

Copyright

by

Scott Douglas Kelman

2008

**The Dissertation Committee for Scott Douglas Kelman certifies that this is the
approved version of the following dissertation:**

**Crosslinking and Stabilization of High Fractional
Free Volume Polymers for the Separation of
Organic Vapors from Permanent Gases**

Committee:

Benny D. Freeman, Supervisor

Donald R. Paul

Isaac C. Sanchez

R. Bruce Eldridge

Chris W. Bielawski

Ingo Pinnau

**Crosslinking and Stabilization of High Fractional
Free Volume Polymers for the Separation of
Organic Vapors from Permanent Gases**

by

Scott Douglas Kelman, B.S.

Dissertation

Presented to the Faculty of the Graduate School of

The University of Texas at Austin

in Partial Fulfillment

of the Requirements

for the Degree of

Doctor of Philosophy

The University of Texas at Austin

May 2008

Dedication

To all those who have helped

Acknowledgements

In my time at the University of Texas at Austin, I have had the pleasure of being associated with many talented and interesting people, and these experiences have made my graduate school career one that I will never forget. My studies have allowed me to grow as a person, both academically, and socially. I would like to start by thanking my supervisor Dr. Benny D. Freeman for his guidance, patience, and encouragement over the course of my studies. Dr. Benny D. Freeman has helped me immensely to develop my connections in the scientific community by introducing me to many of his colleagues, which is something I am very grateful for. I would also like to thank the members of my committee for their guidance and advice given during my time at the University of Texas. I would like to further thank Dr. Don R. Paul, and Dr. Chris W. Bielawski for allowing me access to their laboratory resources. These collaborations have been invaluable to my doctoral work.

Over the course of this Ph.D. many people have contributed their time and effort to the cause. I would like to thank Dr. Anita Hill, and Dr. Steven Pas, and their fellow coworkers at CSIRO in Melbourne, Australia for their work on the PALS analysis of my samples, and for making my stay in Australia such a pleasure. I would like to thank Dr. Tim Merkel, and Dr. Lora Toy for their insight into my project, and their advice has been invaluable. Dr. Ingo Pinnau and the employees at MTR have given many helpful suggestions on the direction of this project, and I am very grateful for their feedback. This Ph.D. project would have not been possible without funding from the U.S.

Department of Energy (grant no. DE-FG03-02ER15362) and the National Science Foundation (grant no. CBET-0515425), and I am thankful for this support.

I have thoroughly enjoyed working with all the members of the Freeman Laboratory, and past and present members of the group have been a valuable source of advice. Many thanks go Scott Matteucci, Roy Raharjo, Rajeev Prabhakar, Ho Bum Park and Haiqing Lin for their guidance and opinions on my dissertation topic. I would also like to thank the other members of the Freeman Laboratory for their willingness to help me out when needed, and for the good times had at Chester Hunt's Icehouse. A special thanks goes to the members of the Texas Graduate rugby team, I have really enjoyed playing rugby during my time in Austin, and being associated with the team both on and off the field. Finally I would like to thank my parents Doug and Jane Kelman and my brother Andy Kelman for their unwavering and enthusiastic support over the course my academic career and the involvement from my family is something that I treasure enormously.

**Crosslinking and Stabilization of High Fractional
Free Volume Polymers for the Separation of
Organic Vapors from Permanent Gases**

Publication No. _____

Scott Douglas Kelman, Ph.D.

The University of Texas at Austin, 2008

Supervisor: Benny D. Freeman

The removal of higher hydrocarbons from natural gas streams is an important separation that has been identified as a growth area for polymer membranes. An ideal membrane material for this separation would be more permeable to higher hydrocarbons (*i.e.*, C₃₊ compounds) than to CH₄. This allows the CH₄ rich permeate to be retained at or near feed pressure, thus minimizing the requirement for repressurization following membrane separation.

A polymer which demonstrates the ability to separate vapor from gases with high efficiency is poly [1-(trimethylsilyl)-1-propyne] (PTMSP). PTMSP is a stiff chain, high free volume glassy polymer well known for its very high gas permeability and outstanding vapor/gas selectivity. However, PTMSP is soluble in many organic

compounds, leading to potential dissolution of the membrane in process streams where its separation properties are of greatest interest. PTMSP also undergoes significant physical aging, which is the gradual relaxation of non-equilibrium excess free volume in glassy polymers. Crosslinking PTMSP with bis(azide)s was undertaken in an attempt to increase the solvent resistance and physical stability of the polymer.

A fundamental investigation into crosslinking PTMSP with a bis(azide) crosslinker was the focus of this thesis. Pure gas transport measurements were conducted with N₂, O₂, CH₄, C₂H₆, C₃H₈, and *n*-C₄H₁₀ over temperatures ranging from -20°C to 35°C and pressures ranging from 0 to 20 atm. Mixed gas permeation experiments were conducted using a 98 mol % CH₄, and 2 mol % *n*-C₄H₁₀ mixture. The mixed gas permeation experiments were conducted at temperatures ranging from -20°C to 35°C, and pressures ranging from 4 to 18 atm. Inorganic nanoparticles such as fumed silica (FS) were added to uncrosslinked and crosslinked PTMSP, and the effects of their addition on the transport properties were investigated.

Crosslinking PTMSP with bis(azide)s increases its solvent resistance, and crosslinked films are insoluble in common PTMSP solvents such as toluene. At all temperatures, the initial pure and mixed gas permeabilities of crosslinked PTMSP films are less than those of uncrosslinked PTMSP. This decrease in permeability is consistent with the fractional free volume (FFV) decrease that accompanies crosslinking. Pure gas solubility coefficients are relatively unaffected by the crosslinking process, so the decrease in permeability is caused by decreases in diffusivity. The addition of FS nanoparticles increases the initial pure and mixed gas permeabilities of uncrosslinked and

crosslinked PTMSP. The pure gas permeabilities and solubilities of all PTMSP films increase when the temperature decreases, while the diffusivities decrease. The rates of change in pure gas transport properties with temperature is similar for all films, so the temperature dependence of pure gas transport properties of PTMSP is unaffected by the addition of crosslinks or FS.

The aging of uncrosslinked and crosslinked PTMSP films was investigated by monitoring N_2 , O_2 and CH_4 permeabilities and FFV over time. The FFV and permeabilities of crosslinked films decreased over time, so crosslinking did not arrest the physical aging of PTMSP, as has been previously reported, and these differences in aging observations are likely to be a consequence of differences in post film casting thermal treatments. The addition of 10 wt % polysiloxysilsesquioxanes (POSS) nanoparticles decreases the permeabilities of uncrosslinked and crosslinked PTMSP by approximately 70 %, and the permeability and FFV values of the resulting nanocomposite films were stable over the course of 200 days.

In all PTMSP films, the mixed gas permeabilities of $n\text{-C}_4\text{H}_{10}$ increase with decreasing temperature, while the mixed gas CH_4 permeabilities decrease with decreasing temperature. As a result, the mixed gas $n\text{-C}_4\text{H}_{10}/CH_4$ permeability selectivities increase with decreasing temperatures. The addition of crosslinks and FS nanoparticles to PTMSP decreases the mixed gas $n\text{-C}_4\text{H}_{10}/CH_4$ permeability selectivities, and changes in the free volume characteristics of PTMSP caused by crosslinking and FS nanoparticles are thought to reduce the blocking of CH_4 permeation by $n\text{-C}_4\text{H}_{10}$.

Table of Contents

List of Tables	xiii
List of Figures	xv
1) Introduction	1
1.1) Membrane Materials for Vapor/Gas Separations	1
1.2) Transport Properties of PTMSP	3
1.3) Modifications to PTMSP to improve its properties	5
1.4) Organization and Goals of the Thesis	7
1.5) References	9
2) Background	13
2.1) Fundamentals of Gas Permeation in Polymers Membranes	13
2.2) Dual-Mode Gas Transport in Glassy Polymers	15
2.3) Free Volume Effects on Gas Transport and Aging	17
2.4) Temperature Effects on Gas Transport	18
2.5) References	19
3) Experimental Methods	22
3.1) Materials	22
3.2) Formation of Polymer Films	25
3.3) Polymer Density Measurement	27
3.4) Ellipsometry Measurements	28
3.5) Pure Gas Sorption Measurement	30
3.6) Pure Gas Permeability Measurement	31

3.7)	Mixed Gas Permeability Measurement.....	32
3.8)	PTMSP Aging Studies	34
3.9)	Positron Annihilation Lifetime Spectroscopy.....	35
3.10)	References.....	36
4)	Effects of Crosslinking on Solvent Resistance and Free Volume	41
4.1)	Solvent Resistance of Crosslinked PTMSP	41
4.2)	Crosslinking Reaction Mechanism	43
4.3)	Effect of Crosslinking on Free Volume and Gas Permeability.....	45
4.4)	Conclusions.....	50
4.5)	References.....	50
5)	Solubility Characteristics of PTMSP.....	53
5.1)	Sorption Isotherms of Neat and Nanocomposite PTMSP.....	53
5.2)	Dual-Mode Sorption in Neat and Nanocomposite PTMSP	63
5.3)	Solubility Coefficients of Neat and Nanocomposite PTMSP.....	70
5.4)	Conclusions.....	74
5.5)	References.....	74
6)	Pure Gas Permeability and Diffusivity.....	76
6.1)	Permanent Gas Permeability.....	76
6.2)	Vapor Permeability	84
6.3)	Gas and Vapor Diffusivity	96
6.4)	Conclusions.....	101
6.5)	References.....	102

7) Physical Stability of PTMSP	105
7.1) Aging of Neat PTMSP	105
7.2) Aging of Nanocomposite POSS/PTMSP Films.....	113
7.3) Permeabilities of PTMSP Compared to Other Polymers.....	117
7.4) Aging of Neat PTMSP Monitored by Ellipsometry	119
7.5) Conclusions.....	124
7.6) References.....	124
8) Mixed Gas Permeability	129
8.1) Pure Gas CH ₄ and <i>n</i> -C ₄ H ₁₀ Permeability	129
8.2) Mixed Gas CH ₄ and <i>n</i> -C ₄ H ₁₀ Permeability	133
8.3) Effect of Upstream <i>n</i> -C ₄ H ₁₀ Activity on Mixed Permeability	141
8.4) Effect of Temperature	147
8.5) Conclusions.....	150
8.6) References.....	151
9) Conclusions and Recommendations.....	153
9.1) Conclusions.....	153
9.2) Recommendations.....	156
9.3) References.....	158
Appendix A – Supplementary Solubility Figures.....	159
Appendix B – Supplementary Permeability and Diffusivity Figures	162
Bibliography	169
Vita.....	181

List of Tables

Table 1.1	Gas permeability coefficients of PTMSP and PDMS at $\Delta p = 0$ and $T = 35^{\circ}\text{C}^{\text{a}}$	3
Table 4.1	Solubility of crosslinked PTMSP films in toluene	42
Table 4.2	Film densities and FFV of various PTMSP films.....	46
Table 4.3	PALS parameters for uncrosslinked and crosslinked PTMSP ^a	47
Table 5.1	Film densities of various PTMSP films.....	59
Table 5.2.	Dual-mode sorption model parameters for CH_4 and $n\text{-C}_4\text{H}_{10}$ in uncrosslinked PTMSP ^a	63
Table 5.3.	Activation energies of sorption for CH_4 and $n\text{-C}_4\text{H}_{10}$ in neat and nanocomposite uncrosslinked PTMSP.	73
Table 6.1	Permeability and PALS parameters of neat and nanocomposite PTMSP ^a	81
Table 6.2.	Activation energies of N_2 , O_2 , and CH_4 permeation for uncrosslinked PTMSP.....	84
Table 6.3.	Dual-mode diffusion coefficients for C_2H_6 in various PTMSP films at 35°C	90
Table 6.4.	Activation energies of C_2H_6 , and C_3H_8 permeation for uncrosslinked and crosslinked PTMSP.....	96
Table 6.5.	Activation energies of diffusivity for uncrosslinked PTMSP.....	101
Table 7.1	van der Waals volumes and molecular mass of TMSP and the bis(azide) crosslinker	110
Table 7.2	PALS parameters for uncrosslinked and nanocomposite PTMSP ^a	114

Table 7.3	PTMSP/POSS nanocomposite film density.....	117
Table 8.1.	Activation energies of pure and mixed gas CH ₄ permeation in various PTMSP films. The activation energies are reported at a CH ₄ fugacity of 11 atm in the feed gas.	149

List of Figures

Figure 1.1	Polymerization reaction to form PTMSP.....	2
Figure 1.2	N ₂ permeability over time of uncrosslinked, unfilled PTMSP, and uncrosslinked PTMSP containing POSS OL1160 nanoparticles. Feed pressure = 50 psig; permeate pressure = atmospheric; T = 23 °C. Films were aged at ambient conditions. POSS OL1160 nanoparticles have a nominal size range of 1-3 nm [30]......	6
Figure 3.1	Chemical structure of bis(azide) crosslinker 3,3'-diazidodiphenylsulfone	22
Figure 3.2	Chemical structure of a) TS 530 FS and b) POSS MS0865	24
Figure 4.1	Proposed reaction scheme for crosslinking PTMSP with bis(azide) [1,2,8]	44
Figure 4.2.	FT-IR spectra of pure PTMSP, PTMSP containing 10 wt % crosslinker (XL) prior to exposing the sample to elevated temperatures to perform the crosslinking reaction, and crosslinked PTMSP containing 10 wt % crosslinker.	45
Figure 4.3.	Effect of crosslinker content on initial N ₂ permeability and FFV of PTMSP and crosslinked PTMSP films. T = 35°C, $f_2 = 4.4$ atm, and $f_1 =$ atmospheric for all measurements. All films were crosslinked in vacuum at 180°C for 90 minutes, then soaked in MeOH for 24 hours, and finally	

	dried at ambient conditions for 72 hours prior to the permeation measurements. Film thickness was approximately 100 μm	48
Figure 4.4.	Permeability of N_2 , O_2 , CH_4 , C_2H_6 , C_3H_8 and $n\text{-C}_4\text{H}_{10}$ in uncrosslinked and crosslinked PTMSP versus $1/\text{FFV}$. $T = 35^\circ\text{C}$, $f_2 = 4.4$ atm (N_2 , O_2 , CH_4 , and C_2H_6), $f_2 = 2.8$ atm (C_3H_8) and $f_2 = 1.7$ atm ($n\text{-C}_4\text{H}_{10}$), $f_1 =$ atmospheric for all measurements. Films were crosslinked at 180°C in vacuum for 90 minutes, soaked in MeOH for 24 hours, then dried for 72 hours before testing began. Film thickness was approximately 100 μm . The numbers at the top of the plot represent the wt % crosslinker initially present in the film.	49
Figure 5.1.	Sorption isotherms of uncrosslinked PTMSP (unfilled symbols) and uncrosslinked PTMSP containing 30 wt % FS (filled symbols) for (a) N_2 at 35°C and 10°C ; (b) N_2 at 0°C and -20°C ; (c) O_2 at 35°C and 10°C ; and (d) O_2 at 0°C and -20°C . The concentration is expressed as cm^3 of penetrant at STP per cm^3 of film in the sorption cell. All films were subjected to vacuum at 180°C for 90 minutes, soaked in MeOH for 24 hours, and then dried for 72 hours in ambient conditions before sorption isotherms were measured. The solid lines represent dual-mode sorption model fits to the sorption isotherms.	54
Figure 5.2.	Sorption isotherms of uncrosslinked PTMSP (unfilled symbols) and uncrosslinked PTMSP containing 30 wt % FS (filled symbols) for (a) CH_4 at 35°C and 10°C ; (b) CH_4 at 0°C and -20°C ; (c) C_2H_6 at 35°C and 10°C ;	

and (d) C_2H_6 at $0^\circ C$ and $-20^\circ C$. The concentration is expressed as cm^3 of penetrant at STP per cm^3 of film in the sorption cell. All films were subjected to vacuum at $180^\circ C$ for 90 minutes, soaked in MeOH for 24 hours, and then dried for 72 hours in ambient conditions before sorption isotherms were measured. The solid lines represent dual-mode sorption model fits to the sorption isotherms. The CH_4 sorption isotherm measured by Merkel et al. is for pure PTMSP at $35^\circ C$ [3]..... 55

Figure 5.3. Sorption isotherms of uncrosslinked PTMSP (unfilled symbols) and uncrosslinked PTMSP containing 30 wt % FS (filled symbols) for (a) C_3H_8 at $35^\circ C$ and $10^\circ C$; (b) C_3H_8 at $0^\circ C$ and $-20^\circ C$; (c) $n-C_4H_{10}$ at $35^\circ C$ and $10^\circ C$; and (d) $n-C_4H_{10}$ at $0^\circ C$ and $-20^\circ C$. The concentration is expressed as cm^3 of penetrant at STP per cm^3 of film in the sorption cell. All films were subjected to vacuum conditions at $180^\circ C$ for 90 minutes, soaked in MeOH for 24 hours, and then dried for 72 hours in ambient conditions before sorption isotherms were measured. The solid lines represent dual-mode sorption model fits to the sorption isotherms. 56

Figure 5.4. Sorption isotherms of PTMSP containing 0 (Δ), 5 (\square), and 10 (\circ) wt % XL, and nanocomposite PTMSP containing 30 wt % FS and 0 (\blacktriangle) or 10 (\bullet) wt % XL for (a) CH_4 at $35^\circ C$; (b) CH_4 at $0^\circ C$; (c) $n-C_4H_{10}$ at $35^\circ C$; and (d) $n-C_4H_{10}$ at $0^\circ C$. The concentration is expressed as cm^3 of penetrant at STP per cm^3 of film in the sorption cell. All films were subjected to vacuum at $180^\circ C$ for 90 minutes, soaked in MeOH for 24 hours, and then

dried for 72 hours in ambient conditions before sorption isotherms were measured. The solid lines represent dual-mode sorption model fits to the sorption isotherms. 58

Figure 5.5. n -C₄H₁₀ sorption isotherms of uncrosslinked PTMSP (unfilled symbols) and uncrosslinked PTMSP containing 30 wt % FS (filled symbols) at 35°C. In all cases, C is the cm³ (STP) of n -C₄H₁₀ sorbed per cm³ of PTMSP (Δ , \blacksquare) or nanocomposite (i.e., PTMSP + fumed silica) (\blacktriangle , \bullet). The volume of the nanocomposite film was estimated using the measured and additive densities in Table 5.1 and the mass of the sample in the sorption cell. The nanocomposite isotherm is also shown for the case when the contribution of FS nanoparticles to the n -C₄H₁₀ sorption is negligible, and only the volume of PTMSP is considered to sorb n -C₄H₁₀ in the nanocomposite film (\blacksquare). All films were subjected to vacuum at 180°C for 90 minutes, soaked in methanol for 24 hours, and then dried for 72 hours in ambient conditions before sorption isotherms were measured. The solid lines represent dual-mode sorption model fits to the sorption isotherms. 60

Figure 5.6. Sorption isotherms of uncrosslinked PTMSP (unfilled symbols), and uncrosslinked PTMSP containing 30 wt % FS (filled symbols) for (a) CH₄; (b) n -C₄H₁₀ at 35°C and 10°C; and (c) n -C₄H₁₀ at 0°C and -20°C. The concentration is expressed as cm³ of penetrant at STP per cm³ of PTMSP in the sorption cell. All films were subjected to vacuum at 180°C for 90 minutes, soaked in MeOH for 24 hours, and then dried for 72 hours in

ambient conditions before sorption isotherms were measured. The solid lines represent dual-mode sorption model fits to the sorption isotherms. 62

Figure 5.7. Effect of temperature on the Langmuir sorption capacity, C'_H , for a) N_2 , b) O_2 , and c) CH_4 in uncrosslinked PTMSP and uncrosslinked PTMSP containing 30 wt % FS. The Langmuir capacity parameter is calculated on the basis of total film volume. All films were crosslinked at 180°C in vacuum for 90 minutes, soaked in MeOH for 24 hours, and then dried at ambient conditions for 72 hours before sorption isotherms were measured. 65

Figure 5.8. Effect of temperature on the Langmuir sorption capacity, C'_H , for a) C_2H_6 , b) C_3H_8 , and c) $n-C_4H_{10}$ in uncrosslinked PTMSP and uncrosslinked PTMSP containing 30 wt % FS. The Langmuir capacity parameter is calculated on the basis of total film volume. All films were crosslinked at 180°C in vacuum for 90 minutes, soaked in MeOH for 24 hours, then dried at ambient conditions for 72 hours before sorption isotherms were measured. 66

Figure 5.9. Effect of temperature on Henry's Law parameter, k_D , for a) CH_4 and C_2H_6 ; and b) C_3H_8 and $n-C_4H_{10}$ in uncrosslinked PTMSP and uncrosslinked PTMSP containing 30 wt % FS. The parameters were calculated using total film volume. All films were subjected to vacuum at 180°C for 90 minutes, soaked in MeOH for 24 hours, and then dried for 72 hours in ambient conditions before sorption isotherms were measured. 68

- Figure 5.10. Effect of temperature on Langmuir affinity parameter, b , of N_2 , O_2 , CH_4 , C_2H_6 , C_3H_8 , and $n-C_4H_{10}$ in uncrosslinked PTMSP and uncrosslinked PTMSP containing 30 wt % FS. The parameters were calculated using total film volume. All films were subjected to vacuum conditions at $180^\circ C$ for 90 minutes, soaked in MeOH for 24 hours, and then dried for 72 hours in ambient conditions before sorption isotherms were measured. 69
- Figure 5.11. Effect of fugacity and temperature on CH_4 , and $n-C_4H_{10}$ solubilities in neat (PTMSP) and nanocomposite (30 FS) uncrosslinked PTMSP. The CH_4 solubilities are plotted as a function of CH_4 fugacity, while the $n-C_4H_{10}$ solubilities are plotted as function of $n-C_4H_{10}$ activity. All films were subjected to vacuum conditions at $180^\circ C$ for 90 minutes, soaked in MeOH for 24 hours, and then dried for 72 hours in ambient conditions before sorption isotherms were measured. The solid lines represent the dual-mode sorption model fit to the solubility data. The saturation fugacity values, f_{sat} , were calculated as described in the literature [14]. 71
- Figure 5.12. Effect of temperature on CH_4 solubility at 10 atm fugacity, and $n-C_4H_{10}$ solubility at an activity of 0.4 in uncrosslinked PTMSP and uncrosslinked PTMSP containing 30 wt % FS. The solubilities were calculated using the dual-mode sorption parameters for the films at the various temperatures. The total volume of the films in the sorption cell was used as the basis to calculate the solubilities. All films were subjected to vacuum at $180^\circ C$ for

	90 minutes, soaked in MeOH for 24 hours, and then dried for 72 hours in ambient conditions before sorption isotherms were measured.	72
Figure 6.1.	Permeability of a) N ₂ , b) O ₂ , and c) CH ₄ as a function of upstream fugacity in various PTMSP films at 35°C. The downstream pressure was fixed at atmospheric. The solid lines represent a nonlinear least squares fit of the dual-mode transport model to the permeability data. All films were subjected to vacuum at 180°C for 90 minutes, soaked in MeOH for 24 hours, and then dried for 72 hours in ambient conditions before permeability was measured. All films were approximately 100 µm thick.	77
Figure 6.2.	Permeability of a) N ₂ , b) O ₂ , and c) CH ₄ as a function of upstream fugacity in various PTMSP films at 0°C. The downstream pressure was fixed at atmospheric. The solid lines represent a nonlinear least squares fit of the dual-mode transport model to the permeability data. All films were subjected to vacuum at 180°C for 90 minutes, soaked in MeOH for 24 hours, and then dried for 72 hours in ambient conditions before permeability was measured. All films were approximately 100 µm thick.	79
Figure 6.3.	Effect of the addition of 30 wt % TiO ₂ nanoparticles to uncrosslinked and crosslinked PTMSP on a) τ_3 and b) τ_4 as measured by PALS. The TiO ₂ nanoparticles have an effective single particle diameter of 15 nm.	82

- Figure 6.4. Temperature dependence of a) N_2 , b) O_2 , and c) CH_4 permeability at 4.4 atm upstream fugacity in various PTMSP films. The downstream pressure was fixed at atmospheric. The data were fit to an Arrhenius relationship shown in Equation 2.14. All films were subjected to vacuum at 180°C for 90 minutes, soaked in MeOH for 24 hours, and then dried for 72 hours in ambient conditions before permeability was measured. All films were approximately 100 μm thick. 83
- Figure 6.5. Permeability of a) C_2H_6 in neat PTMSP, b) C_2H_6 in nanocomposite PTMSP, c) C_3H_8 in neat PTMSP, and d) C_3H_8 in nanocomposite PTMSP as a function of upstream fugacity at 35°C. The downstream pressure was fixed at atmospheric. The C_2H_6 permeability data were fit to the dual-mode transport model, and the C_3H_8 permeability data were fit to a linear function. All films were subjected to vacuum at 180°C for 90 minutes, soaked in MeOH for 24 hours, and then dried for 72 hours in ambient conditions before permeability was measured. All films were approximately 100 μm thick. 86
- Figure 6.6. Permeability of a) C_2H_6 and b) C_3H_8 in as a function of upstream fugacity at 0°C. The downstream pressure was fixed at atmospheric. The C_2H_6 permeability data were fit to the dual-mode transport model, and the C_3H_8 permeability data were fit to a linear function. All films were subjected to vacuum at 180°C for 90 minutes, soaked in MeOH for 24 hours, and then

dried for 72 hours in ambient conditions before permeability was measured. All films were approximately 100 μ m thick..... 87

Figure 6.7. Temperature dependence of a) C₂H₆, and b) C₃H₈ permeability in various PTMSP films. The C₂H₆ and C₃H₈ permeabilities are reported at upstream activities of 0.4, and 0.6, respectively. The data were fit to an Arrhenius relationship shown in Equation 2.14. All films were subjected to vacuum at 180°C for 90 minutes, soaked in MeOH for 24 hours, and then dried for 72 hours in ambient conditions before permeability was measured. All films were approximately 100 μ m thick. 95

Figure 6.8. Concentration averaged diffusivity of a) N₂, b) O₂, c) CH₄, d) C₂H₆ and e) C₃H₈ as a function of penetrant concentration in various PTMSP films at 35°C. The N₂, O₂, CH₄ and C₂H₆ diffusivities were fit to the dual-mode transport model, while the C₃H₈ diffusivities were fit to a linear function.. All films were approximately 100 μ m thick. 97

Figure 6.9. Effect of temperature on the concentration averaged diffusivity of a) N₂ and O₂; b) CH₄; and c) C₂H₆ and C₃H₈ in various PTMSP films. The data were fit to Equation 2.16. All films were subjected to vacuum at 180°C for 90 minutes, soaked in MeOH for 24 hours, and then dried for 72 hours in ambient conditions before transport properties were measured. All films were approximately 100 μ m thick. 100

Figure 7.1. Permeability of a) uncrosslinked PTMSP and b) crosslinked PTMSP as a function of time. The crosslinked film contained 5 wt % bis azide

crosslinker. $T = 35^{\circ}\text{C}$, $f_2 = 4.4 \text{ atm}$, and $f_l = \text{atmospheric}$ for all measurements. The films were thermally annealed in vacuum at 180°C for 90 minutes, soaked in MeOH for 24 hours, and dried at ambient conditions for 72 hours prior to the initial permeation measurements. Film thickness was approximately $100 \mu\text{m}$ 106

Figure 7.2. Measured densities for uncrosslinked and crosslinked PTMSP samples. The densities were measured at ambient conditions using a $\text{Ca}(\text{NO}_3)_2$ salt solution (density = 1.4 g/cm^3) and then calculated using the buoyancy method. The crosslinked film contained 5 wt % crosslinker. All films were thermally treated in vacuum at 180°C for 90 minutes, then soaked in MeOH for 24 hours, and dried at ambient conditions for 72 hours prior to the initial density measurement. Film thickness was approximately $100 \mu\text{m}$ 109

Figure 7.3. Permeability of a) N_2 , b) O_2 , and c) CH_4 in uncrosslinked PTMSP (\blacktriangle) and crosslinked PTMSP (\blacksquare) as a function of $1/\text{FFV}$. The FFV values of the samples were calculated using measured density values and Bondi's group contribution method. $T = 35^{\circ}\text{C}$, $f_2 = 4.4 \text{ atm}$, and $f_l = \text{atmospheric}$ for all measurements. The crosslinked film contained 5 wt % crosslinker. All films were thermally treated in vacuum at 180°C for 90 minutes, soaked in MeOH for 24 hours, and dried at ambient conditions for 72 hours prior to the permeation measurements. Film thickness was approximately $100 \mu\text{m}$ 111

Figure 7.4. Permeability of a) PTMSP + 10 wt % POSS MS0865 nanocomposite film, and b) Crosslinked PTMSP + 10 wt % POSS MS0865 nanocomposite film as a function of time. The crosslinked film contained 5 wt % bis azide crosslinker. $T = 35^{\circ}\text{C}$, $f_2 = 4.4 \text{ atm}$, and $f_1 = \text{atmospheric}$ for all measurements. The films were thermally annealed in vacuum at 180°C for 90 minutes and cooled at ambient conditions for 72 hours prior to the initial permeation measurements. Film thickness was approximately $100 \mu\text{m}$ 113

Figure 7.5. Measured densities for uncrosslinked and crosslinked PTMSP + POSS nanocomposite samples. The densities were measured at ambient conditions using a salt solution (density = 1.4 g/cm^3) and then calculated using the buoyancy method. The crosslinked film contained 5 wt % crosslinker. All films were crosslinked in vacuum at 180°C for 90 minutes, and cooled at ambient conditions for 72 hours prior to the initial density measurement. Film thickness was approximately $100 \mu\text{m}$ 116

Figure 7.6. Permeability of a) N_2 , b) O_2 , and c) CH_4 in uncrosslinked PTMSP and crosslinked PTMSP, other substituted polyacetylenes [22-26], polycarbonates and polysulfones [27-37] as a function of $1/\text{FFV}$. The FFV values were calculated using measured density values and Bondi's group contribution method. 118

Figure 7.7. Effect of aging on the refractive index of uncrosslinked and crosslinked PTMSP. The crosslinked film contains 10 wt % crosslinker, and all films

	were crosslinked in vacuum at 180°C for 90 minutes. Ellipsometry measurements began 1 hour after removal from the vacuum oven.	120
Figure 7.8.	Effect of aging on the film thickness of uncrosslinked and crosslinked PTMSP. The crosslinked film contains 10 wt % crosslinker and all films were crosslinked in vacuum at 180°C for 90 minutes. Ellipsometry measurements began 1 hour after removal from the vacuum oven.	121
Figure 7.9.	Effect of aging on the relative refractive index of uncrosslinked PTMSP and crosslinked PTMSP films. The crosslinked film contains 10 wt. % crosslinker and all films were crosslinked in vacuum at 180°C for 90 minutes. Ellipsometry measurements began 1 hour after removal from the vacuum oven.	122
Figure 7.10.	Effect of free volume on aging rates of various polymers films determined by ellipsometry. All polymer films were approximately 400 nm thick [39,40].	123
Figure 8.1.	Pure gas $n\text{-C}_4\text{H}_{10}$ permeability of various PTMSP films at 35°C. The solid lines are a linear fit to the data measured as feed pressure is increased, and these lines serve as a guide for the eye of the reader. All films were crosslinked at 180°C in vacuum for 90 minutes, soaked in MeOH for 24 hours, then dried at ambient conditions for 72 hours before permeability measurements began. The thickness of the films were approximately 100 μm . In this figure and in figures 8.2 through 8.5, filled data points correspond to measurements made as feed pressure was increased, and	

unfilled data points correspond to measurements made as feed pressure was decreased..... 130

Figure 8.2. Pure gas CH₄ permeability of various PTMSP films at a) 35°C, b) 10°C, c) 0°C, and d) -20°C. The solid lines are smooth fits to the data measured as the pressure is increased, and these lines serve as a guide for the eye of the reader. All films were crosslinked at 180°C in vacuum for 90 minutes, soaked in MeOH for 24 hours, then dried at ambient conditions for 72 hours before permeability measurements began. The thickness of the films were approximately 100 μm. 132

Figure 8.3. Mixed gas *n*-C₄H₁₀ permeabilities of various PTMSP films at a) 35°C, b) 10°C, c) 0°C, and d) -20°C. The solid lines are smooth fits to the data measured as the pressure is increased, and these lines serve as a guide for the eye of the reader. All films were crosslinked at 180°C in vacuum for 90 minutes, soaked in MeOH for 24 hours, then dried at ambient conditions for 72 hours before permeability measurements began. The thickness of the films was approximately 500 μm. 134

Figure 8.4. Mixed gas CH₄ permeability of various PTMSP films at a) 35°C, b) 10°C, c) 0°C, and d) -20°C. The solid lines are smooth fits to the data measured as the pressure is increased, and these lines serve as a guide for the eye of the reader. All films were crosslinked at 180°C in vacuum for 90 minutes, soaked in MeOH for 24 hours, then dried at ambient conditions for 72

hours before permeability measurements began. The thickness of the films was approximately 500 μm 137

Figure 8.5. Mixed gas $n\text{-C}_4\text{H}_{10}/\text{CH}_4$ permeability selectivity of various PTMSP films at a) 35°C, b) 10°C, c) 0°C, and d) -20°C. The solid lines are smooth fits to the data measured as the pressure is increased, and these lines serve as a guide for the eye of the reader. All films were crosslinked at 180°C in vacuum for 90 minutes, soaked in MeOH for 24 hours, then dried at ambient conditions for 72 hours before permeability measurements began. The thickness of the films was approximately 500 μm 139

Figure 8.6. Mixed gas $n\text{-C}_4\text{H}_{10}$ permeabilities of a) uncrosslinked PTMSP, and b) PTMSP + 30 wt % FS (30 FS) and PTMSP + 10 wt % XL (10 XL) as function of upstream $n\text{-C}_4\text{H}_{10}$ activity. The smooth lines are intended to act as guides for the eye of the reader. The mixed gas $n\text{-C}_4\text{H}_{10}$ permeabilities from this study are reported at 35°C, 10°C, 0°C, and -20°C. The mixed gas $n\text{-C}_4\text{H}_{10}$ permeabilities from Raharjo's et al. study are reported at 35°C, 0°C, and -20°C [9]. $n\text{-C}_4\text{H}_{10}$ activity is calculated as f_2/f_{sat} , where the fugacity value at saturation, f_{sat} , was calculated as described by Raharjo *et al.* [12]. 141

Figure 8.7. Mixed gas CH_4 permeabilities of a) uncrosslinked PTMSP, and b) PTMSP + 30 wt % FS (30 FS) and PTMSP + 10 wt % XL (10 XL) as function of upstream $n\text{-C}_4\text{H}_{10}$ activity. The smooth lines are intended to act as guides for the eye of the reader. The mixed gas CH_4 permeabilities from this

	study are reported at 35°C, 10°C, 0°C, and -20°C. The mixed gas CH ₄ permeabilities from Raharjo's <i>et al.</i> study are reported at 35°C, 0°C, and -20°C [9].	143
Figure 8.8	The ratio of mixed gas CH ₄ permeabilities to pure gas CH ₄ permeabilities at infinite dilution as a function of upstream <i>n</i> -C ₄ H ₁₀ activity at a) 35°C, b) 10°C, c) 0°C, and d) -20°C. The filled symbols represent values from this study, while the unfilled symbols represent data from Raharjo <i>et al.</i> , which reports such data for unfilled uncrosslinked PTMSP [9,15].	145
Figure 8.9.	Mixed gas <i>n</i> -C ₄ H ₁₀ /CH ₄ selectivities of a) uncrosslinked PTMSP, and b) PTMSP + 30 wt % FS (30 FS) and PTMSP + 10 wt % XL (10 XL) as function of upstream <i>n</i> -C ₄ H ₁₀ activity. The smooth lines are intended to act as guides for the eye of the reader. The mixed gas <i>n</i> -C ₄ H ₁₀ /CH ₄ selectivities from this study are reported at 35°C, 10°C, 0°C, and -20°C. The mixed gas <i>n</i> -C ₄ H ₁₀ /CH ₄ selectivities from Raharjo's <i>et al.</i> study are reported at 35°C, 0°C, and -20°C [9].	146
Figure 8.10.	The effect of temperature on a) mixed gas <i>n</i> -C ₄ H ₁₀ permeabilities, b) mixed gas CH ₄ permeabilities, c) the ratio of mixed to pure gas CH ₄ permeabilities, and d) mixed gas <i>n</i> -C ₄ H ₁₀ /CH ₄ selectivities of various PTMSP films. The data are reported at a CH ₄ feed fugacity of 11 atm for measurements made as the film was pressurized. The solid lines are an Arrhenius fit to the data. All films were crosslinked at 180°C in vacuum	

for 90 minutes, soaked in MeOH for 24 hours, then dried at ambient conditions for 72 hours before permeability measurements began. 148

Figure A.1. Effect of fugacity and temperature on N_2 , and O_2 solubilities in neat and nanocomposite uncrosslinked PTMSP. The solubilities are plotted as a function of their fugacities. All films were subjected to vacuum conditions at 180°C for 90 minutes, soaked in methanol for 24 hours, then dried for 72 hours in ambient conditions before sorption isotherms were measured. The solid lines represent the dual-mode sorption model fit to the solubility data..... 159

Figure A.2. Effect of activity and temperature on C_2H_6 , and C_3H_8 solubilities in neat and nanocomposite uncrosslinked PTMSP. The solubilities are plotted as a function of their activities. All films were subjected to vacuum conditions at 180°C for 90 minutes, soaked in methanol for 24 hours, then dried for 72 hours in ambient conditions before sorption isotherms were measured. The solid lines represent the dual-mode sorption model fit to the solubility data..... 160

Figure A.3. Effect of temperature on a) N_2 and O_2 ; and b) C_2H_6 and C_3H_8 solubilities in uncrosslinked PTMSP and uncrosslinked PTMSP containing 30 wt % FS. The solubilities were calculated using the dual-mode sorption parameters for the films at the various temperatures specified and fugacities and activities. The total volume of the films in the sorption cell was used as the basis to calculate the solubilities. All films were

crosslinked at 180°C in vacuum for 90 minutes, soaked in MeOH for 24 hours and dried at ambient conditions for 72 hours before sorption isotherms were measured. 161

Figure B.1. Permeability of a) N₂, b) O₂, and c) CH₄ as a function of upstream fugacity in various PTMSP films at 10°C. The downstream pressure was fixed at atmospheric. The solid lines represent a nonlinear least squares fit of the dual-mode transport model to the permeability data. All films were subjected to vacuum at 180°C for 90 minutes, soaked in MeOH for 24 hours, then dried for 72 hours in ambient conditions before permeability was measured. All films were approximately 100 µm thick. 162

Figure B.2. Permeability of a) N₂, b) O₂, and c) CH₄ as a function of upstream fugacity in various PTMSP films at -20°C. The downstream pressure was fixed at atmospheric. The solid lines represent a nonlinear least squares fit of the dual-mode transport model to the permeability data. All films were subjected to vacuum at 180°C for 90 minutes, soaked in MeOH for 24 hours, then dried for 72 hours in ambient conditions before permeability was measured. All films were approximately 100 µm thick 163

Figure B.3. Permeability of a) C₂H₆, and b) C₃H₈ as a function of upstream fugacity in various PTMSP films at 10°C. The downstream pressure was fixed at atmospheric. The C₂H₆ permeability data were fit to the dual-mode transport model, while the C₃H₈ permeability data were fit to a linear function. All films were subjected to vacuum at 180°C for 90 minutes,

soaked in MeOH for 24 hours, then dried for 72 hours in ambient conditions before permeability was measured. All films were approximately 100 μm thick. 164

Figure B.4. Permeability of a) C_2H_6 , and b) C_3H_8 as a function of upstream fugacity in various PTMSP films at -20°C . The downstream pressure was fixed at atmospheric. The C_2H_6 permeability data were fit to the dual-mode transport model, while the C_3H_8 permeability data were fit to a linear function. All films were subjected to vacuum at 180°C for 90 minutes, soaked in MeOH for 24 hours, then dried for 72 hours in ambient conditions before permeability was measured. All films were approximately 100 μm thick. 165

Figure B.5. Concentration averaged diffusivity of a) N_2 , b) O_2 , c) CH_4 , d) C_2H_6 , and e) C_3H_8 as a function of penetrant concentration in various PTMSP films at 10°C . The N_2 , O_2 , CH_4 , and C_2H_6 diffusivity data were fit to the dual-mode transport model, while the C_3H_8 diffusivity data were fit to a linear function. 166

Figure B.6. Concentration averaged diffusivity of a) N_2 , b) O_2 , c) CH_4 , d) C_2H_6 , and e) C_3H_8 as a function of penetrant concentration in various PTMSP films at 0°C . The N_2 , O_2 , CH_4 , and C_2H_6 diffusivity data were fit to the dual-mode transport model, while the C_3H_8 diffusivity data were fit to a linear function. 167

Figure B.7. Concentration averaged diffusivity of a) N_2 , b) O_2 , c) CH_4 , d) C_2H_6 , and e) C_3H_8 as a function of penetrant concentration in various PTMSP films at $-20^\circ C$. The N_2 , O_2 , CH_4 , and C_2H_6 diffusivity data were fit to the dual-mode transport model, while the C_3H_8 diffusivity data were fit to a linear function. 168

1) Introduction

1.1) Membrane Materials for Vapor/Gas Separations

The separation of higher hydrocarbons from permanent gases is an important industrial separation in the processing of natural gas [1]. The primary constituent of natural gas is CH_4 . Other hydrocarbon constituents such as C_2H_6 , C_3H_8 , and $n\text{-C}_4\text{H}_{10}$, and impurities such as N_2 , CO_2 , H_2O , and H_2S are also present in raw natural gas, and the concentration of the non- CH_4 constituents varies significantly from well to well [1-3]. Though the composition of raw natural gas varies significantly, the composition delivered to the pipeline is strictly controlled [1], which means the natural gas processing operations required are tailored to the composition of the raw natural gas stream.

The removal of higher hydrocarbons from natural gas prevents condensation of these materials during pipeline transport and allows a valuable chemical feedstock to be recovered [1]. Membrane technology has been shown to be a commercially viable method for the separation of higher hydrocarbons from CH_4 . An ideal membrane material for this separation would be more permeable to higher hydrocarbons than to CH_4 [4]. This allows the CH_4 rich permeate to be retained at or near feed pressure, thus minimizing the need for repressurization. Membrane materials exhibiting these characteristics are often referred to as “reverse-selective” materials since larger molecules are more permeable than smaller molecules in these materials, which is opposite to the trend often observed for gas permeation in polymers [1,4-7]. Poly[1-(trimethylsilyl)-1-

propyne] (PTMSP) is one such polymer that displays these reverse-selective properties [8-11].

PTMSP is formed by polymerization of substituted polyacetylenes. The polymerization of substituted polyacetylenes was first shown in 1974 when phenylacetylene was polymerized using WCl_6 and other so-called metathesis catalysts based on Mo, Ta and Nb [12]. These catalysts polymerize many other substituted acetylenes into high molecular weight polymers [13]. PTMSP is polymerized using TaCl_5 and NbCl_5 as catalysts, and the reaction scheme for the synthesis of PTMSP is given in *Figure 1.1* [14]:

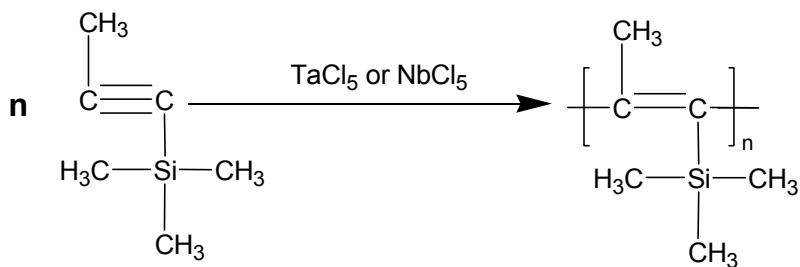


Figure 1.1 Polymerization reaction to form PTMSP

The polymer yield under these reaction conditions was 100 %, and the molecular weight of PTMSP, determined by gel permeation chromatography, ranged from 1×10^5 to 1×10^6 g/mol [14]. The resulting high molecular weight PTMSP is colorless, odorless and thermally stable in air [14]. Since PTMSP was first synthesized in 1983 by Higashimura and Masuda [14] at Kyoto University in Japan, it has attracted intense interest due to its high permeability values and unusual separation characteristics. The notion suggested by PTMSP, that a stiff main chain and bulky side groups result in amorphous, high

permeability materials, has motivated the synthesis of copolymers of PTMSP and many other substituted polyacetylenes [13].

1.2) Transport Properties of PTMSP

PTMSP is the most permeable polymer known [13,14]. As shown in Table 1.1, it exhibits permeability values that are approximately an order of magnitude higher than those of rubbery PDMS. Before the synthesis and characterization of PTMSP, PDMS was regarded as the most gas-permeable polymer [13].

Table 1.1 Gas permeability coefficients of PTMSP and PDMS at $\Delta p = 0$ and $T = 35^\circ\text{C}^a$

Gas	Permeability (barrer ^a)	
	PTMSP [15]	PDMS [16]
H ₂	15,000	890
O ₂	9,000	800
N ₂	6,600	400
CO ₂	27,000	3,800
CH ₄	15,000	1,200
C ₂ H ₆	31,000	3,300
C ₃ H ₈	38,000	4,100

a) 1 Barrer = $10^{-10} \text{ cm}^3(\text{STP}) \cdot \text{cm} / (\text{cm}^2 \cdot \text{s} \cdot \text{cm Hg})$.

PTMSP has a very high fractional free volume (FFV) of 0.29 [17], therefore the polymer has poor size-sieving ability, and the diffusivity selectivity between large and small molecules such as *n*-C₄H₁₀ and CH₄ approaches unity. Conversely, the

n -C₄H₁₀/CH₄ solubility selectivity is far greater than 1 [18]. These two factors contribute to PTMSP having exceptional reverse-selective properties. For example, the n -C₄H₁₀/CH₄ mixed gas selectivity is 35 at 25°C, which is very high [18]. In mixed gas permeation experiments with PTMSP and related reverse-selective materials, the vapor/gas selectivities are enhanced relative to the vapor/gas selectivities of pure gas permeation experiments [18,19]. The enhanced vapor/gas selectivities are caused by blocking of the permanent gas permeation (*i.e.*, CH₄) by the larger, more condensable vapor molecules (*i.e.*, n -C₄H₁₀) [10,20].

The free volume elements of PTMSP are thought to be interconnected, and the majority of the gas permeation is believed to occur through these interconnected free volume elements [10,20]. The transport mechanism of condensable vapors such as n -C₄H₁₀ in PTMSP has been suggested to be similar in some regards to condensable vapor transport in microporous inorganic membranes [10]. In this mechanism the condensable vapor sorbs onto the walls of the small pores, and diffuses along the pore walls. Multilayer absorption of condensable components, which can partially or completely block the pores, reduces the flow of less condensable gases [21,22]. For example, CH₄ permeability in PTMSP at 23°C decreased from 15,400 barrer in pure gas permeation to 1,800 barrer when a mixture of 98 mol % CH₄, and 2 mol % n -C₄H₁₀ was permeated across the film [10]. The decrease of CH₄ permeability in mixed gas experiments is the main reason for the n -C₄H₁₀/CH₄ permeability selectivity increasing from 5 in pure gas experiments to 30 in mixed gas experiments [10].

The pure gas permeability of PTMSP to gases and vapors decreases over time due to physical aging, which is the gradual relaxation and densification of nonequilibrium excess free volume. This process occurs due to the nonequilibrium nature of the glassy state, and this departure from equilibrium provides a driving force for the polymer to densify towards its equilibrium volume [23]. The solvent resistance of PTMSP is low, and it is soluble in a wide range of organic solvents [24]. This high solubility can compromise the utility of PTMSP in natural gas separations, where aliphatic and aromatic contaminants may be present in the feed stream [18]. To improve the performance, and commercialization potential of PTMSP, the physical stability and solvent resistance need to be improved [1,9,10].

1.3) Modifications to PTMSP to improve its properties

PTMSP has been chemically and physically modified using many different methods. PTMSP has been blended with rubbery polymers [25], brominated [26-28], had nanoparticles added [18,29-31], and has been crosslinked [32-34] in attempts to stabilize the gas permeation properties. Fumed silica nanoparticle addition to PTMSP can increase gas and vapor permeability [18,31,35] by disrupting chain packing and creating extra free volume. However, it appears this additional free volume cannot be maintained over time since permeability still decreases, most likely due to a decrease in FFV over time. The addition of polyhedral oligomeric silsesquioxane (POSS) inorganic nanoparticles has been shown to stabilize the permeability of a PTMSP [30]. This result was ascribed to the particles creating barriers that frustrate the relaxation of PTMSP chains. However, a

complete understanding of this phenomenon is still lacking. *Figure 1.2* presents aging data of pure PTMSP and PTMSP containing POSS nanoparticles.

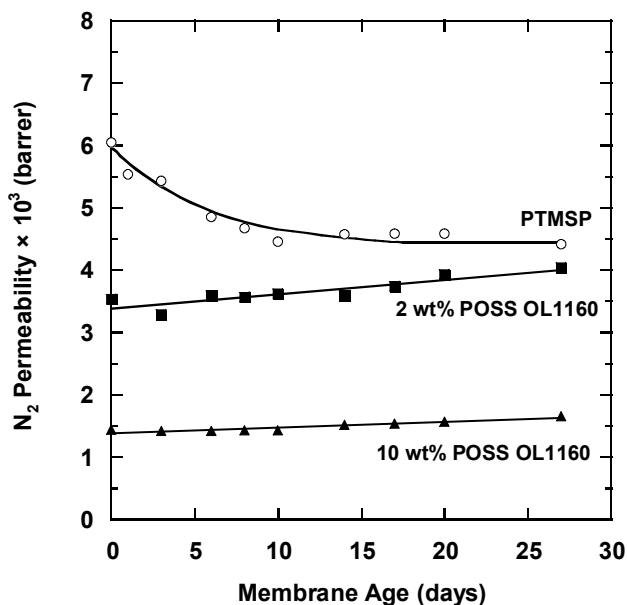


Figure 1.2 N_2 permeability over time of uncrosslinked, unfilled PTMSP, and uncrosslinked PTMSP containing POSS OL1160 nanoparticles. Feed pressure = 50 psig; permeate pressure = atmospheric; $T = 23^\circ\text{C}$. Films were aged at ambient conditions. POSS OL1160 nanoparticles have a nominal size range of 1-3 nm [30].

Crosslinking PTMSP with bis(azide)s has been reported to stabilize permeability over time, and increase the solvent resistance [32]. Crosslinked PTMSP films were insoluble in common PTMSP solvents such as toluene [32]. When crosslinked PTMSP films were stored in vacuum for approximately 29 days, the permeabilities of N_2 and O_2 were stable, while the permeability of an uncrosslinked film decreased to 70 % of its original value [32]. The improved permeability stability was thought to be caused by the crosslinks restricting chain mobility, which reduced the rate of FFV and permeability

decrease over time. However, the crosslinked samples had initial permeability coefficients far below those of uncrosslinked PTMSP. For example, a PTMSP film containing 2 wt. % bis(azide) was crosslinked at 175°C in vacuum for 3 hours. Its initial O₂ permeability at 23°C was 2,100 barrers, while uncrosslinked PTMSP had an O₂ permeability of 8,000 barrers [32]. The lower initial permeability of the crosslinked film presumably reflects a reduced FFV, which may contribute to the stability in permeability of the crosslinked films over time.

1.4) Organization and Goals of the Thesis

Crosslinking has been suggested as method to increase solvent resistance and physically stability of PTMSP [32-34]. However, these early studies focused only on light gases (*e.g.*, O₂ and N₂), so the effects of crosslinking on higher hydrocarbon transport properties was unknown. Moreover, the initial report by Jia *et al.* [32] described only pure gas permeation properties, and PTMSP exhibits unusual and interesting gas/vapor mixture permeation properties [8-10,17]. Therefore, it was not known what influence crosslinking might have on mixed gas permeation and separation properties. The effect of crosslinking on the solubility and diffusivity properties of PTMSP has not been investigated, and such fundamental studies enhance understanding of the basis for the permeability decrease that accompanies crosslinking.

In this study a fundamental study of the effect of crosslinking on the gas transport and aging behavior of PTMSP was undertaken. Pure and mixed gas permeation studies were undertaken to learn if the enhanced vapor/gas selectivity of pure PTMSP in mixed

gas permeation is retained in crosslinked samples. Gas and vapor sorption studies, as well as physical aging studies, were used to complement the permeability studies. The temperature and pressure were varied to understand what effects these variables have on the pure and mixed gas transport properties of uncrosslinked and crosslinked PTMSP. The effects of fumed silica (FS) nanoparticle addition on the transport properties of uncrosslinked and crosslinked PTMSP were also investigated. Additionally, attempts were made to understand the underlying crosslinking chemistry.

This dissertation contains 9 chapters, including the introductory chapter. In Chapter 2 the background and theory of gas transport in polymer membranes is presented. Chapter 3 gives details of the materials and experimental methods used in this study, while in Chapter 4 the crosslinking reaction mechanism is discussed, and the effects of crosslinking on the solvent resistance of PTMSP, and its free volume characteristics are presented.

In Chapter 5 the effects of crosslinking and FS addition on the pure gas sorption properties of PTMSP are presented, while Chapter 6 presents the effects of crosslinking and FS addition on pure gas permeabilities and diffusivities. In both of these chapters, the effects of temperature and pressure on the pure gas transport properties are presented. The effects of crosslinking and POSS addition on the changes in the pure gas permeabilities and FFV of PTMSP over time are presented in Chapter 7. Chapter 8 presents the effects of crosslinking and FS addition on the mixed gas transport properties of PTMSP. The effects of temperature and feed pressure on the mixed gas transport

properties are also discussed in this chapter. In the final chapter, Chapter 9, the conclusions from this study are presented, along with recommendations for future work.

1.5) References

- [1] R. W. Baker, Future directions of membrane gas separation technology, *Industrial & Engineering Chemistry Research*, 41 (2002) 1393-411.
- [2] J. D. Wilkinson and H. M. Hudson, High ethane recovery without inlet carbon dioxide removal, *Proceedings of the Gas Conditioning Conference*, 32nd (1982) N1-N21.
- [3] C. T. Ratcliffe, A. Diaz, C. Nopasit, and G. Munoz, Application of membranes in CO₂ separation from natural gas: pilot plant tests on offshore platforms, *Proceedings - Laurance Reid Gas Conditioning Conference*, (1999) 117-40.
- [4] B. D. Freeman, and I. Pinnau, in: B. D. Freeman, I. Pinnau (Eds.), *Polymer Membranes for Gas and Vapor Separation: Chemistry and Materials Science*. ACS Symposium Series, 1999, pp. 1-27.
- [5] K. Ghosal and B. D. Freeman, Gas separation using polymer membranes: an overview, *Polymers for Advanced Technologies*, 5 (1994) 673-97.
- [6] J. Schultz and K. V. Peinemann, Membranes for separation of higher hydrocarbons from methane, *Journal of Membrane Science*, 110 (1996) 37-45.
- [7] R. W. Spillman, Economics of gas separation membranes, *Chemical Engineering Progress*, 85 (1989) 41-62.
- [8] I. Pinnau, C. G. Casillas, A. Morisato, and B. D. Freeman, Hydrocarbon/hydrogen mixed gas permeation in poly[1-(trimethylsilyl)-1-propyne] (PTMSP), poly(1-phenyl-1-propyne) (PPP), and PTMSP/PPP blends, *Journal of Polymer Science, Part B: Polymer Physics*, 34 (1996) 2613-21.
- [9] I. Pinnau, C. G. Casillas, A. Morisato, and B. D. Freeman, Long-term permeation properties of poly[1-(trimethylsilyl)-1-propyne] membranes in hydrocarbon-vapor environment, *Journal of Polymer Science, Part B: Polymer Physics*, 35 (1997) 1483-90.
- [10] I. Pinnau and L. G. Toy, Transport of organic vapors through poly[1-(trimethylsilyl)-1-propyne], *Journal of Membrane Science*, 116 (1996) 199-209.

- [11] V. V. Teplyakov, D. Roizard, E. Favre, and V. S. Khotimsky, Investigations on the peculiar permeation properties of volatile organic compounds and permanent gases through PTMSP, *Journal of Membrane Science*, 220 (2003) 165-75.
- [12] T. Masuda, K. Hasegawa, and T. Higashimura, Polymerization of phenylacetylenes. I. Polymerization of phenylacetylene catalyzed by tungsten hexachloride and molybdenum pentachloride, *Macromolecules*, 7 (1974) 728-31.
- [13] K. Nagai, T. Masuda, T. Nakagawa, B. D. Freeman, and I. Pinnau, Poly[1-(trimethylsilyl)-1-propyne] and related polymers: synthesis, properties and functions, *Progress in Polymer Science*, 26 (2001) 721-98.
- [14] T. Masuda, E. Isobe, T. Higashimura, and K. Takada, Poly[1-(trimethylsilyl)-1-propyne]: a new high polymer synthesized with transition-metal catalysts and characterized by extremely high gas permeability, *Journal of the American Chemical Society*, 105 (1983) 7473-4.
- [15] T. C. Merkel, V. Bondar, K. Nagai, and B. D. Freeman, Sorption and transport of hydrocarbon and perfluorocarbon gases in poly[1-(trimethylsilyl)-1-propyne], *Journal of Polymer Science, Part B: Polymer Physics*, 38 (2000) 273-96.
- [16] T. C. Merkel, V. I. Bondar, K. Nagai, B. D. Freeman, and I. Pinnau, Gas sorption, diffusion, and permeation in poly(dimethylsiloxane), *Journal of Polymer Science, Part B: Polymer Physics*, 38 (2000) 415-34.
- [17] T. C. Merkel, R. P. Gupta, B. S. Turk, and B. D. Freeman, Mixed-gas permeation of syngas components in poly(dimethylsiloxane) and poly[1-(trimethylsilyl)-1-propyne] at elevated temperatures, *Journal of Membrane Science*, 191 (2001) 85-94.
- [18] T. C. Merkel, Z. He, I. Pinnau, B. D. Freeman, P. Meakin, and A. J. Hill, Effect of nanoparticles on gas sorption and transport in poly[1-(trimethylsilyl)-1-propyne], *Macromolecules*, 36 (2003) 6844-55.
- [19] I. Pinnau and Z. He, Pure- and mixed-gas permeation properties of polydimethylsiloxane for hydrocarbon/methane and hydrocarbon/hydrogen separation, *Journal of Membrane Science*, 244 (2004) 227-33.
- [20] R. Srinivasan, S. R. Auvil, and P. M. Burban, Elucidating the mechanism(s) of gas transport in poly[1-(trimethylsilyl)-1-propyne] (PTMSP) membranes, *Journal of Membrane Science*, 86 (1994) 67-86.

- [21] R. Ash, R. M. Barrer, and R. T. Lowson, Transport of single gases and of binary gas mixtures in a microporous carbon membrane, *Journal of the Chemical Society, Faraday Transactions 1: Physical Chemistry in Condensed Phases*, 69 (1973) 2166-78.
- [22] R. Ash, R. M. Barrer, and P. Sharma, Sorption and flow of carbon dioxide and some hydrocarbons in a microporous carbon membrane, *Journal of Membrane Science*, 1 (1976) 17-32.
- [23] T. S. Chow, Kinetics of free volume and physical aging in polymer glasses, *Macromolecules*, 17 (1984) 2336-40.
- [24] T. Masuda, E. Isobe, and T. Higashimura, Polymerization of 1-(trimethylsilyl)-1-propyne by halides of niobium(V) and tantalum(V) and polymer properties, *Macromolecules*, 18 (1985) 841-5.
- [25] T. Nakagawa, S. Fujisaki, H. Nakano, and A. Higuchi, Physical modification of poly[1-(trimethylsilyl)-1-propyne] membranes for gas separation, *Journal of Membrane Science*, 94 (1994) 183-93.
- [26] G. L. Baker, C. F. Klausner, A. S. Gozdz, J. A. Shelburne, III, and T. N. Bowmer, Brominated poly[1-(trimethylsilyl)-1-propyne]. *Lithography and photochemistry, Advances in Chemistry Series*, 224 (1990) 663-78.
- [27] K. Nagai, A. Higuchi, and T. Nakagawa, Bromination and gas permeability of poly[1-(trimethylsilyl)-1-propyne] membrane, *Journal of Applied Polymer Science*, 54 (1994) 1207-17.
- [28] K. Nagai, A. Higuchi, and T. Nakagawa, Gas permeation and sorption in brominated poly[1-(trimethylsilyl)-1-propyne] membrane, *Journal of Applied Polymer Science*, 54 (1994) 1353-61.
- [29] S. Matteucci, V. A. Kusuma, D. Sanders, S. Swinnea, and B. D. Freeman, Gas transport in TiO₂ nanoparticle-filled poly[1-(trimethylsilyl)-1-propyne], *Journal of Membrane Science*, 307 (2008) 196-217.
- [30] W. A. Reinerth, Sr., J. J. Schwab, J. D. Lichtenhan, Q. Liu, D. Hilton, B. D. Freeman, L. Toy, and H. J. Lee, POSSTM/polymer blends for gas separation, *Abstracts of Papers, 222nd ACS National Meeting, Chicago, IL, United States, August 26-30, 2001*, (2001) MTL-020.
- [31] I. Pinnau and Z. He, Process of separating a fluid mixture by a polymer membrane containing filler. US Patent, 6,326,684 (2001).

- [32] J. Jia and G. L. Baker, Crosslinking of poly[1-(trimethylsilyl)-1-propyne] membranes using bis(aryl azides), *Journal of Polymer Science, Part B: Polymer Physics*, 36 (1998) 959-68.
- [33] C. J. Ruud, J. Jia, and G. L. Baker, Synthesis and characterization of poly[(1-trimethylsilyl-1-propyne)-co-(1-(4-azidobutyldimethylsilyl)-1-propyne)] copolymers, *Macromolecules*, 33 (2000) 8184-91.
- [34] J. Jia, Gas separation and pervaporation of chemically modified poly[1-(trimethylsilyl)-1-propyne] membranes, Ph.D. Dissertation, Michigan State University, 1999.
- [35] T. C. Merkel, L. G. Toy, A. L. Andrady, H. Gracz, and E. O. Stejskal, Investigation of enhanced free volume in nanosilica-filled poly[1-(trimethylsilyl)-1-propyne] by ^{129}Xe NMR spectroscopy, *Macromolecules*, 36 (2003) 353-8.

2) Background

2.1) Fundamentals of Gas Permeation in Polymers Membranes

The principle of using membranes for separation relies on the ability to control the permeation rates of different components in a mixture. One of the first reported examples was in 1866 when Graham enriched air from 21 % to 41 % O₂ [1]. Graham described the gas transport mechanism across polymers as a three step process, where penetrants dissolve into the high pressure side of the membrane, then diffuse through the material, and finally desorb from the low pressure side. Membrane materials used today are understood to obey this same solution-diffusion mechanism [2], and the steady state permeability of gas A , P_A , is defined as follows [3]:

$$P_A = \frac{N_A \cdot l}{p_{2,A} - p_{1,A}} \quad (2.1)$$

where N_A is the steady state gas flux through the film ($\text{cm}^3(\text{STP})/\text{cm}^2\text{s}$), l is the film thickness (cm), and $p_{2,A}$ and $p_{1,A}$ are the upstream and downstream partial pressures of A (cmHg), respectively. Permeability coefficients are often expressed in units of barrer,

where $1 \text{ barrer} = 1 \times 10^{-10} \frac{\text{cm}^3(\text{STP}) \cdot \text{cm}}{\text{cm}^2 \cdot \text{s} \cdot \text{cmHg}}$. When gas behaviour is non-ideal the upstream

and downstream partial pressures of A , $p_{2,A}$ and $p_{1,A}$, are replaced by $f_{2,A}$ and $f_{1,A}$, the upstream and downstream fugacities of A , respectively [4].

The fugacity of gas A is calculated as follows [5]:

$$f_A = \phi_A x_A p \quad (2.2)$$

where ϕ_A is the fugacity coefficient of A , x_A is the mole fraction of A , and p is the total pressure (atm). The information used to calculate fugacity coefficients is provided elsewhere [6]. Fugacity is used for all gas transport calculations instead of pressure because significant non-ideal gas behavior is observed, particularly at higher feed pressures.

For dense polymeric membranes, the solution-diffusion mechanism [2] describes the transport processes of gas molecules in polymers. If the diffusion process is Fickian, the permeability coefficient is [7]:

$$P_A = \frac{C_{2A} - C_{1A}}{f_{2A} - f_{1A}} \times D_A \quad (2.3)$$

where C_{2A} and C_{1A} are the upstream and downstream concentrations of A in the polymer ($\text{cm}^3(\text{STP})/\text{cm}^3$ polymer), and D_A is the concentration averaged effective diffusion coefficient (cm^2/s) of gas A . If the downstream (*i.e.*, permeate) fugacity is significantly less than the upstream (*i.e.*, feed) fugacity, so that $C_{2A} \gg C_{1A}$ and $f_{2A} \gg f_{1A}$, then the permeability of gas A can be expressed as [7]:

$$P_A = D_A \times S_A \quad (2.4)$$

where $S_A = C_{2A}/f_{2A}$ (cm^3 (STP)/ cm^3 polymer cmHg) is the ratio of the concentration of gas A sorbed in the polymer at the upstream face of the film, C_{2A} , (cm^3 (STP)/ cm^3 polymer) to the upstream fugacity of A , f_{2A} (cmHg). S_A is also called the apparent sorption (or solubility) coefficient of penetrant A in the polymer.

The ideal permeability selectivity of a membrane for gas A over gas B is the ratio of gas permeability coefficients. Generally the most permeable gas is in the numerator of the following expression [7]:

$$\alpha_{A/B} = \frac{P_A}{P_B} = \left[\frac{D_A}{D_B} \right] \times \left[\frac{S_A}{S_B} \right] \quad (2.5)$$

where D_A/D_B is the diffusivity selectivity, which is the ratio of the diffusion coefficients of gases A and B . Larger gas molecules normally have lesser diffusion coefficient than smaller gas molecules [7]. The ratio of the solubility coefficients of gases A and B , S_A/S_B , is the solubility selectivity. The term “reverse-selectivity” refers to the polymer being more permeable to larger condensable molecules, such as $n\text{-C}_4\text{H}_{10}$, than to smaller and less condensable permanent gases such as N_2 and CH_4 . This phenomenon can occur when D_A/D_B , the diffusivity selectivity, approaches unity and the solubility selectivity, S_A/S_B , is far greater than 1 [7].

2.2) Dual-Mode Gas Transport in Glassy Polymers

Gas sorption isotherms in glassy polymers typically exhibit nonlinear behavior, and a number of models have been proposed to account for this deviation from Henry’s law [3,7]. Sorption is often described by the dual-mode sorption model, where sorbed penetrants are viewed as being partitioned between the dense equilibrium structure of the polymer (Henry’s law region), and the nonequilibrium excess free volume of the polymer (Langmuir region). The dual-mode sorption model is given by [3,7]:

$$C = C_D + C_H = k_D f + \frac{C'_H b f}{1 + b f} \quad (2.6)$$

where C_D and C_H are the concentrations of penetrant sorbed in the Henry's law and Langmuir regions, respectively ($\text{cm}^3(\text{STP})/\text{cm}^3$ polymer); k_D is the Henry's Law parameter ($\text{cm}^3(\text{STP})/\text{cm}^3$ polymer atm^{-1}), C'_H is the Langmuir sorption capacity ($\text{cm}^3(\text{STP})/\text{cm}^3$ polymer), and b is the Langmuir affinity constant (atm^{-1}).

Solubility coefficients can be calculated from the dual-mode sorption model as follows [8,9]:

$$S = \frac{C}{f} = k_D + \frac{C'_H b}{1 + b f} \quad (2.7)$$

where C is the penetrant concentration sorbed in the polymer at fugacity f . Infinite dilution solubility is calculated by setting $f = 0$ on the right hand side of Equation 2.7.

Within the context of the dual-mode model, permeability is given by [3]:

$$P = k_D \bar{D}_D + \frac{C'_H b \bar{D}_H}{(1 + b f_1)(1 + b f_2)} \quad (2.8)$$

where \bar{D}_D and \bar{D}_H are the effective diffusion coefficients of penetrant molecules in the Henry's law and Langmuir regions, respectively.

The concentration-averaged effective diffusion coefficients can also be calculated from the dual-mode transport model [3]:

$$D = \bar{D}_D \left[\frac{k_D + \frac{b C'_H \bar{D}_H / \bar{D}_D}{(1 + b f_1)(1 + b f_2)}}{k_D + \frac{b C'_H}{(1 + b f_1)(1 + b f_2)}} \right] \quad (2.9)$$

2.3) Free Volume Effects on Gas Transport and Aging

The fractional free volume (FFV) of a polymer is typically calculated using a group contribution method [10-12]. The van der Waals volume of each molecular group in a polymer is summed and multiplied by 1.3 to find the total occupied volume of the crosslinked polymer [10-12]. The FFV is related to the occupied volume and the polymer specific volume as follows [11]:

$$FFV = \frac{V - V_o}{V} \quad (2.10)$$

where V is the specific volume of the polymer film (cm^3/g), and V_o is the occupied volume of the polymer (cm^3/g).

Diffusion of small molecules in dense polymeric films is also understood to be a function of polymer free volume, and the following model is often used to describe this dependence [13]:

$$D_A = C \exp\left(-\frac{\gamma}{\langle V_f \rangle} V_A^*\right) \quad (2.11)$$

where C is a pre-exponential factor, γ is a numerical factor introduced to account for overlap of free volume, V_A^* is the minimum free volume element size needed to accommodate a gas molecule, and $\langle V_f \rangle$ is the average free volume in the polymer. In this model, the diffusion coefficient is a function of penetrant size and polymer average free volume. As average free volume increases, the effect of penetrant size on diffusivity diminishes, so the polymer becomes less size-sieving. This trend is especially true for

high free volume PTMSP, and it is an important consideration for understanding the transport properties of reverse-selective separation materials [7]. $\langle V_f \rangle$ is usually replaced by FFV in gas diffusion studies. The solubility is typically a weak function of free volume, as the condensability of a penetrant is the primary determinate of its solubility [7], therefore, permeability often exhibits a similar dependence on free volume as diffusivity [13]:

$$P_A = S_A C \exp\left(-\frac{\gamma}{\langle V_f \rangle} V_A^*\right) \quad (2.12)$$

Volume relaxation, or physical aging of polymers, is often described by the following equation [12]:

$$\frac{dV}{dt} = \frac{V - V_{eq}}{\tau} \quad (2.13)$$

where V is specific volume (*i.e.*, 1/density), t is time, V_{eq} is the hypothetical equilibrium specific volume, and τ is a time constant. As specific volume decreases (*i.e.*, as density increases), τ increases, and molecular motion is slowed [14]. The density of polymer films can be tracked using variable angle spectroscopic ellipsometry, which is a valuable tool for studying the physical aging in thin polymer films [15,16]. This sensitive and precise technique measures changes in surface and film properties over time.

2.4) Temperature Effects on Gas Transport

The influence of temperature on gas permeability, solubility, and diffusivity in polymers is typically described by the following Arrhenius-van't Hoff equations [3]:

$$P = P_0 \exp\left[\frac{-E_P}{RT}\right] \quad (2.14)$$

$$S = S_0 \exp\left[\frac{-\Delta H_s}{RT}\right] \quad (2.15)$$

$$D = D_0 \exp\left[\frac{-E_D}{RT}\right] \quad (2.16)$$

where E_P , and E_D are the activation energies of permeation and diffusivity, respectively; ΔH_s is the enthalpy of sorption, and $E_P = E_D + \Delta H_s$. E_D is always positive, while the sign of E_P depends on the magnitudes and signs of E_D and ΔH_s [7]. This framework was developed for polymers in which the gas sorption and transport properties do not change markedly with pressure or, equivalently, gas concentration in the polymer. If this restriction is not obeyed, then this framework must be applied to the experimental data with caution [17]. High free volume polymers such as PTMSP that exhibit “reverse-selectivity” are weakly size-sieving, so the energy barriers to diffusion are low (*i.e.* low E_D values) [7]. As a result, often $E_D < |\Delta H_s|$, which leads to negative E_P values. Consequently, the permeability of PTMSP often increases as temperature decreases [18-20].

2.5) References

- [1] T. Graham, On the absorption and dialytic separation of gases by colloid septa Part I.-Action of a septum of caoutchouc, Journal of Membrane Science, 100 (1995) 27-31.
- [2] J. G. Wijmans and R. W. Baker, The solution-diffusion model: a review, Journal of Membrane Science, 107 (1995) 1-21.

- [3] K. Ghosal and B. D. Freeman, Gas separation using polymer membranes: an overview, *Polymers for Advanced Technologies*, 5 (1994) 673-97.
- [4] R. D. Raharjo, B. D. Freeman, and E. S. Sanders, Pure and mixed gas CH₄ and *n*-C₄H₁₀ sorption and dilation in poly(dimethylsiloxane), *Journal of Membrane Science*, 292 (2007) 45-61.
- [5] J. M. Smith, H. C. Van Ness, and M. M. Abbot, *Chemical Engineering Thermodynamics* 5th ed., McGraw Hill, New York, 1995.
- [6] H. Lin and B. D. Freeman, Gas and vapor solubility in cross-linked poly(ethylene glycol diacrylate), *Macromolecules*, 38 (2005) 8394-407.
- [7] S. Matteucci, Y. Yampolskii, B. D. Freeman, and I. Pinnau, in: Y. Yampolskii, B. D. Freeman, I. Pinnau (Eds.), *Material Science of Membranes for Gas and Vapor Separation*, John Wiley & Sons, New York, 2006, pp. 1-47.
- [8] J. H. Petropoulos, in: D. R. Paul, Y. P. Yampol'skii (Eds.), *Polymeric Gas Separation Membranes*, CRC Press, Boca Raton, FL, 1994, pp. 17-81.
- [9] T. C. Merkel, V. Bondar, K. Nagai, and B. D. Freeman, Sorption and transport of hydrocarbon and perfluorocarbon gases in poly[1-(trimethylsilyl)-1-propyne], *Journal of Polymer Science, Part B: Polymer Physics*, 38 (2000) 273-96.
- [10] A. Bondi, van der Waals volumes and radii, *Journal of Physical Chemistry*, 68 (1964) 441-51.
- [11] A. Bondi, *Physical Properties of Molecular Crystals, Liquids and Glasses*, Wiley, New York, 1968.
- [12] D. W. Van Krevelen, *Properties of Polymers*, 3rd ed., Elsevier, Amsterdam, 2003.
- [13] M. H. Cohen and D. Turnbull, Molecular transport in liquids and glasses, *Journal of Chemical Physics*, 31 (1959) 1164-9.
- [14] M. S. McCaig, D. R. Paul, and J. W. Barlow, Effect of film thickness on the changes in gas permeability of a glassy polyarylate due to physical aging part II. Mathematical model, *Polymer*, 41 (1999) 639-48.
- [15] Y. Huang and D. R. Paul, Physical aging of thin glassy polymer films monitored by optical properties, *Macromolecules*, 39 (2006) 1554-9.

- [16] J. H. Kim, W. J. Koros, and D. R. Paul, Physical aging of thin 6FDA-based polyimide membranes containing carboxyl acid groups. Part II. Optical properties, *Polymer*, 47 (2006) 3104-11.
- [17] R. S. Prabhakar, R. Raharjo, L. G. Toy, H. Lin, and B. D. Freeman, Self-consistent model of concentration and temperature dependence of permeability in rubbery polymers, *Industrial & Engineering Chemistry Research*, 44 (2005) 1547-56.
- [18] S. V. Dixon-Garrett, K. Nagai, and B. D. Freeman, Sorption, diffusion, and permeation of ethylbenzene in poly[1-(trimethylsilyl)-1-propyne], *Journal of Polymer Science, Part B: Polymer Physics*, 38 (2000) 1078-89.
- [19] T. Masuda, Y. Iguchi, B. Z. Tang, and T. Higashimura, Diffusion and solution of gases in substituted polyacetylene membranes, *Polymer*, 29 (1988) 2041-9.
- [20] R. Srinivasan, S. R. Auvil, and P. M. Burban, Elucidating the mechanism(s) of gas transport in poly[1-(trimethylsilyl)-1-propyne] (PTMSP) membranes, *Journal of Membrane Science*, 86 (1994) 67-86.

3) Experimental Methods

3.1) Materials

PTMSP was kindly supplied by Air Products and Chemicals, Inc, and its synthesis have been described in the introduction. The following bis(azide) crosslinkers were initially chosen to crosslink PTMSP: 3,3'-diazidodiphenylsulfone, 2,6-di(p-azidobenzyl)-4-methylcyclohexanone, and 2,6-bis(4-azidobenzylidene)cyclohexanone. All were supplied by Sigma Aldrich Chemicals. These bis(azide)s were chosen because they are chemically safe at the conditions of film formation and crosslinking, and had been shown to crosslink polymeric materials effectively [1-5].

The most effective crosslinker for PTMSP was 3,3'-diazidodiphenylsulfone. Its chemical structure is shown in *Figure 3.1*.

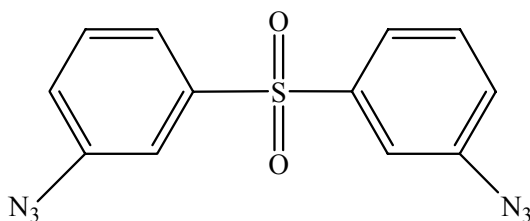


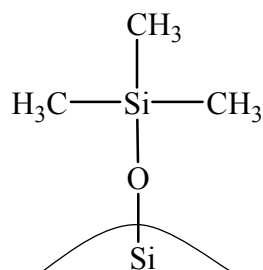
Figure 3.1 Chemical structure of bis(azide) crosslinker 3,3'-diazidodiphenylsulfone

This crosslinker was chosen because films crosslinked with 3,3'-diazidodiphenylsulfone were less soluble in toluene (a good solvent for PTMSP) than films crosslinked with equivalent amounts of other the two bis(azide)s considered. A possible reason for this behavior is these two crosslinkers contain 30 wt % water (to allow safe handling of

them); since PTMSP has a low affinity for water, the water content is thought to make the bis(azide)s less compatible with PTMSP [6].

Nonporous, hydrophobic fumed silica nanoparticles (FS), (Cab-O-Sil TS530, a grade of FS available from Cabot Corp., Tuscola, IL) were added to PTMSP to form nanocomposite films. TS-530 FS nanoparticles have a characteristic dimension of 13 nm, and they have been chemically treated with hexamethyldisilazane to replace hydrophilic hydroxyl surface groups with hydrophobic trimethylsilyl surface groups [7]. Non-porous POSS particles (MS0865, an octatrimethylsiloxy POSS available from Hybrid Plastics, Hattiesburg, MS) were added to PTMSP to form nanocomposite films. The POSS nanoparticles have a characteristic dimension of approximately 1.2 nm [8]. The structure of the FS and POSS nanoparticles are shown in *Figure 3.2*.

a)



b)

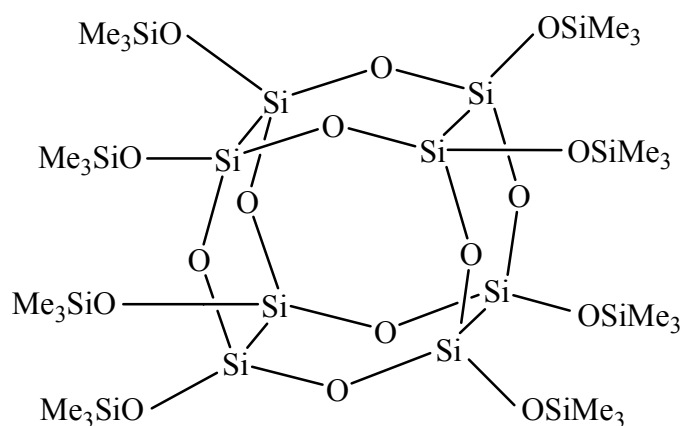


Figure 3.2 Chemical structure of a) TS 530 FS and b) POSS MS0865

Ultra high purity (99.99 %) cylinders of N_2 and O_2 , and chemical purity (99 %) cylinders of CH_4 , C_2H_6 , C_3H_8 , and $n\text{-C}_4\text{H}_{10}$ were received from Air Gas Southwest Inc. (Corpus Christi, TX). Mixtures of CH_4 and $n\text{-C}_4\text{H}_{10}$ were received from Air Liquide America Corporation (Houston, TX). All solvents used in the experiments had a purity of at least 99.8 %. All materials, chemicals, and gases were used as received unless otherwise indicated.

3.2) Formation of Polymer Films

Dense films of PTMSP and bis(azide) crosslinker were cast from a toluene solution containing 1.5 wt % polymer. To form nanocomposite films the FS or POSS nanoparticles were added to these solutions. The reported wt % of crosslinker or nanoparticles in a film, w_A , is given by:

$$w_A = \frac{m_A}{m_A + m_p} \quad (3.1)$$

where m_A is the crosslinker or nanoparticle mass, and m_p is the polymer mass. This calculation is based on the films before they are crosslinked. The wt % of crosslinker in the films decreases after crosslinking because each bis(azide) loses 2 N₂ molecules. The toluene solutions were stirred for 2 days using a magnetic stir bar, and the cast films were dried at ambient conditions for approximately 1 week until all toluene had evaporated.

All films in this study were thermally treated in a vacuum oven at 180°C for 90 minutes to initiate the crosslinking reaction. For films containing no crosslinker, the thermal treatment is still performed to normalize the thermal histories of all films. The crosslinking is performed in vacuum so that no oxygen is present, because nitrene molecules readily oxidize to nitroso compounds, which reduces the effectiveness of the crosslinking reaction [5]. At lower temperatures, the reaction did not proceed at a reasonable rate. The reaction time was set to 90 minutes because it was sufficient to cause the peak associated with the azide group in the FT-IR spectrum at 2120 cm⁻¹ to disappear, indicating that the azides had reacted to form nitrenes [9]. It is important that no contaminants (*e.g.*, vacuum pump oil vapors) contact the film during casting and

crosslinking [10], because these materials can significantly alter transport properties [11]. To minimize contamination by vacuum pump oil vapors during the crosslinking process, two liquid N₂ traps were placed on the line between the vacuum pump and the vacuum oven.

PTMSP transport properties, FFV, and positron annihilation lifetime spectroscopy parameters are strongly influenced by hysteresis effects [11-15]. To insure preparation of PTMSP samples with reproducible properties, all films not containing POSS particles were soaked in methanol (MeOH), which is a swelling non-solvent for PTMSP, for 24 hours following the thermal annealing required for crosslinking. The PTMSP/POSS films were not soaked in MeOH because the POSS nanoparticles diffused out of the nanocomposite and into the MeOH. The length of MeOH immersion insures that MeOH reaches equilibrium with the PTMSP films [12]. This preparation step helps minimize sample to sample variability due to slight differences in film histories [12]. After MeOH immersion, the films were dried for 72 hours at ambient conditions. The length of drying is long enough to insure that all MeOH had evaporated [12]. Afterwards, film thickness and film density were measured, and transport property testing was commenced. Films used in the pure gas permeation and sorption experiments were approximately 100 μm thick, while films used in mixed gas permeation experiments were approximately 500 μm thick.

3.3) Polymer Density Measurement

Film densities were determined using the buoyancy method. The weight of PTMSP films in air and in a $\text{Ca}(\text{NO}_3)_2$ solution of known density was measured, and the following expression was used to calculate the experimental film density [16].

$$\rho_{Film} = \frac{M_{Air}}{M_{Air} - M_{Sol}} \times \rho_{Sol} \quad (3.2)$$

where ρ_{Film} is the film density (g/cm^3), M_{Air} is the film mass in air (g), M_{Sol} is the film mass in solution (g), and ρ_{Sol} is the solution density (g/cm^3). The PTMSP films used in the density measurements are from the same films used for permeation and sorption measurements, and they have undergone the same crosslinking and MeOH conditioning treatments described earlier for films used in the transport studies. The film density is used to calculate the specific volume of the film, where $V = 1/\rho_{film}$, and the FFV using equation 2.10. The film density is also used to calculate the film volume of the polymer samples in the sorption experiments.

The ideal additive density, ρ_{Add} , of a nanocomposite film containing uncrosslinked or crosslinked PTMSP and FS or POSS nanoparticles is defined by [17]:

$$\rho_{Add} = \frac{W_{PTMSP} + W_N}{W_{PTMSP} / \rho_{PTMSP} + W_N / \rho_N} \quad (3.3)$$

where W_{PTMSP} is the weight fraction of uncrosslinked or crosslinked PTMSP in the nanocomposite film, W_N is the weight fraction of nanoparticles in the film, and ρ_{PTMSP} and ρ_N are the densities of the neat polymer and nanoparticles, respectively. This

equation assumes ideal mixing. Deviations from this idealized situation may be captured by determining the void volume fraction, ϕ_v , as follows [17]:

$$\phi_v = 1 - \frac{\rho_{Film}}{\rho_{Add}} \quad (3.4)$$

Positive values of ϕ_v indicate the presence of additional volume in the film (*i.e.*, voids), above and beyond that expected based on the polymer and particle densities and concentrations, and negative values of ϕ_v indicate more compact mixing of the polymer and particles than anticipated based on the pure component properties.

3.4) Ellipsometry Measurements

Variable angle spectroscopic ellipsometry, a sensitive and precise technique for measuring surface and film properties, is a valuable tool for studying physical aging in thin polymer films [18,19]. Ellipsometry measures the change in the polarization state of light reflected from a sample. Sample thickness and optical properties (*e.g.*, refractive index) are obtained by fitting the experimental data to a model. The Lorentz-Lorenz equation provides a fundamental relationship between density and refractive index, \bar{n} [20]:

$$\frac{\bar{n}^2 - 1}{\bar{n}^2 + 2} = \frac{\rho N_{av} \alpha}{3 M_0 \epsilon_0} \quad (3.5)$$

where ρ is the polymer density, N_{av} is Avogadro's number, α is the average polarizability of the polymer repeat unit, M_0 is the polymer repeat unit molecular weight, and ϵ_0 is the

permittivity of free space. Only refractive index and density are expected to change with physical aging, simplifying the Lorentz-Lorenz equation to [20]:

$$L = \frac{\bar{n}^2 - 1}{\bar{n}^2 + 2} = \rho C \quad (3.6)$$

where L is defined as the Lorentz-Lorenz parameter, and C is the specific refraction, which is presumed to be a constant for a given substance. The Lorentz-Lorenz equation has been tested with remarkable success for many systems including gases, liquids, solids and polymers [20-25].

A variable angle spectroscopic ellipsometer manufactured by J.A. Woollam Company, Model 2000D, was used to determine thickness and refractive index in this study. Measurements were taken at wavelengths from 400 to 1000 nm at three angles of incidence: 65°, 70°, and 75°. The program WVASE32 was used to fit the data to a model of the polymer film and substrate system. The polymer refractive index was calculated using the Cauchy equation [26]:

$$\bar{n} = A + B / \lambda^2 + C / \lambda^4 \quad (3.7)$$

where A , B , and C are constants, and λ is the light wavelength. All refractive index values are reported at the sodium D line. Because PTMSP is uv light sensitive [27-29], the deuterium lamp in the ellipsometer, which supplies short wavelength light, was switched off during measurements. Tests were performed to ensure film properties did not change during the course of the ellipsometry experiments due to light exposure; these results are not included for brevity. The ellipsometer was in an environmental chamber where the relative humidity was controlled to 10 ± 0.3 % with dry nitrogen, as measured by a

Tracable Hygrometer from Fischer Scientific. The sample temperature was controlled to 25 ± 0.1 °C using a Melcor thermoelectric heater/cooler and temperature controller.

3.5) Pure Gas Sorption Measurement

Pure gas sorption isotherms were determined in a high pressure barometric sorption apparatus [30]. The sorption apparatus consists of a charge cell and a sample cell, and a ball valve separates the two cells. The volumes of each cell are known, and a known volume of polymer film was placed in the sample cell. The film volume was calculated by measuring the mass and density of the film. The charge and sample cells were exposed to vacuum overnight to degas the polymer film sample. The valve between the charge and sample cells was then closed, penetrant gas was introduced into the charge cell, and the pressure was measured once equilibrium is reached. The valve between the charge and sample cells was opened and then closed, thereby introducing penetrant gas into the sample cell. When the system had equilibrated, the pressure was measured in both cells. This process was repeated, and penetrant uptake was measured as a function of pressure. The time required to reach equilibrium in the sorption cell was, at most, a few hours. After measuring each sorption isotherm, the polymer film was degassed overnight under vacuum before the next isotherm was measured.

Sorption isotherms for N₂, O₂, CH₄, C₂H₆, C₃H₈, and *n*-C₄H₁₀ were measured at 35°C, 10°C, 0°C, and -20°C over a pressure range of 0 to 20 atm. At each temperature the sorption isotherms were measured in the following order; N₂, O₂, CH₄, C₂H₆, C₃H₈, *n*-C₄H₁₀, and N₂. The same film was used to measure all the sorption isotherms at each

temperature, and the N₂ sorption isotherm was measured after *n*-C₄H₁₀ sorption to test for conditioning effects of the previously sorbed gases. At each temperature a new film was placed in the sample cell, which helps eliminate any hysteresis effects associated with the previous measurements at a different temperature. The sorption apparatus was kept at constant temperature in a water bath. To allow sorption isotherms to be measured at 0°C and -20°C, MeOH was added to the water to lower the freezing point of the bath liquid. The error in the reported sorption data points is approximately $\pm 10\%$, which accounts for the measurement error and sample to sample variability.

3.6) Pure Gas Permeability Measurement

Pure gas permeabilities were measured in a constant pressure, variable volume permeation cell [31]. At steady state, the permeability of gas *A* in a film is calculated according to [32]:

$$P_A = \frac{1}{A} \times \frac{V}{t} \times \frac{l}{f_2 - f_1} \times \frac{273.15K}{T} \times \frac{p_a}{76} \times 10^{10} \quad (3.8)$$

where P_A is the permeability coefficient (barrer), A is the film area (cm²), V is the volume of permeating gas (cm³) collected during time t (s), l is film thickness (cm), f_2 is gas fugacity of *A* on the upstream (*i.e.*, high pressure) side of the film (cmHg), f_1 is the gas fugacity on the downstream (*i.e.*, low pressure) side of the film (cmHg), T is the measurement temperature (K), and p_a is atmospheric pressure (cmHg). The films used in the pure gas permeation experiments had an area of 13.8 cm², and a bubble flowmeter was used to measure the gas flow rates. The gas permeabilities were measured in the

following order: N₂, O₂, CH₄, C₂H₆, C₃H₈, and *n*-C₄H₁₀. To check for conditioning effects, N₂ permeability was measured before and after each gas. The permeation measurements were conducted at 35°C, 10°C, 0°C, and -20°C over a feed pressure range from 1.5 atm to 18 atm. The downstream pressure in all cases was 1 atm. The permeability of each gas was measured at 5 pressures as the film was pressurized to its maximum value, and at 3 – 4 pressures as the film was depressurized to atmospheric pressure. Permeability was measured as the film was depressurized to characterize any conditioning effects of the permeating gas. At each temperature, a new film was loaded into the permeation cell, which helps eliminate any hysteresis effects of the previous permeation measurements. The N₂ permeability was measured at 35°C, and 4.4 atm to confirm that each film had the same initial transport properties. The error in the reported permeability coefficients is approximately $\pm 10\%$, which accounts for the measurement error and sample to sample variability.

3.7) Mixed Gas Permeability Measurement

Mixed gas permeabilities were measured in a constant pressure, variable volume system connected to a gas chromatograph that was equipped with a thermal conductivity detector (TCD) and a flame ionization detector (FID) [33]. The permeate stream was swept from the low-pressure side of the film by Helium. The permeate concentration of gas *A* in the sweep, x_{IA} , and the sweep gas flow rate, S (cm³/s) were measured, and the mixed gas permeability of gas *A* was calculated as follows [33]:

$$P_A = \frac{x_{1A} Sl}{x_c^P A(f_{2,A} - f_{1,A})} \times \frac{273.15K}{T} \times \frac{p_a}{76} \times 10^{10} \quad (3.9)$$

where, x_c^P is the mole fraction of sweep gas in the permeate stream, and $f_{2,A}$ and $f_{1,A}$ are the feed and permeate fugacities of gas A . The ratio of permeate to feed flow rate (*i.e.*, the stage cut), was always less than 1 %, which insures the residue and feed compositions remain essentially equal [34]. The area of films used in the mixed gas experiments was $0.31 \pm 0.01 \text{ cm}^2$, and the film thickness was $500 \pm 40 \text{ }\mu\text{m}$. In mixed gas permeation experiments, the film area was less, and film thickness was greater, than that of the films used for pure gas permeation experiments. Decreasing film area, and increasing film thickness reduced the amount of gas permeating across the film, therefore decreasing the flow rate of residue gas required to maintain the stage cut below 1 %, which minimized the consumption of feed gas.

The pure gas CH_4 permeability was measured at 35°C and 4.4 atm pressure at the beginning of each mixed gas experiment to confirm that the each PTMSP film being tested had the same initial transport properties as their like films. The temperature of the cell was then adjusted to the required experimental temperature, and the gas mixture was introduced to the feed side of the film at 4.4 atm. For all experiments in this study, the mixed gas feed composition was 98 mol % CH_4 , and 2 mol % $n\text{-C}_4\text{H}_{10}$. The mixed gas permeabilities were measured at 5 pressures as the feed (or upstream) pressure was increased to its maximum value, and at 4 pressures as the film was depressurized to atmospheric pressure. Permeability was measured as the film was depressurized to understand the conditioning effects of the mixed gas feed. At each temperature

considered, a new film was loaded into the mixed gas permeation cell, which minimized the hysteresis effects of previous permeability measurements.

For all PTMSP films and at all temperatures considered, pure gas CH₄ permeabilities measured in the mixed gas permeation cell were the same as those measured in the pure gas permeation cell. Thus, the pure gas CH₄ permeabilities can be compared to the mixed gas CH₄ permeabilities, thereby permitting meaningful comparisons to be made between the pure and mixed gas transport properties. The thicknesses of the films in the pure gas permeation experiments (~100 μm) and mixed gas permeation experiments (~500 μm) are different, and it has been reported in the literature that film thickness can affect the permeability of PTMSP [14,35]. However no thickness dependence of the pure and mixed gas permeabilities was observed for films in this study. This result could be caused by the film thicknesses not being as relatively dissimilar in this study as they were in other studies where film thickness affected the PTMSP permeabilities [14,35].

3.8) PTMSP Aging Studies

Films used to study the change of pure gas PTMSP permeability over time were kept in storage cell blanketed with N₂ that had been filtered through a PTMSP film to sorb any organic impurities. The storage cell was filled with N₂ to prevent exposure to contaminants from the ambient air, and it was opaque to prevent sample degradation due to ultraviolet light exposure [27,36-38]. Films were only removed from the storage cell in

order to measure their permeabilities, and once the permeability measurements were completed the films were returned into the storage cell.

The permeabilities reported in the aging studies were measured in the pure gas permeation cell, and the gases were tested in the following order: N₂, O₂, and CH₄. N₂ permeability was measured before and after each gas to check for any conditioning effects that the previous permeating gas may have had on the PTMSP films. The permeation measurements were performed at 35°C and at an upstream pressure of 4.4 atm. The downstream pressure in all cases was atmospheric.

The thin films used in the ellipsometry study were stored at 35°C in an opaque cell in dry ambient air. Oxidation of the thin films due to exposure to air should be insignificant because oxidation of PTMSP is not significant at the temperatures and times considered [39,40]. The permeability of PTMSP films used in the ellipsometry studies was not measured because of difficulty in creating defect-free thin films. Ellipsometry measures film properties over an area of several square millimeters, and the measurements are not affected by defects in the films, which would effectively compromise films for gas transport studies.

3.9) Positron Annihilation Lifetime Spectroscopy

The PALS experiment uses *ortho*-positronium (*o*-Ps) to determine the size and number of free volume elements in the polymer. Prior to annihilation the *o*-Ps will localize in low density regions of a sample (*i.e.*, free volume elements). As the free volume element gets larger the *o*-Ps lifetime increases, hence *o*-Ps lifetime reflects the

size of the free volume element. The number of positrons annihilating as *o*-Ps, as determined by the intensity parameter, gives information on the number of pores. PALS measurements were performed using an automated EG&G Ortec fast-fast coincidence system with plastic scintillators and a resolution of 260 ps (^{60}Co source with the energy windows set to ^{22}Na events). Polymer films were stacked (≥ 1 mm thick) on either side of a 30 μCi $^{22}\text{NaCl}$ foil (2.54 μm Ti) source, and wrapped in aluminum foil (which serves to ground the samples and has no influence on the measured *o*-Ps lifetimes). At least five spectra of 30,000 peak counts were collected for each sample in a dry N_2 atmosphere, and each spectrum took approximately 2.5 hours to collect. Data analysis was performed using LT9. The spectra were best fitted with four components with the shortest lifetime fixed to 125ps, characteristic of para-positronium (*p*-Ps) self annihilation [34]. Only the ortho-positronium (*o*-Ps) components with the longest measured lifetimes, which are the third (τ_3) and fourth (τ_4), and their intensities I_3 and I_4 , were considered further since they are ascribed to annihilations in free volume cavities of the polymer matrix [34]. PALS analysis of POSS MS0865 nanoparticles was also performed, in a dry nitrogen atmosphere, where the nanoparticles were packed on either side of the sources.

3.10) References

- [1] M. Pinteala, V. Harabagiu, B. C. Simionescu, P. Guegan, and H. Cheradame, Ionically conducting networks derived from PEO containing aziridine groups, *Polymer International*, 48 (1999) 1147-54.
- [2] V. M. Treushnikov, T. V. Telepneva, A. V. Oleinik, E. L. Sorin, V. V. Korshak, E. S. Krongauz, and N. M. Belomoina, Photochemical crosslinking of poly(phenylquinoxalines) with aromatic azides, *Vysokomolekulyarnye Soedineniya, Seriya A*, 28 (1986) 2129-34.

- [3] M. Yan, S. X. Cai, M. N. Wybourne, and J. F. W. Keana, Evaluation of bis(perfluorophenyl azide)s as cross-linkers for a soluble polyimide, *Journal of Materials Chemistry*, 6 (1996) 1249-52.
- [4] N. Yasuda, S. Yamamoto, H. Adachi, S. Nagae, Y. Wada, and S. Yanagida, A novel photosensitive silicone ladder polymer: synthesis, photochemical, and thermal characteristics, *Bulletin of the Chemical Society of Japan*, 74 (2001) 991-6.
- [5] N. Yasuda, S. Yamamoto, Y. Wada, and S. Yanagida, Photocrosslinking reaction of vinyl-functional polyphenylsilsesquioxane sensitized with aromatic bis(azide) compounds, *Journal of Polymer Science, Part A: Polymer Chemistry*, 39 (2001) 4196-205.
- [6] S. Ulutan and T. Nakagawa, Separability of ethanol and water mixtures through PTMSP-silica membranes in pervaporation, *Journal of Membrane Science*, 143 (1998) 275-84.
- [7] CAB-O-SIL TS-530 Treated Fumed Silica: Technical Data, Cabot Corp., 1991.
- [8] N. Auner, B. Ziemer, B. Herrschaft, W. Ziche, P. John, and J. Weis, Structural studies of novel siloxysilsesquioxanes, *European Journal of Inorganic Chemistry*, (1999) 1087-94.
- [9] S. D. Kelman, S. Matteucci, C. W. Bielawski, and B. D. Freeman, Crosslinking poly[1-(trimethylsilyl)-1-propyne] and its effect on solvent resistance and transport properties, *Polymer*, 48 (2007) 6881-92.
- [10] K. Nagai, T. Masuda, T. Nakagawa, B. D. Freeman, and I. Pinnau, Poly[1-(trimethylsilyl)-1-propyne] and related polymers: synthesis, properties and functions, *Progress in Polymer Science*, 26 (2001) 721-98.
- [11] H. Shimomura, K. Nakanishi, H. Odani, and M. Kurata, Effects of physical aging on permeation of gases in a disubstituted polyacetylene, *Reports on Progress in Polymer Physics in Japan*, 30 (1987) 233-6.
- [12] A. J. Hill, S. J. Pas, T. J. Bastow, M. I. Burgar, K. Nagai, L. G. Toy, and B. D. Freeman, Influence of methanol conditioning and physical aging on carbon spin-lattice relaxation times of poly[1-(trimethylsilyl)-1-propyne], *Journal of Membrane Science*, 243 (2004) 37-44.

- [13] K. Nagai, B. D. Freeman, and A. J. Hill, Effect of physical aging of poly[1-(trimethylsilyl)-1-propyne] films synthesized with TaCl₅ and NbCl₅ on gas permeability, fractional free volume, and positron annihilation lifetime spectroscopy parameters, *Journal of Polymer Science, Part B: Polymer Physics*, 38 (2000) 1222-39.
- [14] K. Nagai, A. Higuchi, and T. Nakagawa, Gas permeability and stability of poly(1-trimethylsilyl-1-propyne-co-1-phenyl-1-propyne) membranes, *Journal of Polymer Science, Part B: Polymer Physics*, 33 (1995) 289-98.
- [15] K. Nagai and T. Nakagawa, Effects of aging on the gas permeability and solubility in poly[1-(trimethylsilyl)-1-propyne] membranes synthesized with various catalysts, *Journal of Membrane Science*, 105 (1995) 261-72.
- [16] Mettler-Toledo Density Determination Kit for AT/AG Balances, 1997.
- [17] S. Matteucci, V. A. Kusuma, D. Sanders, S. Swinnea, and B. D. Freeman, Gas transport in TiO₂ nanoparticle-filled poly(1-trimethylsilyl-1-propyne), *Journal of Membrane Science*, 307 (2008) 196-217.
- [18] Y. Huang and D. R. Paul, Physical aging of thin glassy polymer films monitored by optical properties, *Macromolecules*, 39 (2006) 1554-9.
- [19] J. H. Kim, W. J. Koros, and D. R. Paul, Physical aging of thin 6FDA-based polyimide membranes containing carboxyl acid groups. Part II. Optical properties, *Polymer*, 47 (2006) 3104-11.
- [20] H. A. Lorentz, *The Theory of Electrons and Its Applications*, 2nd ed., Dover, New York, 1953.
- [21] R. K. Krishnaswamy and J. Janzen, Exploiting refractometry to estimate the density of polyethylene: The Lorentz-Lorenz approach re-visited, *Polymer Testing*, 24 (2005) 762-5.
- [22] S. S. Kurtz, Jr. and A. L. Ward, Refractivity intercept and the specific refraction equation of Newton. I. Development of the refractivity intercept and comparison with specific-refraction equations, *Journal of the Franklin Institute*, 222 (1936) 563-92.
- [23] S. S. Kurtz, Jr. and A. L. Ward, The refractivity intercept and the specific refraction equation of Newton. II. The electronic interpretation of the refractivity intercept and of the specific refraction equations of Newton, Eykman and Lorentz-Lorenz, *Journal of the Franklin Institute*, 224 (1937) 583-601.

- [24] J. H. Van Santen and W. Opechowski, A generalization of the Lorentz-Lorenz formula, *Physica (The Hague)*, 14 (1948) 545-52.
- [25] S. Spinner and R. M. Waxler, Relation between refractive index and density of glasses resulting from annealing compared with corresponding relation resulting from compression, *Applied Optics*, 5 (1966) 1887-9.
- [26] M. Born, and E. Wolf, *Principles of Optics*, 7th ed., Cambridge University Press, Cambridge, United Kingdom, 1999.
- [27] K. K. Hsu, S. Nataraj, R. M. Thorogood, and P. S. Puri, Oxygen/nitrogen selectivity improvement for poly[1-(trimethylsilyl)-1-propyne] membranes by UV irradiation and further enhancement by subambient temperature operation, *Journal of Membrane Science*, 79 (1993) 1-10.
- [28] J. Jia, Gas separation and pervaporation of chemically modified poly[1-(trimethylsilyl)-1-propyne] membranes, Ph.D. Dissertation, Michigan State University, 1999.
- [29] J. Jia and G. L. Baker, Crosslinking of poly[1-(trimethylsilyl)-1-propyne] membranes using bis(aryl azides), *Journal of Polymer Science, Part B: Polymer Physics*, 36 (1998) 959-68.
- [30] Y. Ichiraku, S. A. Stern, and T. Nakagawa, An investigation of the high gas permeability of poly[1-(trimethylsilyl)-1-propyne], *Journal of Membrane Science*, 34 (1987) 5-18.
- [31] B. D. Freeman, H. Lin, in: H. Czichos, T. Saito, L. Smith (Eds.), *Springer Handbook of Materials Measurement Methods*, Springer, Berlin, German, 2006, pp. 371-87.
- [32] K. Ghosal and B. D. Freeman, Gas separation using polymer membranes: an overview, *Polymers for Advanced Technologies*, 5 (1994) 673-97.
- [33] T. C. Merkel, R. P. Gupta, B. S. Turk, and B. D. Freeman, Mixed-gas permeation of syngas components in poly(dimethylsiloxane) and poly[1-(trimethylsilyl)-1-propyne] at elevated temperatures, *Journal of Membrane Science*, 191 (2001) 85-94.
- [34] T. C. Merkel, Z. He, I. Pinnau, B. D. Freeman, P. Meakin, and A. J. Hill, Effect of nanoparticles on gas sorption and transport in poly[1-(trimethylsilyl)-1-propyne], *Macromolecules*, 36 (2003) 6844-55.

- [35] K. D. Dorkenoo and P. H. Pfromm, Accelerated physical aging of thin poly[1-(trimethylsilyl)-1-propyne] films, *Macromolecules*, 33 (2000) 3747-51.
- [36] G. L. Baker, C. F. Klausner, A. S. Gozdz, J. A. Shelburne, III, and T. N. Bowmer, Brominated poly[1-(trimethylsilyl)-1-propyne]. *Lithography and photochemistry, Advances in Chemistry Series*, 224 (1990) 663-78.
- [37] B. Z. Tang, T. Masuda, T. Higashimura, and H. Yamaoka, Radiation effects on silicon-containing polyacetylenes, *Journal of Polymer Science, Part A: Polymer Chemistry*, 27 (1989) 1197-209.
- [38] K. Tsuchihara, T. Masuda, and T. Higashimura, Effects of ultraviolet irradiation on substituted polyacetylenes, *Journal of Polymer Science, Part A: Polymer Chemistry*, 29 (1991) 471-8.
- [39] V. L. Khodzhaeva, V. G. Zaikin, and V. S. Khotimskii, Thermal oxidation of poly[1-(trimethylsilyl)-1-propyne] studied by IR spectroscopy, *Russian Chemical Bulletin (Translation of Izvestiya Akademii Nauk, Seriya Khimicheskaya)*, 52 (2003) 1333-9.
- [40] K. Nagai and T. Nakagawa, Oxidation of poly[1-(trimethylsilyl)-1-propyne], *Journal of Applied Polymer Science*, 54 (1994) 1651-8.

4) Effects of Crosslinking on Solvent Resistance and Free Volume

This chapter presents the influence of crosslinking on the solvent resistance of PTMSP at ambient conditions. The crosslinking reaction mechanism is discussed, and a plausible crosslinking mechanism is presented. The change in the free volume characteristics of PTMSP due to crosslinking is discussed and the effects of free volume on the gas and vapor permeabilities at 35°C are examined.

4.1) Solvent Resistance of Crosslinked PTMSP

Crosslinking renders PTMSP insoluble in solvents that readily dissolve the uncrosslinked polymer [1-3]. Therefore, a preliminary indication of successful crosslinking is the lack of solubility of crosslinked films in known solvents for PTMSP. In this study, crosslinked PTMSP was insoluble in toluene, cyclohexane and tetrahydrofuran (THF), all of which are excellent solvents for uncrosslinked PTMSP [4]. For example, as shown in Table 4.1, when the crosslinker concentration is 2.4 wt % or greater, PTMSP films are insoluble in toluene. Insolubility of crosslinked PTMSP films is defined when there is less than 1 % weight loss in a dry film before and after soaking in toluene for 24 hours.

Table 4.1 Solubility of crosslinked PTMSP films in toluene

Wt % Crosslinker	0	0.7	1.4	2.4	4.9	7.7	10	20
Toluene Soluble^a	Yes	Yes	Partially	No	No	No	No	No
Monomer Units Between Crosslinks^b	-	-	90	55	26	16	12	6

- a) Films were soaked in toluene for 24 hours. The films mass was measured before and after toluene immersion once all of the toluene had evaporated from the sample.
- b) Calculated according to Equation 4.1.

Uncrosslinked PTMSP films that were subjected to the same thermal crosslinking conditions as crosslinked PTMSP films are soluble in toluene, cyclohexane and THF. This result confirms that crosslinking, and not the thermal treatment, is responsible for the solvent resistance of crosslinked PTMSP. Crosslinked PTMSP films were soaked in toluene for up to 4 years, and the films remain insoluble even after this long exposure period.

The theoretical number of monomers between each crosslink is estimated using the following expression [5]:

$$N_m = \frac{m_P / M_P}{m_{XL} / (2M_{XL})} \quad (4.1)$$

where N_m is the average number of monomer units between crosslinks, m_P is the mass of PTMSP in the film (g), M_P is the molecular weight of the PTMSP repeat unit (g/mol), m_{XL} is the mass of bis(azide) in the film (g), and M_{XL} (g/mol) is the bis(azide) molecular

weight. This calculation assumes that every azide moiety reacts and abstracts one hydrogen from a PTMSP repeat unit.

4.2) Crosslinking Reaction Mechanism

A plausible mechanism for the reaction of PTMSP with the bis(azide) crosslinker is presented in *Figure 4.1* [1,2]. After azide decomposition, the resulting nitrene is thought to insert into a carbon-hydrogen bond in PTMSP, forming a substituted amine. Since allylic C-H bonds are significantly weaker (~85 kcal/mol) [6] than the C-H bonds in $\text{Si}(\text{CH}_3)_3$ (~100 kcal/mol) [6], reaction at the allylic methyl groups ($\text{C}=\text{C}-\text{CH}_3$) along the PTMSP backbone should be strongly favored [7].

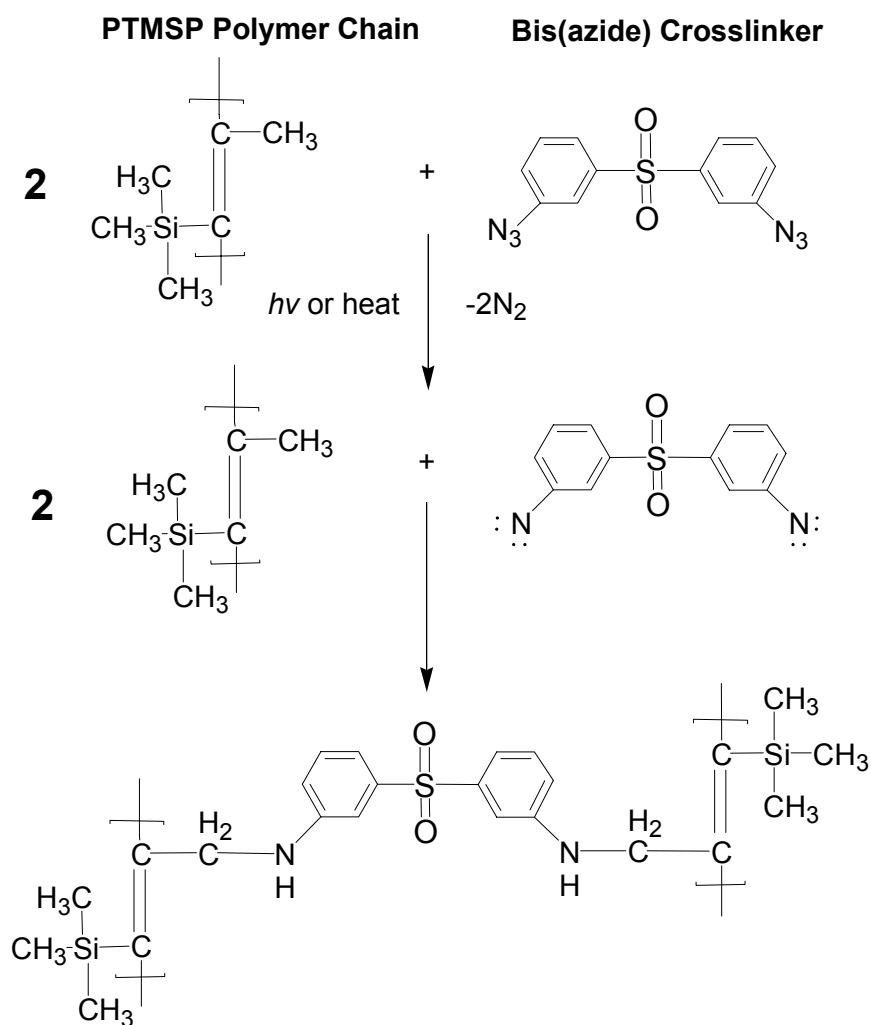


Figure 4.1 Proposed reaction scheme for crosslinking PTMSP with bis(azide) [1,2,8]

Further support for this mechanism is obtained by examining the FT-IR spectra of the crosslinked PTMSP films in *Figure 4.2*. The intensity of the characteristic signals attributed to the alkene units in PTMSP (1600 cm^{-1} , C=C stretching) did not decrease upon crosslinking. This result effectively minimizes the possibility of a nitrene addition-type mechanism which would connect polymer chains via an aziridine linkage. The azide

peak at 2120 cm^{-1} disappears when the PTMSP film is crosslinked, indicating conversion of the bis(azide) crosslinker to a reactive bis(nitrene).

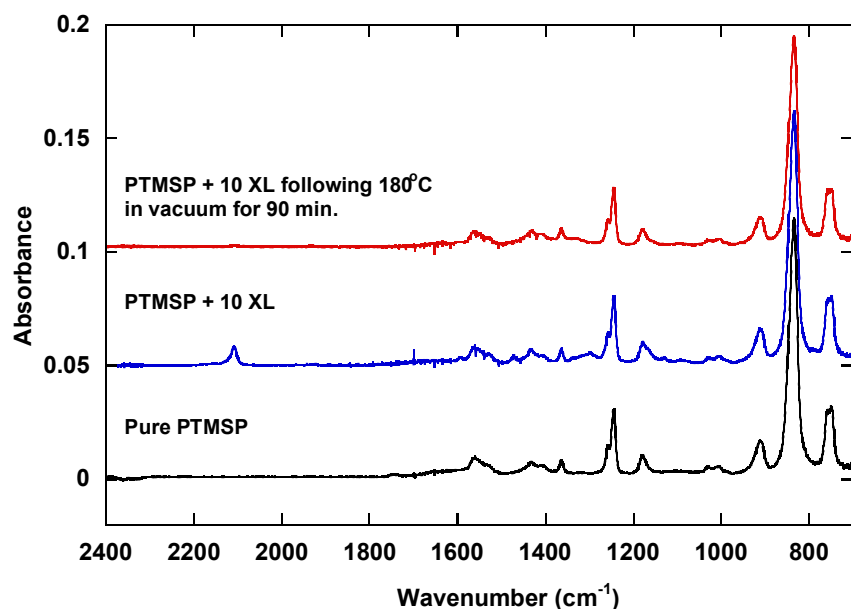


Figure 4.2. FT-IR spectra of pure PTMSP, PTMSP containing 10 wt % crosslinker (XL) prior to exposing the sample to elevated temperatures to perform the crosslinking reaction, and crosslinked PTMSP containing 10 wt % crosslinker.

4.3) Effect of Crosslinking on Free Volume and Gas Permeability

Crosslinking PTMSP with a bis(azide) crosslinker increases the film density markedly, and this effect is illustrated in Table 4.2. The film labeled “5 XL” refers to a film of PTMSP containing 5 wt % of the crosslinker; the film containing 10 wt % crosslinker was named “10 XL”. The density of PTMSP increases from 0.76 g/cm^3 in its uncrosslinked state to 0.81 g/cm^3 when the film is crosslinked with 10 wt % crosslinker. The increase in density causes a decrease in FFV, and the above increase in density

caused the FFV to decrease from 0.295 to 0.260. The FFV values were calculated using measured density values and Bondi's group contribution method [9-11].

Table 4.2 Film densities and FFV of various PTMSP films.

Film	Measured Density, $\rho_{film} [g/cm^3]$	FFV
PTMSP	0.760 ± 0.010	0.295 ± 0.005
5 XL	0.785 ± 0.010	0.275 ± 0.005
10 XL	0.810 ± 0.010	0.260 ± 0.005

It is of interest to understand whether the decrease in FFV associated with higher crosslinker content is due to the presence of the crosslinker in PTMSP or related to densification induced by the thermal annealing protocol. In this regard, the FFV of a PTMSP film containing 5 wt % crosslinker is the same before and after exposure to the crosslinking conditions (180°C for 90 minutes in vacuum). Therefore, the reduction in free volume is due to the mixing of high free volume PTMSP with the initially crystalline crosslinker, which is expected to have a much lower inherent FFV than PTMSP, rather than to thermally-induced densification of the polymer.

Positron annihilation lifetime spectroscopy (PALS) is a powerful tool for characterizing the size and concentration of free volume sites in polymer systems [12]. PALS was performed on uncrosslinked and crosslinked PTMSP films to understand the changes in free volume that occur due crosslinking, and Table 4.3 presents the PALS results.

Table 4.3 PALS parameters for uncrosslinked and crosslinked PTMSP^a

Film	P _{N2} (barrers)	τ_3 (ns)	I ₃ (%)	τ_4 (ns)	I ₄ (%)
PTMSP	6,500 ± 900	2.0 ± 0.1	6.5 ± 0.2	9.7 ± 0.1	38.8 ± 0.2
5 XL	4,200 ± 700	2.08 ± 0.04	6.1 ± 0.1	9.6 ± 0.1	29.0 ± 0.1

- a) All films were thermally annealed in vacuum at 180°C for 90 minutes, then soaked in MeOH for 24 hours, and dried at ambient conditions for 72 hours prior to the PALS and permeation measurements.
- b) T = 35°C, $f_2 = 4.4$ atm, and f_1 = atmospheric for all permeation measurements.

Similar to previously published results [13-16] the PALS of the uncrosslinked and crosslinked PTMSP films show a bi-modal or very broad free volume element size distribution with two *o*-Ps lifetimes clearly resolved. The parameters τ_3 and I₃, represent the *o*-Ps lifetime and intensity of the smaller free volume elements, while τ_4 and I₄ correspond to the *o*-Ps lifetime and intensity of the large free volume elements. The intensity of large free volume elements, I₄, decreases from 38.8 % in uncrosslinked PTMSP to 29.0 % in crosslinked PTMSP, while there is no significant change in the average τ_4 values between the two films. No significant changes in τ_3 and I₃ due to crosslinking were observed. Consistent with these results, aging of MeOH conditioned PTMSP, which is accompanied by a decrease in permeability, has been shown previously to decrease the concentration of large free volume elements [15].

For all gases considered, gas and vapor permeability decreases as crosslinker content increases and FFV decreases. *Figure 4.3* presents a typical example of such results. N₂ permeability decreases from 7,000 barrers to 2,000 barrers as crosslinker content increases from 0 to 20 wt %, while FFV decreases from 0.295 to 0.24.

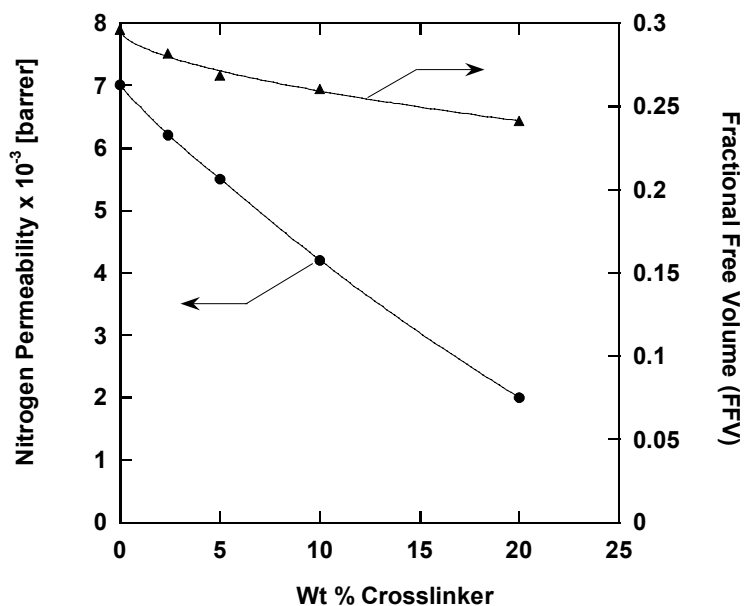


Figure 4.3. Effect of crosslinker content on initial N_2 permeability and FFV of PTMSP and crosslinked PTMSP films. $T = 35^\circ\text{C}$, $f_2 = 4.4$ atm, and $f_1 =$ atmospheric for all measurements. All films were crosslinked in vacuum at 180°C for 90 minutes, then soaked in MeOH for 24 hours, and finally dried at ambient conditions for 72 hours prior to the permeation measurements. Film thickness was approximately $100\ \mu\text{m}$.

The decrease in permeability can be correlated with the decrease in FFV using Equation 2.12 [17], and the relationship between gas permeability and FFV is presented in Figure 4.4.

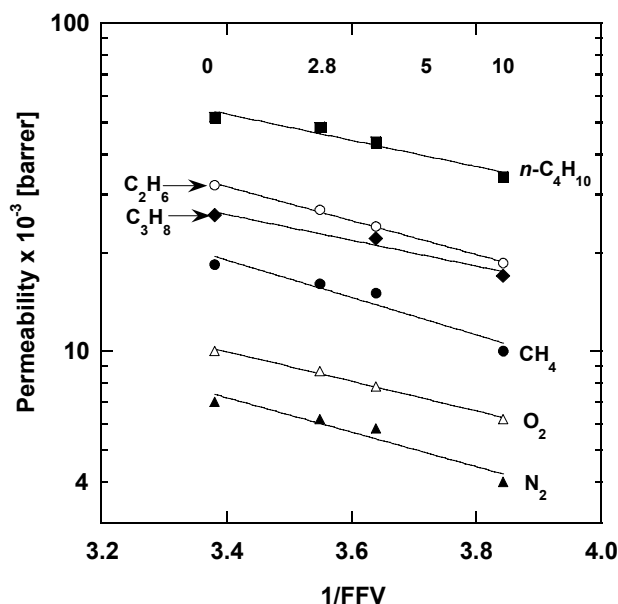


Figure 4.4. Permeability of N₂, O₂, CH₄, C₂H₆, C₃H₈ and *n*-C₄H₁₀ in uncrosslinked and crosslinked PTMSP versus 1/FFV. T = 35°C, $f_2 = 4.4$ atm (N₂, O₂, CH₄, and C₂H₆), $f_2 = 2.8$ atm (C₃H₈) and $f_2 = 1.7$ atm (*n*-C₄H₁₀), f_1 = atmospheric for all measurements. Films were crosslinked at 180°C in vacuum for 90 minutes, soaked in MeOH for 24 hours, then dried for 72 hours before testing began. Film thickness was approximately 100 μ m. The numbers at the top of the plot represent the wt % crosslinker initially present in the film.

The N₂ permeability decreases from 7,000 barrers to 4,000 barrers, and the *n*-C₄H₁₀ permeability decreases from 51,000 barrers to 34,000 barrers as the bis(azide) content increases from 0 to 10 wt %. The gas and vapor permeabilities for uncrosslinked PTMSP are comparable to the values reported at the same pressures and temperatures by Merkel *et al.* [18]. A strong relationship between permeability and 1/FFV is observed for all

gases considered, which is consistent with Equation 2.12. An increase in the O_2/N_2 selectivity from 1.43 to 1.55 is observed as crosslinker content increases from 0 to 10 wt %, suggesting a slight increase in size selectivity upon crosslinking. These results are consistent with the tradeoff between permeability and selectivity commonly observed in polymers [19,20]. Changes in pure gas solubility and diffusivity of PTMSP due to crosslinking are discussed in Chapters 5 and 6.

4.4) Conclusions

Crosslinking PTMSP with a bis(azide) successfully increased the solvent resistance of the polymer. Crosslinked PTMSP is insoluble in common PTMSP solvents, such as toluene. The gas permeability of PTMSP decreases upon crosslinking and the decrease is related to a decrease in FFV that accompanies crosslinking. An increase in O_2/N_2 selectivity is observed in crosslinked samples, suggesting a slight increase in size selectivity upon crosslinking.

4.5) References

- [1] J. Jia, Gas separation and pervaporation of chemically modified poly[1-(trimethylsilyl)-1-propyne] membranes, Ph.D. Dissertation, Michigan State University, 1999.
- [2] J. Jia and G. L. Baker, Crosslinking of poly[1-(trimethylsilyl)-1-propyne] membranes using bis(aryl azides), *Journal of Polymer Science, Part B: Polymer Physics*, 36 (1998) 959-68.
- [3] C. J. Ruud, J. Jia, and G. L. Baker, Synthesis and characterization of poly[(1-trimethylsilyl-1-propyne)-co-(1-(4-azidobutyldimethylsilyl)-1-propyne)] copolymers, *Macromolecules*, 33 (2000) 8184-91.

- [4] T. Masuda, E. Isobe, T. Higashimura, and K. Takada, Poly[1-(trimethylsilyl)-1-propyne]: a new high polymer synthesized with transition-metal catalysts and characterized by extremely high gas permeability, *Journal of the American Chemical Society*, 105 (1983) 7473-4.
- [5] H. Allcock, Lampe, F., *Contemporary Polymer Chemistry*, 2nd ed., Prentice-Hall, London, 1990.
- [6] J. A. Dean, *Lange's Handbook of Chemistry*, 15th ed., McGraw-Hill, New York, 1999.
- [7] V. L. Khodzhaeva, V. G. Zaikin, and V. S. Khotimskii, Thermal oxidation of poly[1-(trimethylsilyl)-1-propyne] studied by IR spectroscopy, *Russian Chemical Bulletin (Translation of Izvestiya Akademii Nauk, Seriya Khimicheskaya)*, 52 (2003) 1333-9.
- [8] S. D. Kelman, S. Matteucci, C. W. Bielawski, and B. D. Freeman, Crosslinking poly[1-(trimethylsilyl)-1-propyne] and its effect on solvent resistance and transport properties, *Polymer*, 48 (2007) 6881-92.
- [9] A. Bondi, van der Waals volumes and radii, *Journal of Physical Chemistry*, 68 (1964) 441-51.
- [10] A. Bondi, *Physical Properties of Molecular Crystals, Liquids and Glasses*, Wiley, New York, 1968.
- [11] D. W. Van Krevelen, *Properties of Polymers*, 3rd ed., Elsevier, Amsterdam, 2003.
- [12] P. E. Mallon, in: Y. C. Dean, P. E. Mallon, D. M. Schrader (Eds.), *Positron and Positronium Chemistry*, World Scientific Publishing Co., Singapore, 2003, pp. 253-80.
- [13] G. Consolati, I. Genco, M. Pegoraro, and L. Zangerighi, Positron annihilation lifetime (PAL) in poly[1-(trimethylsilyl)-1-propyne] (PTMSP): free volume determination and time dependence of permeability, *Journal of Polymer Science, Part B: Polymer Physics*, 34 (1996) 357-67.
- [14] T. C. Merkel, Z. He, I. Pinnau, B. D. Freeman, P. Meakin, and A. J. Hill, Effect of nanoparticles on gas sorption and transport in poly[1-(trimethylsilyl)-1-propyne], *Macromolecules*, 36 (2003) 6844-55.

- [15] K. Nagai, B. D. Freeman, and A. J. Hill, Effect of physical aging of poly[1-(trimethylsilyl)-1-propyne] films synthesized with TaCl₅ and NbCl₅ on gas permeability, fractional free volume, and positron annihilation lifetime spectroscopy parameters, *Journal of Polymer Science, Part B: Polymer Physics*, 38 (2000) 1222-39.
- [16] Y. P. Yampolskii, A. P. Korikov, V. P. Shantarovich, K. Nagai, B. D. Freeman, T. Masuda, M. Teraguchi, and G. Kwak, Gas permeability and free volume of highly branched substituted acetylene polymers, *Macromolecules*, 34 (2001) 1788-96.
- [17] T. C. Merkel, L. G. Toy, A. L. Andrady, H. Gracz, and E. O. Stejskal, Investigation of enhanced free volume in nanosilica-filled poly[1-(trimethylsilyl)-1-propyne] by ¹²⁹Xe NMR spectroscopy, *Macromolecules*, 36 (2003) 353-8.
- [18] T. C. Merkel, V. Bondar, K. Nagai, and B. D. Freeman, Sorption and transport of hydrocarbon and perfluorocarbon gases in poly[1-(trimethylsilyl)-1-propyne], *Journal of Polymer Science, Part B: Polymer Physics*, 38 (2000) 273-96.
- [19] L. M. Robeson, Correlation of separation factor versus permeability for polymeric membranes, *Journal of Membrane Science*, 62 (1991) 165-85.
- [20] B. D. Freeman, Basis of permeability/selectivity tradeoff relations in polymeric gas separation membranes, *Macromolecules*, 32 (1999) 375-80.

5) Solubility Characteristics of PTMSP

This chapter discusses the influence of crosslinking and FS addition on the solubility characteristics of PTMSP. The N_2 , O_2 , CH_4 , C_2H_6 , C_3H_8 , and $n-C_4H_{10}$ sorption isotherms were measured in various PTMSP films at temperatures ranging from -20°C to 35°C and at fugacities ranging from 0 to 20 atm. The sorption isotherms were fit to the dual-mode sorption model. Changes in the sorption isotherms due to nanoparticle addition and temperature effects were related to changes in the values of the dual-mode sorption model parameters.

5.1) Sorption Isotherms of Neat and Nanocomposite PTMSP

The sorption isotherms of N_2 , O_2 , CH_4 , C_2H_6 , C_3H_8 , and $n-C_4H_{10}$ in uncrosslinked PTMSP, and uncrosslinked PTMSP containing 30 wt % FS at were measured at 35°C , 10°C , 0°C , and -20°C , and the isotherms are presented in *Figure 5.1*, *Figure 5.2* and *Figure 5.3*. The sorption isotherms of the nanocomposite uncrosslinked PTMSP films in this study are 10 – 20 % less than that of their neat analogs at all fugacities. The decrease in nanocomposite sorption is similar at all temperatures, and the reduction in sorption due to FS addition is similar for all penetrants. For all gases and vapors, the sorption isotherms increase as temperature decreases, which is consistent with previous results in PTMSP [1,2].

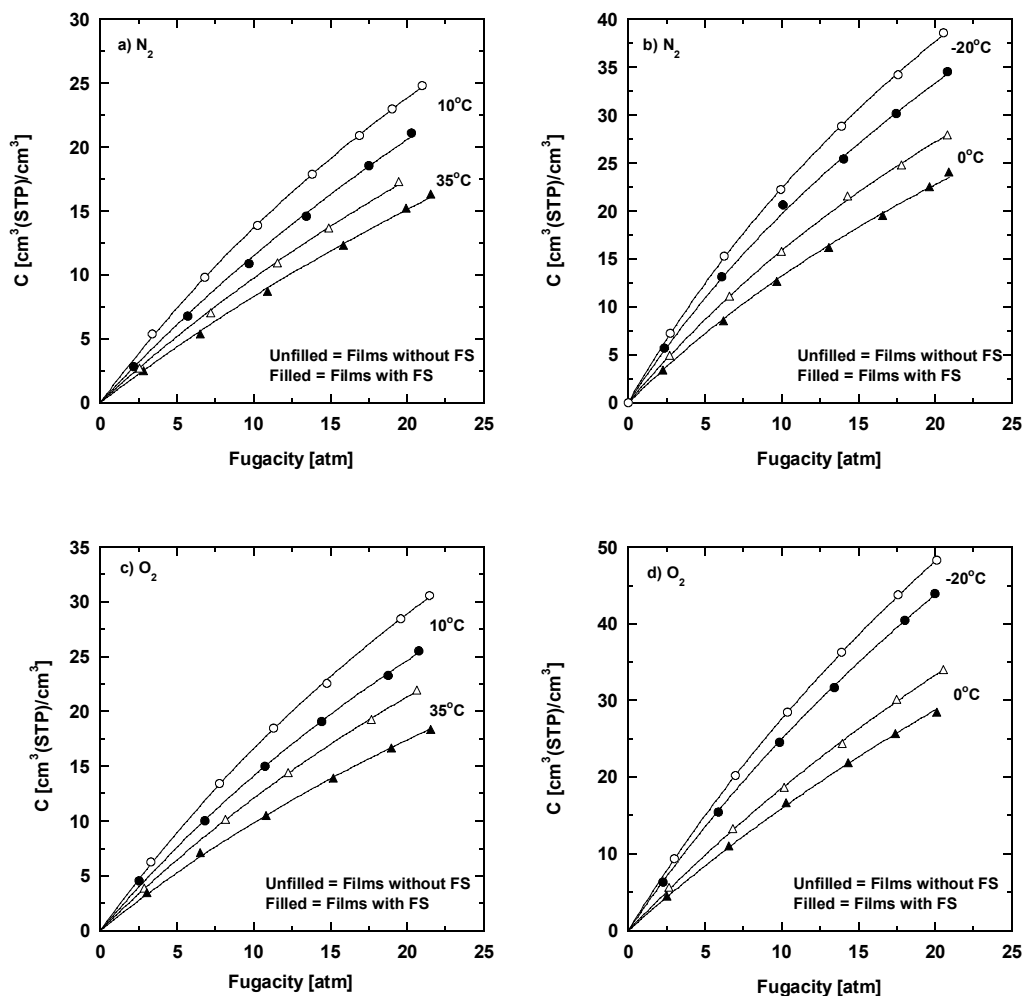


Figure 5.1. Sorption isotherms of uncrosslinked PTMSP (unfilled symbols) and uncrosslinked PTMSP containing 30 wt % FS (filled symbols) for (a) N_2 at 35°C and 10°C ; (b) N_2 at 0°C and -20°C ; (c) O_2 at 35°C and 10°C ; and (d) O_2 at 0°C and -20°C . The concentration is expressed as cm^3 of penetrant at STP per cm^3 of film in the sorption cell. All films were subjected to vacuum at 180°C for 90 minutes, soaked in MeOH for 24 hours, and then dried for 72 hours in ambient conditions before sorption isotherms were measured. The solid lines represent dual-mode sorption model fits to the sorption isotherms.

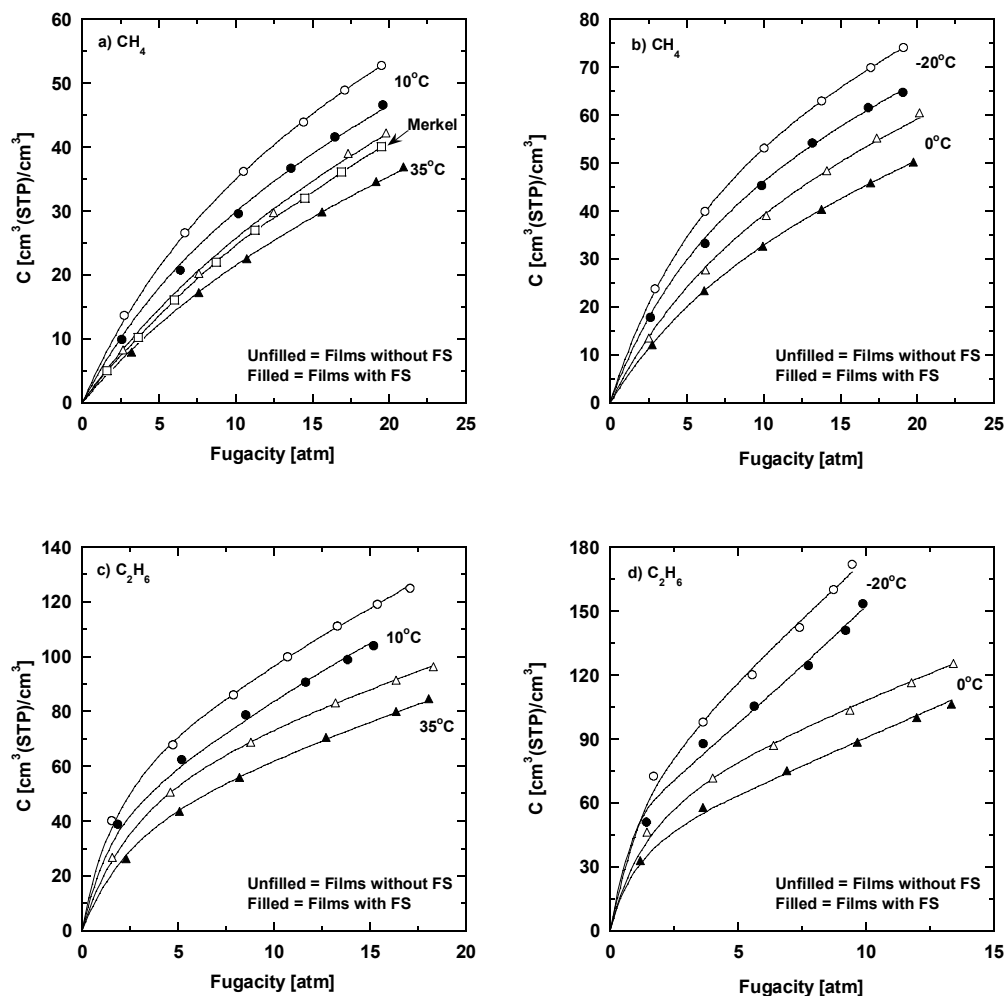


Figure 5.2. Sorption isotherms of uncrosslinked PTMSP (unfilled symbols) and uncrosslinked PTMSP containing 30 wt % FS (filled symbols) for (a) CH_4 at 35°C and 10°C ; (b) CH_4 at 0°C and -20°C ; (c) C_2H_6 at 35°C and 10°C ; and (d) C_2H_6 at 0°C and -20°C . The concentration is expressed as cm^3 of penetrant at STP per cm^3 of film in the sorption cell. All films were subjected to vacuum at 180°C for 90 minutes, soaked in MeOH for 24 hours, and then dried for 72 hours in ambient conditions before sorption isotherms were measured. The solid lines represent dual-mode sorption model fits to the sorption isotherms. The CH_4 sorption isotherm measured by Merkel et al. is for pure PTMSP at 35°C [3].

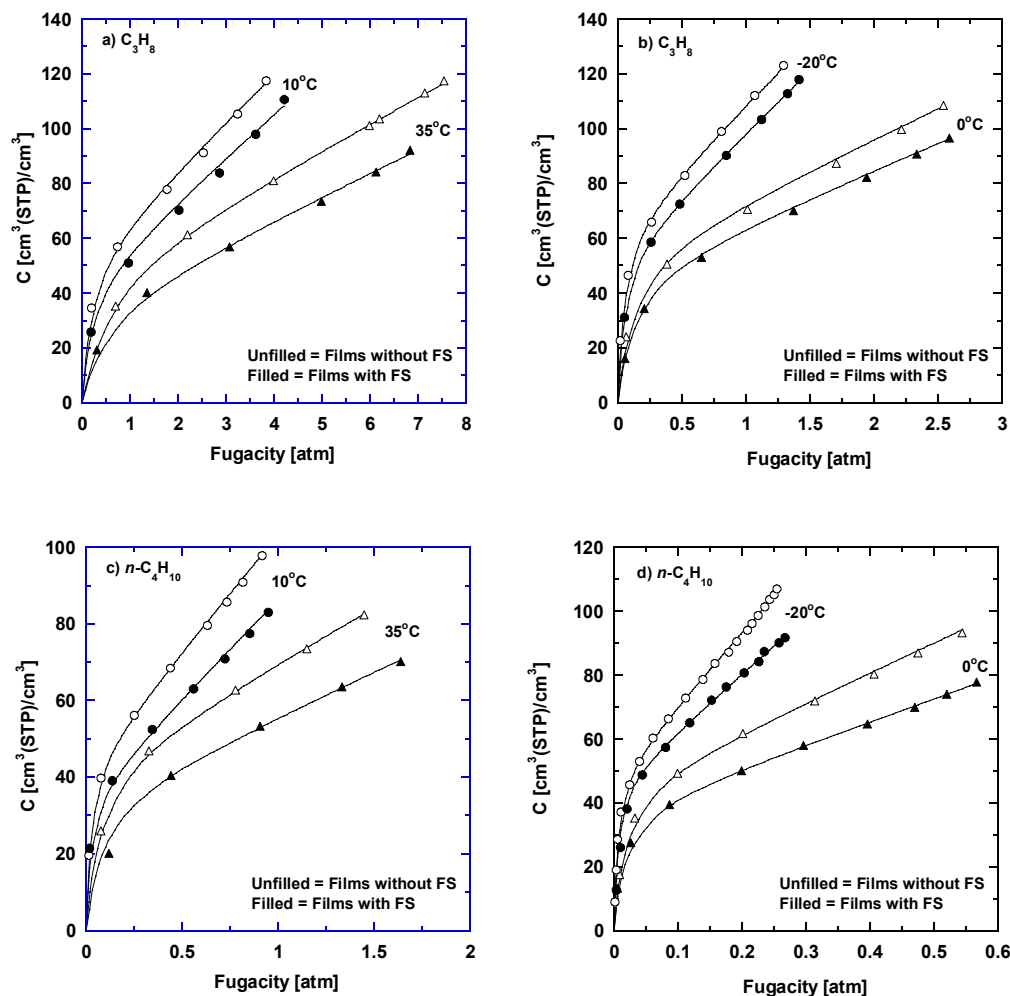


Figure 5.3. Sorption isotherms of uncrosslinked PTMSP (unfilled symbols) and uncrosslinked PTMSP containing 30 wt % FS (filled symbols) for (a) C₃H₈ at 35°C and 10°C; (b) C₃H₈ at 0°C and -20°C; (c) n-C₄H₁₀ at 35°C and 10°C; and (d) n-C₄H₁₀ at 0°C and -20°C. The concentration is expressed as cm³ of penetrant at STP per cm³ of film in the sorption cell. All films were subjected to vacuum conditions at 180°C for 90 minutes, soaked in MeOH for 24 hours, and then dried for 72 hours in ambient conditions before sorption isotherms were measured. The solid lines represent dual-mode sorption model fits to the sorption isotherms.

In *Figure 5.4*, the sorption isotherms of uncrosslinked PTMSP and uncrosslinked PTMSP containing 30 wt % FS are compared to sorption isotherms of crosslinked PTMSP containing 5 and 10 wt % bis(azide) crosslinker, and crosslinked PTMSP containing 10 wt % bis(azide) crosslinker and 30 wt % FS. The film labeled “5 XL” refers to a film of PTMSP containing 5 wt % of the crosslinker; films containing 10 wt % crosslinker were named “10 XL”. Likewise, the sample labeled “30 FS” indicates a PTMSP film containing 30 wt % fumed silica. Finally, the sample labeled “10 XL + 30 FS” refers to a PTMSP film containing 10 wt % crosslinker and 30 wt % fumed silica. This naming scheme is used for the rest of this document.

The CH₄ and *n*-C₄H₁₀ sorption isotherms at 35°C and 0°C of neat uncrosslinked PTMSP films are essentially equivalent to those of neat crosslinked PTMSP films. For all other gases, and at all other temperatures, the sorption isotherms of neat uncrosslinked and crosslinked PTMSP films are also equivalent. The sorption isotherms of the nanocomposite uncrosslinked and crosslinked PTMSP films are also equivalent. Therefore, gas solubility in neat and nanocomposite PTMSP is not measurably influenced by the presence of crosslinker.

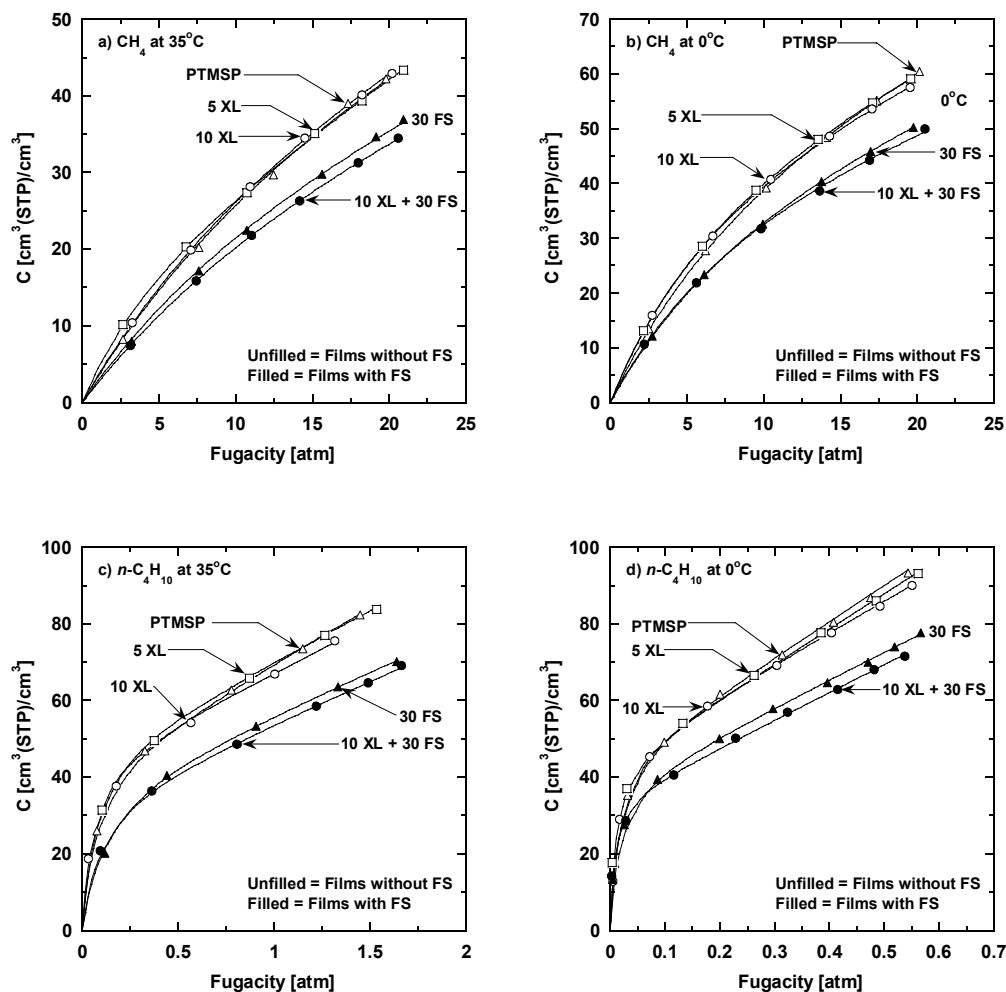


Figure 5.4. Sorption isotherms of PTMSP containing 0 (Δ), 5 (\square), and 10 (\circ) wt % XL, and nanocomposite PTMSP containing 30 wt % FS and 0 (\blacktriangle) or 10 (\bullet) wt % XL for (a) CH₄ at 35°C; (b) CH₄ at 0°C; (c) *n*-C₄H₁₀ at 35°C; and (d) *n*-C₄H₁₀ at 0°C. The concentration is expressed as cm³ of penetrant at STP per cm³ of film in the sorption cell. All films were subjected to vacuum at 180°C for 90 minutes, soaked in MeOH for 24 hours, and then dried for 72 hours in ambient conditions before sorption isotherms were measured. The solid lines represent dual-mode sorption model fits to the sorption isotherms.

Merkel *et al.* observed no decrease in gas and vapor sorption at 25°C when 30 wt % FS nanoparticles were added to PTMSP [4]. However, in this study, the gas and vapor solubility of nanocomposite PTMSP is less than the gas and vapor solubility of neat PTMSP (cf., Figures 5.1 – 5.4) To explain the discrepancy in the observed sorption behavior of neat and nanocomposite PTMSP in this study, and the study by Merkel *et al.*, the method used to calculate film volume in the sorption cell needs to be considered.

In this study, the measured density and the measured sample mass was used to estimate the volume of sample in the sorption cell. Merkel *et al.* [4] used the additive density model (Equation 3.3) to estimate the sample density and then estimated the sample volume using the measured sample mass and the estimated density. The measured nanocomposite PTMSP densities are less than the additive nanocomposite densities, as shown in Table 5.1.

Table 5.1 Film densities of various PTMSP films.

Film	Measured Density, ρ_{film} [g/cm³]	Additive Density, ρ_{Add} [g/cm³]	Void Fraction, ϕ_v
PTMSP	0.76 ± 0.01	-	-
5 XL	0.78 ± 0.01	-	-
10 XL	0.81 ± 0.01	-	-
30 FS	0.81 ± 0.01	0.95	0.14
10 XL + 30 FS	0.85 ± 0.01	1.00	0.15

If the sample volume is estimated using the additive density model, the apparent penetrant concentration in the nanocomposite film increases. This effect is illustrated in *Figure 5.5* where *n*-C₄H₁₀ sorption isotherms at 35°C are presented for uncrosslinked PTMSP and uncrosslinked PTMSP containing 30 wt % FS nanoparticles.

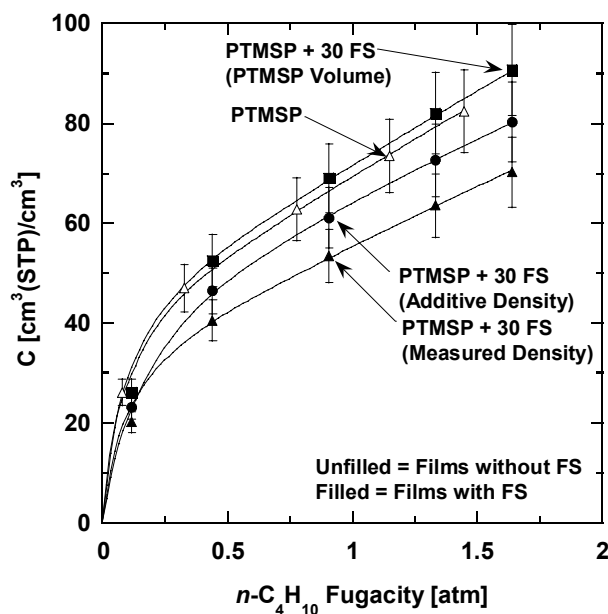


Figure 5.5. n -C₄H₁₀ sorption isotherms of uncrosslinked PTMSP (unfilled symbols) and uncrosslinked PTMSP containing 30 wt % FS (filled symbols) at 35°C. In all cases, C is the cm³ (STP) of n -C₄H₁₀ sorbed per cm³ of PTMSP (Δ , \blacksquare) or nanocomposite (*i.e.*, PTMSP + fumed silica) (\blacktriangle , \bullet). The volume of the nanocomposite film was estimated using the measured and additive densities in Table 5.1 and the mass of the sample in the sorption cell. The nanocomposite isotherm is also shown for the case when the contribution of FS nanoparticles to the n -C₄H₁₀ sorption is negligible, and only the volume of PTMSP is considered to sorb n -C₄H₁₀ in the nanocomposite film (\blacksquare). All films were subjected to vacuum at 180°C for 90 minutes, soaked in methanol for 24 hours, and then dried for 72 hours in ambient conditions before sorption isotherms were measured. The solid lines represent dual-mode sorption model fits to the sorption isotherms.

When the nanocomposite sample volume in the sorption cell is calculated using the measured density, the n -C₄H₁₀ sorption isotherm of nanocomposite PTMSP is slightly less than that reported when the additive density model is used to estimate nanocomposite sample volume. The n -C₄H₁₀ sorption isotherm is also presented using only the volume of PTMSP in the nanocomposite film, and the n -C₄H₁₀ sorption isotherm of the PTMSP in

the nanocomposite film is comparable, within the experimental error, to the isotherms of both uncrosslinked PTMSP and nanocomposite PTMSP when the additive density model is used to calculate nanocomposite film volume.

So, when the additive density model is used to estimate the nanocomposite sample volume, as Merkel *et al.* did, the same result as Merkel *et al.* (*i.e.*, that the presence of the nanoparticles does not influence gas sorption levels) is obtained. When the experimental measured density is used to estimate nanocomposite volume, then the nanoparticles do appear to slightly depress gas solubility in the nanocomposite by about 20 %, as indicated in *Figure 5.5*.

To further understand the sorption decrease in nanocomposite PTMSP, the sorption isotherms were calculated using the volume of only PTMSP in neat and nanocomposite films, rather than the total volume of the film, which would include both PTMSP and nanoparticles. These sorption isotherms are shown in *Figure 5.6* for CH₄ and *n*-C₄H₁₀. The sorption isotherms of neat and nanocomposite uncrosslinked films are the same within experimental error. This result is consistent with the combined affects of the low volume fraction of FS in the nanocomposite film (*i.e.*, 13 volume % of the additive film volume at a loading of 30 wt % FS – calculated based on the additive model), and the gas sorption of FS being an order of magnitude less than that of PTMSP [4] causing the FS contribution to penetrant sorption of nanocomposite films to be small. For all sorption isotherms other than those presented in *Figure 5.5* and *Figure 5.6* for comparison purposes, the nanocomposite volume was calculated based on measured

density values, and the sorption isotherms are reported as volume of gas sorbed per unit volume of nanocomposite sample (*i.e.*, PTMSP and FS).

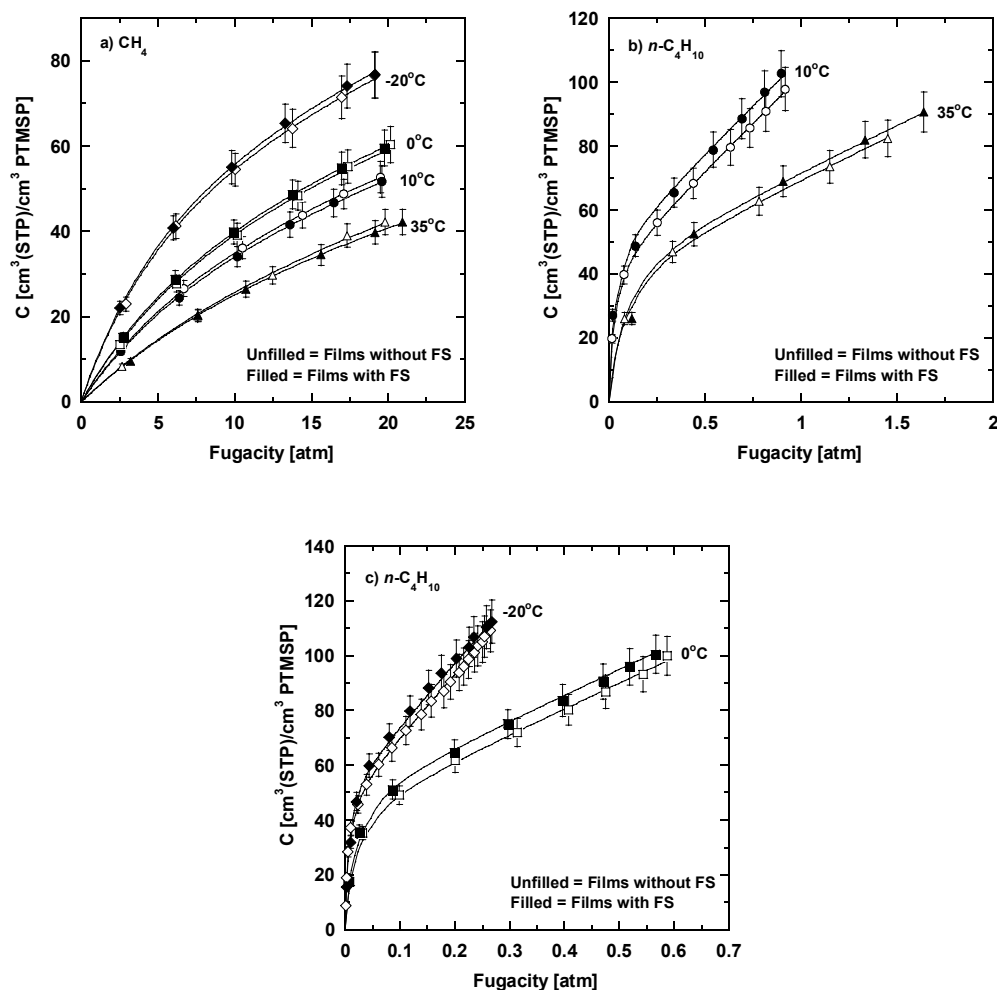


Figure 5.6. Sorption isotherms of uncrosslinked PTMSP (unfilled symbols), and uncrosslinked PTMSP containing 30 wt % FS (filled symbols) for (a) CH_4 ; (b) $n\text{-C}_4\text{H}_{10}$ at 35°C and 10°C ; and (c) $n\text{-C}_4\text{H}_{10}$ at 0°C and -20°C . The concentration is expressed as cm^3 of penetrant at STP per cm^3 of PTMSP in the sorption cell. All films were subjected to vacuum at 180°C for 90 minutes, soaked in MeOH for 24 hours, and then dried for 72 hours in ambient conditions before sorption isotherms were measured. The solid lines represent dual-mode sorption model fits to the sorption isotherms.

5.2) Dual-Mode Sorption in Neat and Nanocomposite PTMSP

The sorption isotherms of neat uncrosslinked PTMSP in *Figure 5.1*, *Figure 5.2*, and *Figure 5.3* were fit to the dual-mode sorption model, which has been used extensively to model the sorption of gases and vapors in PTMSP [3,5-9]. The dual-mode sorption parameters for CH₄ and *n*-C₄H₁₀, are recorded in Table 5.2 for neat uncrosslinked PTMSP at 35°C, 10°C, 0°C, and -20°C.

Table 5.2. Dual-mode sorption model parameters for CH₄ and *n*-C₄H₁₀ in uncrosslinked PTMSP^a.

Gas	T	k_D	C'_H	b	Reference
CH ₄	35°C	0.65 ± 0.04	57 ± 3	0.05 ± 0.01	This work
		0.60 ± 0.05	56 ± 5	0.05 ± 0.01	Raharjo <i>et al.</i> [9]
		0.5	62	0.05	Merkel <i>et al.</i> [3]
CH ₄	10°C	0.82 ± 0.05	60 ± 4	0.08 ± 0.01	This work
CH ₄	0°C	0.89 ± 0.08	65 ± 6	0.09 ± 0.01	This work
		0.83 ± 0.05	63 ± 5	0.09 ± 0.01	Raharjo <i>et al.</i> [9]
CH ₄	-20°C	1.04 ± 0.08	77 ± 7	0.13 ± 0.01	This work
		1.00 ± 0.07	79 ± 7	0.12 ± 0.01	Raharjo <i>et al.</i> [9]
<i>n</i> -C ₄ H ₁₀	35°C	29 ± 2	43 ± 2	17 ± 3	This work
		27.7	44	14.8	Morisato <i>et al.</i> [6]
		29 ± 2	40 ± 2	16 ± 2	Raharjo <i>et al.</i> [9]
<i>n</i> -C ₄ H ₁₀	10°C	60 ± 4	44 ± 2	50 ± 6	This work
<i>n</i> -C ₄ H ₁₀	0°C	91 ± 6	46 ± 2	77 ± 10	This work
		96 ± 7	47 ± 2	85 ± 9	Raharjo <i>et al.</i> [9]
<i>n</i> -C ₄ H ₁₀	-20°C	223 ± 20	50 ± 2	160 ± 25	This work
		213 ± 17	53 ± 3	188 ± 20	Raharjo <i>et al.</i> [9]

a) The units of k_D , C'_H , and b are [cm³(STP)/cm³atm], [cm³(STP)/cm³], and [atm⁻¹], respectively.

The dual-mode sorption parameters for CH₄ and *n*-C₄H₁₀ sorption in neat crosslinked PTMSP are essentially identical to those in Table 5.2 due to the equivalency of the neat uncrosslinked and crosslinked PTMSP sorption isotherms. The parameters from this study are in good agreement with those obtained by Merkel *et al.* [3], Morisato *et al.* [6], and Raharjo *et al.* [9]. The dual-mode sorption parameters of N₂, O₂, C₂H₆, and C₃H₈ in neat uncrosslinked PTMSP are also equivalent to their values in neat crosslinked PTMSP, and these values also agree reasonably well with values from the literature [3].

To further characterize the decrease in sorption of uncrosslinked PTMSP containing 30 wt % FS nanoparticles, the dual-mode sorption model was fit to the nanocomposite PTMSP sorption isotherms in *Figure 5.1*, *Figure 5.2*, and *Figure 5.3*. The dual-mode parameters of neat uncrosslinked PTMSP for the same gas and at the same temperature were used as initial estimates to fit the nanocomposite sorption isotherms. To achieve a better fit, one parameter was allowed to vary, while the other two were held constant. Using this approach, a good fit of the model was obtained for the N₂, O₂, CH₄, and C₂H₆ nanocomposite sorption isotherms when C'_H was varied, and k_D and b were fixed at the values obtained for neat PTMSP. To achieve a good fit to the nanocomposite C₃H₈ and *n*-C₄H₁₀ sorption isotherms, both C'_H and k_D needed to be varied. The dual-mode parameters of nanocomposite crosslinked PTMSP are similar to those of nanocomposite uncrosslinked PTMSP, due to the similarity of their sorption isotherms.

Figure 5.7 and Figure 5.8 present the Langmuir sorption capacity parameter, C'_H , for N_2 , O_2 , CH_4 , C_2H_6 , C_3H_8 , and $n-C_4H_{10}$ in neat uncrosslinked PTMSP and nanocomposite uncrosslinked PTMSP as a function of temperature.

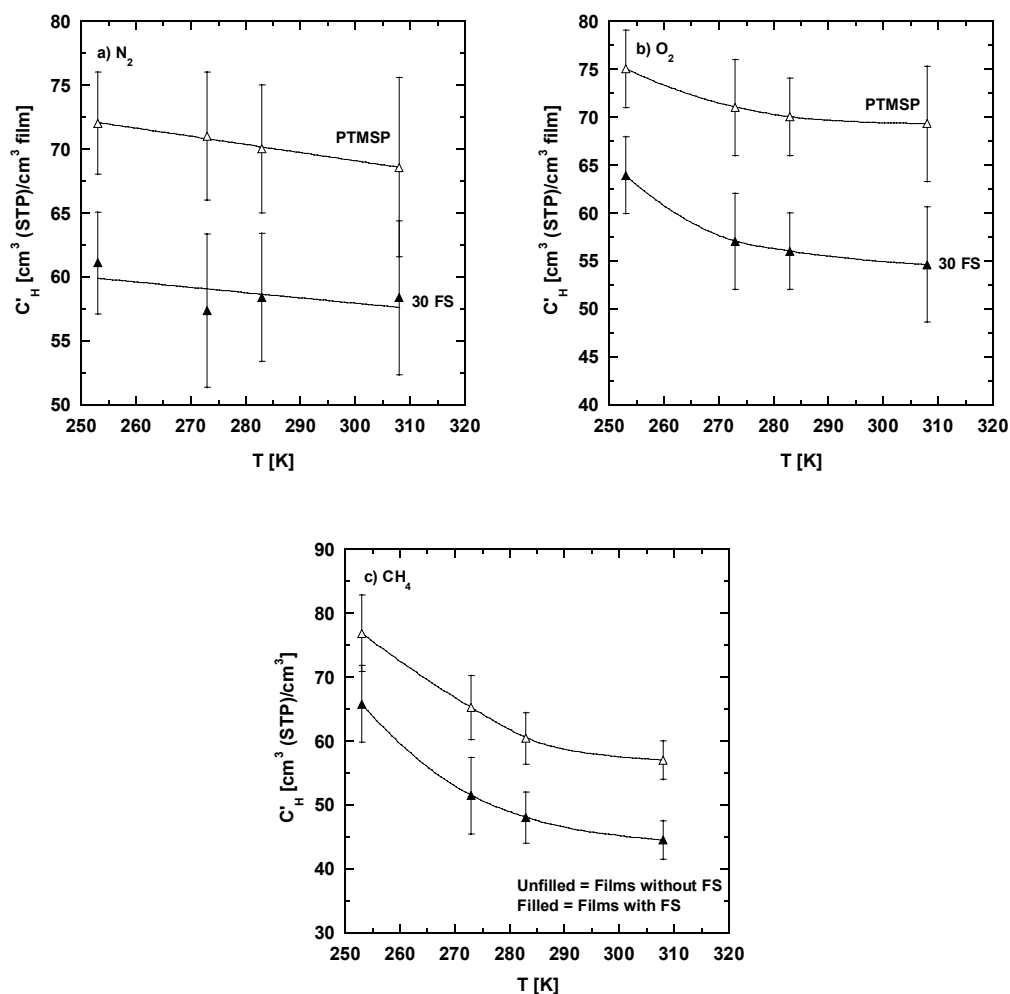


Figure 5.7. Effect of temperature on the Langmuir sorption capacity, C'_H , for a) N_2 , b) O_2 , and c) CH_4 in uncrosslinked PTMSP and uncrosslinked PTMSP containing 30 wt % FS. The Langmuir capacity parameter is calculated on the basis of total film volume. All films were crosslinked at 180°C in vacuum for 90 minutes, soaked in MeOH for 24 hours, and then dried at ambient conditions for 72 hours before sorption isotherms were measured.

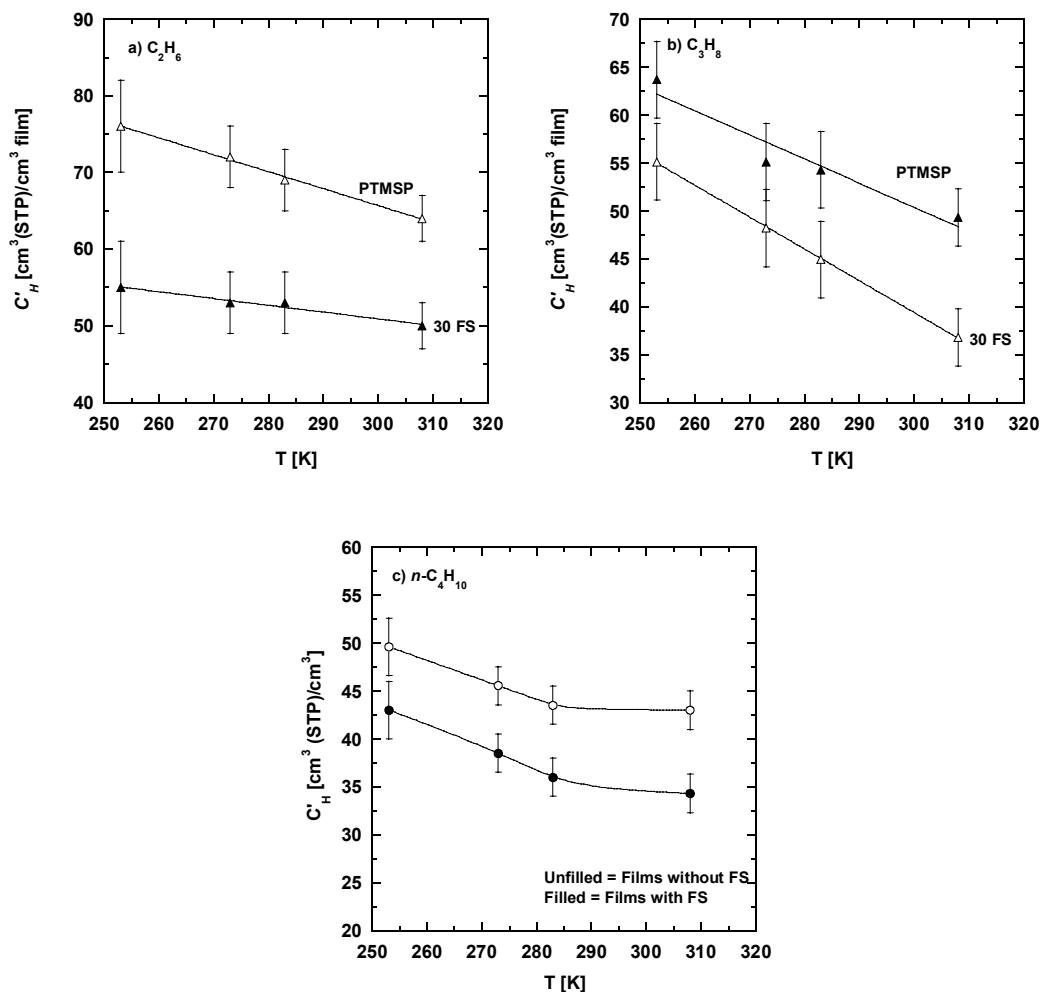


Figure 5.8. Effect of temperature on the Langmuir sorption capacity, C'_H , for a) C_2H_6 , b) C_3H_8 , and c) $n\text{-C}_4\text{H}_{10}$ in uncrosslinked PTMSP and uncrosslinked PTMSP containing 30 wt % FS. The Langmuir capacity parameter is calculated on the basis of total film volume. All films were crosslinked at 180°C in vacuum for 90 minutes, soaked in MeOH for 24 hours, then dried at ambient conditions for 72 hours before sorption isotherms were measured.

At all temperatures, there is a decrease in Langmuir sorption capacity of all gases and vapors when 30 wt % FS nanoparticles were added to PTMSP. The Langmuir sorption capacity characterizes sorption in the nonequilibrium excess free volume of a

glassy polymer [10]. The addition of low sorbing FS nanoparticles dilutes the nonequilibrium excess free volume in the nanocomposite films. The FS and the voids that are introduced with the FS contribute to the overall film volume, but they contribute little to gas sorption, so the sorption properties of PTMSP are diluted by the presence of the particles and voids, which acts, in this case, to reduce the effective Langmuir capacity parameter. For both neat and nanocomposite films, C'_H increases as temperature decreases. This result is consistent with the non-equilibrium excess volume in a glassy polymer increasing as temperature decreases [3,9,11].

In *Figure 5.9* the Henry's law parameter, k_D , of CH_4 , C_2H_6 , C_3H_8 , and $n\text{-C}_4\text{H}_{10}$ are presented as a function of temperature for neat and nanocomposite uncrosslinked PTMSP. The nanocomposite samples have measurably lower Henry's law constants for C_3H_8 and $n\text{-C}_4\text{H}_{10}$ sorption than those associated with the neat samples, while the k_D values of CH_4 and C_2H_6 are unchanged by the FS addition.

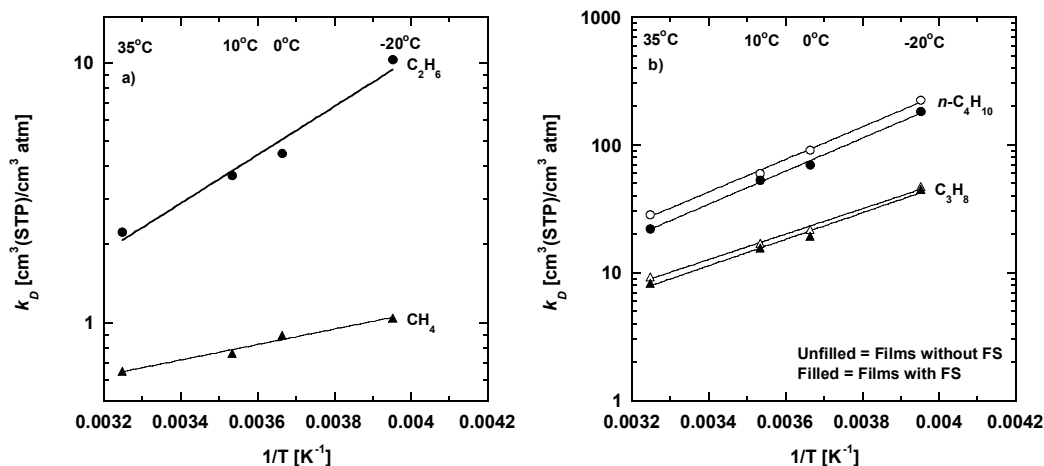


Figure 5.9. Effect of temperature on Henry's Law parameter, k_D , for a) CH₄ and C₂H₆; and b) C₃H₈ and *n*-C₄H₁₀ in uncrosslinked PTMSP and uncrosslinked PTMSP containing 30 wt % FS. The parameters were calculated using total film volume. All films were subjected to vacuum at 180°C for 90 minutes, soaked in MeOH for 24 hours, and then dried for 72 hours in ambient conditions before sorption isotherms were measured.

In Figure 5.10 the Langmuir affinity parameter, b , for N₂, O₂, CH₄, C₂H₆, C₃H₈, and *n*-C₄H₁₀ are presented as a function of temperature for neat and nanocomposite uncrosslinked PTMSP. The Langmuir affinity parameters of all gases and vapors are not affected by FS addition, so FS nanoparticles do not appear to interfere with the affinity of these gases for the Langmuir sites.

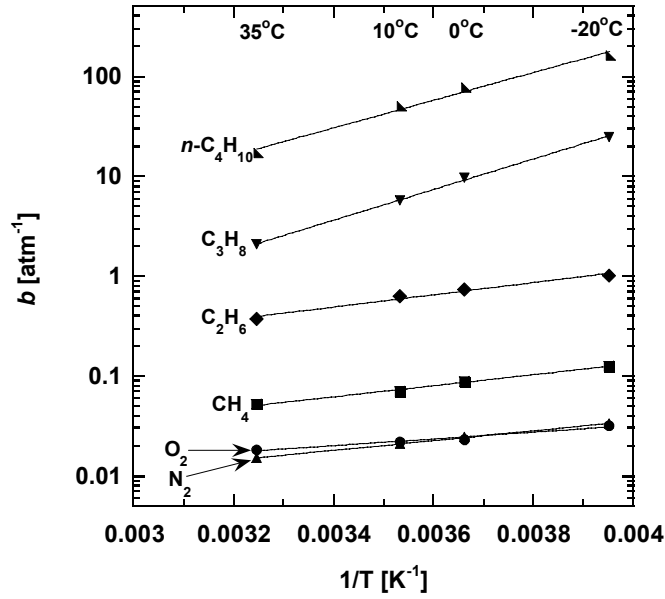


Figure 5.10. Effect of temperature on Langmuir affinity parameter, b , of N_2 , O_2 , CH_4 , C_2H_6 , C_3H_8 , and $n-C_4H_{10}$ in uncrosslinked PTMSP and uncrosslinked PTMSP containing 30 wt % FS. The parameters were calculated using total film volume. All films were subjected to vacuum conditions at 180°C for 90 minutes, soaked in MeOH for 24 hours, and then dried for 72 hours in ambient conditions before sorption isotherms were measured.

The effect of temperature on k_D and b is typically described as follows [12]:

$$k_D = k_{D0} \exp\left(\frac{-\Delta H_D}{RT}\right) \quad (5.1)$$

$$b = b_0 \exp\left(\frac{-\Delta H_b}{RT}\right) \quad (5.2)$$

where k_{D0} and b_0 are constants, ΔH_D is the enthalpy change of sorption in the Henry's law region, and ΔH_b is the enthalpy change of the Langmuir affinity parameter. The values of k_D and b increase with decreasing temperature for all gases and vapors in this study, and the increase is mainly caused by penetrant condensability increasing with decreasing

temperature. The values of ΔH_D for CH_4 and $n\text{-C}_4\text{H}_{10}$ in neat uncrosslinked PTMSP are -5.7 ± 0.7 kJ/mol, and -24 ± 2 kJ/mol, respectively. The value of ΔH_D for $n\text{-C}_4\text{H}_{10}$ in nanocomposite uncrosslinked PTMSP is also -24 ± 2 kJ/mol. These values are very similar to those reported by Raharjo *et al.* of -5.8 ± 0.5 kJ/mol, and -24 ± 2 kJ/mol [9]. The enthalpy of condensation of $n\text{-C}_4\text{H}_{10}$ at 7.5°C (*i.e.*, the midpoint temperature of this study) is -22 kJ/mol [13], which is comparable to ΔH_D of $n\text{-C}_4\text{H}_{10}$ in PTMSP. The values of ΔH_b for CH_4 and $n\text{-C}_4\text{H}_{10}$ in PTMSP are -11 ± 1 kJ/mol, and -26 ± 2 kJ/mol, respectively. These values are very similar to those reported by Raharjo *et al.* (*i.e.*, -11 ± 1 kJ/mol and -29 ± 2 kJ/mol, respectively).

5.3) Solubility Coefficients of Neat and Nanocomposite PTMSP

The solubility coefficients of CH_4 and $n\text{-C}_4\text{H}_{10}$ in neat and nanocomposite PTMSP are presented at various temperatures in *Figure 5.11*. The solubility coefficients are presented as a function of fugacity or, in the case of $n\text{-C}_4\text{H}_{10}$, activity. The dual-mode sorption model fit to the solubilities, based on the parameters presented in Table 5.2, is shown as the smooth lines through the data. The solubilities of neat and nanocomposite crosslinked films are very similar to their uncrosslinked analogues due to the equivalency of their sorption isotherms. Similar figures presenting the solubility of N_2 , O_2 , C_2H_6 , and C_3H_8 in neat and nanocomposite PTMSP are presented in the appendix and are qualitatively consistent with the results presented in *Figure 5.11*.

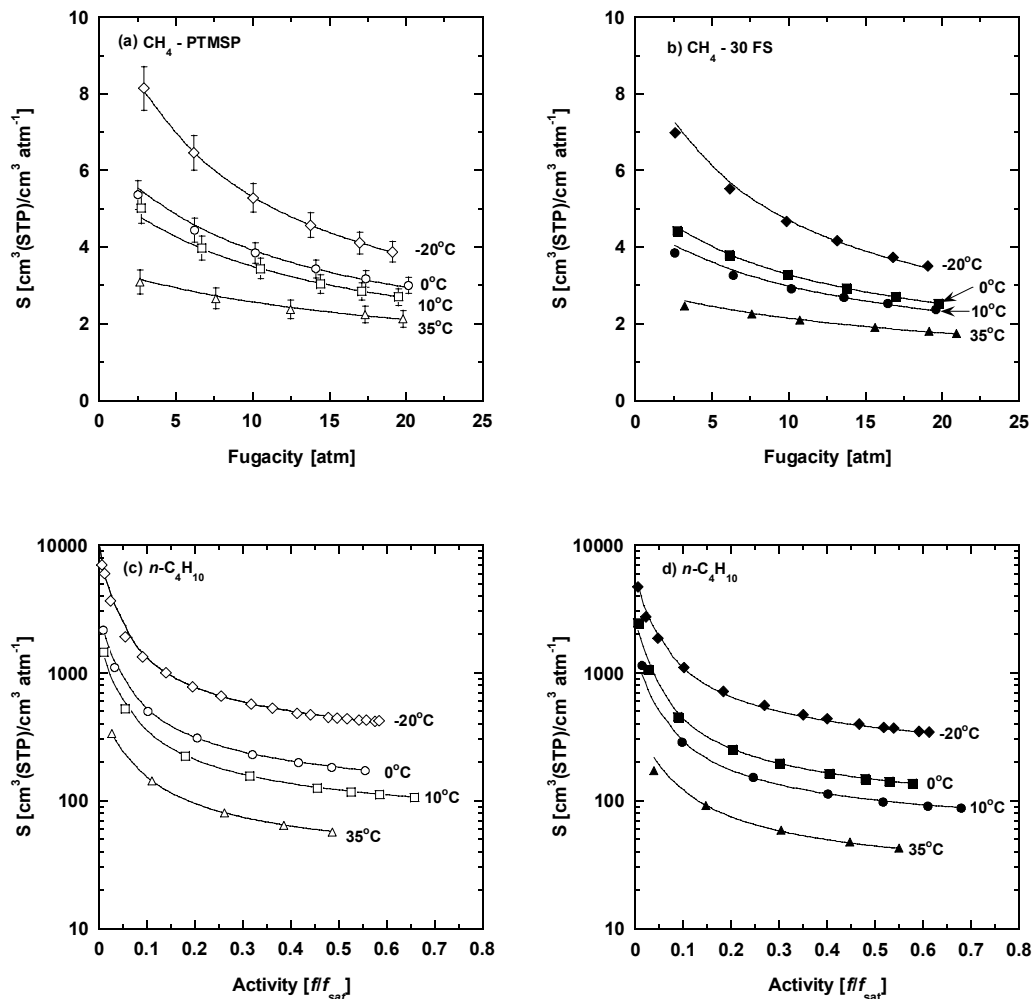


Figure 5.11. Effect of fugacity and temperature on CH_4 , and $n\text{-C}_4\text{H}_{10}$ solubilities in neat (PTMSP) and nanocomposite (30 FS) uncrosslinked PTMSP. The CH_4 solubilities are plotted as a function of CH_4 fugacity, while the $n\text{-C}_4\text{H}_{10}$ solubilities are plotted as function of $n\text{-C}_4\text{H}_{10}$ activity. All films were subjected to vacuum conditions at 180°C for 90 minutes, soaked in MeOH for 24 hours, and then dried for 72 hours in ambient conditions before sorption isotherms were measured. The solid lines represent the dual-mode sorption model fit to the solubility data. The saturation fugacity values, f_{sat} , were calculated as described in the literature [14].

At all experimental points the solubilities of neat uncrosslinked films are greater than the solubilities of nanocomposite films, which is a consequence of the sorption

isotherms of nanocomposite films being less than the neat films. The solubility of CH_4 and $n\text{-C}_4\text{H}_{10}$ in PTMSP increases as temperature decreases, and a greater relative increase in solubility with decreasing temperature is observed for the more condensable $n\text{-C}_4\text{H}_{10}$.

Figure 5.12 presents the influence of temperature on the solubility coefficients of CH_4 at 10 atm fugacity and $n\text{-C}_4\text{H}_{10}$ at an activity of 0.4 for neat uncrosslinked PTMSP and nanocomposite uncrosslinked PTMSP containing 30 wt % FS. The CH_4 and $n\text{-C}_4\text{H}_{10}$ solubility coefficients were fit to Equation 2.15.

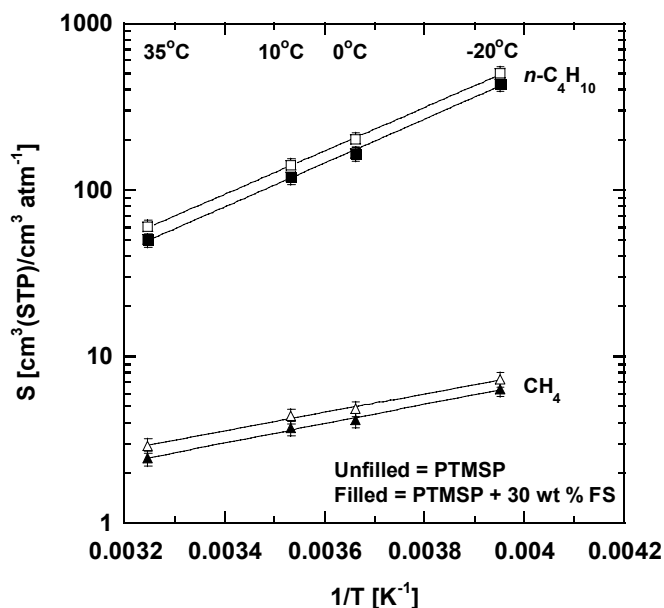


Figure 5.12. Effect of temperature on CH_4 solubility at 10 atm fugacity, and $n\text{-C}_4\text{H}_{10}$ solubility at an activity of 0.4 in uncrosslinked PTMSP and uncrosslinked PTMSP containing 30 wt % FS. The solubilities were calculated using the dual-mode sorption parameters for the films at the various temperatures. The total volume of the films in the sorption cell was used as the basis to calculate the solubilities. All films were subjected to vacuum at 180°C for 90 minutes, soaked in MeOH for 24 hours, and then dried for 72 hours in ambient conditions before sorption isotherms were measured.

As temperature decreases, the $n\text{-C}_4\text{H}_{10}$ solubility coefficients increase more than the CH_4 solubility coefficients. The solubility coefficients of neat PTMSP are greater than those of nanocomposite PTMSP, but the relative change in solubility with temperature is similar. The enthalpies of sorption for CH_4 and $n\text{-C}_4\text{H}_{10}$ in neat and nanocomposite PTMSP are shown in Table 5.3.

Table 5.3. Activation energies of sorption for CH_4 and $n\text{-C}_4\text{H}_{10}$ in neat and nanocomposite uncrosslinked PTMSP.

Gas	Film	ΔH_S [kJ/mol]	Reference
CH_4	PTMSP	-11 ± 1	This work
	PTMSP	- 9.9	Raharjo <i>et al.</i> [9]
	30 FS	-11 ± 1	This work
$n\text{-C}_4\text{H}_{10}$	PTMSP	-25 ± 2	This work
	PTMSP	- 25.5	Raharjo <i>et al.</i> [9]
	30 FS	-25 ± 2	This work

The enthalpies of sorption of neat uncrosslinked PTMSP are in good agreement with values from Raharjo *et al.* [9]. The enthalpy of sorption of $n\text{-C}_4\text{H}_{10}$ is less than that of CH_4 , which is expected since enthalpies of sorption often decrease with increasing critical temperature [4]. N_2 , O_2 , C_2H_6 , and C_3H_8 solubility coefficients exhibit qualitatively similar trends with temperature as CH_4 and $n\text{-C}_4\text{H}_{10}$, and the relationships between N_2 , O_2 , C_2H_6 , and C_3H_8 solubility and temperature are presented in the appendix.

5.4) Conclusions

The addition of crosslinks causes no significant change in gas and vapor solubility of PTMSP, while the addition of 30 wt % FS to uncrosslinked and crosslinked samples decreases gas and vapor solubility by 10 – 20 %. The dual-mode sorption model was successfully fitted to the sorption isotherms for all PTMSP films, and the decrease in solubility of the nanocomposite samples could be described by a decrease in the number of non-equilibrium sorption sites, represented by C'_H , the Langmuir sorption capacity. No change in the relative increase in solubility with decreasing temperature was observed for PTMSP when crosslinks and FS nanoparticles were added to the polymer.

5.5) References

- [1] S. V. Dixon-Garrett, K. Nagai, and B. D. Freeman, Sorption, diffusion, and permeation of ethylbenzene in poly[1-(trimethylsilyl)-1-propyne], *Journal of Polymer Science, Part B: Polymer Physics*, 38 (2000) 1078-89.
- [2] T. Masuda, Y. Iguchi, B. Z. Tang, and T. Higashimura, Diffusion and solution of gases in substituted polyacetylene membranes, *Polymer*, 29 (1988) 2041-9.
- [3] T. C. Merkel, V. Bondar, K. Nagai, and B. D. Freeman, Sorption and transport of hydrocarbon and perfluorocarbon gases in poly[1-(trimethylsilyl)-1-propyne], *Journal of Polymer Science, Part B: Polymer Physics*, 38 (2000) 273-96.
- [4] T. C. Merkel, Z. He, I. Pinnau, B. D. Freeman, P. Meakin, and A. J. Hill, Effect of nanoparticles on gas sorption and transport in poly[1-(trimethylsilyl)-1-propyne], *Macromolecules*, 36 (2003) 6844-55.
- [5] S. D. Kelman, S. Matteucci, C. W. Bielawski, and B. D. Freeman, Crosslinking poly[1-(trimethylsilyl)-1-propyne] and its effect on solvent resistance and transport properties, *Polymer*, 48 (2007) 6881-92.
- [6] A. Morisato, B. D. Freeman, I. Pinnau, and C. G. Casillas, Pure hydrocarbon sorption properties of poly[1-(trimethylsilyl)-1-propyne] (PTMSP), poly(1-

- phenyl-1-propyne) (PPP), and PTMSP/PPP blends, *Journal of Polymer Science, Part B: Polymer Physics*, 34 (1996) 1925-34.
- [7] R. Srinivasan, S. R. Auvil, and P. M. Burban, Elucidating the mechanism(s) of gas transport in poly[1-(trimethylsilyl)-1-propyne] (PTMSP) membranes, *Journal of Membrane Science*, 86 (1994) 67-86.
- [8] L. C. Witchey-Lakshmanan, H. B. Hopfenberg, and R. T. Chern, Sorption and transport of organic vapors in poly[1-(trimethylsilyl)-1-propyne], *Journal of Membrane Science*, 48 (1990) 321-31.
- [9] R. D. Raharjo, B. D. Freeman, and E. S. Sanders, Pure and mixed gas CH₄ and *n*-C₄H₁₀ sorption and dilation in poly[1-(trimethylsilyl)-1-propyne], *Polymer*, 48 (2007) 6097-114.
- [10] S. Matteucci, Y. Yampolskii, B. D. Freeman, and I. Pinnau, in: Y. Yampolskii, B. D. Freeman, I. Pinnau (Eds.), *Material Science of Membranes for Gas and Vapor Separation*, John Wiley & Sons, New York, 2006, pp. 1-47.
- [11] M. S. McCaig, D. R. Paul, and J. W. Barlow, Effect of film thickness on the changes in gas permeability of a glassy polyarylate due to physical aging part II. Mathematical model, *Polymer*, 41 (1999) 639-48.
- [12] W. J. Koros, D. R. Paul, and G. S. Huvar, Energetics of gas sorption in glassy polymers, *Polymer*, 20 (1979) 956-60.
- [13] <http://dippr.byu.edu/public/chemsearch.asp>
- [14] R. D. Raharjo, B. D. Freeman, and E. S. Sanders, Pure and mixed gas CH₄ and *n*-C₄H₁₀ sorption and dilation in poly(dimethylsiloxane), *Journal of Membrane Science*, 292 (2007) 45-61.

6) Pure Gas Permeability and Diffusivity

This chapter presents the influence of crosslinking and FS addition on the pure gas permeability and diffusivity of PTMSP. The N_2 , O_2 , CH_4 , C_2H_6 , C_3H_8 , and $n-C_4H_{10}$ permeabilities were measured in various PTMSP films at temperatures ranging from -20°C to 35°C , and at fugacities ranging from 0 to 18 atm. The permeability coefficients were fit to the dual-mode transport model where applicable. Conditioning effects of the permeating gases were studied by measuring the permeability as the films were depressurized from their maximum pressure to atmospheric pressure. The diffusivities were calculated from the measured permeabilities and solubilities, and the diffusivities were related to the concentration of penetrant in the polymer via the dual-mode transport model.

6.1) Permanent Gas Permeability

The N_2 , O_2 , and CH_4 permeabilities of neat and nanocomposite uncrosslinked and crosslinked PTMSP at 35°C are presented in *Figure 6.1* as a function of upstream fugacity. The light gas permeabilities of uncrosslinked PTMSP at 35°C are similar to those reported by Merkel *et al.* [1]. The addition of crosslinks to PTMSP causes N_2 , O_2 , and CH_4 permeabilities to decrease substantially, and this result has been correlated with a decrease in FFV that accompanies crosslinking [2]. The addition of 30 wt % FS to uncrosslinked and crosslinked PTMSP increases the light gas permeability by 50 - 65 %, and this increase is similar to that reported by Merkel *et al.*, and De Sitter *et al.* at the

same FS loading [3,4]. This result suggests the FS dispersion properties of our films should be similar to those reported in the literature [3,5].

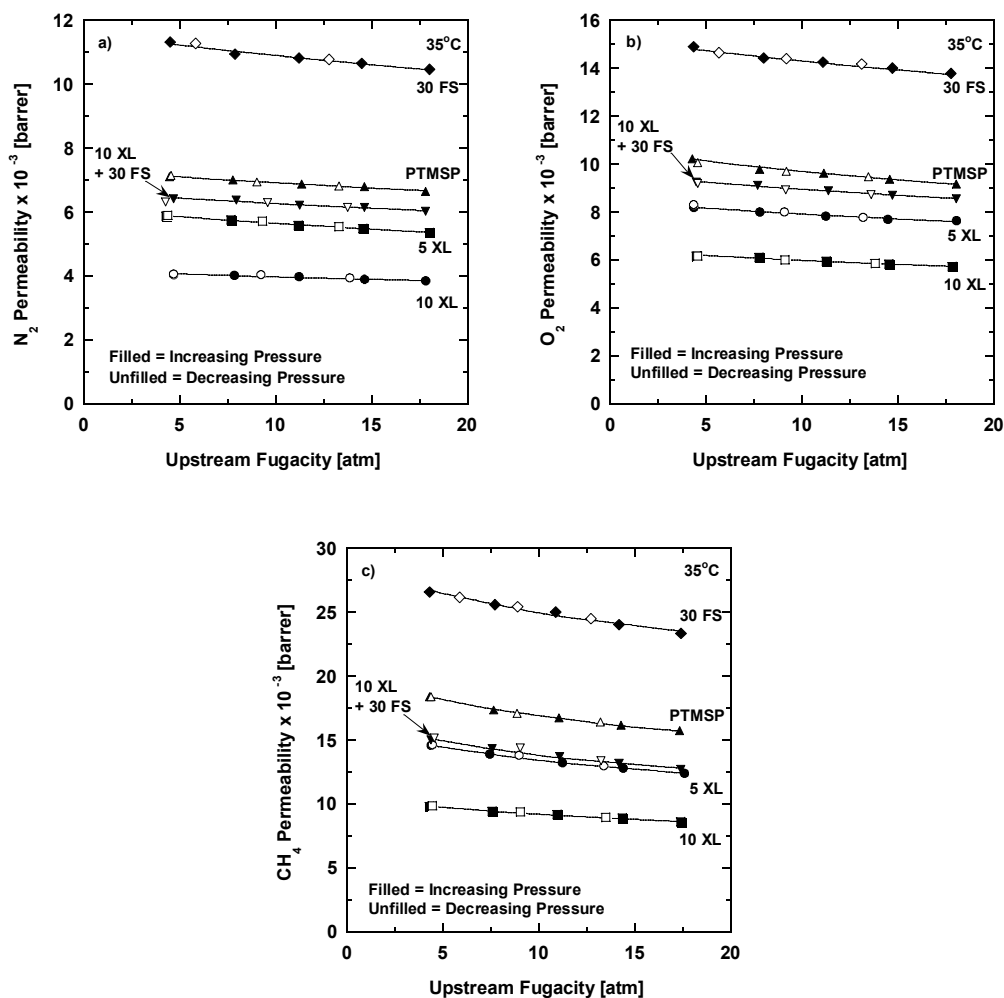


Figure 6.1. Permeability of a) N_2 , b) O_2 , and c) CH_4 as a function of upstream fugacity in various PTMSP films at 35°C. The downstream pressure was fixed at atmospheric. The solid lines represent a nonlinear least squares fit of the dual-mode transport model to the permeability data. All films were subjected to vacuum at 180°C for 90 minutes, soaked in MeOH for 24 hours, and then dried for 72 hours in ambient conditions before permeability was measured. All films were approximately 100 μm thick.

In *Figure 6.2* the N_2 , O_2 , and CH_4 permeabilities at 0°C of various PTMSP films are presented as a function of fugacity. Analogous to the results at 35°C , the addition of crosslinks decreases permeability, while FS nanoparticle addition increases permeability. The magnitudes of the changes in N_2 , O_2 , and CH_4 permeability at 0°C due to crosslink and FS addition are similar to those observed at 35°C . For brevity, the N_2 , O_2 , and CH_4 permeabilities at 10°C and -20°C are presented in the appendix. At 10°C and -20°C the addition of crosslinks and FS to PTMSP causes changes in permeability similar to those observed at 35°C and 0°C .

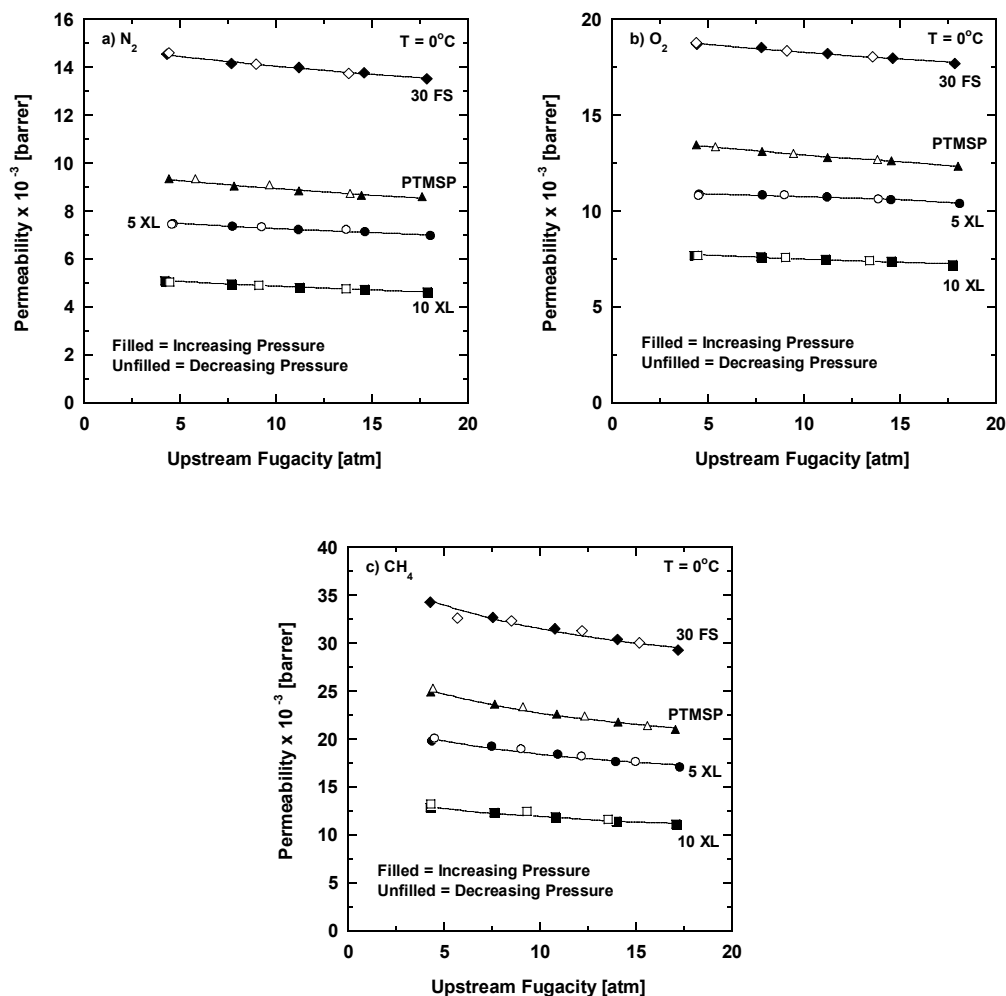


Figure 6.2. Permeability of a) N₂, b) O₂, and c) CH₄ as a function of upstream fugacity in various PTMSP films at 0°C. The downstream pressure was fixed at atmospheric. The solid lines represent a nonlinear least squares fit of the dual-mode transport model to the permeability data. All films were subjected to vacuum at 180°C for 90 minutes, soaked in MeOH for 24 hours, and then dried for 72 hours in ambient conditions before permeability was measured. All films were approximately 100 μm thick.

The N₂, O₂, and CH₄ permeabilities decrease with increasing fugacity at all temperatures, and this result is consistent with previous studies for PTMSP [1]. The relative decreases in N₂, O₂, and CH₄ permeabilities at 35°C with increasing fugacity are

similar for all films, so the addition of crosslinks and FS nanoparticles does not affect the pressure dependence of light gas permeability. This same result is also found at 10°C, 0°C and -20°C. The decrease in the light gas permeability with increasing fugacity is slightly greater for CH₄ than for N₂ and O₂. For example, at 35°C the CH₄ permeabilities of the 5 films in this study decrease by an average of 13 % when the gas fugacity increases from 4.5 atm to 18 atm, while the N₂ and O₂ permeabilities of the same films decrease by an average of 7 % over the same fugacity range. The decreases in N₂, O₂, and CH₄ permeabilities at 10°C, 0°C, and -20°C with increasing fugacity are similar, within experimental error, to those observed at 35°C. The permeabilities in *Figure 6.1* and *Figure 6.2* were fit to the dual-mode transport model shown in Equation 2.8, and a good fit is found for all gases and for all films. The dual-mode transport model also fits well to the N₂, O₂, and CH₄ permeability data for the various PTMSP films at 10°C, and -20°C (*cf.*, appendix).

The N₂, O₂ and CH₄ permeabilities were measured as films were depressurized, and these data points are the unfilled symbols in *Figure 6.1* and *Figure 6.2*. For all films, the N₂, O₂, and CH₄ permeabilities measured as the pressure decreases lie on the same trendline formed by the permeability values measured as feed pressure was increased. This same result is also observed at 10°C, and -20°C (*cf.*, appendix). Therefore, no conditioning was observed for N₂, O₂, and CH₄ permeation.

It is shown in Chapter 4 that the addition of crosslinks decreases the number of large free volume elements in PTMSP according to PALS. The changes in the free volume characteristics of PTMSP caused by the addition of FS nanoparticles were not

investigated by PALS. However, PALS was undertaken on uncrosslinked and crosslinked films containing 30 wt % TiO_2 nanoparticles. Similar to FS, the addition of TiO_2 nanoparticles increases the permeability of uncrosslinked and crosslinked PTMSP substantially, and the permeabilities and PALS parameters of the neat and nanocomposite films are recorded in Table 6.1. It is expected that changes in the PALS parameters of PTMSP due to FS addition will be analogous to the changes observed for TiO_2 addition, because a similar mechanism is thought to cause the permeability increase of PTMSP films containing FS and TiO_2 nanoparticles [4,6].

Table 6.1 Permeability and PALS parameters of neat and nanocomposite PTMSP^a

Film	P_{N_2} (barrer)^b	τ_4 (ns)	I_4 (%)
PTMSP	6,500 \pm 900	9.6 \pm 0.1	38.8 \pm 0.1
5 XL	4,200 \pm 700	9.4 \pm 0.1	29.1 \pm 0.1
30 TiO_2	11,000 \pm 2,000	10.2 \pm 0.1	27.2 \pm 0.1
5 XL + 30 TiO_2	8,000 \pm 1,000	9.9 \pm 0.1	22.8 \pm 0.1

a) TiO_2 nanoparticles have effective single particle diameter of 15 nm.

b) $T = 35^\circ\text{C}$, $f_2 = 4.4$ atm, and $f_1 =$ atmospheric for all permeation measurements.

The addition of TiO_2 nanoparticles increases the size of the large free volume elements represented by τ_4 in uncrosslinked and crosslinked PTMSP. Merkel *et al.* found a similar effect for FS addition to uncrosslinked PTMSP [4]. There is a decrease in the concentration of the large free volume elements (τ_4) in uncrosslinked and crosslinked films due to TiO_2 addition, and this decrease could be caused by nanoparticles diluting the concentration of large free volume elements. The change in the values of the two longest lifetimes, τ_3 and τ_4 , observed by PALS is presented graphically in *Figure 6.3*.

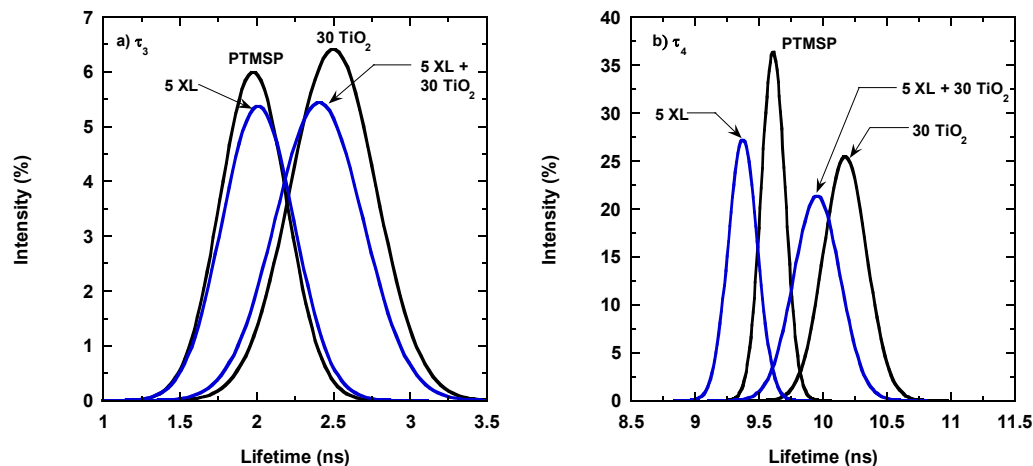


Figure 6.3. Effect of the addition of 30 wt % TiO_2 nanoparticles to uncrosslinked and crosslinked PTMSP on a) τ_3 and b) τ_4 as measured by PALS. The TiO_2 nanoparticles have an effective single particle diameter of 15 nm.

The values of τ_4 and its associated intensity, or concentration, change significantly when 30 wt % TiO_2 is added to the uncrosslinked and crosslinked films, while there is a small increase in the size of the small free volume elements, represented by τ_3 , and no significant change in the intensity of τ_3 .

Figure 6.4 presents the influence of temperature on N_2 , O_2 , and CH_4 permeabilities at 4.4 atm upstream fugacity. This upstream fugacity value was chosen for comparison since data were available for all gases at this fugacity.

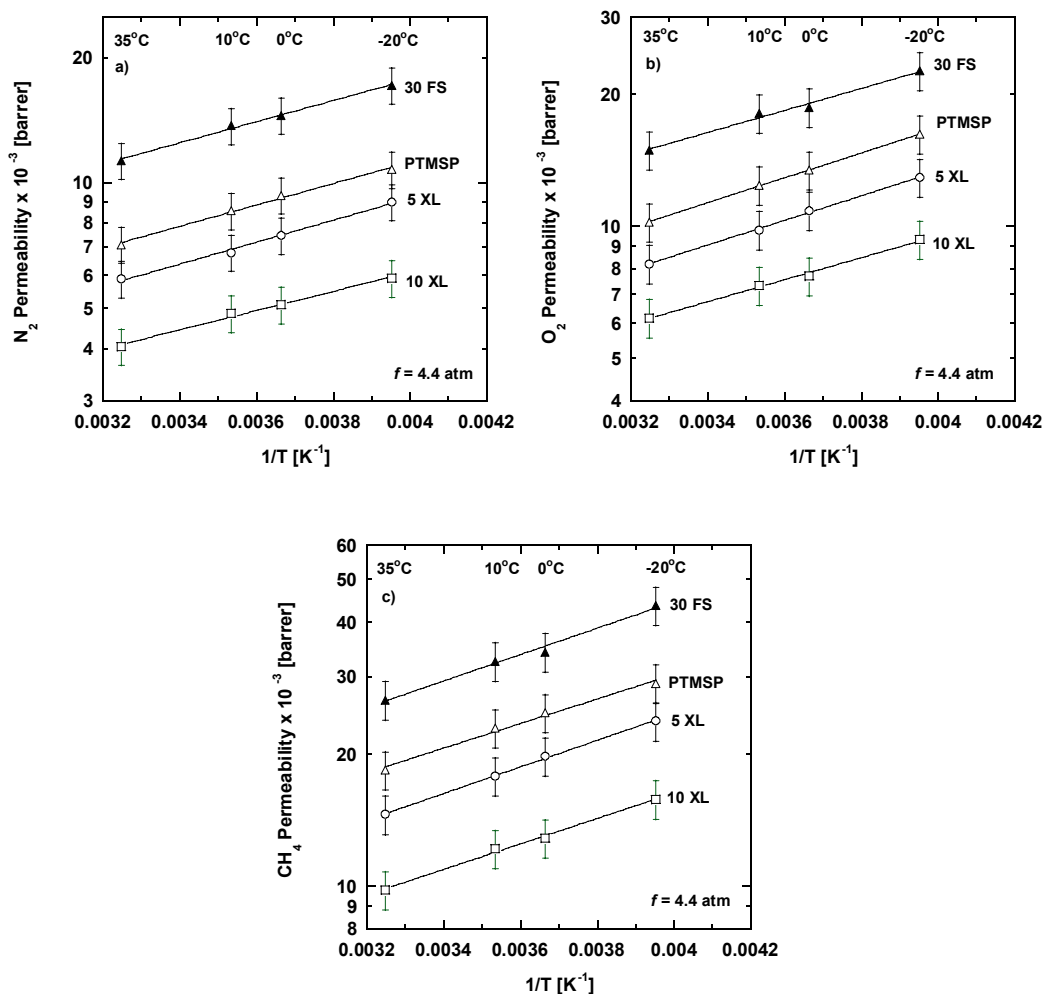


Figure 6.4. Temperature dependence of a) N_2 , b) O_2 , and c) CH_4 permeability at 4.4 atm upstream fugacity in various PTMSP films. The downstream pressure was fixed at atmospheric. The data were fit to an Arrhenius relationship shown in Equation 2.14. All films were subjected to vacuum at 180°C for 90 minutes, soaked in MeOH for 24 hours, and then dried for 72 hours in ambient conditions before permeability was measured. All films were approximately 100 μm thick.

All permeabilities increase as temperature decreases, and this result is in good agreement with previous literature reports [5,7-9]. The magnitude of the permeability increase is similar in uncrosslinked and crosslinked PTMSP, so the addition of crosslinks does not

influence the temperature dependence of light gas permeation. The addition of 30 wt % FS to PTMSP also causes no change in the temperature dependence of light gas permeation, which agrees with results reported by Merkel *et al.* [4]. The activation energies of permeation for uncrosslinked PTMSP were calculated using Equation 2.14, and they are recorded in Table 6.2. These values are in good agreement with those reported by Masuda *et al.* [7].

Table 6.2. Activation energies of N₂, O₂, and CH₄ permeation for uncrosslinked PTMSP.

Gas	E_P [kJ/mol]	Reference
N ₂	- 4.9 ± 0.7	This study
	- 5.1	Masuda <i>et al.</i> [7]
O ₂	- 5.5 ± 0.9	This study
	- 6.7	Masuda <i>et al.</i> [7]
CH ₄	- 5.4 ± 0.9	This study
	-6.3	Masuda <i>et al.</i> [7]

6.2) Vapor Permeability

Figure 6.5 presents C₂H₆ and C₃H₈ permeabilities at 35°C for various neat and nanocomposite uncrosslinked and crosslinked PTMSP films. As observed for N₂, O₂, and CH₄ permeation, crosslinking decreases C₂H₆ and C₃H₈ permeabilities. The addition of 30 wt % FS nanoparticles increases the C₂H₆ and C₃H₈ permeabilities of uncrosslinked and crosslinked PTMSP by 30 – 40 %, and this increase is less than the increase in N₂, O₂ and CH₄ permeabilities due to 30 wt % FS nanoparticle addition. This result is consistent

with findings by Merkel *et al.*, where the permeability increase due to the addition of 50 wt % FS nanoparticles was less for C_2H_6 and C_3H_8 than for smaller, lighter gases such as H_2 and CH_4 . The incorporation of FS nanoparticles into PTMSP may lead to an increase in pore-flow transport mechanisms (*e.g.*, Knudsen flow), and smaller molecules will gain access to these faster transport processes more readily than larger gas molecules [4]. Consequently, the relative increase in permeability of small gas molecules is higher than that of larger gas molecules when FS nanoparticles are added to PTMSP [4].

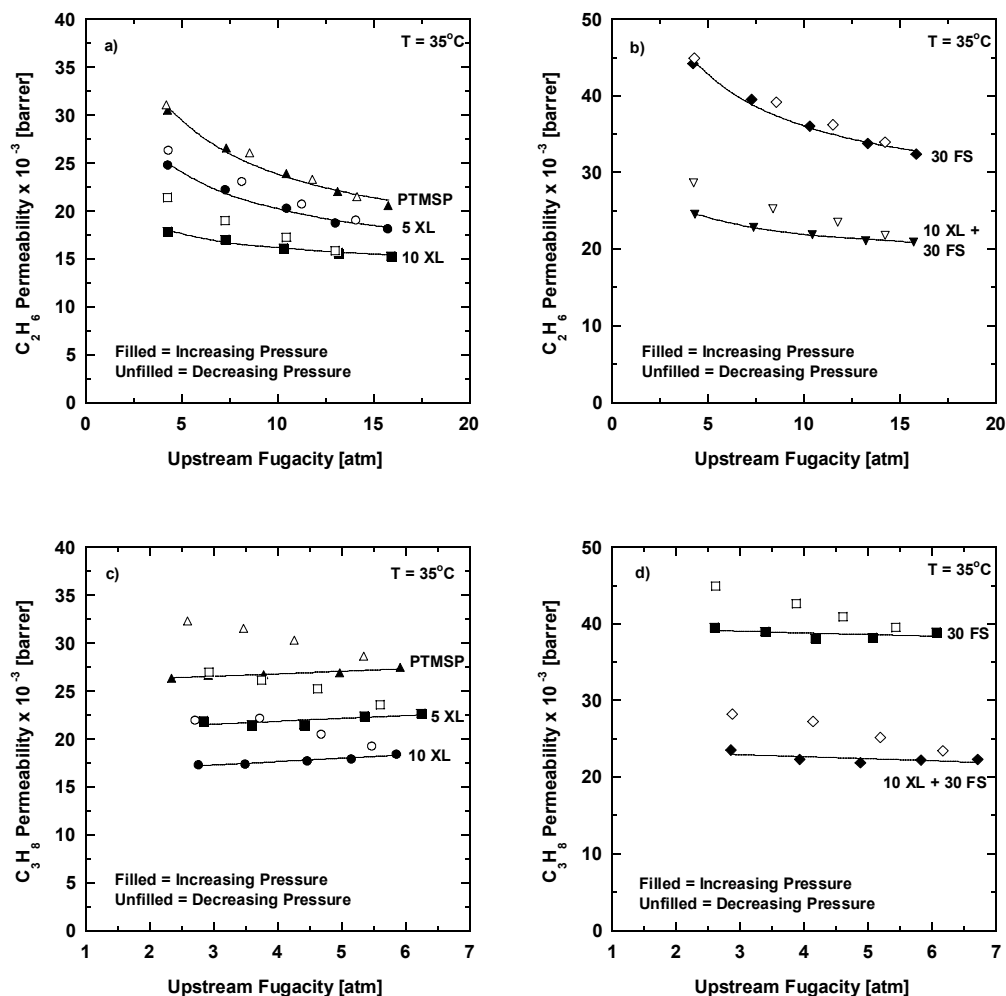


Figure 6.5. Permeability of a) C_2H_6 in neat PTMSP, b) C_2H_6 in nanocomposite PTMSP, c) C_3H_8 in neat PTMSP, and d) C_3H_8 in nanocomposite PTMSP as a function of upstream fugacity at $35^\circ C$. The downstream pressure was fixed at atmospheric. The C_2H_6 permeability data were fit to the dual-mode transport model, and the C_3H_8 permeability data were fit to a linear function. All films were subjected to vacuum at $180^\circ C$ for 90 minutes, soaked in MeOH for 24 hours, and then dried for 72 hours in ambient conditions before permeability was measured. All films were approximately $100\ \mu m$ thick.

The permeabilities of C_2H_6 and C_3H_8 at $0^\circ C$ are presented in *Figure 6.6*. Similar to the observations made at $35^\circ C$ the increase in C_2H_6 permeability due to the addition of

30 wt % FS nanoparticles is less than the increase observed for N_2 , O_2 and CH_4 at $0^\circ C$. The permeabilities of C_2H_6 and C_3H_8 at $10^\circ C$, and $-20^\circ C$ are presented in the appendix, and the same trends observed for C_2H_6 and C_3H_8 permeation at $35^\circ C$ and $0^\circ C$ are observed at these temperatures.

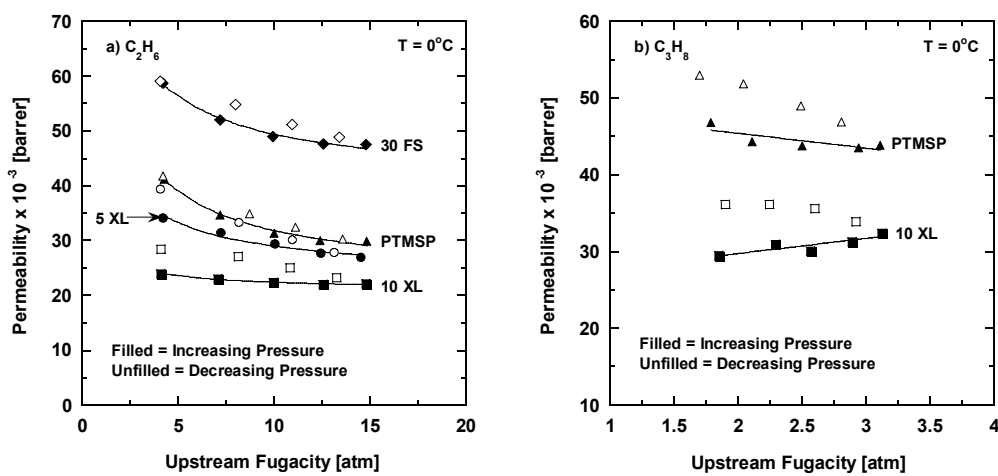


Figure 6.6. Permeability of a) C_2H_6 and b) C_3H_8 in as a function of upstream fugacity at $0^\circ C$. The downstream pressure was fixed at atmospheric. The C_2H_6 permeability data were fit to the dual-mode transport model, and the C_3H_8 permeability data were fit to a linear function. All films were subjected to vacuum at $180^\circ C$ for 90 minutes, soaked in MeOH for 24 hours, and then dried for 72 hours in ambient conditions before permeability was measured. All films were approximately $100\mu m$ thick.

The C_2H_6 permeabilities and the fugacity dependence of the C_2H_6 permeabilities in uncrosslinked PTMSP shown in *Figure 6.5* are similar to those reported by Merkel *et al.* at $35^\circ C$ [1]. For example, the C_2H_6 permeability of uncrosslinked PTMSP decreases from 30,000 barrer to 20,000 barrer as the upstream C_2H_6 fugacity increases from 4.2 atm to 16 atm, while Merkel *et al.* observed the C_2H_6 permeabilities of PTMSP to decrease from 27,000 barrer to 17,000 barrer when upstream C_2H_6 fugacity increased from 2.5 atm

to 11 atm [1]. In contrast, the C_3H_8 permeabilities and the fugacity dependence of C_3H_8 permeabilities in uncrosslinked PTMSP observed in this study (*cf.* Figure 6.5) are somewhat different from those reported by Merkel *et al.* at 35°C [1]. For example, the C_3H_8 permeability of uncrosslinked PTMSP increases from 26,000 barrer to 27,000 barrer as the upstream C_3H_8 fugacity increases from 2.3 atm to 5.9 atm. An increase in the C_3H_8 permeability with increasing C_3H_8 fugacity is consistent with C_3H_8 lightly plasticizing PTMSP [4]. Merkel *et al.* observed the C_3H_8 permeability of PTMSP to decrease from 35,000 barrer to 27,000 barrer when upstream C_3H_8 fugacity increased from 1.2 atm to 4.0 atm [1].

A possible explanation for the difference in the fugacity dependence of the C_3H_8 permeabilities could be that related to differences in film processing history. An example of film history effecting the fugacity dependence of C_3H_8 permeation in PTMSP can be seen by comparing the reported C_3H_8 permeabilities of PTMSP in two studies by Merkel *et al.* [1,4]. The first study by Merkel *et al.* is the study used to compare the results for uncrosslinked PTMSP, and films in this study were soaked in MeOH after being cast [1]. In another study by Merkel *et al.*, the C_3H_8 permeability at 25°C of PTMSP increased from 37,000 barrer to 48,000 barrer as the upstream fugacity of C_3H_8 increased from 1.7 atm to 7.3 atm [4]. The PTMSP films in the second Merkel *et al.* study were not soaked in MeOH after the film casting [4]. The dependence of C_2H_6 permeabilities on upstream C_2H_6 fugacity were similar in both Merkel *et al.* studies [1,4]. Therefore, soaking PTMSP in MeOH apparently significantly changes the fugacity dependence of C_3H_8 permeation in PTMSP. The two Merkel *et al.* studies were performed at different temperatures [1,4].

However, this difference in temperature should not change the fugacity dependence of C_2H_6 and C_3H_8 permeation in PTMSP, because the fugacity dependence of C_2H_6 and C_3H_8 permeability in uncrosslinked PTMSP in this study is similar at 35°C, 10°C, 0°C, and -20°C.

The two Merkel *et al.* studies suggest that film history plays a role in determining the fugacity dependence of C_3H_8 permeation in PTMSP. In this work, the uncrosslinked PTMSP films were thermally annealed at 180°C in vacuum for 90 minutes after film casting, while PTMSP films in the Merkel *et al.* study were not subjected to any such thermal treatment [1]. This difference in thermal history could lead to differences in the fugacity dependence of C_3H_8 permeation in PTMSP, presumably as a result of the influence of the thermal treatment process on the resulting non-equilibrium excess volume and excess volume distribution in the samples.

In *Figure 6.5* and *Figure 6.6* the relative decrease in C_2H_6 permeability of neat and nanocomposite crosslinked PTMSP films with increasing fugacity is less than the relative decrease in C_2H_6 permeability of neat and nanocomposite uncrosslinked PTMSP films. The C_2H_6 permeabilities were fit to the dual-mode transport model in Equation 2.8, and the effective diffusion coefficients of C_2H_6 in the Henry's law and Langmuir regions at 35°C are recorded in Table 6.3.

Table 6.3. Dual-mode diffusion coefficients for C₂H₆ in various PTMSP films at 35°C.

Film	$\bar{D}_D \times 10^5 [\text{cm}^2/\text{s}]$	$\bar{D}_H \times 10^5 [\text{cm}^2/\text{s}]$
PTMSP	5.2 ± 0.5	1.8 ± 0.2
5 XL	4.9 ± 0.5	1.2 ± 0.1
10 XL	4.7 ± 0.5	0.5 ± 0.1
30 FS	8.8 ± 0.9	2.7 ± 0.3
10 XL + 30 FS	6.3 ± 0.6	0.9 ± 0.1

In the Henry's law region, the diffusion coefficients are similar for the neat uncrosslinked PTMSP film and the neat crosslinked PTMSP films. The addition of FS nanoparticles to uncrosslinked and crosslinked PTMSP increases the Henry's law diffusivity of the uncrosslinked and crosslinked PTMSP films. This result is consistent with the observed free volume increases due to FS nanoparticle addition [4]. The C₂H₆ diffusivity in the Langmuir sites of the crosslinked PTMSP films is significantly less than the Langmuir diffusivity of C₂H₆ in the uncrosslinked PTMSP films. The decrease in the Langmuir diffusivity of C₂H₆ in crosslinked PTMSP is a result of C₂H₆ permeability of crosslinked PTMSP films being less sensitive to changes in C₂H₆ fugacity. The trends of the diffusion coefficients in the Henry's and Langmuir regions at 35°C are indicative of the trends observed at 10°C, 0°C and -20°C for C₂H₆ permeation in the various PTMSP films.

The permeabilities of C₂H₆ and C₃H₈ were measured as a function of increasing and decreasing fugacity, and the unfilled points in *Figure 6.5* and *Figure 6.6* represent the permeabilities measured during depressurization. An increase in permeability on depressurization suggests conditioning of PTMSP [1,10-12]. Conditioning has the effect

of “opening up” the polymer (*i.e.*, increasing its FFV), which increases penetrant permeability [13]. Increases in the permeability of PTMSP upon depressurization have also been reported for C₃F₈ [1] and ethylbenzene [10].

The neat and nanocomposite uncrosslinked PTMSP films show little increase in C₂H₆ permeability during depressurization at 35°C and 0°C (*cf.* Figure 6.5 and Figure 6.6), while a significant increase in C₂H₆ permeability is observed in the neat and nanocomposite crosslinked PTMSP films. For example, the C₂H₆ permeability at 35°C and 4.3 atm of crosslinked PTMSP containing 10 wt % crosslinker increases from 17,500 barrer initially to 21,500 barrer after depressurization. The increase in C₂H₆ permeability is maximized at lower fugacities. The difference in the C₂H₆ conditioning behavior of uncrosslinked and crosslinked PTMSP films could be related to the differences in how the free volume elements of uncrosslinked and crosslinked PTMSP films relax after exposure to highly sorbing penetrants such as C₂H₆ and C₃H₈ [11].

Koros *et al.* described the conditioning of glassy polymers as a process where highly sorbing penetrants introduce chain packing disruptions to the polymer matrix [11,12,14-16]. Upon depressurization, the free volume elements reorganize as the penetrant is removed from the polymer matrix, and if penetrant removal is sufficiently fast, the polymer free volume can be trapped in out-of-equilibrium conformations. These out-of-equilibrium conformations may display greater penetrant permeability than the conformations found during the initial pressurization of the film. The permeability increase on depressurization can be stable over time scales that are long relative to the measurement timescale [11].

Based upon the analysis by Koros *et al.*, when C_2H_6 is depressurized from crosslinked PTMSP films, the free volume distributions formed are different from those existing when the film is first pressurized with C_2H_6 . The free volume distributions produced on depressurization are likely to have a greater FFV than those existing prior to exposure to high feed pressures of C_2H_6 . Therefore, the C_2H_6 permeabilities in crosslinked PTMSP films measured during depressurization, and shown in *Figure 6.5* and *Figure 6.6*, are greater than C_2H_6 permeabilities measured as the films are pressurized. In contrast, the free volume distributions of uncrosslinked PTMSP films during C_2H_6 depressurization appear to be similar to the free volume distributions existing prior to pressurization. This conclusion is reached because there is no significant increase in C_2H_6 permeability in uncrosslinked PTMSP film during depressurization.

All PTMSP films in this study show significant increases in C_3H_8 permeability during depressurization, as illustrated in *Figure 6.5* and *Figure 6.6*. For example, the C_3H_8 permeability of uncrosslinked PTMSP at 35°C and 2.5 atm increases from 26,000 barrer initially to 32,000 barrer after depressurization. Unlike C_2H_6 permeation, the uncrosslinked PTMSP films show similar increases in C_3H_8 permeability on depressurization as crosslinked PTMSP films. Therefore, based on the picture of conditioning developed by Koros *et al.* [11], the free volume elements in uncrosslinked and crosslinked PTMSP films relax to conformations during C_3H_8 depressurization that have greater FFV than the free volume element distributions existing prior to exposure to high pressures of C_3H_8 . The increase in FFV on C_3H_8 depressurization should be similar

in all PTMSP films, as all films are observed to have similar increases in C_3H_8 permeability during C_3H_8 depressurization.

The relationship between the fugacity dependence of PTMSP permeability and conditioning behavior can be used to probe differences in the conditioning of various PTMSP films. Based on the C_2H_6 permeability data in *Figure 6.5* and *Figure 6.6* the lower the relative decrease in PTMSP permeability with increasing fugacity, the greater the increase in permeability when the film is depressurized. For example, the C_2H_6 permeability of uncrosslinked PTMSP at 35°C decreases from 30,000 barrer to 20,000 barrer (a 33 % decrease), as the fugacity increases from 4.2 atm to 16 atm, while the permeability of crosslinked PTMSP containing 10 wt % crosslinker decreases from 17,500 barrer to 15,000 barrer (a 14 % decrease), as fugacity increases from 4.3 atm to 16.2 atm. No increase in C_2H_6 permeability of uncrosslinked PTMSP occurs on depressurization at 35°C, while a 23 % increase in C_2H_6 permeability at 4.2 atm is observed for the crosslinked PTMSP film. The trends in C_2H_6 permeation observed at 10°C, 0°C, and -20°C are analogous to the trends observed at 35°C.

The C_3H_8 permeability of all films in this study is relatively stable or increases slightly with increasing C_3H_8 fugacity. For example, in *Figure 6.5* the C_3H_8 permeability of uncrosslinked PTMSP at 35°C increases from 26,000 barrer to 27,000 barrer as the fugacity increases from 2.3 atm to 5.9 atm, and upon depressurization a 23 % increase in C_3H_8 permeability is observed at 2.5 atm. Merkel *et al.* observed the C_3H_8 permeability of PTMSP at 35°C decreased from 35,000 barrer to 27,000 barrer as fugacity increased from 1.2 atm to 4.0 atm, and on depressurization no increase in C_3H_8 permeability was

observed [1]. This difference in C_3H_8 permeation behavior on depressurization could be explained by differences in the fugacity dependence of C_3H_8 permeability, where conditioning by C_3H_8 is more likely to occur if the decrease in C_3H_8 permeability is small when C_3H_8 fugacity increases. These trends are likely due to subtle differences in distributions of nonequilibrium excess volume among the various samples.

The C_3H_8 permeation behavior at $10^\circ C$, $0^\circ C$ and $-20^\circ C$ of the various PTMSP films is similar to that observed at $35^\circ C$. C_3H_8 permeabilities at $0^\circ C$ and $-20^\circ C$ were only measured in uncrosslinked PTMSP and in crosslinked PTMSP containing 10 wt % crosslinker. This step was taken to save experimental time, and testing these two films allowed comparison of the effects of crosslinking, and the influence of FS nanoparticle addition on uncrosslinked and crosslinked PTMSP transport properties at $0^\circ C$ and $-20^\circ C$ is expected to be similar to the effects observed at $35^\circ C$ and $10^\circ C$.

Figure 6.7 presents the effect of temperature on the C_2H_6 and C_3H_8 permeabilities of the PTMSP films in this study. The C_2H_6 and C_3H_8 permeabilities are reported at activities of 0.4, and 0.6, respectively. The permeabilities are reported at these activities because these are the only C_2H_6 and C_3H_8 activities that are common at all temperatures for the experimental data in this study.

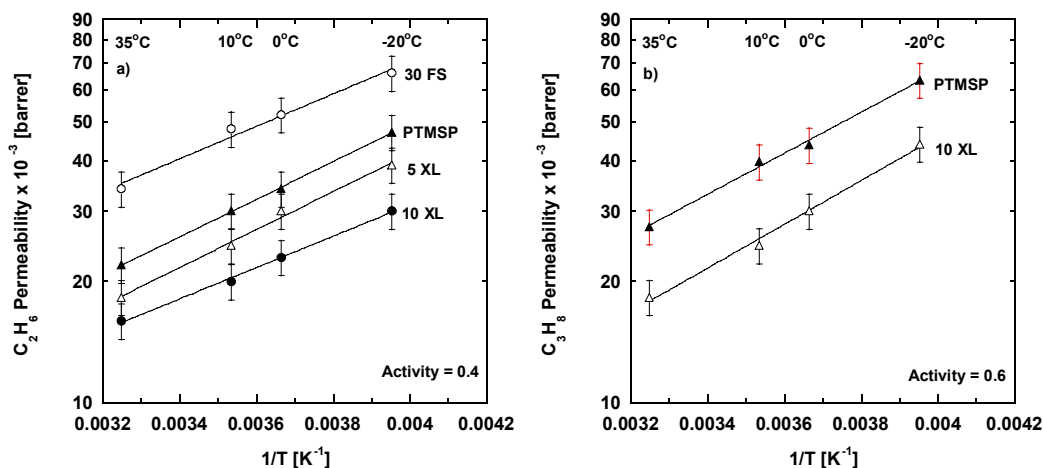


Figure 6.7. Temperature dependence of a) C_2H_6 , and b) C_3H_8 permeability in various PTMSP films. The C_2H_6 and C_3H_8 permeabilities are reported at upstream activities of 0.4, and 0.6, respectively. The data were fit to an Arrhenius relationship shown in Equation 2.14. All films were subjected to vacuum at 180°C for 90 minutes, soaked in MeOH for 24 hours, and then dried for 72 hours in ambient conditions before permeability was measured. All films were approximately 100 μm thick.

The permeabilities of C_2H_6 and C_3H_8 were measured at fugacities close to saturation, so when comparing the C_2H_6 and C_3H_8 permeabilities at different temperatures, it is more accurate to compare the permeabilities at the same activity, as this helps to normalize the conditioning effects that occur with high activity penetrants in PTMSP films [9,17]. The activation energies of permeation for C_2H_6 and C_3H_8 in uncrosslinked PTMSP and crosslinked PTMSP containing 10 wt % crosslinker are recorded in Table 6.4. The activation energies of C_2H_6 and C_3H_8 permeation are similar for uncrosslinked and crosslinked PTMSP, so the addition of crosslinks does not change the temperature dependence of C_2H_6 and C_3H_8 permeation in PTMSP.

Table 6.4. Activation energies of C₂H₆, and C₃H₈ permeation for uncrosslinked and crosslinked PTMSP

Gas	Film	E_p [kJ/mol]	Reference
C ₂ H ₆	PTMSP	- 9 ± 2	This study
	PTMSP	- 9.4	Merkel <i>et al.</i> [4]
	10 XL	- 8 ± 2	This study
C ₃ H ₈	PTMSP	- 10 ± 2	This study
	10 XL	- 11 ± 2	This study

6.3) Gas and Vapor Diffusivity

Figure 6.8 presents the concentration averaged diffusion coefficients of N₂, O₂, CH₄, C₂H₆, and C₃H₈ at 35°C as a function of penetrant concentration. For brevity, the diffusion coefficients at 10°C, 0°C, and -20°C are presented in the appendix. The diffusion coefficients were calculated using Equation 2.3, where the measured permeability coefficients and concentrations calculated from the dual-mode sorption model were used to determine diffusion coefficients at the upstream fugacities of the measured permeabilities.

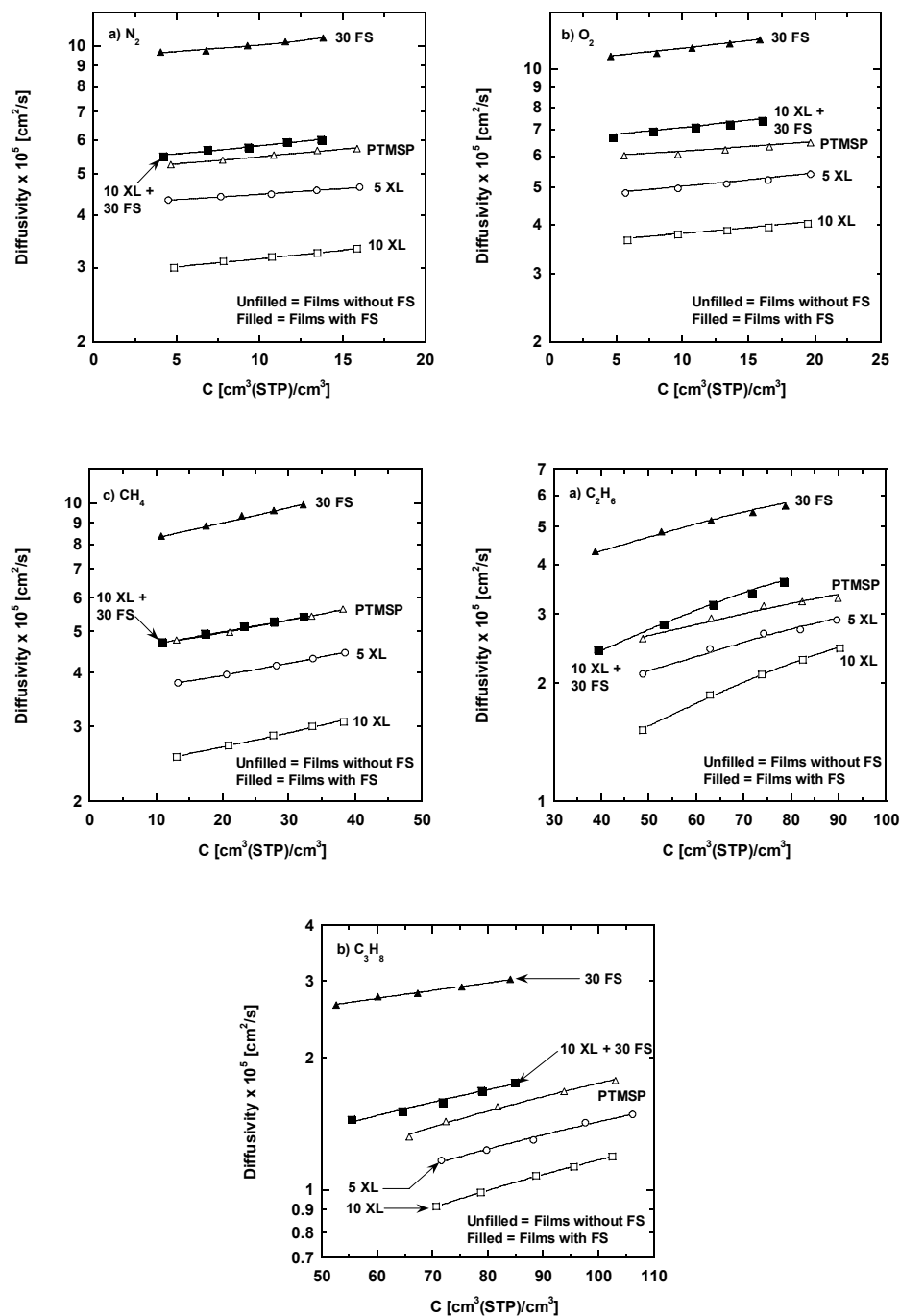


Figure 6.8. Concentration averaged diffusivity of a) N_2 , b) O_2 , c) CH_4 , d) C_2H_6 and e) C_3H_8 as a function of penetrant concentration in various PTMSP films at 35°C . The N_2 , O_2 , CH_4 and C_2H_6 diffusivities were fit to the dual-mode transport model, while the C_3H_8 diffusivities were fit to a linear function.. All films were approximately $100 \mu\text{m}$ thick.

For all gases shown in *Figure 6.8*, the diffusivities of crosslinked PTMSP are less than those of uncrosslinked PTMSP. The decrease in diffusivity in crosslinked PTMSP is correlated with a decrease in FFV that accompanies the crosslinking reaction [2]. The addition of 30 wt % FS nanoparticles to PTMSP increases the diffusivity of both uncrosslinked and crosslinked PTMSP significantly. The relative increase in nanocomposite PTMSP diffusivity is greater than the relative increase in nanocomposite permeability because the gas and vapor solubilities of nanocomposite PTMSP are less than those of neat PTMSP.

The N_2 , O_2 , CH_4 , and C_2H_6 diffusivities at 35°C, 10°C, 0°C, and -20°C were fit to Equation 2.9, and in all cases a good fit to the diffusivity data was obtained. Within the experimental error, the N_2 and O_2 diffusion coefficients of all films at 35°C are independent of penetrant concentration. The trends in N_2 and O_2 diffusivities at 10°C, 0°C, and -20°C, shown in the appendix, are similar to those observed at 35°C. The CH_4 diffusivities of all PTMSP films at 35°C, 10°C, 0°C, and -20°C increase with increasing CH_4 concentration, and the increases are relatively similar at all temperatures and for all films.

As shown in *Figure 6.8*, the C_2H_6 diffusivities of all PTMSP films increase significantly over the range of concentrations observed at 35°C. The relative increase in C_2H_6 diffusivity with C_2H_6 concentration is somewhat greater for crosslinked PTMSP films than for uncrosslinked PTMSP films. This result occurs because the decrease in C_2H_6 permeability with increasing fugacity is less for crosslinked PTMSP than for uncrosslinked PTMSP, while the C_2H_6 solubilities of uncrosslinked and crosslinked

samples are the same at all fugacities. At 10°C, 0°C, and -20°C the trends in C₂H₆ diffusivity are similar to those observed at 35°C. The diffusivities of C₃H₈ in *Figure 6.8* increase with increasing C₃H₈ concentration in the polymer, and the relative increase is similar for all films at 35°C. At 10°C, the trends in C₃H₈ diffusivity are similar to those observed at 35°C, while at 0°C and -20°C the increase in C₃H₈ diffusivity with increasing C₃H₈ concentration is slightly greater for the crosslinked PTMSP film.

Figure 6.9 presents the effect of temperature on the concentration averaged diffusion coefficients of N₂, O₂, CH₄, C₂H₆, and C₃H₈ in neat and nanocomposite uncrosslinked PTMSP and neat crosslinked PTMSP. The diffusivities of N₂, O₂, and CH₄ are calculated at an upstream fugacity of 4.4 atm, while the diffusivities of C₂H₆ and C₃H₈ are calculated at activities of 0.4, and 0.6, respectively. In this way, a comparison of the C₂H₆ and C₃H₈ diffusivities at a fixed activity can be made for all temperatures considered. Calculating the C₂H₆ and C₃H₈ diffusivities at fixed activities should help normalize for the possibility that conditioning effects by highly sorbing penetrants might change the diffusion coefficients in PTMSP [9,17].

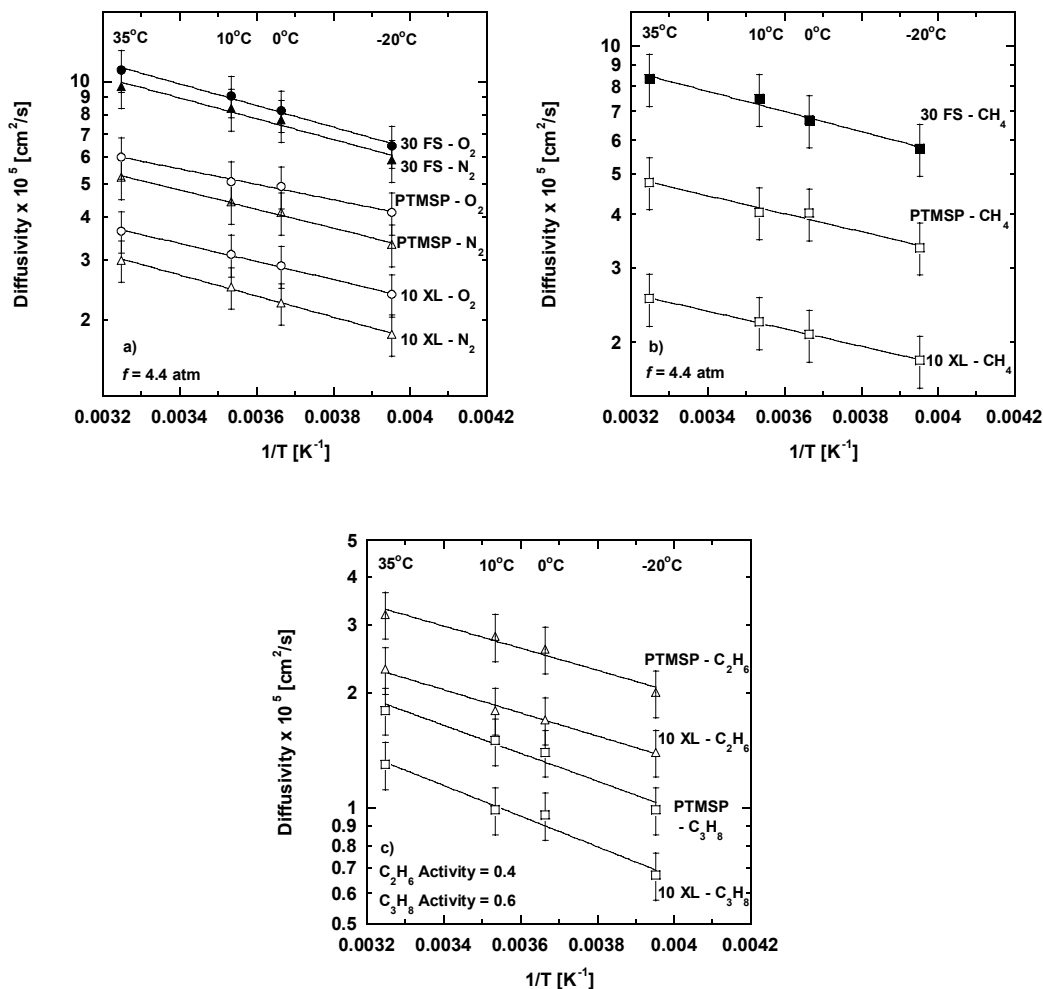


Figure 6.9. Effect of temperature on the concentration averaged diffusivity of a) N_2 and O_2 ; b) CH_4 ; and c) C_2H_6 and C_3H_8 in various PTMSP films. The data were fit to Equation 2.16. All films were subjected to vacuum at 180°C for 90 minutes, soaked in MeOH for 24 hours, and then dried for 72 hours in ambient conditions before transport properties were measured. All films were approximately $100 \mu\text{m}$ thick.

For all films in *Figure 6.9*, the N_2 , O_2 , CH_4 , C_2H_6 , and C_3H_8 diffusion coefficients decrease with decreasing temperature. The activation energies of the concentration averaged diffusion coefficients of N_2 , O_2 , CH_4 , C_2H_6 , and C_3H_8 were calculated using Equation 2.16 and are reported in Table 6.5.

Table 6.5. Activation energies of diffusivity for uncrosslinked PTMSP

Gas	Kinetic Diameter [Å] [13]	E_D [kJ/mol]	Reference
N ₂	3.64	5.3 ± 1.0 5.0	This study Masuda <i>et al.</i> [7]
O ₂	3.46	5.9 ± 0.8 5.0	This study Masuda <i>et al.</i> [7]
CH ₄	3.8	4.0 ± 1.0 4.9	This study Masuda <i>et al.</i> [7]
C ₂ H ₆	-	5.6 ± 1.0	This study
C ₃ H ₈	4.3	7.0 ± 1.0	This study

The activation energies of diffusion in neat uncrosslinked PTMSP are comparable, within experimental error, to those of neat crosslinked PTMSP, and nanocomposite uncrosslinked PTMSP. Therefore, the addition of crosslinks or FS did not change the temperature dependence of diffusivity. The activation energies of diffusion for N₂, O₂ and CH₄ agree with the literature values reported by Masuda *et al.* [7]. The activation energies of C₂H₆ and C₃H₈ diffusion are similar to the values observed for N₂, O₂ and CH₄. All other factors being equal, activation energies of diffusion should increase with increasing penetrant size [13]. However this trend was not observed and this result could be caused by the highly sorbing C₂H₆ and C₃H₈ molecules conditioning the PTMSP films, and thereby increasing the C₂H₆ and C₃H₈ diffusivities relatively more at lower temperatures than would otherwise occur in the absence of conditioning.

6.4) Conclusions

The addition of crosslinks to PTMSP decreases the permeability. The addition of 30 wt % FS nanoparticles to uncrosslinked and crosslinked samples increases

permeability by 30 – 65 %. The addition of crosslinks and FS nanoparticles has differing effects on PTMSP diffusivity; crosslinking decreases diffusivity, while FS addition increases diffusivity. The permeability of N₂, O₂, CH₄, C₂H₆, and C₃H₈ in PTMSP increases as temperature decreases, and the increase in permeability with decreasing temperature is similar for all PTMSP films studied. At all temperatures, the N₂, O₂, and CH₄ permeabilities measured during depressurization were equivalent to the permeabilities measured as the film was pressurized. The C₂H₆ permeability of crosslinked PTMSP was greater during depressurization, while no increase in C₂H₆ permeability in uncrosslinked PTMSP was observed upon depressurization. For both uncrosslinked and crosslinked PTMSP films, the C₃H₈ permeability increased by 20 – 30 % on depressurization. The magnitude of the C₂H₆ and C₃H₈ permeability increases on depressurization were similar at all temperatures.

6.5) References

- [1] T. C. Merkel, V. Bondar, K. Nagai, and B. D. Freeman, Sorption and transport of hydrocarbon and perfluorocarbon gases in poly[1-(trimethylsilyl)-1-propyne], *Journal of Polymer Science, Part B: Polymer Physics*, 38 (2000) 273-96.
- [2] S. D. Kelman, S. Matteucci, C. W. Bielawski, and B. D. Freeman, Crosslinking poly[1-(trimethylsilyl)-1-propyne] and its effect on solvent resistance and transport properties, *Polymer*, 48 (2007) 6881-92.
- [3] K. De Sitter, P. Winberg, J. D'Haen, C. Dotremont, R. Leysen, J. A. Martens, S. Mullens, F. H. J. Maurer, and I. F. J. Vankelecom, Silica filled poly[1-(trimethylsilyl)-1-propyne] nanocomposite membranes: Relation between the transport of gases and structural characteristics, *Journal of Membrane Science*, 278 (2006) 83-91.

- [4] T. C. Merkel, Z. He, I. Pinnau, B. D. Freeman, P. Meakin, and A. J. Hill, Effect of nanoparticles on gas sorption and transport in poly[1-(trimethylsilyl)-1-propyne], *Macromolecules*, 36 (2003) 6844-55.
- [5] T. C. Merkel, B. D. Freeman, R. J. Spontak, Z. He, I. Pinnau, P. Meakin, and A. J. Hill, Sorption, transport, and structural evidence for enhanced free volume in poly(4-methyl-2-pentyne)/fumed silica nanocomposite membranes, *Chemistry of Materials*, 15 (2003) 109-23.
- [6] S. Matteucci, V. A. Kusuma, D. Sanders, S. Swinnea, and B. D. Freeman, Gas transport in TiO₂ nanoparticle-filled poly[1-(trimethylsilyl)-1-propyne], *Journal of Membrane Science*, 307 (2008) 196-217.
- [7] T. Masuda, Y. Iguchi, B. Z. Tang, and T. Higashimura, Diffusion and solution of gases in substituted polyacetylene membranes, *Polymer*, 29 (1988) 2041-9.
- [8] J. Qiu, J. M. Zheng, and K. V. Peinemann, Gas transport properties in a novel poly[1-(trimethylsilyl)-1-propyne] composite membrane with nanosized organic filler trimethylsilylglucose, *Macromolecules*, 39 (2006) 4093-100.
- [9] R. D. Raharjo, B. D. Freeman, and E. S. Sanders, Pure and mixed gas CH₄ and *n*-C₄H₁₀ sorption and dilation in poly[1-(trimethylsilyl)-1-propyne], *Polymer*, 48 (2007) 6097-114.
- [10] S. V. Dixon-Garrett, K. Nagai, and B. D. Freeman, Sorption, diffusion, and permeation of ethylbenzene in poly[1-(trimethylsilyl)-1-propyne], *Journal of Polymer Science, Part B: Polymer Physics*, 38 (2000) 1078-89.
- [11] S. M. Jordan, G. K. Fleming, and W. J. Koros, Permeability of carbon dioxide at elevated pressures in substituted polycarbonates, *Journal of Polymer Science, Part B: Polymer Physics*, 28 (1990) 2305-27.
- [12] S. M. Jordan, W. J. Koros, and G. K. Fleming, The effects of carbon dioxide exposure on pure and mixed gas permeation behavior: comparison of glassy polycarbonate and silicone rubber, *Journal of Membrane Science*, 30 (1987) 191-212.
- [13] S. Matteucci, Y. Yampolskii, B. D. Freeman, and I. Pinnau, in: Y. Yampolskii, B. D. Freeman, I. Pinnau (Eds.), *Material Science of Membranes for Gas and Vapor Separation*, John Wiley & Sons, New York, 2006, pp. 1-47.

- [14] G. K. Fleming and W. J. Koros, Dilation of polymers by sorption of carbon dioxide at elevated pressures. 1. Silicone rubber and unconditioned polycarbonate, *Macromolecules*, 19 (1986) 2285-91.
- [15] S. M. Jordan, M. A. Henson, and W. J. Koros, The effects of carbon dioxide conditioning on the permeation behavior of hollow fiber asymmetric membranes, *Journal of Membrane Science*, 54 (1990) 103-18.
- [16] S. M. Jordan and W. J. Koros, Characterization of carbon dioxide-induced conditioning of substituted polycarbonates using various "exchange" penetrants, *Journal of Membrane Science*, 51 (1990) 233-47.
- [17] I. Pinnau, C. G. Casillas, A. Morisato, and B. D. Freeman, Long-term permeation properties of poly[1-(trimethylsilyl)-1-propyne] membranes in hydrocarbon-vapor environment, *Journal of Polymer Science, Part B: Polymer Physics*, 35 (1997) 1483-90.

7) Physical Stability of PTMSP

This chapter presents the influence of crosslinking on the physical stability of PTMSP. The densities and N₂, O₂, and CH₄ permeabilities of thick (*i.e.*, ~100 μm) uncrosslinked and crosslinked PTMSP films were monitored over time, and changes in permeability were related to changes in the film density and free volume. Ellipsometry was used to monitor the changes in the density of thin (*i.e.*, ~400 nm) uncrosslinked and crosslinked PTMSP films, and the aging rates of thick and thin uncrosslinked and crosslinked films were compared. POSS nanoparticles were added to thick uncrosslinked and crosslinked PTMSP films, and the densities and permeabilities of the nanocomposite films were measured over time to understand the effects of POSS addition on the physical stability of the films.

7.1) Aging of Neat PTMSP

The pure gas N₂, O₂, and CH₄ permeabilities of uncrosslinked and crosslinked PTMSP are presented as a function of membrane age in *Figure 7.1*. Time zero is defined when the films are removed from the MeOH soak. In both samples, after 4,900 hours, the permeabilities decrease to 55 - 80 % of their initial values. In contrast, Jia *et al.* observed stable permeability values in their crosslinked PTMSP samples [1]. In this study, the permeability decrease with time is slightly greater for crosslinked PTMSP than for uncrosslinked PTMSP. The initial O₂ permeability of the crosslinked film in this study was 8,000 barrer, while the crosslinked film from the Jia *et al.* study had an initial O₂ permeability of 2,200 barrer [1]. The differences in the aging behavior and starting

permeabilities of samples from the two studies are most likely related to differences in film histories.

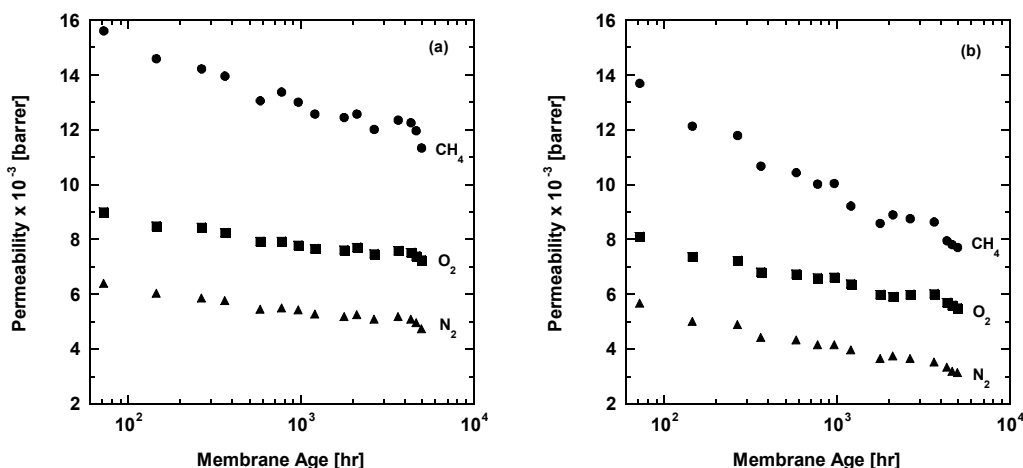


Figure 7.1. Permeability of a) uncrosslinked PTMSP and b) crosslinked PTMSP as a function of time. The crosslinked film contained 5 wt % bis azide crosslinker. $T = 35^{\circ}\text{C}$, $f_2 = 4.4$ atm, and $f_1 =$ atmospheric for all measurements. The films were thermally annealed in vacuum at 180°C for 90 minutes, soaked in MeOH for 24 hours, and dried at ambient conditions for 72 hours prior to the initial permeation measurements. Film thickness was approximately $100\text{ }\mu\text{m}$.

One reason for the substantial difference in starting permeability values is that the films in this study were conditioned in MeOH before the initial permeation measurements, while Jia *et al.* did not undertake this conditioning step. MeOH swells the PTMSP polymer matrix, which increases the FFV [2] and, therefore, the initial permeability. However, the higher initial FFV of a MeOH soaked film should also lead to more rapid physical aging [3] than films prepared without the methanol soak [1]. A PTMSP film with a lower initial FFV and permeability ages less because the driving force to age is reduced (*cf.*, Equation 2.13) [3,4]. For example, Dorkenoo *et al.* [5]

observed that an 85 μm thick PTMSP film annealed at 250°C exhibited a N_2 permeability of 1,200 barrer, while the crosslinked PTMSP film in this study initially had a N_2 permeability of 5,600 barrer. The N_2 permeability of Dorkenoo's annealed PTMSP film was constant over the course of 200 hours, while over the same period of time, the crosslinked film permeability in this study decreased from 5,600 to 4,700 barrer.

Nagai *et al.* observed aging-induced decreases in gas permeability in PTMSP similar to those observed in this study (*cf. Figure 7.1*) [4,6]. The films in this study were of a similar thickness to those used by Nagai *et al.* [4,6]; the thickness is important to note because accelerated aging has been observed in thin (1 – 3 μm) PTMSP films, which is hypothesized to be caused by increased elimination of FFV by diffusion processes [5]. The rate of permeability decrease of uncrosslinked and crosslinked PTMSP films in this study is less than that observed in uncrosslinked PTMSP by Shimomura *et al.*, [7] Yampol'skii *et al.*, [8] Nagai *et al.*, [9] and Consolati *et al.* [10] because the films in those studies were exposed to vacuum conditions or ambient conditions where contamination of the films by high sorbing organic vapors could occur. Nagai *et al.* noted that contamination effects were the dominant factor causing a significant decrease in PTMSP permeability as a film aged from 90 to 2200 days at ambient conditions [6].

Based on the data in *Figure 7.1*, the rate of permeability decrease in uncrosslinked and crosslinked PTMSP films is greatest at the start of the experiment. Within the first 500 hours, approximately half of the total observed loss in permeability occurs. This result is consistent with the fact that excess FFV and, therefore, the driving force to reduce the FFV, is greatest initially [2-4]. Faster initial aging has also been observed by

Hill *et al.*, [2] Nagai *et al.*, [4] and Pinnau *et al.*[11]. This finding is also consistent with the self-retarding nature of physical aging [12]. After 4900 hours, the relative decrease in the N₂ and CH₄ permeability in uncrosslinked and crosslinked PTMSP is greater than the decrease in O₂ permeability. N₂ (3.64 Å) and CH₄ (3.80 Å) are larger than O₂ (3.46 Å) [13], and permeabilities of larger gases should be more sensitive to decreases in FFV than smaller gases [13,14]. Consistent with this picture, during the aging experiment, the O₂/N₂ selectivity increases from 1.41 to 1.53 in uncrosslinked PTMSP, and from 1.43 to 1.76 in crosslinked PTMSP, while the CH₄/O₂ selectivity decreases from 1.73 to 1.56 in uncrosslinked PTMSP, and from 1.69 to 1.40 in crosslinked PTMSP.

In *Figure 7.2*, the densities of uncrosslinked and crosslinked PTMSP films are presented as a function of aging time. The density measurements were performed on the same day that the permeabilities were measured.

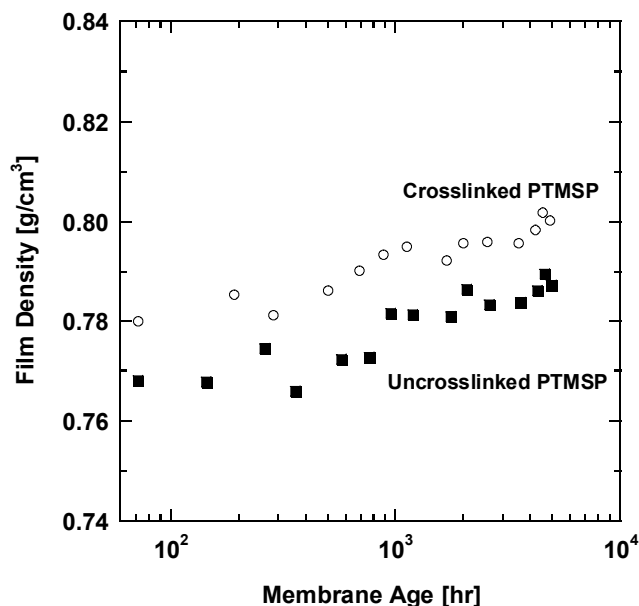


Figure 7.2. Measured densities for uncrosslinked and crosslinked PTMSP samples. The densities were measured at ambient conditions using a $\text{Ca}(\text{NO}_3)_2$ salt solution (density = 1.4 g/cm^3) and then calculated using the buoyancy method. The crosslinked film contained 5 wt % crosslinker. All films were thermally treated in vacuum at 180°C for 90 minutes, then soaked in MeOH for 24 hours, and dried at ambient conditions for 72 hours prior to the initial density measurement. Film thickness was approximately $100 \mu\text{m}$.

The densities of both uncrosslinked and crosslinked PTMSP films increase by approximately 2.5 % after 4900 hours. Because the magnitude of the density increases of the uncrosslinked and crosslinked films are similar, crosslinking PTMSP *per se* does not prevent densification under the experimental conditions in this study. Consolati *et al.* [10] observed a density increase of 1.2 % after 60 days of aging an uncrosslinked PTMSP sample, and a similar increase in density over this time period was observed in this study. The densities from Figure 7.2 were used to calculate FFV values using the group contribution method [15-17] shown in Equation 2.10. The van der Waals volumes and

molecular weight of TMSP (*i.e.*, the PTMSP repeat unit) and the bis(azide) crosslinker used in this calculation are recorded in Table 7.1.

Table 7.1 van der Waals volumes and molecular mass of TMSP and the bis(azide) crosslinker

Molecule	van der Waals Volume (cm³/mol) [17]	Molecular Mass in Reacted Film
TMSP	79.56	112.23
Bis(azide) Crosslinker^a	114.9	244.26

- a) Molecular mass of crosslinker is 300.30 g/mol before crosslinking reaction. Two N₂ molecules are released from each bis(azide) during the crosslinking reaction.

The N₂, O₂, and CH₄ permeabilities of uncrosslinked and crosslinked PTMSP are presented as a function of 1/FFV in *Figure 7.3*. For both uncrosslinked PTMSP and crosslinked PTMSP, permeability decreases as FFV decreases. During these experiments, the FFV of uncrosslinked PTMSP decreases from 0.292 to 0.274, while the FFV of crosslinked PTMSP decreases from 0.289 to 0.272. The magnitude of the FFV decrease is similar for uncrosslinked and crosslinked PTMSP.

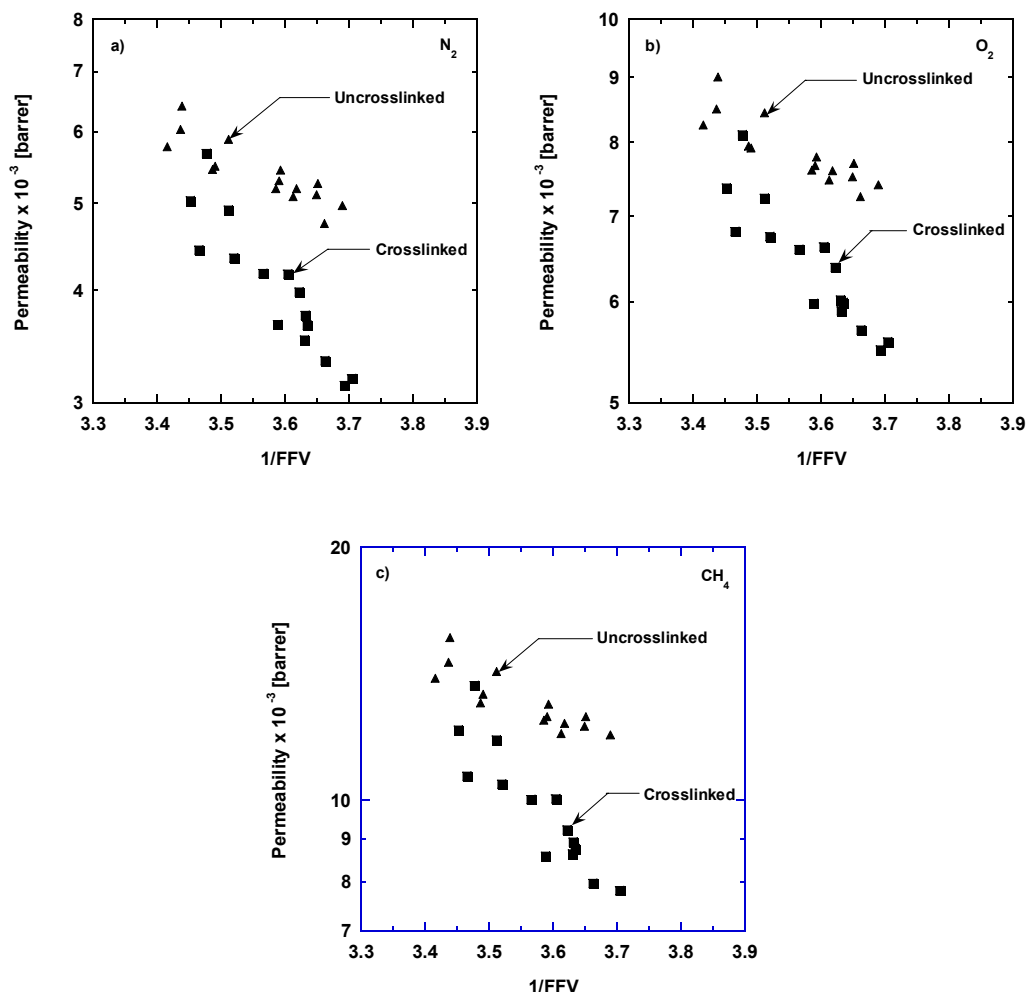


Figure 7.3. Permeability of a) N₂, b) O₂, and c) CH₄ in uncrosslinked PTMSP (▲) and crosslinked PTMSP (■) as a function of 1/FFV. The FFV values of the samples were calculated using measured density values and Bondi's group contribution method. T = 35°C, $f_2 = 4.4$ atm, and f_1 = atmospheric for all measurements. The crosslinked film contained 5 wt % crosslinker. All films were thermally treated in vacuum at 180°C for 90 minutes, soaked in MeOH for 24 hours, and dried at ambient conditions for 72 hours prior to the permeation measurements. Film thickness was approximately 100 μ m.

The N₂, O₂, and CH₄ permeability decrease of crosslinked PTMSP is greater than that of uncrosslinked PTMSP. During the experiment, the N₂ permeability of uncrosslinked PTMSP decreased from 6,500 barrer to 4,900 barrer, while the crosslinked PTMSP N₂

permeability decreased from 5,600 barrer to 3,200 barrer. The uncertainty in FFV and permeability are $\pm 1 \%$, and $\pm 15 \%$, respectively. For a similar decrease in FFV, there is a greater permeability decrease in crosslinked PTMSP, so crosslinked PTMSP permeability is more sensitive to FFV change than uncrosslinked PTMSP.

A possible explanation for this result may come from the PALS data presented in Chapter 4 of uncrosslinked and crosslinked PTMSP films. The size of large free volume elements, τ_4 , was constant during crosslinking, while the intensity of large free volume elements, I_4 , decreases from 38.8 % in uncrosslinked PTMSP to 29.0 % in crosslinked PTMSP. Consistent with these results, aged MeOH conditioned PTMSP films show a decrease in the concentration of large free volume elements, and the decrease in the large free volume elements is correlated with the decrease in the permeability over time [4].

The large free volume elements of PTMSP are thought to be interconnected [18,19], so a decrease in the concentration of large free volume elements should decrease interconnectivity, thereby decreasing permeability. The relative decrease of I_4 over the course of the experiment should be similar for both uncrosslinked and crosslinked PTMSP, as this would correlate with the observation that the FFV of both films decrease at a similar rate [4]. For a similar relative decrease in I_4 , a greater loss of interconnectivity, and therefore permeability, may occur in crosslinked PTMSP because crosslinked PTMSP initially has fewer large free volume elements than uncrosslinked PTMSP.

7.2) Aging of Nanocomposite POSS/PTMSP Films

Reinerth *et al.*, observed that the addition of 10 wt % inorganic POSS nanoparticles to PTMSP reduced its permeability by approximately 75 %. However, the permeability of the nanocomposite films were stable for 27 days [20], demonstrating that physical aging was slowed markedly by the addition of POSS particles. In *Figure 7.4* the N_2 , O_2 , and CH_4 permeabilities of uncrosslinked and crosslinked PTMSP films containing 10 wt % POSS MS0865 particles are shown. AFM analysis of the PTMSP/POSS nanocomposites showed there was no significant agglomeration of the POSS particles in the polymer matrix. The addition of POSS particles did not affect the solvent resistance of crosslinked PTMSP.

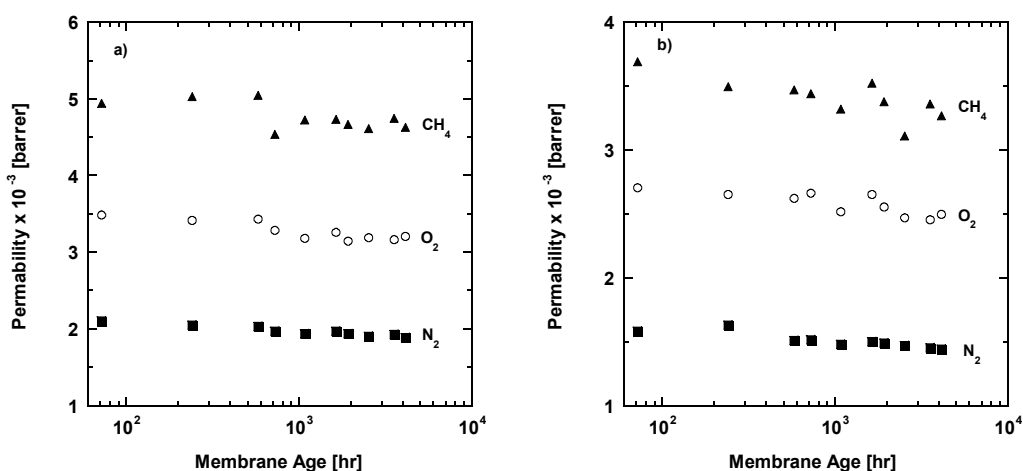


Figure 7.4. Permeability of a) PTMSP + 10 wt % POSS MS0865 nanocomposite film, and b) Crosslinked PTMSP + 10 wt % POSS MS0865 nanocomposite film as a function of time. The crosslinked film contained 5 wt % bis azide crosslinker. $T = 35^{\circ}\text{C}$, $f_2 = 4.4$ atm, and $f_1 =$ atmospheric for all measurements. The films were thermally annealed in vacuum at 180°C for 90 minutes and cooled at ambient conditions for 72 hours prior to the initial permeation measurements. Film thickness was approximately 100 μm .

The initial permeabilities of the uncrosslinked and crosslinked PTMSP/POSS nanocomposite films are approximately 30 % of the values observed in the particle-free uncrosslinked and crosslinked films, and this decrease is similar to that observed by Reinerth *et al.* at the same POSS loading [20]. The permeabilities of N₂, O₂ and CH₄ were stable over 4,100 hours, in contrast to the results for the particle-free uncrosslinked and crosslinked PTMSP films in *Figure 7.1*. Therefore, the addition of POSS particles suppresses aging. However, it does so at the expense of a significant reduction in permeability.

Table 7.2 presents permeabilities and PALS data for uncrosslinked PTMSP, pure POSS MS0865 nanoparticles and uncrosslinked PTMSP containing 10 wt % POSS MS0865. The uncrosslinked PTMSP film presented in Table 7.2 was not soaked in MeOH after the thermal treatment. This protocol ensures that the neat uncrosslinked film and the PTMSP/POSS films have the same treatment history, because PTMSP/POSS films were not soaked in MeOH.

Table 7.2 PALS parameters for uncrosslinked and nanocomposite PTMSP^a

Film	P _{N2} (barrers)	τ_3 (ns)	I ₃ (%)	τ_4 (ns)	I ₄ (%)
Uncrosslinked PTMSP	4,000 ± 700	2.1 ± 0.3	5.5 ± 0.4	5.9 ± 0.1	28.0 ± 0.4
POSS MS0865	-	1.85 ± 0.05	39.0 ± 0.6	4.3 ± 0.1	7.0 ± 0.4
Uncrosslinked PTMSP + 10 wt % POSS	1,800 ± 300	2.3 ± 0.2	9.1 ± 0.4	5.4 ± 0.1	28.7 ± 0.3

- a) All films were thermally annealed in vacuum at 180°C for 90 minutes and aged in ambient conditions for 20 days prior to the PALS and permeation measurements.

Pure POSS MS0865 has a broad oPs-accessible free volume distribution even though it is considered nonporous to gas molecules. POSS has fewer large free volume elements and more small free volume elements than PTMSP. The addition of 10 wt % POSS to PTMSP should result in fewer large free volume elements if the effect is purely additive. However, as shown in Table 7.2, I_4 is not appreciably changed upon addition of POSS to PTMSP. Thus, the addition of POSS to PTMSP apparently props open the larger free volume elements. Although POSS has its own free volume distribution, these free volume elements are not accessible to gas molecules, and therefore POSS acts as a nonporous filler which reduces permeability. However, POSS also mitigates physical aging. The PALS and permeability data suggest that POSS particles may occupy some of the larger free volume elements, thereby preventing their collapse but also restricting the passage of gas molecules through the structure.

In *Figure 7.5*, the densities of uncrosslinked and crosslinked PTMSP containing 10 wt % POSS MS0865 nanoparticles are presented.

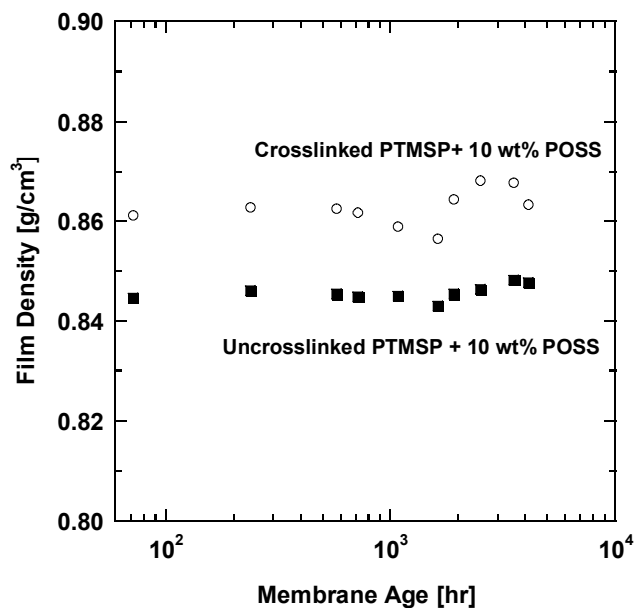


Figure 7.5. Measured densities for uncrosslinked and crosslinked PTMSP + POSS nanocomposite samples. The densities were measured at ambient conditions using a salt solution (density = 1.4 g/cm³) and then calculated using the buoyancy method. The crosslinked film contained 5 wt % crosslinker. All films were crosslinked in vacuum at 180°C for 90 minutes, and cooled at ambient conditions for 72 hours prior to the initial density measurement. Film thickness was approximately 100 μ m.

The film densities and, therefore, the FFV values are relatively constant for the 4,100 hour duration of this experiment. This result is consistent with the fact that the permeability is stable over this time period. The densities of the PTMSP/POSS nanocomposites are further investigated in Table 7.3. The calculated density of the individual MS0865 POSS particles [21], and the PTMSP/POSS nanocomposite film densities are known. Using Equations 3.2 3.3, and 3.4 the polymer density, ρ_p , and polymer volume fraction, ϕ_p , of uncrosslinked and crosslinked PTMSP in the nanocomposites can be calculated.

Table 7.3 PTMSP/POSS nanocomposite film density

Film	ρ Nanocomposite – measured (g/cm ³)	ρ Polymer – calculated (g/cm ³)	Vol. % POSS
Uncrosslinked PTMSP + 10 wt. % POSS	0.845 \pm 0.003	0.820	7.2
Crosslinked PTMSP + 10 wt. % POSS ^a	0.860 \pm 0.003	0.835	7.3

a) Crosslinked PTMSP/POSS nanocomposite contains 5 wt % crosslinker.

The densities of uncrosslinked and crosslinked PTMSP/POSS nanocomposites are significantly greater than that of their particle-free analogues. These results are consistent with the fact that the PTMSP/POSS nanocomposites are much less permeable than their particle-free analogues.

7.3) Permeabilities of PTMSP Compared to Other Polymers

In *Figure 7.6*, the N₂, O₂, and CH₄ permeabilities are plotted as a function of 1/FFV for films from this study. This figure also includes values for other substituted polyacetylenes [22-26], polycarbonates and polysulfones [27-37].

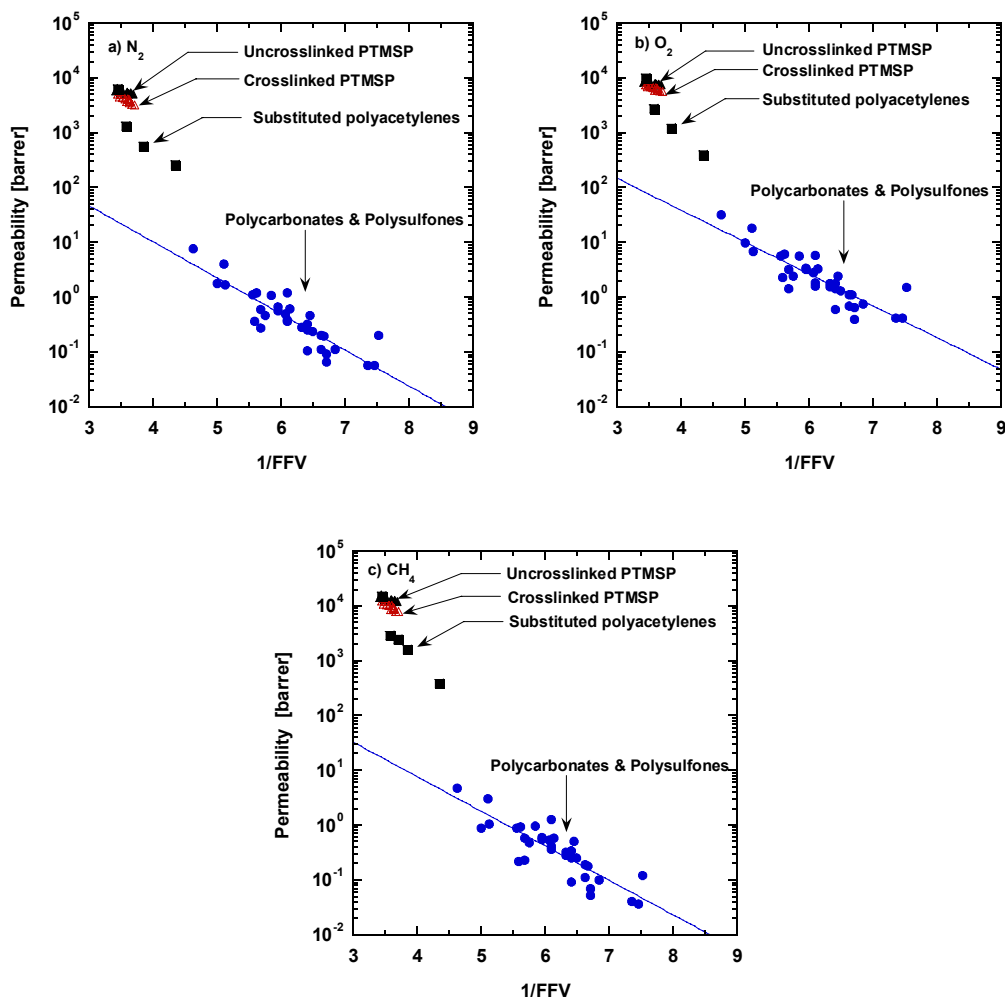


Figure 7.6. Permeability of a) N_2 , b) O_2 , and c) CH_4 in uncrosslinked PTMSP and crosslinked PTMSP, other substituted polyacetylenes [22-26], polycarbonates and polysulfones [27-37] as a function of $1/FFV$. The FFV values were calculated using measured density values and Bondi's group contribution method.

The permeabilities of uncrosslinked and crosslinked PTMSP from this study are significantly greater than that of other substituted polyacetylenes having similar FFV values. This difference could be caused by differences in the free volume element distribution in these materials. PTMSP has higher values of τ_4 and I_4 [4] than substituted

polyacetylenes such as PMP [23], which may contribute to the higher permeability of PTMSP [38]. At a FFV of 0.275 (*i.e.*, $1/\text{FFV} = 3.64$), the permeabilities of PTMSP and other substituted polyacetylenes are 2-3 orders of magnitude greater than the line of best fit permeabilities for the polycarbonates and polysulfones. PALS analysis of low permeability glassy polymers (such as the polycarbonates and polysulfones plotted on the graph) show no I_4 and τ_4 components in the PALS spectra [38], so the distribution of free volume in these polymers does not favor high permeability as it does in PTMSP.

7.4) Aging of Neat PTMSP Monitored by Ellipsometry

The refractive indices of thin ($\sim 400 - 480$ nm) uncrosslinked and crosslinked PTMSP films aged at 35°C are shown in *Figure 7.7*.

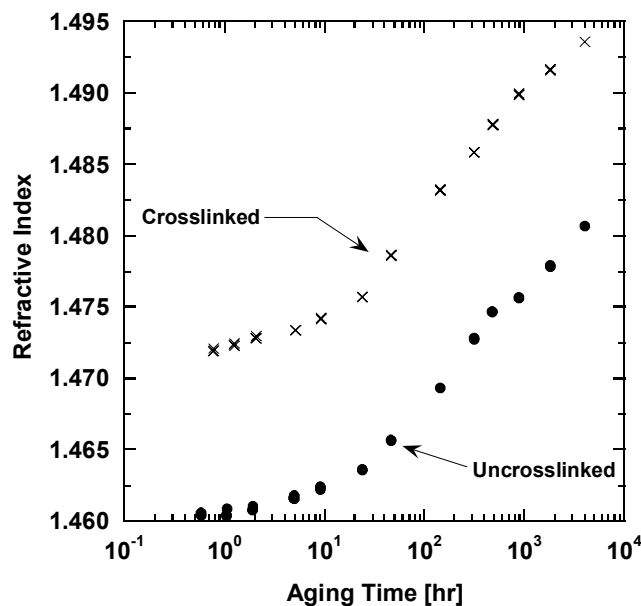


Figure 7.7. Effect of aging on the refractive index of uncrosslinked and crosslinked PTMSP. The crosslinked film contains 10 wt % crosslinker, and all films were crosslinked in vacuum at 180°C for 90 minutes. Ellipsometry measurements began 1 hour after removal from the vacuum oven.

The refractive index of both films increase linearly with log time after an initial aging time of approximately 24 hours. This behavior is consistent with other reports in the literature [39-42]. The crosslinked film had a higher refractive index than the uncrosslinked film. This difference is comparable to the slightly greater density in the thick crosslinked PTMSP films as compared to uncrosslinked films. The density increased 3.7 % and 3.9 % over 4,100 hours in the uncrosslinked and crosslinked films, respectively. This increase is independent of the specific refraction, C , because the values are relative. These density increases are slightly larger than those observed in thicker films and are consistent with accelerated aging in thinner films. The permeabilities of these thin PTMSP films were not measured because of trans-membrane pinhole defects.

Figure 7.8 presents the effect of aging time on the film thickness of uncrosslinked and crosslinked PTMSP. The small decrease in film thickness with aging time is caused by volume relaxation of the polymer, as discussed by Huang and Paul [39]. The aging rate of thin films can depend on film thickness; however, the small difference in thickness between these two films would result in a negligible difference in aging rate.

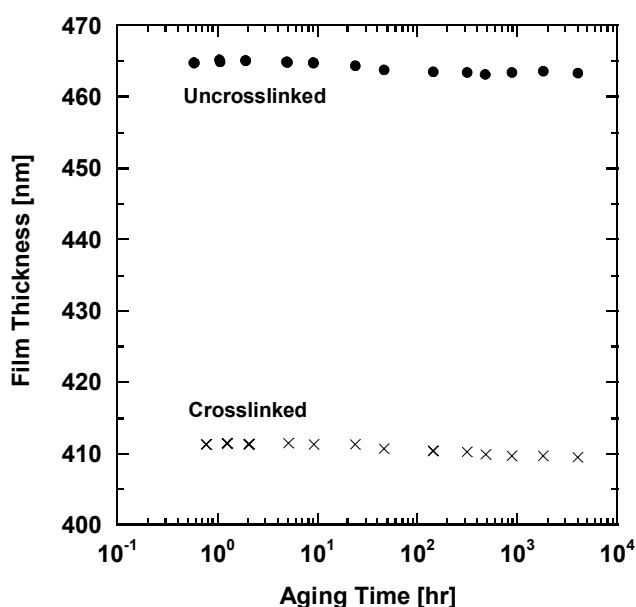


Figure 7.8. Effect of aging on the film thickness of uncrosslinked and crosslinked PTMSP. The crosslinked film contains 10 wt % crosslinker and all films were crosslinked in vacuum at 180°C for 90 minutes. Ellipsometry measurements began 1 hour after removal from the vacuum oven.

The relative refractive index of the uncrosslinked and crosslinked PTMSP films is shown in Figure 7.9 as a function of aging time. This illustration clearly shows the similarity in the aging response of the two films.

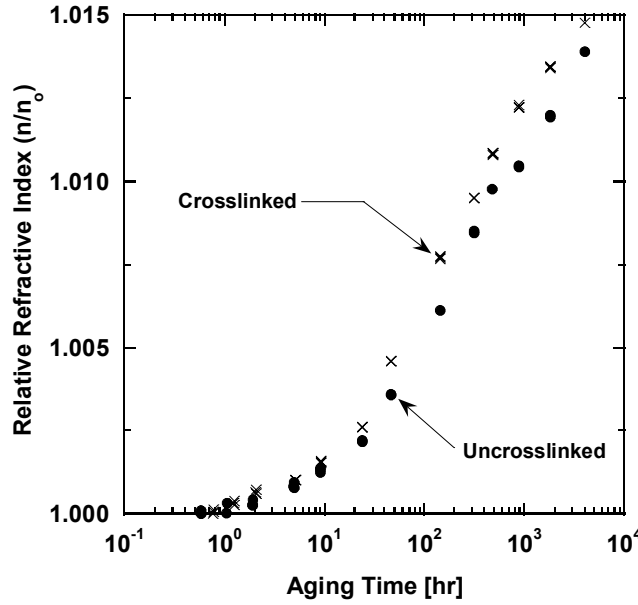


Figure 7.9. Effect of aging on the relative refractive index of uncrosslinked PTMSP and crosslinked PTMSP films. The crosslinked film contains 10 wt. % crosslinker and all films were crosslinked in vacuum at 180°C for 90 minutes. Ellipsometry measurements began 1 hour after removal from the vacuum oven.

Using the Lorentz-Lorenz equation to relate refractive index to density, a volumetric aging rate, r , can be defined as

$$r = -\frac{1}{V} \left(\frac{\partial V}{\partial \ln t} \right)_{P,T} = \left(\frac{\partial \ln \rho}{\partial \ln t} \right)_{P,T} = \left(\frac{\partial \log L}{\partial \log t} \right)_{P,T} \quad (7.1)$$

where V is the specific volume, P is the pressure, and T is the aging temperature. The aging rate for each polymer film was calculated by applying a best fit line to the log-log plot of L vs t after an initial aging period of 24 hours. The uncrosslinked and crosslinked PTMSP aging rates were 60×10^{-4} and 62×10^{-4} , respectively. This result is qualitatively consistent with the fact that FFV of crosslinked and uncrosslinked samples decreases

over time at similar rates (see *Figure 7.3*). The aging rates, as measured using ellipsometry, of other glassy polymer films of similar thickness have been reported, including: polysulfone (PSF), poly(2,6-dimethyl-1,4-phenylene oxide) (PPO), Matrimid, and several 6FDA-based polyimides [39,40]. The aging rates of these polymers and the polymers considered in this study are plotted vs $1/FFV$ in *Figure 7.10*.

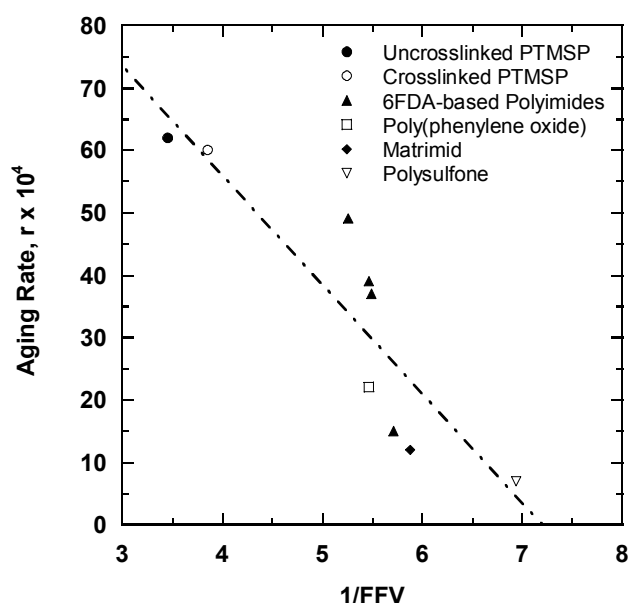


Figure 7.10. Effect of free volume on aging rates of various polymers films determined by ellipsometry. All polymer films were approximately 400 nm thick [39,40].

Figure 7.10 is meant to illustrate the general notion that higher free volume polymers tend to age more rapidly than lower free volume polymers. Because physical aging is dependent on other factors besides free volume (*e.g.*, polymer structure, thermal transitions, *etc.*), the actual relationship is likely to be more complex than indicated in *Figure 7.10*. The aging rates of polymers (other than PTMSP) used in this comparison are

for films freshly quenched from above T_g , presumably leading to more rapid aging rates than if these films had been thermally annealed similar to the PTMSP films.

7.5) Conclusions

The gas permeability and FFV of uncrosslinked and crosslinked PTMSP decreased over time. The rate of permeability decrease was greater for crosslinked PTMSP, while the rate of FFV decrease was similar for uncrosslinked and crosslinked PTMSP. The addition of 10 wt % POSS nanoparticles decreased the permeability of uncrosslinked and crosslinked PTMSP by approximately 70 %, and the permeability and FFV values were stable over time. PALS results suggest that the POSS nanoparticles prop open the larger free volume elements of PTMSP, mitigating the physical aging by preventing the collapse of larger free volume elements. The permeability of PTMSP at a given FFV was greater than that of other substituted polyacetylenes, polysulfones and polycarbonates. This result presumably relates to differences in the distribution of free volume in these various materials. Physical aging of thin PTMSP films studied using ellipsometry showed little difference in aging rates between uncrosslinked and crosslinked films, corroborating the findings of the permeability studies. The thin PTMSP films in this study age more rapidly than any other thin polymer film studied to date using ellipsometry.

7.6) References

- [1] J. Jia and G. L. Baker, Crosslinking of poly[1-(trimethylsilyl)-1-propyne] membranes using bis(aryl azides), *Journal of Polymer Science, Part B: Polymer Physics*, 36 (1998) 959-68.

- [2] A. J. Hill, S. J. Pas, T. J. Bastow, M. I. Burgar, K. Nagai, L. G. Toy, and B. D. Freeman, Influence of methanol conditioning and physical aging on carbon spin-lattice relaxation times of poly[1-(trimethylsilyl)-1-propyne], *Journal of Membrane Science*, 243 (2004) 37-44.
- [3] M. S. McCaig, D. R. Paul, and J. W. Barlow, Effect of film thickness on the changes in gas permeability of a glassy polyarylate due to physical aging part II. Mathematical model, *Polymer*, 41 (1999) 639-48.
- [4] K. Nagai, B. D. Freeman, and A. J. Hill, Effect of physical aging of poly[1-(trimethylsilyl)-1-propyne] films synthesized with TaCl₅ and NbCl₅ on gas permeability, fractional free volume, and positron annihilation lifetime spectroscopy parameters, *Journal of Polymer Science, Part B: Polymer Physics*, 38 (2000) 1222-39.
- [5] K. D. Dorkenoo and P. H. Pfromm, Accelerated physical aging of thin poly[1-(trimethylsilyl)-1-propyne] films, *Macromolecules*, 33 (2000) 3747-51.
- [6] K. Nagai and T. Nakagawa, Effects of aging on the gas permeability and solubility in poly[1-(trimethylsilyl)-1-propyne] membranes synthesized with various catalysts, *Journal of Membrane Science*, 105 (1995) 261-72.
- [7] H. Shimomura, K. Nakanishi, H. Odani, and M. Kurata, Effects of physical aging on permeation of gases in a disubstituted polyacetylene, *Reports on Progress in Polymer Physics in Japan*, 30 (1987) 233-6.
- [8] Y. P. Yampol'skii, S. M. Shishatskii, V. P. Shantorovich, E. M. Antipov, N. N. Kuzmain, S. V. Rykov, V. L. Khodjaeva, and N. A. Plate, Transport characteristics and other physicochemical properties of aged poly[1-(trimethylsilyl)-1-propyne], *Journal of Applied Polymer Science*, 48 (1993) 1935-44.
- [9] K. Nagai, A. Higuchi, and T. Nakagawa, Gas permeability and stability of poly(1-trimethylsilyl-1-propyne-co-1-phenyl-1-propyne) membranes, *Journal of Polymer Science, Part B: Polymer Physics*, 33 (1995) 289-98.
- [10] G. Consolati, I. Genco, M. Pegoraro, and L. Zangerighi, Positron annihilation lifetime (PAL) in poly[1-(trimethylsilyl)-1-propyne] (PTMSP): free volume determination and time dependence of permeability, *Journal of Polymer Science, Part B: Polymer Physics*, 34 (1996) 357-67.

- [11] I. Pinnau, C. G. Casillas, A. Morisato, and B. D. Freeman, Long-term permeation properties of poly[1-(trimethylsilyl)-1-propyne] membranes in hydrocarbon-vapor environment, *Journal of Polymer Science, Part B: Polymer Physics*, 35 (1997) 1483-90.
- [12] L. C. E. Struik, *Physical Aging in Amorphous Polymers and Other Materials*, Amsterdam, 1978.
- [13] S. Matteucci, Y. Yampolskii, B. D. Freeman, and I. Pinnau, in: Y. Yampolskii, B. D. Freeman, I. Pinnau (Eds.), *Material Science of Membranes for Gas and Vapor Separation*, John Wiley & Sons, New York, 2006, pp. 1-47.
- [14] M. H. Cohen and D. Turnbull, Molecular transport in liquids and glasses, *Journal of Chemical Physics*, 31 (1959) 1164-9.
- [15] A. Bondi, van der Waals volumes and radii, *Journal of Physical Chemistry*, 68 (1964) 441-51.
- [16] A. Bondi, *Physical Properties of Molecular Crystals, Liquids and Glasses*, Wiley, New York, 1968.
- [17] D. W. Van Krevelen, *Properties of Polymers*, 3rd ed., Elsevier, Amsterdam, 2003.
- [18] I. Pinnau and L. G. Toy, Transport of organic vapors through poly[1-(trimethylsilyl)-1-propyne], *Journal of Membrane Science*, 116 (1996) 199-209.
- [19] R. Srinivasan, S. R. Auvil, and P. M. Burban, Elucidating the mechanism(s) of gas transport in poly[1-(trimethylsilyl)-1-propyne] (PTMSP) membranes, *Journal of Membrane Science*, 86 (1994) 67-86.
- [20] W. A. Reinerth, Sr., J. J. Schwab, J. D. Lichtenhan, Q. Liu, D. Hilton, B. D. Freeman, L. Toy, and H. J. Lee, POSSTM/polymer blends for gas separation, Abstracts of Papers, 222nd ACS National Meeting, Chicago, IL, United States, August 26-30, 2001, (2001) MTL-020.
- [21] N. Auner, B. Ziemer, B. Herrschaft, W. Ziche, P. John, and J. Weis, Structural studies of novel siloxysilsesquioxanes, *European Journal of Inorganic Chemistry*, (1999) 1087-94.
- [22] T. C. Merkel, V. Bondar, K. Nagai, and B. D. Freeman, Sorption and transport of hydrocarbon and perfluorocarbon gases in poly[1-(trimethylsilyl)-1-propyne], *Journal of Polymer Science, Part B: Polymer Physics*, 38 (2000) 273-96.

- [23] T. C. Merkel, B. D. Freeman, R. J. Spontak, Z. He, I. Pinnau, P. Meakin, and A. J. Hill, Sorption, transport, and structural evidence for enhanced free volume in poly(4-methyl-2-pentyne)/fumed silica nanocomposite membranes, *Chemistry of Materials*, 15 (2003) 109-23.
- [24] T. C. Merkel, Z. He, I. Pinnau, B. D. Freeman, P. Meakin, and A. J. Hill, Effect of nanoparticles on gas sorption and transport in poly[1-(trimethylsilyl)-1-propyne], *Macromolecules*, 36 (2003) 6844-55.
- [25] R. D. Raharjo, H. J. Lee, B. D. Freeman, T. Sakaguchi, and T. Masuda, Pure gas and vapor permeation properties of poly[1-phenyl-2-[p-(trimethylsilyl)phenyl]acetylene] (PTMSDPA) and its desilylated analog, poly[diphenylacetylene] (PDPA), *Polymer*, 46 (2005) 6316-24.
- [26] L. G. Toy, Gas and hydrocarbon vapor transport properties of novel disubstituted polyacetylene membranes, Ph.D. Dissertation, North Carolina State University, 2001.
- [27] C. L. Aitken, W. J. Koros, and D. R. Paul, Gas transport properties of biphenol polysulfones, *Macromolecules*, 25 (1992) 3651-8.
- [28] J. S. McHattie, W. J. Koros, and D. R. Paul, Gas transport properties of polysulfones: 3. Comparison of tetramethyl-substituted bisphenols, *Polymer*, 33 (1992) 1701-11.
- [29] C. L. Aitken, W. J. Koros, and D. R. Paul, Effect of structural symmetry on gas transport properties of polysulfones, *Macromolecules*, 25 (1992) 3424-34.
- [30] M. W. Hellums, W. J. Koros, G. R. Husk, and D. R. Paul, Gas transport in halogen-containing aromatic polycarbonates, *Journal of Applied Polymer Science*, 43 (1991) 1977-86.
- [31] J. S. McHattie, W. J. Koros, and D. R. Paul, Gas transport properties of polysulfones. 2. Effect of bisphenol connector groups, *Polymer*, 32 (1991) 2618-25.
- [32] J. S. McHattie, W. J. Koros, and D. R. Paul, Gas transport properties of polysulfones. 1. Role of symmetry of methyl group placement on bisphenol, *Polymer*, 32 (1991) 840-50.
- [33] J. S. McHattie, W. J. Koros, and D. R. Paul, Effect of isopropylidene replacement on gas transport properties of polycarbonates, *Journal of Polymer Science, Part B: Polymer Physics*, 29 (1991) 731-46.

- [34] M. W. Hellums, W. J. Koros, G. R. Husk, and D. R. Paul, Fluorinated polycarbonates for gas separation applications, *Journal of Membrane Science*, 46 (1989) 93-112.
- [35] M. Aguilar-Vega and D. R. Paul, Gas transport properties of polycarbonates and polysulfones with aromatic substitutions on the bisphenol connector group, *Journal of Polymer Science, Part B: Polymer Physics*, 31 (1993) 1599-610.
- [36] C. L. Aitken, D. R. Paul, and D. K. Mohanty, Gas transport properties of poly(aryl ether bissulfones) and poly(aryl ether bisketones), *Journal of Polymer Science, Part B: Polymer Physics*, 31 (1993) 983-9.
- [37] C. L. Aitkin and D. R. Paul, Gas transport properties of polysulfones based on dihydroxynaphthalene isomers, *Journal of Polymer Science Part B: Polymer Physics*, 31 (1993) 1061-5.
- [38] Y. P. Yampolskii, A. P. Korikov, V. P. Shantarovich, K. Nagai, B. D. Freeman, T. Masuda, M. Teraguchi, and G. Kwak, Gas permeability and free volume of highly branched substituted acetylene polymers, *Macromolecules*, 34 (2001) 1788-96.
- [39] Y. Huang and D. R. Paul, Physical aging of thin glassy polymer films monitored by optical properties, *Macromolecules*, 39 (2006) 1554-9.
- [40] J. H. Kim, W. J. Koros, and D. R. Paul, Physical aging of thin 6FDA-based polyimide membranes containing carboxyl acid groups. Part II. Optical properties, *Polymer*, 47 (2006) 3104-11.
- [41] C. G. Robertson and G. L. Wilkes, Refractive index: a probe for monitoring volume relaxation during physical aging of glassy polymers, *Polymer*, 39 (1998) 2129-33.
- [42] N. Tanio and T. Nakanishi, Physical aging and refractive index of poly(methyl methacrylate) glass, *Polymer Journal (Tokyo, Japan)*, 38 (2006) 814-8.

8) Mixed Gas Permeability

This chapter presents the influence of crosslinking and FS nanoparticles addition on mixed gas permeabilities and selectivities of PTMSP. The mixed gas permeabilities of CH₄ and *n*-C₄H₁₀ were measured in various PTMSP films using a gas mixture containing 98 mol % CH₄ and 2 mol % *n*-C₄H₁₀. The mixed gas transport properties are reported at 35°C, 10°C, 0°C, and -20°C. These temperatures were chosen to provide a more complete fundamental understanding of the impact of nanoparticle addition and crosslinking on the gas separation properties and because natural gas separations can be performed over this temperature range [1]. The changes in mixed gas permeation properties were related to changes in the free volume characteristics of the films due to crosslinking and FS addition. Conditioning effects of the permeating gases were studied by measuring the permeability as the films were depressurized from their maximum pressure to atmospheric pressure. Pure gas permeabilities are presented at the beginning of this chapter to allow the reader to compare the pure and mixed gas permeation properties of PTMSP.

8.1) Pure Gas CH₄ and *n*-C₄H₁₀ Permeability

Figure 8.1 presents pure gas *n*-C₄H₁₀ permeabilities at 35°C of uncrosslinked PTMSP, uncrosslinked PTMSP containing 30 wt % FS nanoparticles (30 FS), crosslinked PTMSP containing 10 wt % bis(azide) crosslinker (10 XL), and crosslinked PTMSP containing 10 wt % bis(azide) crosslinker and 30 wt % FS nanoparticles (10 XL + 30 FS)

as a function of $n\text{-C}_4\text{H}_{10}$ fugacity at the upstream side of the film. The addition of crosslinks decreases permeability, and this decrease is consistent with the lower FFV of crosslinked material [2]. Upon addition of FS, the $n\text{-C}_4\text{H}_{10}$ permeability increases by approximately 30 %, relative to that of uncrosslinked PTMSP, and this increase is consistent with an increase in free volume caused by FS nanoparticles disrupting the polymer chain packing [3].

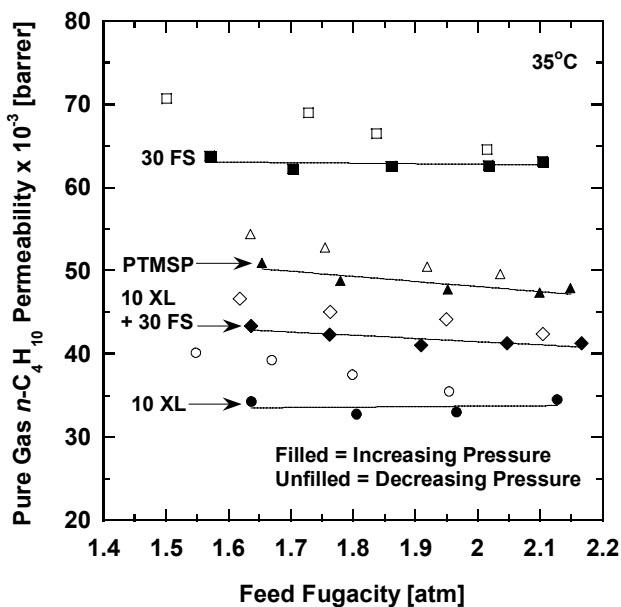


Figure 8.1. Pure gas $n\text{-C}_4\text{H}_{10}$ permeability of various PTMSP films at 35°C . The solid lines are a linear fit to the data measured as feed pressure is increased, and these lines serve as a guide for the eye of the reader. All films were crosslinked at 180°C in vacuum for 90 minutes, soaked in MeOH for 24 hours, then dried at ambient conditions for 72 hours before permeability measurements began. The thickness of the films were approximately $100\ \mu\text{m}$. In this figure and in figures 8.2 through 8.5, filled data points correspond to measurements made as feed pressure was increased, and unfilled data points correspond to measurements made as feed pressure was decreased.

The n -C₄H₁₀ permeabilities of all films are slightly higher when the permeability was measured as the film was depressurized (unfilled symbols in Fig. 1), which indicates slight conditioning of the films by n -C₄H₁₀. Conditioning occurs when penetrant sorption leads to dilation of the polymer sample as feed pressure is increased. In glassy polymers, the dilation of the sample may be slow to relax, resulting in films, when measured during depressurization, that have a slightly higher free volume than they had when the permeability measurement was made upon increasing feed pressure [4]. The increase in free volume upon depressurization often correlates with increased permeability [5]. Increases in the pure gas permeability of PTMSP upon depressurization have been shown for C₂H₆, C₃H₈, C₃F₈ [6] and ethylbenzene [7].

Figure 8.2 presents pure gas CH₄ permeabilities as function of upstream CH₄ fugacity. The permeabilities are presented at 35°C, 10°C, 0°C, and -20°C. At all temperatures, the permeability of the crosslinked film is lower than that of its uncrosslinked analog, presumably due to the lower FFV in crosslinked samples [2]. The addition of 30 wt % FS nanoparticles increases the permeability of both uncrosslinked and crosslinked PTMSP by approximately 50 %, relative to their unfilled analogs, and the permeability increase is qualitatively consistent with FS nanoparticles disrupting the polymer chain packing, thereby increasing the free volume of the resulting nanocomposites [3]. In this regard, the increases in CH₄ and n -C₄H₁₀ permeabilities upon addition of 30 wt % FS are similar to those reported by De Sitter *et al.* [8], and Merkel *et al.* [3]. Therefore, the dispersion of FS nanoparticles in the PTMSP films in this study should be similar to that observed by De Sitter *et al.* [8], and Merkel *et al.* [3], where FS

nanoparticles where observed to be aggregated in agglomerates in the size range of several hundred nanometers [3,8].

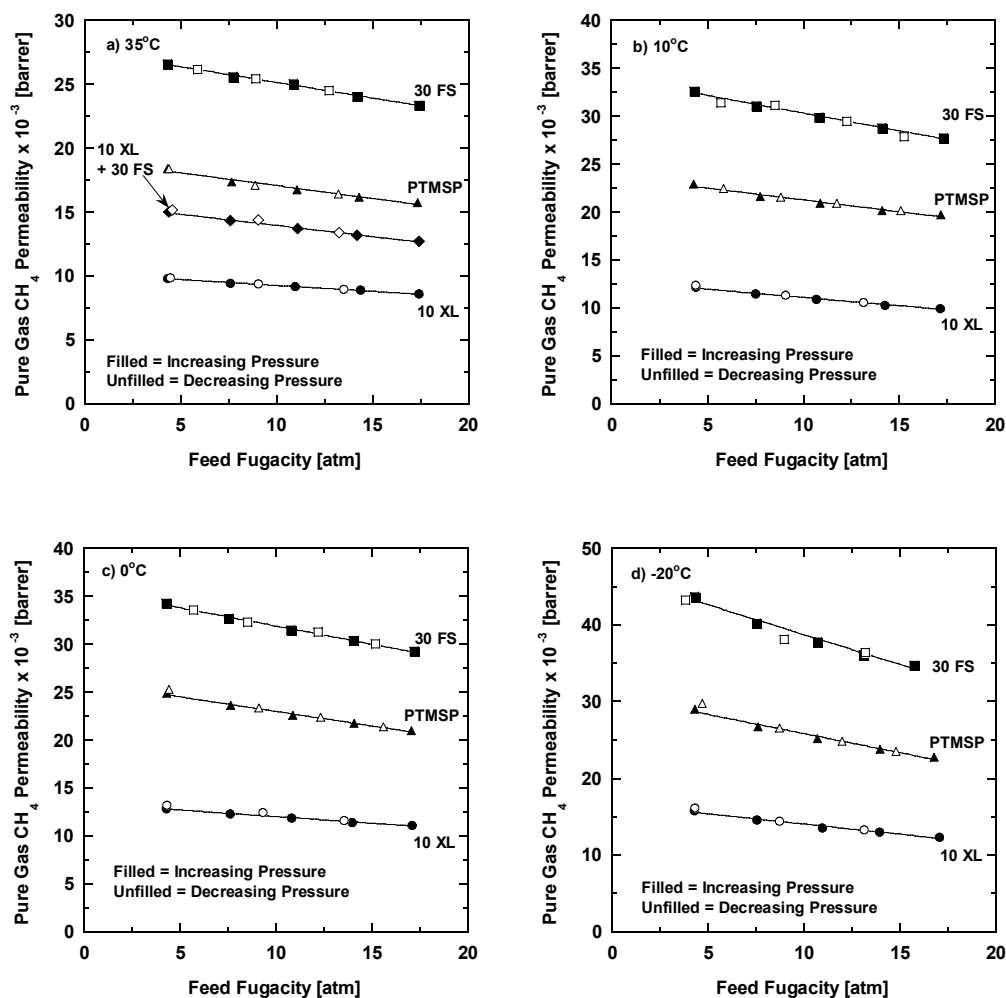


Figure 8.2. Pure gas CH_4 permeability of various PTMSP films at a) 35°C, b) 10°C, c) 0°C, and d) -20°C. The solid lines are smooth fits to the data measured as the pressure is increased, and these lines serve as a guide for the eye of the reader. All films were crosslinked at 180°C in vacuum for 90 minutes, soaked in MeOH for 24 hours, then dried at ambient conditions for 72 hours before permeability measurements began. The thickness of the films were approximately 100 μm .

As shown in *Figure 8.2*, the increase in pure gas CH₄ permeability due to 30 wt % FS addition is greater than the increase observed in pure gas *n*-C₄H₁₀ permeability. A similar result was found by Merkel *et al.*, where the pure gas CH₄ permeability of PTMSP increased by 60 % when 40 wt % FS nanoparticles were added to PTMSP, while the pure gas *n*-C₄H₁₀ permeability increased by 35 % [3]. These results follow a trend where the increase in PTMSP permeability due to FS addition is less for larger molecules. This finding is consistent with transport mechanisms other than solution-diffusion, (such as Knudsen flow in the extra free volume introduced by FS addition, which would preferentially increase the permeability of smaller molecules such as CH₄ [3]) beginning to play a role in the permeability properties of the nanocomposite films.

8.2) Mixed Gas CH₄ and *n*-C₄H₁₀ Permeability

Figure 8.3 presents mixed gas *n*-C₄H₁₀ permeabilities of the PTMSP films considered in this study. The crosslinked unfilled (10 XL) and nanocomposite (10 XL + 30 FS) samples are about 40 % less permeable to *n*-C₄H₁₀ than their uncrosslinked analogs (PTMSP and 30 FS, respectively) at 35°C, which is consistent with lower free volume in the crosslinked samples [2]. This decrease in permeability is similar at all temperatures for the unfilled crosslinked samples (10 XL). The addition of 30 wt % FS nanoparticles increases the mixed gas permeability coefficients at all temperatures, and this permeability increase is ascribed to FS nanoparticles disrupting chain packing, which increases free volume [3]. The addition of 30 wt % FS nanoparticles increases mixed gas *n*-C₄H₁₀ permeabilities of both uncrosslinked and crosslinked samples by approximately

30 %, which is similar to the increase in pure gas $n\text{-C}_4\text{H}_{10}$ permeability observed in *Figure 8.1* when 30 wt % FS was added to uncrosslinked and crosslinked PTMSP.

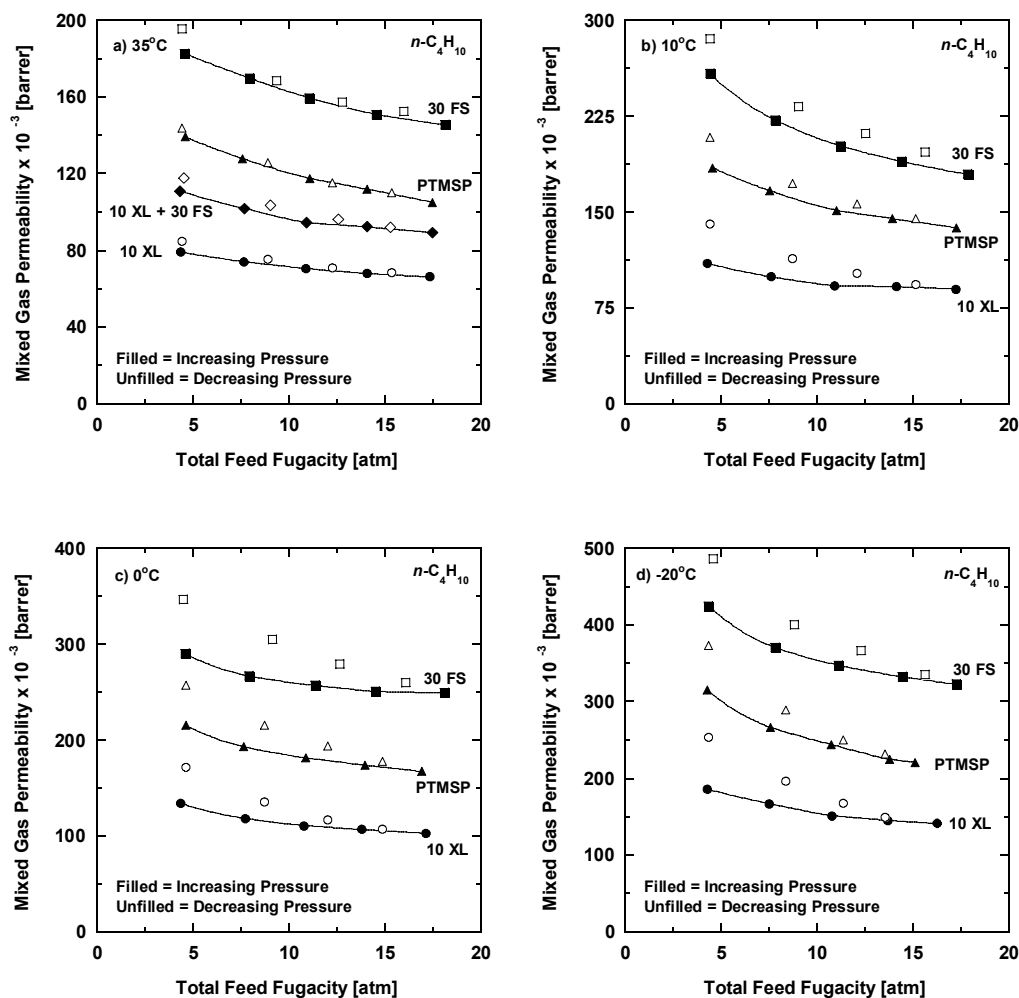


Figure 8.3. Mixed gas $n\text{-C}_4\text{H}_{10}$ permeabilities of various PTMSP films at a) 35°C, b) 10°C, c) 0°C, and d) -20°C. The solid lines are smooth fits to the data measured as the pressure is increased, and these lines serve as a guide for the eye of the reader. All films were crosslinked at 180°C in vacuum for 90 minutes, soaked in MeOH for 24 hours, then dried at ambient conditions for 72 hours before permeability measurements began. The thickness of the films was approximately 500 μm .

The mixed gas $n\text{-C}_4\text{H}_{10}$ permeabilities presented in *Figure 8.3* decrease with increasing upstream fugacity. There is no significant difference in the relative decrease of $n\text{-C}_4\text{H}_{10}$ permeabilities for different PTMSP films, and there is no qualitative difference observed when temperature decreases. Raharjo *et al.* also observed similar decreases in $n\text{-C}_4\text{H}_{10}$ permeabilities in uncrosslinked PTMSP [9] and ascribed the decrease to a reduction in the mixed gas $n\text{-C}_4\text{H}_{10}$ solubility coefficient as $n\text{-C}_4\text{H}_{10}$ fugacity increased [9,10].

As shown in *Figure 8.3*, mixed gas $n\text{-C}_4\text{H}_{10}$ permeabilities were measured as the films were depressurized to investigate conditioning effects. At all temperatures, the $n\text{-C}_4\text{H}_{10}$ permeabilities measured as the films were depressurized were equal to or greater than the mixed gas $n\text{-C}_4\text{H}_{10}$ permeabilities measured as feed pressure was increased. At any given feed fugacity and temperature for any of the films (*i.e.*, PTMSP, 10 XL, and 30 FS), the relative change in mixed gas $n\text{-C}_4\text{H}_{10}$ permeabilities between pressurization and depressurization is similar. Therefore, the addition of crosslinks or FS does not change the relative degree of conditioning. At 10°C, 0°C, and -20°C there are significant increases in mixed gas $n\text{-C}_4\text{H}_{10}$ permeabilities when the films were depressurized, and the increases are more significant when the temperature and upstream gas fugacity were lower. At 35°C, the increases in mixed gas $n\text{-C}_4\text{H}_{10}$ permeabilities for all films upon depressurization are not significant within the resolution of the experiment. The negligible change in mixed gas $n\text{-C}_4\text{H}_{10}$ permeabilities on depressurization at 35°C may be a consequence of lower $n\text{-C}_4\text{H}_{10}$ activities in the mixed gas feed stream at higher temperatures. At higher activities, penetrants sorb to a greater extent, thereby dilating the

polymer and disrupting polymer chain packing to a greater degree [4], causing a greater increase in conditioning effects.

Figure 8.4 presents mixed gas CH₄ permeabilities of various PTMSP films as a function of total upstream fugacity. The addition of crosslinks decreases mixed gas CH₄ permeabilities of PTMSP, while the addition of FS nanoparticles increases mixed gas CH₄ permeabilities, similar to the trends observed in the pure gas case (*cf.*, Fig. 8.2). The decrease in mixed gas CH₄ permeability of the unfilled samples in *Figure 8.4* upon crosslinking is approximately 30 % at all temperatures. The decrease in mixed gas CH₄ permeability in the nanocomposite sample at 35°C upon crosslinking is approximately 40 %. The mixed gas CH₄ permeability of uncrosslinked and crosslinked PTMSP increases by 100 – 130 % due to addition of 30 wt % FS. This increase is substantially greater than the 40 % increase in mixed gas *n*-C₄H₁₀ permeability in both uncrosslinked and crosslinked films when FS nanoparticles were added.

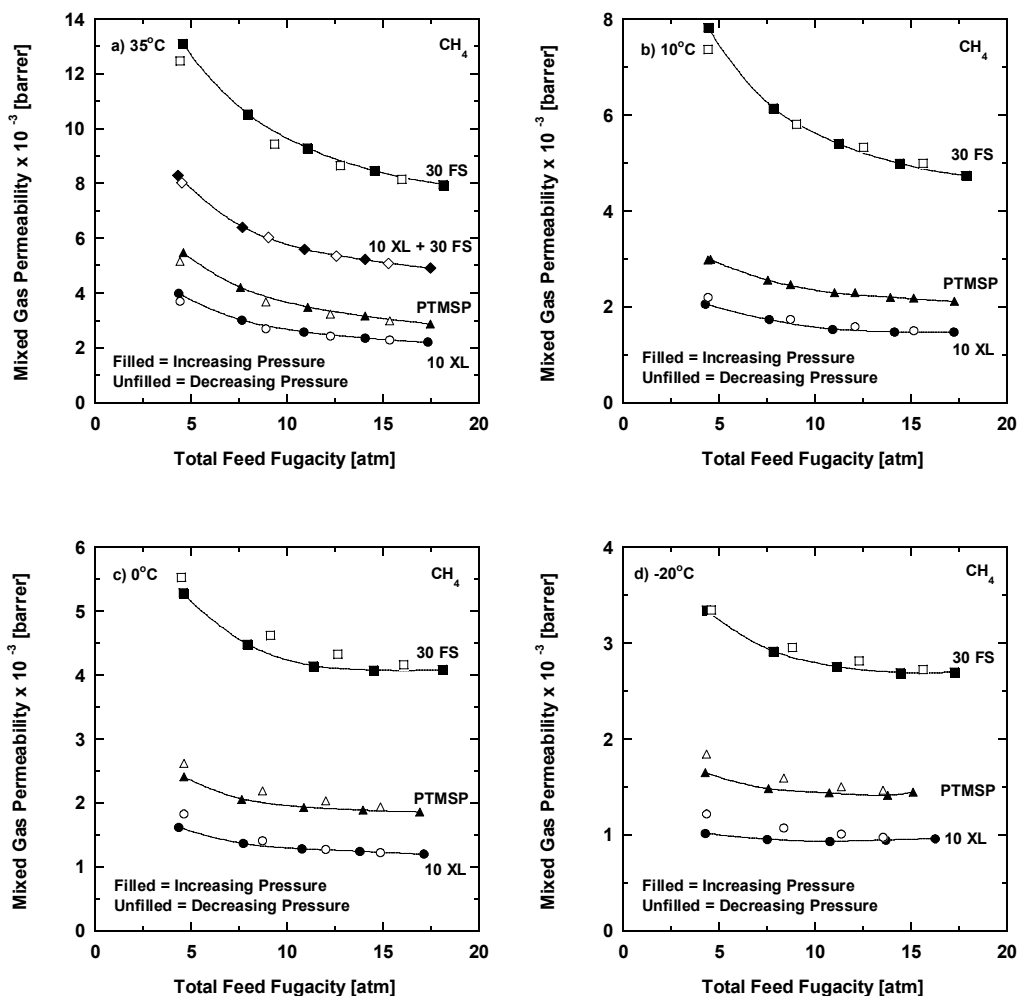


Figure 8.4. Mixed gas CH_4 permeability of various PTMSP films at a) 35°C, b) 10°C, c) 0°C, and d) -20°C. The solid lines are smooth fits to the data measured as the pressure is increased, and these lines serve as a guide for the eye of the reader. All films were crosslinked at 180°C in vacuum for 90 minutes, soaked in MeOH for 24 hours, then dried at ambient conditions for 72 hours before permeability measurements began. The thickness of the films was approximately 500 μm .

As shown in *Figure 8.4*, there are at most only slightly differences in the mixed gas CH_4 permeabilities measured during pressurization and depressurization. Therefore, any conditioning that is occurring has weak effect on CH_4 permeability. The uncertainty

in the mixed gas CH_4 permeabilities measured during depressurization is approximately $\pm 5\%$.

Figure 8.5 presents the mixed gas $n\text{-C}_4\text{H}_{10}/\text{CH}_4$ selectivities of various PTMSP films as a function of total feed fugacity. At all temperatures, the mixed gas $n\text{-C}_4\text{H}_{10}/\text{CH}_4$ selectivities decrease when PTMSP is crosslinked (*e.g.*, compare PTMSP to 10 XL in Fig. 8.5), which is consistent with previous results [2]. The addition of FS causes a substantial decrease in mixed gas selectivity (*e.g.*, compare PTMSP to 30 FS in Fig. 8.5), which is consistent with previous results [2,3]. For example, at 35°C , the mixed gas $n\text{-C}_4\text{H}_{10}/\text{CH}_4$ selectivities of 30 FS are approximately 50 % less than those of PTMSP, while at -20°C a 30 % decrease in mixed gas selectivity is observed.

Crosslinking PTMSP decreases its FFV [2], so the crosslinked films are likely to be more size-sieving than their uncrosslinked analogs [5], which would favor a reduction in the mixed gas $n\text{-C}_4\text{H}_{10}/\text{CH}_4$ permeability selectivity upon crosslinking. When FS is added to PTMSP, the decrease in mixed gas $n\text{-C}_4\text{H}_{10}/\text{CH}_4$ selectivities is thought to be caused by FS-induced creation of structures (*e.g.*, pores large enough to permit Knudsen flow) that are CH_4 selective [3]. In the case of crosslinking and addition of FS, the overall effect is a reduction in the mixed gas $n\text{-C}_4\text{H}_{10}/\text{CH}_4$ permeability selectivity, but the molecular basis for this effect is probably different for crosslinking and FS addition.

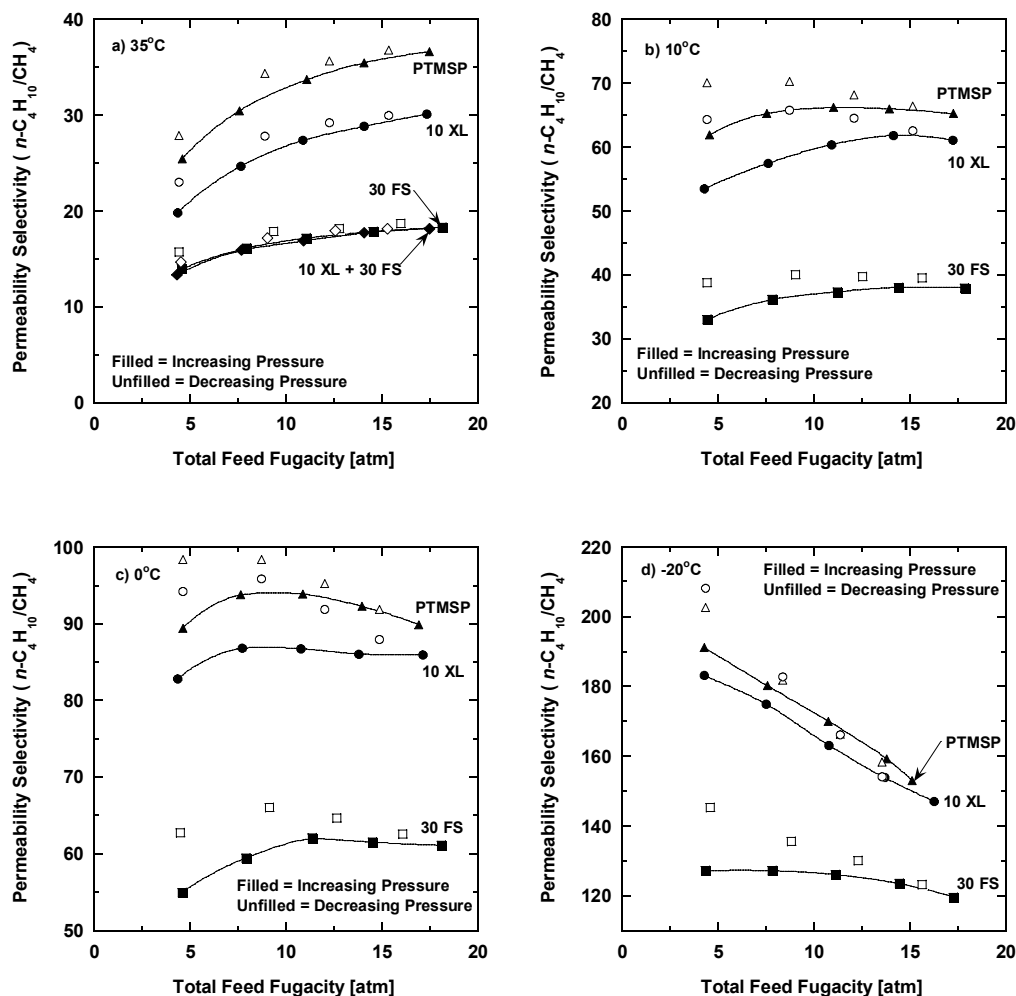


Figure 8.5. Mixed gas $n\text{-C}_4\text{H}_{10}/\text{CH}_4$ permeability selectivity of various PTMSP films at a) 35°C, b) 10°C, c) 0°C, and d) -20°C. The solid lines are smooth fits to the data measured as the pressure is increased, and these lines serve as a guide for the eye of the reader. All films were crosslinked at 180°C in vacuum for 90 minutes, soaked in MeOH for 24 hours, then dried at ambient conditions for 72 hours before permeability measurements began. The thickness of the films was approximately 500 μm .

As shown in *Figure 8.5*, when temperature decreases, the mixed gas permeability selectivities of crosslinked PTMSP (10 XL) and nanocomposite uncrosslinked PTMSP (30 FS) become more comparable to the selectivities of uncrosslinked PTMSP. This

effect could be caused by the increase in $n\text{-C}_4\text{H}_{10}$ activity in the feed gas as temperature decreases. At higher activity, more $n\text{-C}_4\text{H}_{10}$ sorbs in the films and can block the permeation of CH_4 . Higher concentrations of $n\text{-C}_4\text{H}_{10}$ may reduce the effect that crosslinks and FS addition have on decreasing mixed gas $n\text{-C}_4\text{H}_{10}/\text{CH}_4$ permeability selectivity. However, a complete explanation of this phenomenon is not currently available. The shape of the permeability versus fugacity plots changes with temperature, and the reason for this will be discussed in greater detail later in this chapter.

The mixed gas $n\text{-C}_4\text{H}_{10}/\text{CH}_4$ selectivities were also measured as the films were depressurized, and these values are displayed as the unfilled symbols in *Figure 8.5*. At 10°C , 0°C , and -20°C , the mixed gas $n\text{-C}_4\text{H}_{10}/\text{CH}_4$ selectivities measured during depressurization are greater than those measured as the films were pressurized, and the difference is most significant at the lowest fugacities. In contrast, at 35°C there was no significant increase in mixed gas selectivity upon depressurization. For all films, and at all temperatures, the relative increase in mixed gas selectivity upon depressurization is similar. The increase in mixed gas $n\text{-C}_4\text{H}_{10}/\text{CH}_4$ selectivities upon depressurization is a consequence of the mixed gas $n\text{-C}_4\text{H}_{10}$ permeabilities increasing significantly more than the mixed gas CH_4 permeabilities during depressurization, as shown in *Figure 8.3* and *Figure 8.4*. That is, conditioning influences the permeation properties of the larger penetrant ($n\text{-C}_4\text{H}_{10}$) more than that of the smaller penetrant (CH_4).

8.3) Effect of Upstream $n\text{-C}_4\text{H}_{10}$ Activity on Mixed Permeability

Figure 8.6 presents mixed gas $n\text{-C}_4\text{H}_{10}$ permeabilities of various PTMSP films as function of $n\text{-C}_4\text{H}_{10}$ upstream activity and temperature. The mixed gas $n\text{-C}_4\text{H}_{10}$ permeabilities of all films decrease as $n\text{-C}_4\text{H}_{10}$ activity increases, which is consistent with the decrease in $n\text{-C}_4\text{H}_{10}$ solubility coefficients with increasing $n\text{-C}_4\text{H}_{10}$ activity observed in pure gas sorption studies [2,6,10]. The mixed gas $n\text{-C}_4\text{H}_{10}$ permeabilities increase as temperature decreases, which agrees with prior reports of negative activation energies of permeation for gases and vapors in PTMSP [3,9,11]. Similar trends in mixed gas $n\text{-C}_4\text{H}_{10}$ permeability were reported by Raharjo *et al.* [9], and data from their study are presented in Figure 8.6 for comparison.

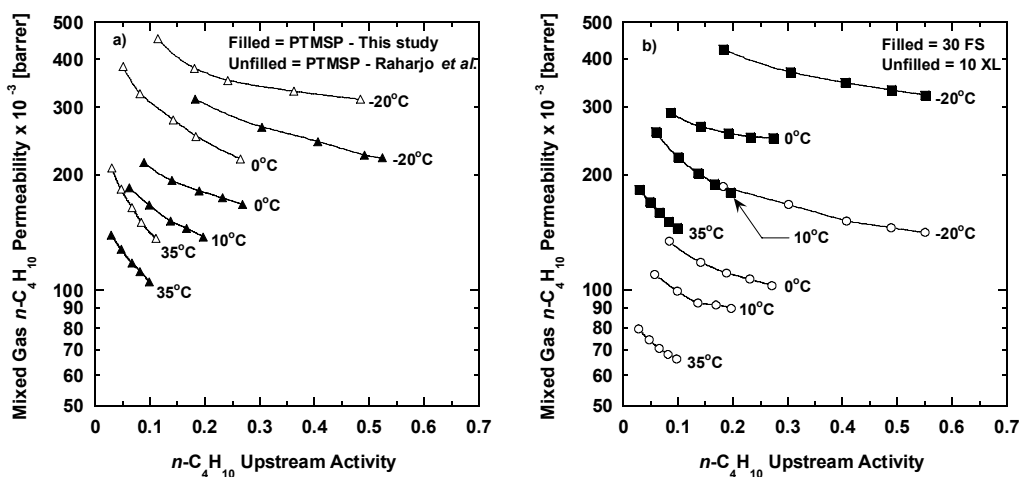


Figure 8.6. Mixed gas $n\text{-C}_4\text{H}_{10}$ permeabilities of a) uncrosslinked PTMSP, and b) PTMSP + 30 wt % FS (30 FS) and PTMSP + 10 wt % XL (10 XL) as function of upstream $n\text{-C}_4\text{H}_{10}$ activity. The smooth lines are intended to act as guides for the eye of the reader. The mixed gas $n\text{-C}_4\text{H}_{10}$ permeabilities from this study are reported at 35°C, 10°C, 0°C, and -20°C. The mixed gas $n\text{-C}_4\text{H}_{10}$ permeabilities from Raharjo's *et al.* study are reported at 35°C, 0°C, and -20°C [9]. $n\text{-C}_4\text{H}_{10}$ activity is calculated as f_2/f_{sat} , where the fugacity value at saturation, f_{sat} , was calculated as described by Raharjo *et al.* [12].

At similar temperature and activity, the mixed gas $n\text{-C}_4\text{H}_{10}$ permeabilities of uncrosslinked PTMSP in this study are slightly less than those reported by Raharjo *et al.*, and this variation can be explained by differences in the thermal histories of the films. All films in this study were thermally annealed at 180°C in a vacuum oven for 90 minutes, while films in the Raharjo *et al.* study were not subjected to any thermal treatment [9]. The thermal annealing treatment decreases pure gas CH_4 permeabilities and increases the density of PTMSP [5]. For example, the uncrosslinked PTMSP films in this study had a density of $0.76 \pm 0.01 \text{ g/cm}^3$, and a pure gas CH_4 permeability at 35°C and 4.4 atm of 18,000 barrer. In the Raharjo *et al.* study, the density of PTMSP was $0.73 \pm 0.01 \text{ g/cm}^3$, and the pure gas CH_4 permeability at 35°C and 4.4 atm was 26,000 barrer [9]. Therefore, the thermal annealing treatment used in this study is believed to be the basis for differences in $n\text{-C}_4\text{H}_{10}$ permeabilities between this study and that of Raharjo *et al.*

Figure 8.7 presents mixed gas CH_4 permeabilities of various PTMSP films as a function of temperature and upstream $n\text{-C}_4\text{H}_{10}$ activity. The mixed gas CH_4 permeabilities from Raharjo *et al.* [9] are slightly greater than those of the uncrosslinked PTMSP films in this study, and this difference is related to differences in thermal histories of the films.

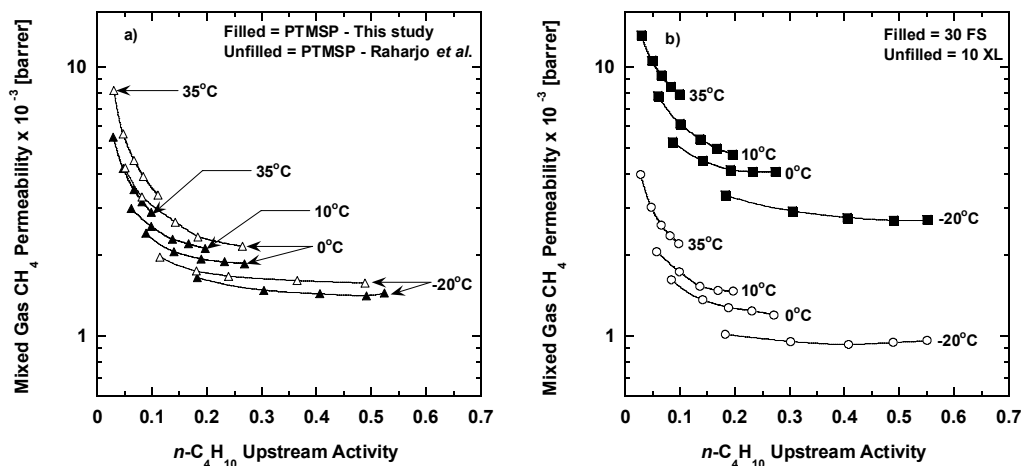


Figure 8.7. Mixed gas CH_4 permeabilities of a) uncrosslinked PTMSP, and b) PTMSP + 30 wt % FS (30 FS) and PTMSP + 10 wt % XL (10 XL) as function of upstream $n\text{-C}_4\text{H}_{10}$ activity. The smooth lines are intended to act as guides for the eye of the reader. The mixed gas CH_4 permeabilities from this study are reported at 35°C, 10°C, 0°C, and -20°C. The mixed gas CH_4 permeabilities from Raharjo's *et al.* study are reported at 35°C, 0°C, and -20°C [9].

The mixed gas CH_4 permeabilities of all films decrease as upstream $n\text{-C}_4\text{H}_{10}$ activity increases. For all films, the mixed gas CH_4 permeabilities decrease with decreasing temperature, and this result is opposite to the behaviour observed for pure gas CH_4 permeation in PTMSP, where CH_4 permeability increases with decreasing temperature [3,9,11]. This interesting trend results from a competition among several factors [13,14]. As temperature decreases, CH_4 solubility would, in the absence of $n\text{-C}_4\text{H}_{10}$, increase more than the CH_4 diffusion coefficient decreases, resulting in an increase in CH_4 permeability [9,11]. However, in the presence of $n\text{-C}_4\text{H}_{10}$, as temperature decreases, the amount of $n\text{-C}_4\text{H}_{10}$ sorbed in the film, at fixed activity, increases and, due to the resulting competitive sorption effects, the CH_4 solubility actually decreases (rather than increases)

[10]. As temperature decreases, CH₄ diffusivity decreases in both pure gas and mixed gas cases [9,11]. However, in the presence of *n*-C₄H₁₀ at fixed activity, the decrease in CH₄ diffusivity with temperature is greater than in the absence of *n*-C₄H₁₀ [9]. Consequently, the CH₄ permeability, in the presence of *n*-C₄H₁₀, decreases as temperature decreases, but, in the absence of *n*-C₄H₁₀, the CH₄ permeability increases as temperature decreases (*cf.*, Fig. 8.2).

Figure 8.8 presents CH₄ blocking ratios (*i.e.*, the ratios of mixed gas CH₄ permeabilities to pure gas CH₄ permeabilities) as a function of upstream *n*-C₄H₁₀ activity. The ratios of mixed to pure gas CH₄ permeabilities of uncrosslinked, unfilled PTMSP are similar to the values reported by Raharjo *et al.* [9,15]. At all temperatures, the ratios of mixed to pure gas CH₄ permeabilities are greater for crosslinked PTMSP (10 XL) and nanocomposite uncrosslinked PTMSP (30 FS) than for uncrosslinked PTMSP. This increase is thought to be caused by crosslinks and FS nanoparticles changing the free volume characteristics of PTMSP such that the blocking of CH₄ permeation by *n*-C₄H₁₀ is reduced in the 10 XL and 30 FS samples.

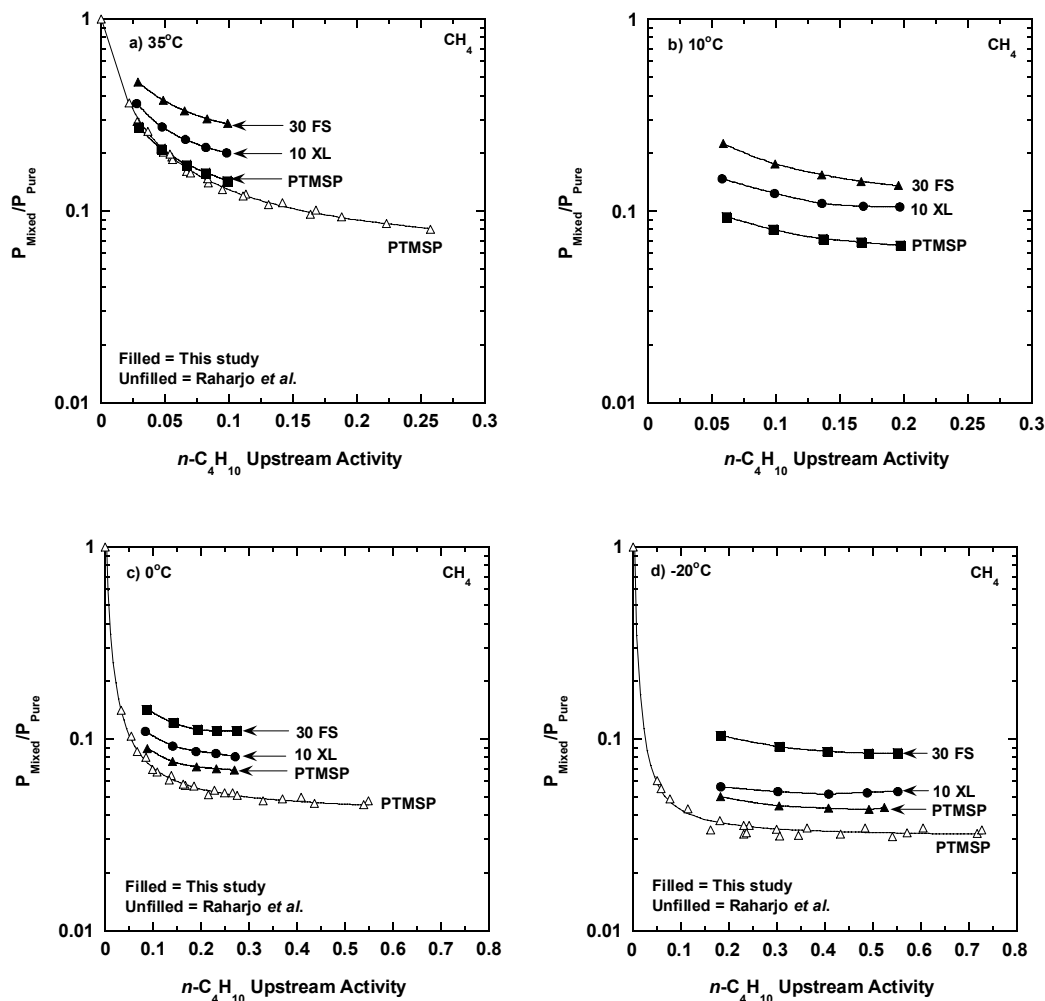


Figure 8.8 The ratio of mixed gas CH_4 permeabilities to pure gas CH_4 permeabilities at infinite dilution as a function of upstream $n\text{-C}_4\text{H}_{10}$ activity at a) 35°C , b) 10°C , c) 0°C , and d) -20°C . The filled symbols represent values from this study, while the unfilled symbols represent data from Raharjo et al., which reports such data for unfilled uncrosslinked PTMSP [9,15].

Figure 8.9 presents the mixed gas $n\text{-C}_4\text{H}_{10}/\text{CH}_4$ selectivities of various PTMSP films as a function of $n\text{-C}_4\text{H}_{10}$ activity and temperature. Some of these data were presented earlier in Figure 8.5, but the shape of the selectivity versus fugacity was not discussed at that point. The $n\text{-C}_4\text{H}_{10}/\text{CH}_4$ selectivities of all films increase as temperature

decreases. This increase occurs because mixed gas $n\text{-C}_4\text{H}_{10}$ permeabilities increase with decreasing temperature, while mixed gas CH_4 permeabilities decrease with decreasing temperature (*cf.*, Fig. 8.6 and 8.7).

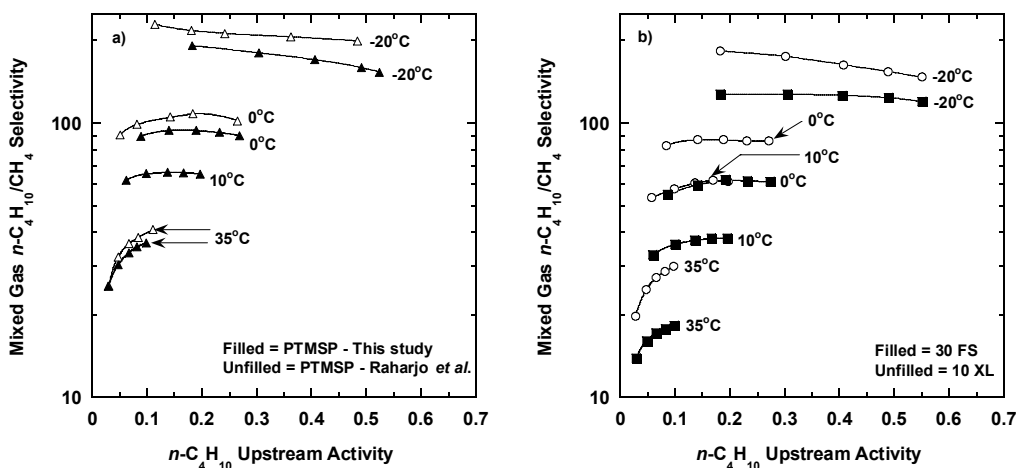


Figure 8.9. Mixed gas $n\text{-C}_4\text{H}_{10}/\text{CH}_4$ selectivities of a) uncrosslinked PTMSP, and b) PTMSP + 30 wt % FS (30 FS) and PTMSP + 10 wt % XL (10 XL) as function of upstream $n\text{-C}_4\text{H}_{10}$ activity. The smooth lines are intended to act as guides for the eye of the reader. The mixed gas $n\text{-C}_4\text{H}_{10}/\text{CH}_4$ selectivities from this study are reported at 35°C, 10°C, 0°C, and -20°C. The mixed gas $n\text{-C}_4\text{H}_{10}/\text{CH}_4$ selectivities from Raharjo's et al. study are reported at 35°C, 0°C, and -20°C [9].

At 35°C, the $n\text{-C}_4\text{H}_{10}/\text{CH}_4$ selectivities increase with increasing $n\text{-C}_4\text{H}_{10}$ activity. For example, the $n\text{-C}_4\text{H}_{10}/\text{CH}_4$ selectivity of uncrosslinked PTMSP increases from 25 to 36 when $n\text{-C}_4\text{H}_{10}$ activity increases from 0.03 to 0.10. This increase in selectivity occurs because, over this activity range, CH_4 permeability is decreasing faster than that of $n\text{-C}_4\text{H}_{10}$ with increasing activity [9]. At all temperatures other than -20°C, the $n\text{-C}_4\text{H}_{10}/\text{CH}_4$ selectivities are relatively constant when $n\text{-C}_4\text{H}_{10}$ activity is greater than about 0.15, because at higher activity values, the blocking of CH_4 transport by $n\text{-C}_4\text{H}_{10}$

reaches an asymptote. At 0°C and 10°C, a significant increase in $n\text{-C}_4\text{H}_{10}/\text{CH}_4$ selectivity with increasing activity is not observed because the lowest activity value that was experimentally accessible was probably in a range where blocking had already reached its asymptotic value. At -20°C, $n\text{-C}_4\text{H}_{10}/\text{CH}_4$ selectivity decreases slightly with increasing activity, and this result is consistent with the findings of Raharjo *et al* [9].

8.4) Effect of Temperature

Figure 8.10 presents the effect of temperature on the mixed gas transport properties of various PTMSP films. All mixed and pure gas permeabilities and selectivities are reported for an upstream CH_4 fugacity of 11 atm, which was selected because it provides a convenient reference point for comparison with pure gas CH_4 data in *Figure 8.2*. In *Figure 8.10a*, the mixed gas $n\text{-C}_4\text{H}_{10}$ permeabilities increase as temperature decreases, and the data follows Equation 2.14. The activation energies of $n\text{-C}_4\text{H}_{10}$ permeation were calculated using Equation 2.14. The addition of crosslinks or nanoparticles to PTMSP did not change the temperature dependence of the mixed gas $n\text{-C}_4\text{H}_{10}$ permeation. For all films in this study, the activation energy of mixed gas $n\text{-C}_4\text{H}_{10}$ permeation is -9 ± 1 kJ/mol.

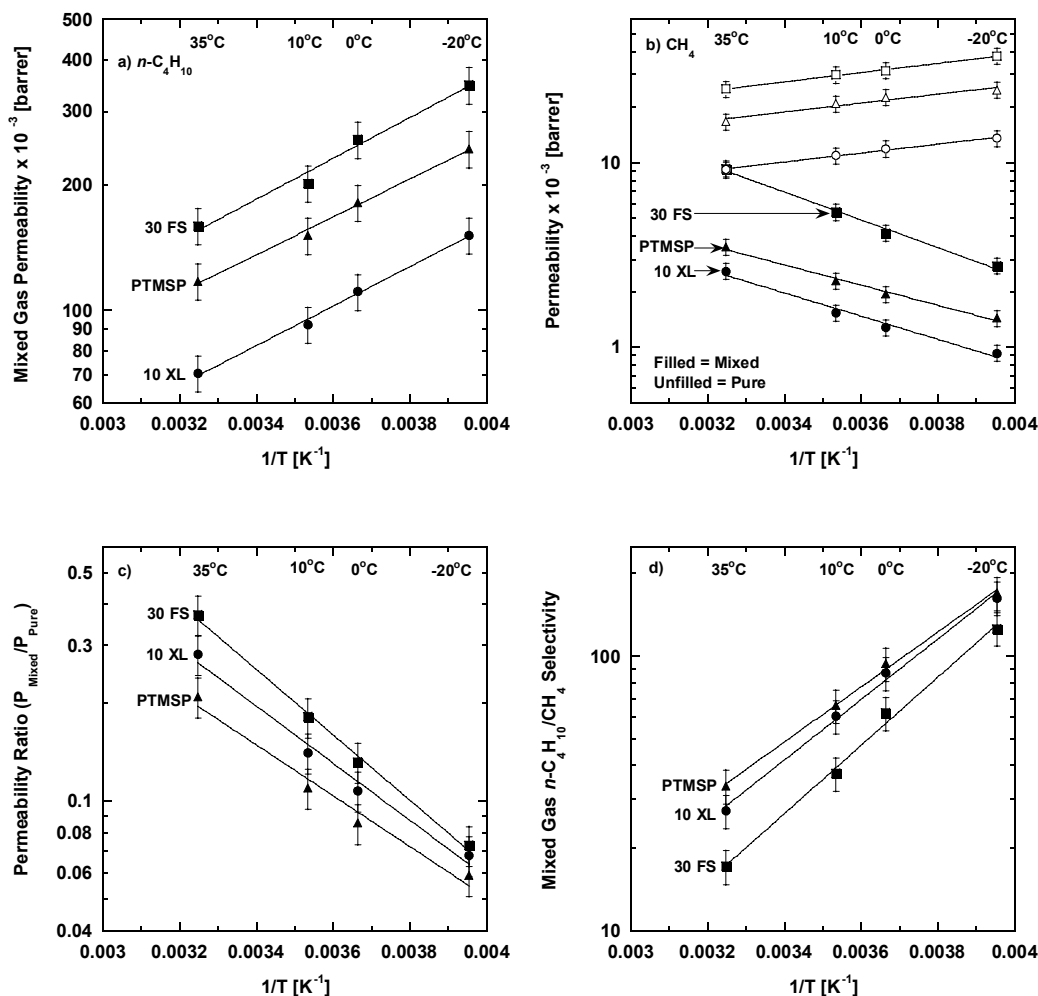


Figure 8.10. The effect of temperature on a) mixed gas $n\text{-C}_4\text{H}_{10}$ permeabilities, b) mixed gas CH_4 permeabilities, c) the ratio of mixed to pure gas CH_4 permeabilities, and d) mixed gas $n\text{-C}_4\text{H}_{10}/\text{CH}_4$ selectivities of various PTMSP films. The data are reported at a CH_4 feed fugacity of 11 atm for measurements made as the film was pressurized. The solid lines are an Arrhenius fit to the data. All films were crosslinked at 180°C in vacuum for 90 minutes, soaked in MeOH for 24 hours, then dried at ambient conditions for 72 hours before permeability measurements began.

The activation energies of pure and mixed gas CH_4 permeation are calculated from the data presented in *Figure 8.10b*, and the values are recorded in Table 8.1. For all

films, the pure gas activation energies are negative, while the activation energies of mixed gas CH₄ permeation are positive.

Table 8.1. Activation energies of pure and mixed gas CH₄ permeation in various PTMSP films. The activation energies are reported at a CH₄ fugacity of 11 atm in the feed gas.

Film	E_p (kJ/mol) - Pure	E_p (kJ/mol) - Mixed
PTMSP	- 4.6 ± 1.0	11 ± 1
10 XL	- 4.6 ± 1.0	12 ± 1
30 FS	- 4.8 ± 1.0	14 ± 1

The activation energies of pure gas CH₄ permeation are similar for all films. Likewise, the activation energies of mixed gas CH₄ permeation are similar for all films. As indicated earlier the presence of *n*-C₄H₁₀ in the feed gas has a profound influence on CH₄ permeation properties, and the activation energy data are one further example of this phenomenon.

In *Figure 8.10c*, the ratios of mixed to pure gas CH₄ permeabilities are observed to decrease as temperature decreases. This decrease could be related to the activity of *n*-C₄H₁₀ in the feed gas in the mixed gas permeation experiments. When the fugacity is fixed, as it is for the data reported in *Figure 8.10c*, the activity of *n*-C₄H₁₀ in the feed gas increases as temperature decreases. Consequently, more *n*-C₄H₁₀ is present at lower temperatures in the PTMSP films to block the permeation of CH₄ [9], which results in lower mixed gas CH₄ permeabilities, and lower mixed to pure gas CH₄ permeability ratios.

The mixed gas $n\text{-C}_4\text{H}_{10}/\text{CH}_4$ selectivities of all PTMSP films shown in *Figure 8.10d* are observed to increase as temperature decreases. The reason for the increase in selectivity is caused by $n\text{-C}_4\text{H}_{10}$ permeabilities increasing and CH_4 permeabilities decreasing when temperature decreases (*cf.*, Fig. 8.6 and 8.7). At all temperatures, the mixed gas selectivities of crosslinked PTMSP films and nanocomposite uncrosslinked PTMSP films are less than that of the uncrosslinked PTMSP films.

8.5) Conclusions

The addition of crosslinks to PTMSP decreases the mixed gas CH_4 and $n\text{-C}_4\text{H}_{10}$ permeabilities, and the decrease is consistent with a decrease in FFV of crosslinked PTMSP. FS nanoparticle addition to uncrosslinked and crosslinked PTMSP increases the mixed gas CH_4 and $n\text{-C}_4\text{H}_{10}$ permeabilities, as FS nanoparticles are thought to disrupt the polymer chain packing, causing additional free volume to be created. The mixed gas $n\text{-C}_4\text{H}_{10}/\text{CH}_4$ selectivities of crosslinked PTMSP and nanocomposite PTMSP were less than those of uncrosslinked PTMSP. Crosslinking PTMSP decreases FFV. Consequently, the CH_4 permeability is reduced less by crosslinking than $n\text{-C}_4\text{H}_{10}$ permeability. In samples containing FS, enough free volume is added to permit the onset of transport mechanisms that are CH_4 selective. Consequently, $n\text{-C}_4\text{H}_{10}/\text{CH}_4$ selectivity decreases in sample containing FS. As temperature decreased, mixed gas $n\text{-C}_4\text{H}_{10}$ permeabilities increased, while mixed gas CH_4 permeabilities decreased. Overall, $n\text{-C}_4\text{H}_{10}/\text{CH}_4$ permeability selectivities increase with decreasing temperature. The decrease in mixed gas CH_4 permeability with decreasing temperature is opposite to that observed for pure

gas CH₄ permeation, where an increase in permeability is observed with decreasing temperature. This difference in behavior is thought to be related to the blocking of CH₄ permeation by *n*-C₄H₁₀ in the gas mixture.

8.6) References

- [1] R. W. Baker, Future directions of membrane gas separation technology, *Industrial & Engineering Chemistry Research*, 41 (2002) 1393-411.
- [2] S. D. Kelman, S. Matteucci, C. W. Bielawski, and B. D. Freeman, Crosslinking poly[1-(trimethylsilyl)-1-propyne] and its effect on solvent resistance and transport properties, *Polymer*, 48 (2007) 6881-92.
- [3] T. C. Merkel, Z. He, I. Pinnau, B. D. Freeman, P. Meakin, and A. J. Hill, Effect of nanoparticles on gas sorption and transport in poly[1-(trimethylsilyl)-1-propyne], *Macromolecules*, 36 (2003) 6844-55.
- [4] S. M. Jordan, G. K. Fleming, and W. J. Koros, Permeability of carbon dioxide at elevated pressures in substituted polycarbonates, *Journal of Polymer Science, Part B: Polymer Physics*, 28 (1990) 2305-27.
- [5] S. Matteucci, Y. Yampolskii, B. D. Freeman, and I. Pinnau, in: Y. Yampolskii, B. D. Freeman, I. Pinnau (Eds.), *Material Science of Membranes for Gas and Vapor Separation*, John Wiley & Sons, New York, 2006, pp. 1-47.
- [6] T. C. Merkel, V. Bondar, K. Nagai, and B. D. Freeman, Sorption and transport of hydrocarbon and perfluorocarbon gases in poly[1-(trimethylsilyl)-1-propyne], *Journal of Polymer Science, Part B: Polymer Physics*, 38 (2000) 273-96.
- [7] S. V. Dixon-Garrett, K. Nagai, and B. D. Freeman, Sorption, diffusion, and permeation of ethylbenzene in poly[1-(trimethylsilyl)-1-propyne], *Journal of Polymer Science, Part B: Polymer Physics*, 38 (2000) 1078-89.
- [8] K. De Sitter, P. Winberg, J. D'Haen, C. Dotremont, R. Leysen, J. A. Martens, S. Mullens, F. H. J. Maurer, and I. F. J. Vankelecom, Silica filled poly[1-(trimethylsilyl)-1-propyne] nanocomposite membranes: Relation between the transport of gases and structural characteristics, *Journal of Membrane Science*, 278 (2006) 83-91.

- [9] R. D. Raharjo, B. D. Freeman, D. R. Paul, and E. S. Sanders, Pure and mixed gas CH₄ and *n*-C₄H₁₀ permeability and diffusivity in poly[1-(trimethylsilyl)-1-propyne], *Polymer*, 48 (2007) 7329-44.
- [10] R. D. Raharjo, B. D. Freeman, and E. S. Sanders, Pure and mixed gas CH₄ and *n*-C₄H₁₀ sorption and dilation in poly[1-(trimethylsilyl)-1-propyne], *Polymer*, 48 (2007) 6097-114.
- [11] T. Masuda, Y. Iguchi, B. Z. Tang, and T. Higashimura, Diffusion and solution of gases in substituted polyacetylene membranes, *Polymer*, 29 (1988) 2041-9.
- [12] R. D. Raharjo, B. D. Freeman, and E. S. Sanders, Pure and mixed gas CH₄ and *n*-C₄H₁₀ sorption and dilation in poly(dimethylsiloxane), *Journal of Membrane Science*, 292 (2007) 45-61.
- [13] W. J. Koros, R. T. Chern, V. Stannett, and H. B. Hopfenberg, A model for permeation of mixed gases and vapors in glassy polymers, *Journal of Polymer Science, Polymer Physics Edition*, 19 (1981) 1513-30.
- [14] E. S. Sanders, W. J. Koros, H. B. Hopfenberg, and V. T. Stannett, Pure and mixed gas sorption of carbon dioxide and ethylene in poly(methyl methacrylate), *Journal of Membrane Science*, 18 (1984) 53-74.
- [15] R. D. Raharjo, Mixed gas sorption and transport study in solubility selective polymers, Ph.D. Dissertation, University of Texas at Austin, 2007.

9) Conclusions and Recommendations

9.1) Conclusions

This dissertation focused on a systematic study of changes in gas transport properties of poly[1-(trimethylsilyl)-1-propyne] (PTMSP) caused by the addition of bis(azide) crosslinks and fumed silica (FS) nanoparticles. PTMSP was chosen because of its very high gas permeability, and outstanding vapor/gas selectivity [1,2]. Crosslinks were added to PTMSP to improve its solvent resistance and physical stability [3], while FS nanoparticles were added to increase the permeability [4]. The crosslinking of PTMSP greatly increased its solvent resistance, and the crosslinked polymer was insoluble in good solvents for PTMSP, such as toluene [5]. The addition of crosslinks and FS to PTMSP had differing effects on the free volume of the resulting films, where crosslinking decreases the free volume, and FS addition increases the free volume.

9.1.1) Pure Gas Solubility, Permeability, and Diffusivity

The addition of crosslinks causes no significant change in the solubility of gases and vapors in PTMSP, while the addition of 30 wt % FS nanoparticles to uncrosslinked and crosslinked samples decreases the nanocomposite gas and vapor solubility by 10 – 20 %. The dual-mode sorption model was successfully fitted to the sorption isotherms for all PTMSP films, and the decrease in solubility of the nanocomposite samples could be described by a decrease in the number of non-equilibrium sorption sites, represented by C'_H , the Langmuir sorption capacity. The addition of crosslinks causes a decrease in the

permeability of PTMSP. The addition of 30 wt % FS nanoparticles to uncrosslinked and crosslinked samples increases the permeability by 30 – 65 %. The addition of crosslinks and FS nanoparticles has differing effects on the PTMSP diffusivity; where crosslinking decreases diffusivity, while FS nanoparticle addition increases diffusivity. The solubilities and permeabilities of N₂, O₂, CH₄, C₂H₆, and C₃H₈ in PTMSP increase as temperature decreases, while the diffusivities decrease with decreasing temperature. The changes in permeability, solubility and diffusivity with temperature are similar for all PTMSP films studied, so the addition of crosslinks or FS did not change the temperature dependence of pure gas PTMSP transport properties.

9.1.2) Aging Studies

The gas permeability and FFV of uncrosslinked and crosslinked PTMSP decreases over time. The rate of permeability decrease is greater for crosslinked PTMSP, while the rate of FFV decrease is similar for uncrosslinked and crosslinked PTMSP. The addition of 10 wt % POSS nanoparticles decreases the permeability of uncrosslinked and crosslinked PTMSP by approximately 70 %, and the permeability and FFV values of PTMSP films containing POSS were then stable over time. PALS results suggest that the POSS nanoparticles fill the larger free volume elements of PTMSP, mitigating physical aging by preventing the free volume collapse. Physical aging of thin PTMSP films, studied using ellipsometry, show little difference in aging rates (*i.e.*, density increase) between uncrosslinked and crosslinked films. The thin PTMSP films in this study age more rapidly than any other thin glassy polymer film studied to date using ellipsometry.

9.1.3) Mixed Gas Permeability, and Selectivity

The addition of crosslinks to PTMSP decreases mixed gas CH_4 and $n\text{-C}_4\text{H}_{10}$ permeabilities, and the decrease is consistent with the decrease in FFV in crosslinked PTMSP that occurs. FS nanoparticle addition to uncrosslinked and crosslinked PTMSP increases mixed gas CH_4 and $n\text{-C}_4\text{H}_{10}$ permeabilities, as FS nanoparticles are thought to disrupt the polymer chain packing, causing additional free volume to be created. The mixed gas $n\text{-C}_4\text{H}_{10}/\text{CH}_4$ selectivities of crosslinked PTMSP and nanocomposite PTMSP are less than those of uncrosslinked PTMSP. Crosslinking PTMSP decreases FFV, and the polymer is thought to become more size-selective in the mixed gas experiments, which increases the CH_4 permeability relative to that of $n\text{-C}_4\text{H}_{10}$. In the additional free volume created by FS addition, CH_4 selective transport may be favored, which causes the $n\text{-C}_4\text{H}_{10}/\text{CH}_4$ selectivity to decrease. As temperature decreased, the mixed gas $n\text{-C}_4\text{H}_{10}$ permeabilities of all films increased, while the mixed gas CH_4 permeabilities decreased. Consequently, $n\text{-C}_4\text{H}_{10}/\text{CH}_4$ permeability selectivities increase with decreasing temperature. The decrease in mixed gas CH_4 permeability with decreasing temperature is opposite to that observed for pure gas CH_4 permeation, where an increase is observed with decreasing temperature. This difference in behavior is thought to be caused by the blocking of CH_4 permeation by $n\text{-C}_4\text{H}_{10}$ in the gas mixture increasing as temperature decreases.

9.2) Recommendations

9.2.1) Optimization of Crosslinking Process

The current method to crosslink PTMSP involves placing the polymer film containing unreacted bis(azide) in a vacuum oven for 90 minutes at 180°C. This method is satisfactory for producing crosslinked films on a small scale. However to produce crosslinked films on a large scale, a continuous membrane forming operation would likely be employed. *UV* irradiation would be the most suitable method to initiate the crosslinking reaction for continuous membrane formation. In this study, PTMSP was crosslinked using *uv* irradiation, however it took 3 hours to effect the crosslinking reaction with the *uv* lamp and bis azide crosslinker that were available. Investigations to shorten this reaction time could involve studying the effects of the intensity of *uv* source on reaction time, and examining different crosslinkers which require a less energetic *uv* source than the current crosslinker, to initiate their reaction.

9.2.2) Testing of Different Gas Mixtures

At the moment the understanding of changes in mixed gas transport properties of PTMSP caused by crosslinking and FS addition is limited. It is currently proposed that decreases in the mixed gas selectivities of crosslinked and nanocomposite PTMSP are a result of changes in their free volume characteristics. The study of the mixed gas transport properties of *n*-C₄H₁₀/H₂ mixtures would further the understanding of the effect of free volume changes on the mixed gas transport properties of PTMSP. H₂ (2.89 Å) is substantially smaller than CH₄ (3.8 Å) [6], and mixed gas *n*-C₄H₁₀/H₂ selectivities of

crosslinked and nanocomposite PTMSP should show greater deviation from the $n\text{-C}_4\text{H}_{10}/\text{H}_2$ selectivities of unfilled, uncrosslinked PTMSP, than the deviations observed from permeation experiments using a $n\text{-C}_4\text{H}_{10}/\text{CH}_4$ mixture. The reasoning for this hypothesis is the increased size sieving ability of crosslinked PTMSP, and the increased Knudsen flow characteristics of nanocomposite PTMSP should effect the transport properties of H_2 significantly more than CH_4 as H_2 is smaller than CH_4 [4]. If these effects were borne out in $n\text{-C}_4\text{H}_{10}/\text{H}_2$ mixtures, the initial conclusions on the reasoning for changes in mixed gas selectivities due to crosslinking and FS addition would be substantiated.

9.2.3) Concentration Polarization Effects

It has been reported in the literature that concentration polarization reduces the separation factors of highly permeable materials such as polydimethylsiloxane (PDMS) [7]. Mixed gas selectivities are reduced by concentration polarization when the resistance to gas permeation of the boundary layer along the membrane surface becomes significant relative to the resistance of the separating membrane layer [7,8]. As PTMSP is an order of magnitude more permeable than PDMS [1], it is expected that concentration polarization effects would be much more severe in PTMSP, and would cause substantial reductions in the mixed gas selectivities. Investigations into these effects and the effects of crosslinking, FS and POSS addition on the amount of concentration polarization would help in evaluating whether PTMSP could be used as a practical material for use in industrial gas separation membranes.

9.3) References

- [1] K. Nagai, T. Masuda, T. Nakagawa, B. D. Freeman, and I. Pinnau, Poly[1-(trimethylsilyl)-1-propyne] and related polymers: synthesis, properties and functions, *Progress in Polymer Science*, 26 (2001) 721-98.
- [2] I. Pinnau and L. G. Toy, Transport of organic vapors through poly[1-(trimethylsilyl)-1-propyne], *Journal of Membrane Science*, 116 (1996) 199-209.
- [3] J. Jia and G. L. Baker, Crosslinking of poly[1-(trimethylsilyl)-1-propyne] membranes using bis(aryl azides), *Journal of Polymer Science, Part B: Polymer Physics*, 36 (1998) 959-68.
- [4] T. C. Merkel, Z. He, I. Pinnau, B. D. Freeman, P. Meakin, and A. J. Hill, Effect of nanoparticles on gas sorption and transport in poly[1-(trimethylsilyl)-1-propyne], *Macromolecules*, 36 (2003) 6844-55.
- [5] T. Masuda, E. Isobe, T. Higashimura, and K. Takada, Poly[1-(trimethylsilyl)-1-propyne]: a new high polymer synthesized with transition-metal catalysts and characterized by extremely high gas permeability, *Journal of the American Chemical Society*, 105 (1983) 7473-4.
- [6] S. Matteucci, Y. Yampolskii, B. D. Freeman, and I. Pinnau, in: Y. Yampolskii, B. D. Freeman, I. Pinnau (Eds.), *Material Science of Membranes for Gas and Vapor Separation*, John Wiley & Sons, New York, 2006, pp. 1-47.
- [7] O. Ludtke, R. D. Behling, and K. Ohlrogge, Concentration polarization in gas permeation, *Journal of Membrane Science*, 146 (1998) 145-57.
- [8] S. Bhattacharya and S.-T. Hwang, Concentration polarization, separation factor, and Peclet number in membrane processes, *Journal of Membrane Science*, 132 (1997) 73-90.

Appendix A – Supplementary Solubility Figures

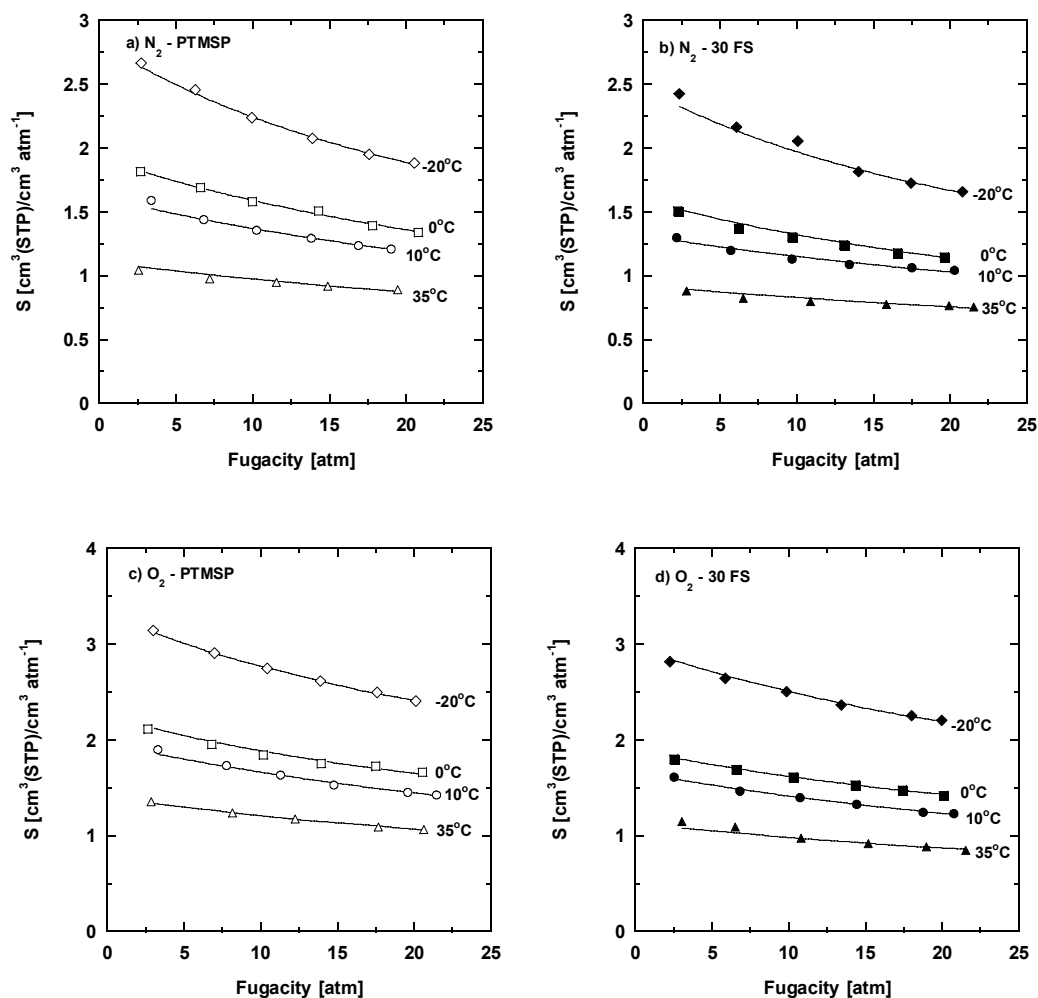


Figure A.1. Effect of fugacity and temperature on N_2 and O_2 solubilities in neat and nanocomposite uncrosslinked PTMSP. The solubilities are plotted as a function of their fugacities. All films were subjected to vacuum conditions at 180°C for 90 minutes, soaked in methanol for 24 hours, then dried for 72 hours in ambient conditions before sorption isotherms were measured. The solid lines represent the dual-mode sorption model fit to the solubility data.

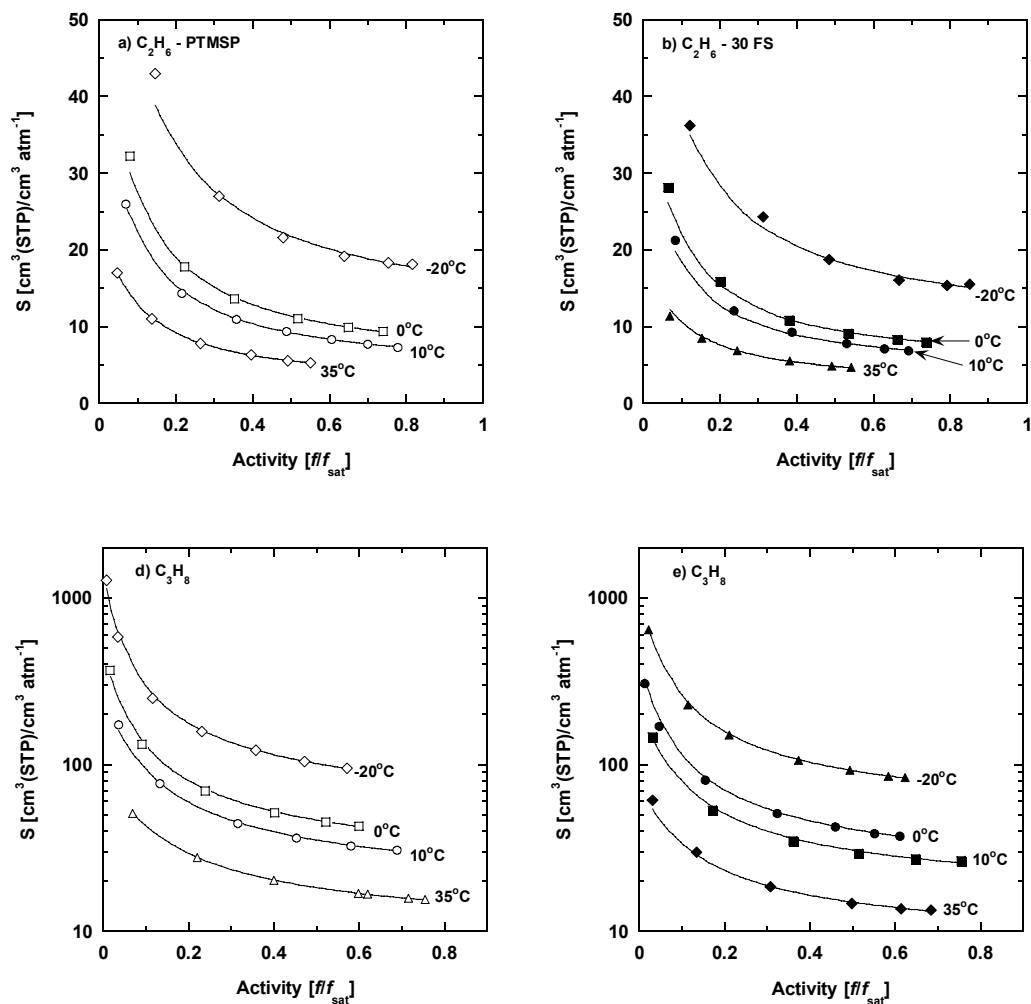


Figure A.2. Effect of activity and temperature on C_2H_6 and C_3H_8 solubilities in neat and nanocomposite uncrosslinked PTMSP. The solubilities are plotted as a function of their activities. All films were subjected to vacuum conditions at 180°C for 90 minutes, soaked in methanol for 24 hours, then dried for 72 hours in ambient conditions before sorption isotherms were measured. The solid lines represent the dual-mode sorption model fit to the solubility data.

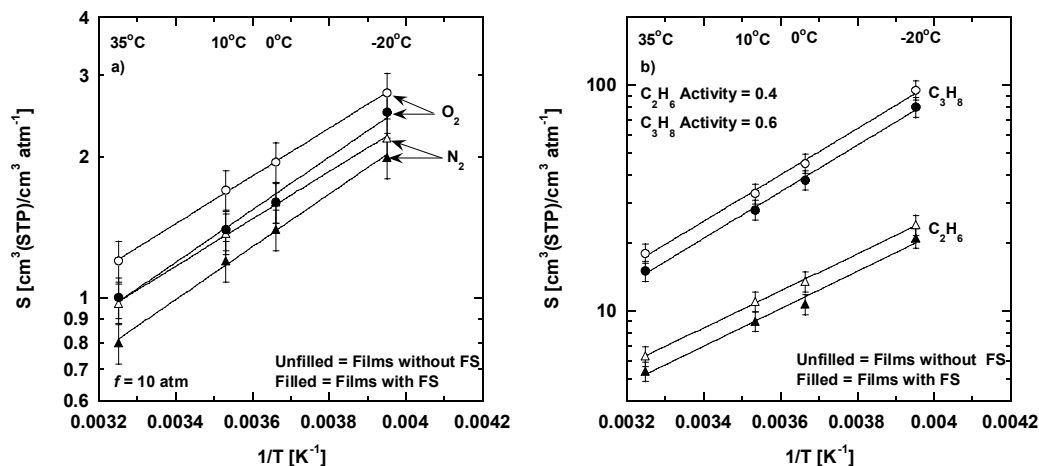


Figure A.3. Effect of temperature on a) N_2 and O_2 ; and b) C_2H_6 and C_3H_8 solubilities in uncrosslinked PTMSP and uncrosslinked PTMSP containing 30 wt % FS. The solubilities were calculated using the dual-mode sorption parameters for the films at the various temperatures specified and fugacities and activities. The total volume of the films in the sorption cell was used as the basis to calculate the solubilities. All films were crosslinked at 180°C in vacuum for 90 minutes, soaked in MeOH for 24 hours and dried at ambient conditions for 72 hours before sorption isotherms were measured.

Appendix B – Supplementary Permeability and Diffusivity Figures

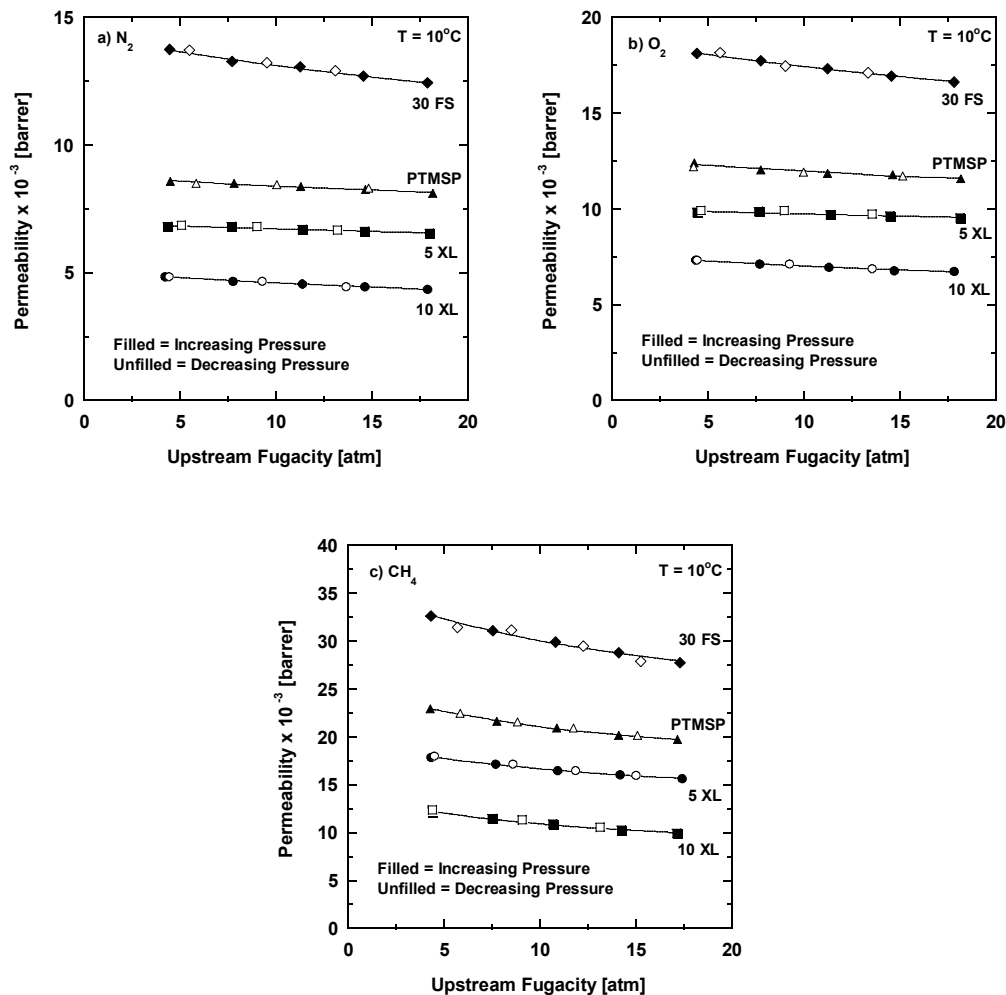


Figure B.1. Permeability of a) N_2 , b) O_2 , and c) CH_4 as a function of upstream fugacity in various PTMSP films at 10°C . The downstream pressure was fixed at atmospheric. The solid lines represent a nonlinear least squares fit of the dual-mode transport model to the permeability data. All films were subjected to vacuum at 180°C for 90 minutes, soaked in MeOH for 24 hours, then dried for 72 hours in ambient conditions before permeability was measured. All films were approximately $100\ \mu\text{m}$ thick.

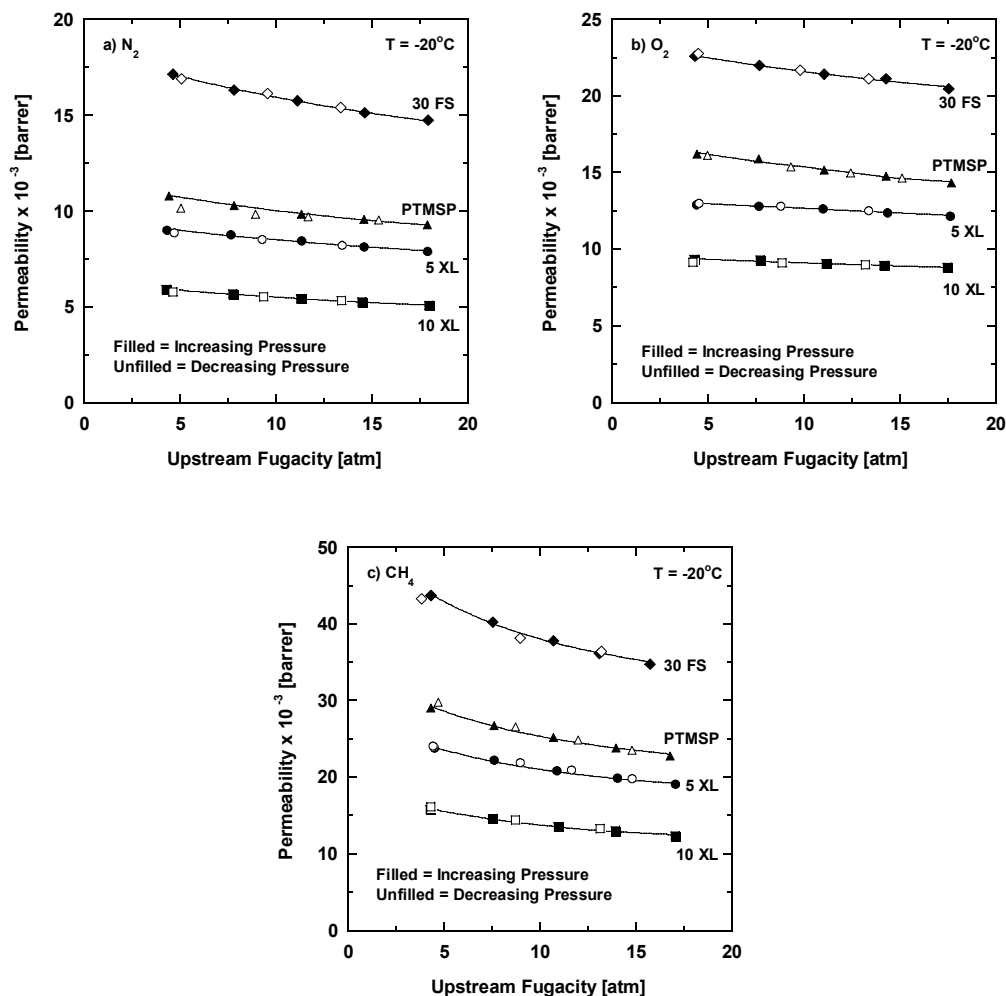


Figure B.2. Permeability of a) N_2 , b) O_2 , and c) CH_4 as a function of upstream fugacity in various PTMSP films at -20°C . The downstream pressure was fixed at atmospheric. The solid lines represent a nonlinear least squares fit of the dual-mode transport model to the permeability data. All films were subjected to vacuum at 180°C for 90 minutes, soaked in MeOH for 24 hours, then dried for 72 hours in ambient conditions before permeability was measured. All films were approximately $100\text{ }\mu\text{m}$ thick

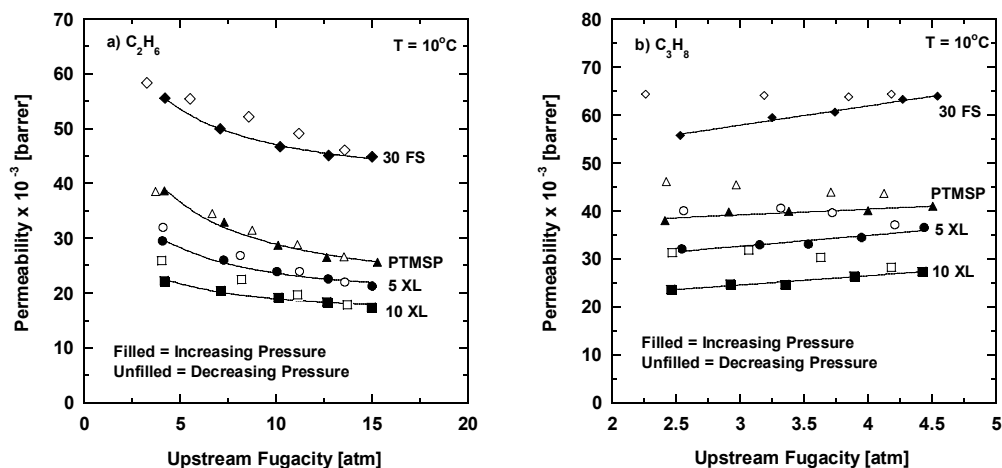


Figure B.3. Permeability of a) C_2H_6 , and b) C_3H_8 as a function of upstream fugacity in various PTMSP films at $10^\circ C$. The downstream pressure was fixed at atmospheric. The C_2H_6 permeability data were fit to the dual-mode transport model, while the C_3H_8 permeability data were fit to a linear function. All films were subjected to vacuum at $180^\circ C$ for 90 minutes, soaked in MeOH for 24 hours, then dried for 72 hours in ambient conditions before permeability was measured. All films were approximately $100\ \mu m$ thick.

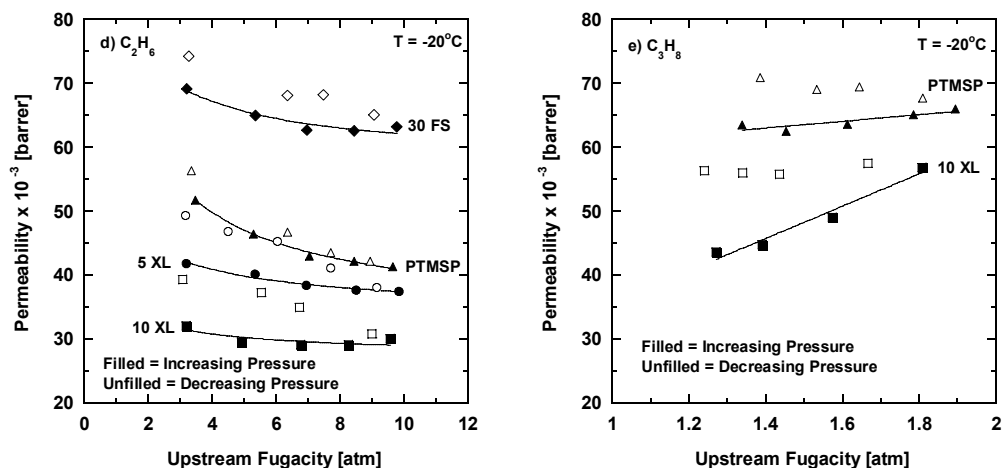


Figure B.4. Permeability of a) C_2H_6 , and b) C_3H_8 as a function of upstream fugacity in various PTMSP films at $-20^\circ C$. The downstream pressure was fixed at atmospheric. The C_2H_6 permeability data were fit to the dual-mode transport model, while the C_3H_8 permeability data were fit to a linear function. All films were subjected to vacuum at $180^\circ C$ for 90 minutes, soaked in MeOH for 24 hours, then dried for 72 hours in ambient conditions before permeability was measured. All films were approximately $100\ \mu m$ thick.

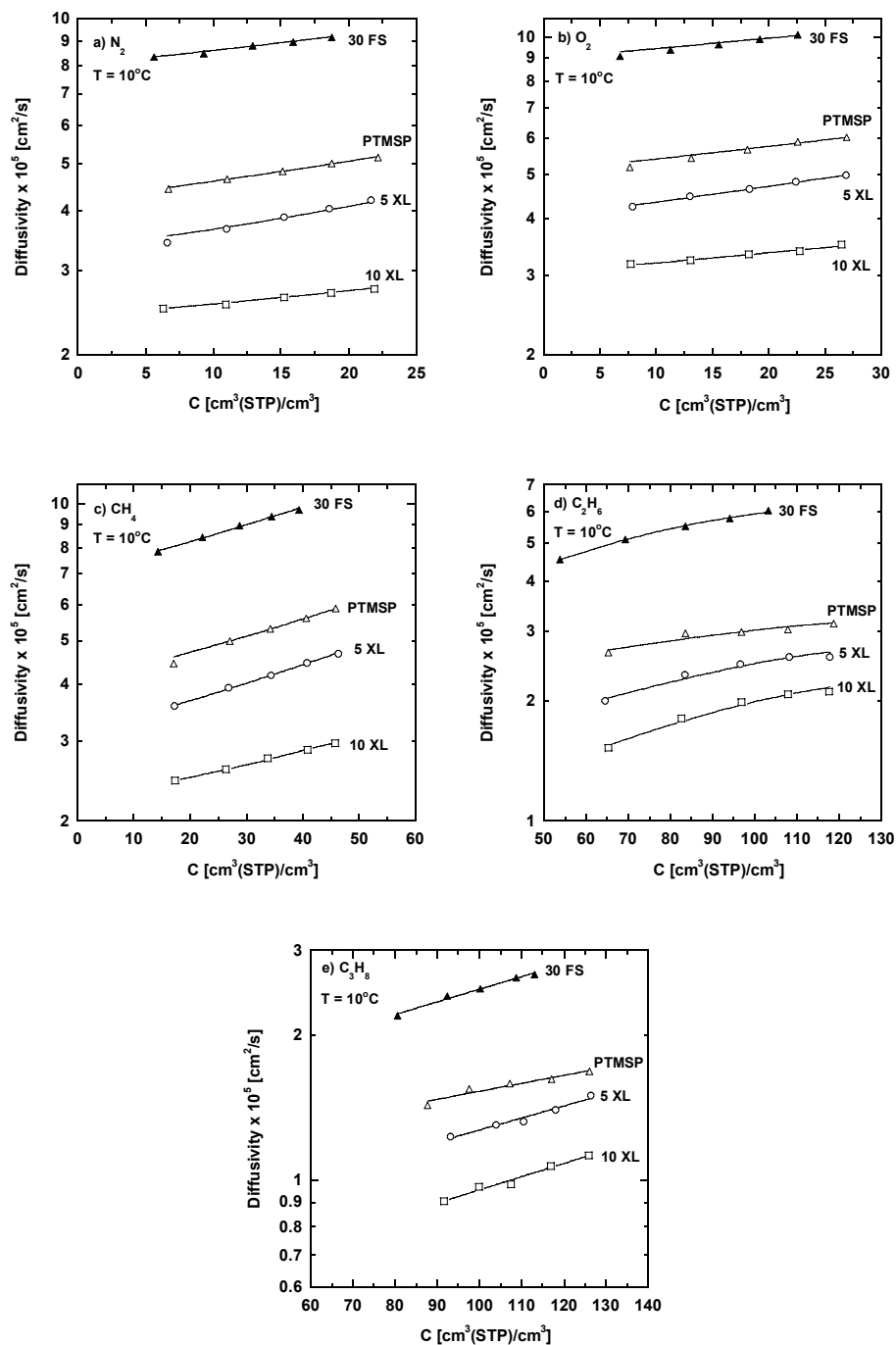


Figure B.5. Concentration averaged diffusivity of a) N_2 , b) O_2 , c) CH_4 , d) C_2H_6 , and e) C_3H_8 as a function of penetrant concentration in various PTMSP films at 10°C . The N_2 , O_2 , CH_4 , and C_2H_6 diffusivity data were fit to the dual-mode transport model, while the C_3H_8 diffusivity data were fit to a linear function.

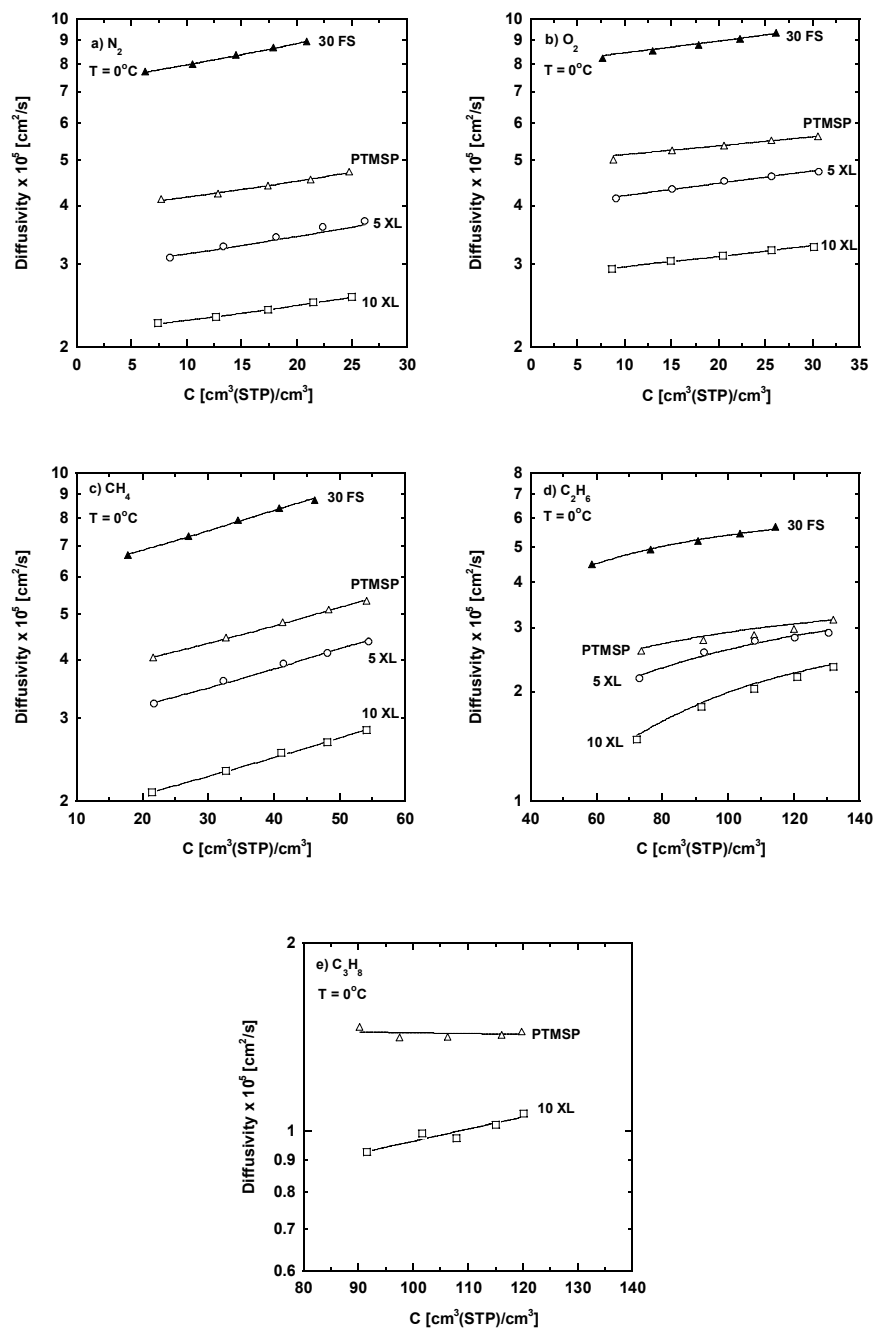


Figure B.6. Concentration averaged diffusivity of a) N_2 , b) O_2 , c) CH_4 , d) C_2H_6 , and e) C_3H_8 as a function of penetrant concentration in various PTMSP films at 0°C . The N_2 , O_2 , CH_4 , and C_2H_6 diffusivity data were fit to the dual-mode transport model, while the C_3H_8 diffusivity data were fit to a linear function.

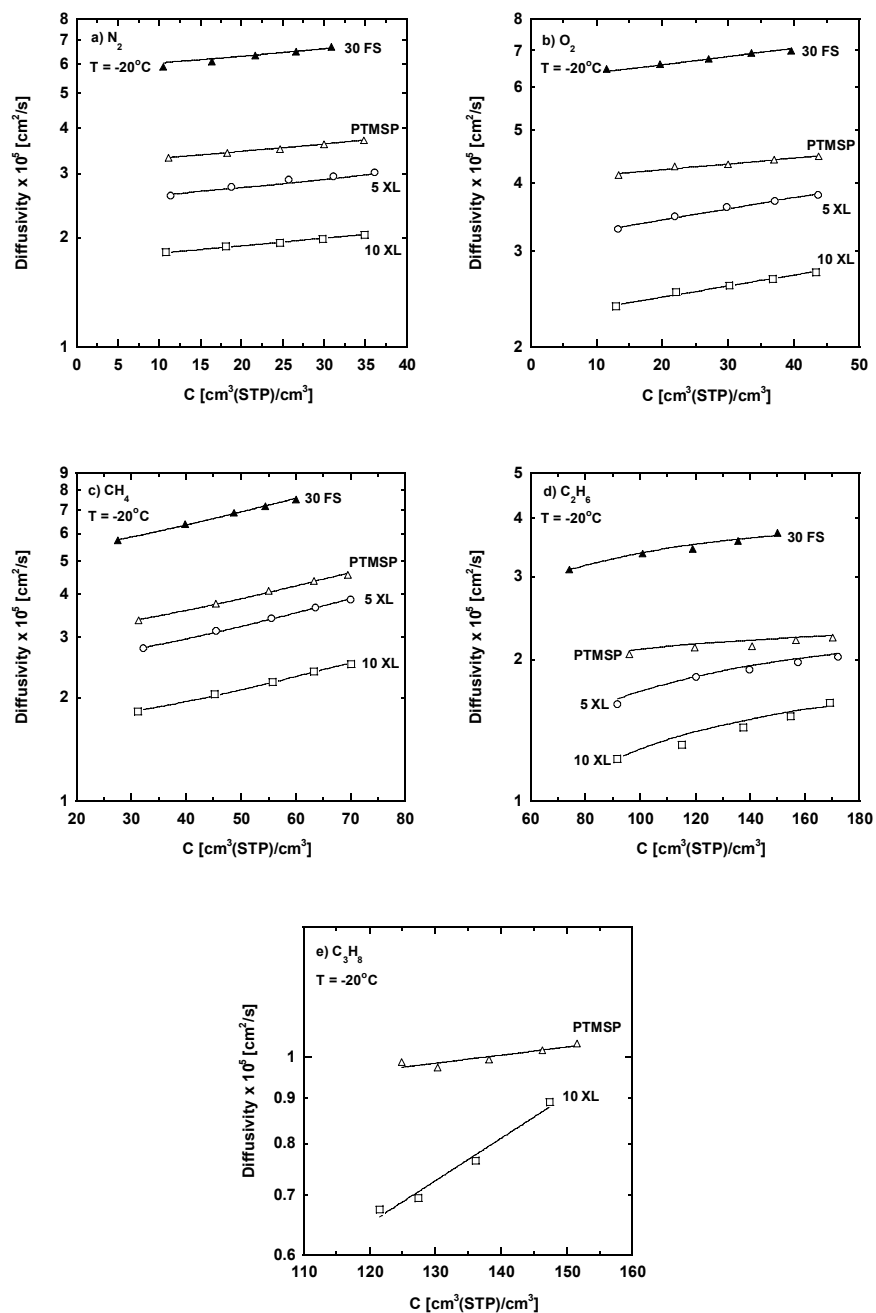


Figure B.7. Concentration averaged diffusivity of a) N_2 , b) O_2 , c) CH_4 , d) C_2H_6 , and e) C_3H_8 as a function of penetrant concentration in various PTMSP films at -20°C . The N_2 , O_2 , CH_4 , and C_2H_6 diffusivity data were fit to the dual-mode transport model, while the C_3H_8 diffusivity data were fit to a linear function.

Bibliography

CAB-O-SIL TS-530 Treated Fumed Silica: Technical Data, Cabot Corp., 1991.

<http://dippr.byu.edu/public/chemsearch.asp>

Mettler-Toledo Density Determination Kit for AT/AG Balances, 1997.

M. Aguilar-Vega and D. R. Paul, Gas transport properties of polycarbonates and polysulfones with aromatic substitutions on the bisphenol connector group, *Journal of Polymer Science, Part B: Polymer Physics*, 31 (1993) 1599-610.

C. L. Aitken, W. J. Koros, and D. R. Paul, Gas transport properties of biphenol polysulfones, *Macromolecules*, 25 (1992) 3651-8.

C. L. Aitken, W. J. Koros, and D. R. Paul, Effect of structural symmetry on gas transport properties of polysulfones, *Macromolecules*, 25 (1992) 3424-34.

C. L. Aitken, D. R. Paul, and D. K. Mohanty, Gas transport properties of poly(aryl ether bissulfones) and poly(aryl ether bisketones), *Journal of Polymer Science, Part B: Polymer Physics*, 31 (1993) 983-9.

C. L. Aitkin and D. R. Paul, Gas transport properties of polysulfones based on dihydroxynaphthalene isomers, *Journal of Polymer Science Part B: Polymer Physics*, 31 (1993) 1061-5.

H. Allcock, Lampe, F., *Contemporary Polymer Chemistry*, 2nd ed., Prentice-Hall, London, 1990.

R. Ash, R. M. Barrer, and R. T. Lowson, Transport of single gases and of binary gas mixtures in a microporous carbon membrane, *Journal of the Chemical Society, Faraday Transactions 1: Physical Chemistry in Condensed Phases*, 69 (1973) 2166-78.

R. Ash, R. M. Barrer, and P. Sharma, Sorption and flow of carbon dioxide and some hydrocarbons in a microporous carbon membrane, *Journal of Membrane Science*, 1 (1976) 17-32.

N. Auner, B. Ziemer, B. Herrschaft, W. Ziche, P. John, and J. Weis, Structural studies of novel siloxysilsesquioxanes, *European Journal of Inorganic Chemistry*, (1999) 1087-94.

- G. L. Baker, C. F. Klausner, A. S. Gozdz, J. A. Shelburne, III, and T. N. Bowmer, Brominated poly[1-(trimethylsilyl)-1-propyne]. Lithography and photochemistry, *Advances in Chemistry Series*, 224 (1990) 663-78.
- R. W. Baker, Future directions of membrane gas separation technology, *Industrial & Engineering Chemistry Research*, 41 (2002) 1393-411.
- S. Bhattacharya and S.-T. Hwang, Concentration polarization, separation factor, and Peclet number in membrane processes, *Journal of Membrane Science*, 132 (1997) 73-90.
- A. Bondi, van der Waals volumes and radii, *Journal of Physical Chemistry*, 68 (1964) 441-51.
- A. Bondi, *Physical Properties of Molecular Crystals, Liquids and Glasses*, Wiley, New York, 1968.
- M. Born, and E. Wolf, *Principles of Optics*, 7th ed., Cambridge University Press, Cambridge, United Kingdom, 1999.
- T. S. Chow, Kinetics of free volume and physical aging in polymer glasses, *Macromolecules*, 17 (1984) 2336-40.
- M. H. Cohen and D. Turnbull, Molecular transport in liquids and glasses, *Journal of Chemical Physics*, 31 (1959) 1164-9.
- G. Consolati, I. Genco, M. Pegoraro, and L. Zangerighi, Positron annihilation lifetime (PAL) in poly[1-(trimethylsilyl)-1-propyne] (PTMSP): free volume determination and time dependence of permeability, *Journal of Polymer Science, Part B: Polymer Physics*, 34 (1996) 357-67.
- K. De Sitter, P. Winberg, J. D'Haen, C. Dotremont, R. Leysen, J. A. Martens, S. Mullens, F. H. J. Maurer, and I. F. J. Vankelecom, Silica filled poly[1-(trimethylsilyl)-1-propyne] nanocomposite membranes: Relation between the transport of gases and structural characteristics, *Journal of Membrane Science*, 278 (2006) 83-91.
- J. A. Dean, *Lange's Handbook of Chemistry*, 15th ed., McGraw-Hill, New York, 1999.
- S. V. Dixon-Garrett, K. Nagai, and B. D. Freeman, Sorption, diffusion, and permeation of ethylbenzene in poly[1-(trimethylsilyl)-1-propyne], *Journal of Polymer Science, Part B: Polymer Physics*, 38 (2000) 1078-89.

- K. D. Dorkenoo and P. H. Pfromm, Accelerated physical aging of thin poly[1-(trimethylsilyl)-1-propyne] films, *Macromolecules*, 33 (2000) 3747-51.
- G. K. Fleming and W. J. Koros, Dilation of polymers by sorption of carbon dioxide at elevated pressures. 1. Silicone rubber and unconditioned polycarbonate, *Macromolecules*, 19 (1986) 2285-91.
- B. D. Freeman, Basis of permeability/selectivity tradeoff relations in polymeric gas separation membranes, *Macromolecules*, 32 (1999) 375-80.
- B. D. Freeman, and I. Pinnau, in: B. D. Freeman, I. Pinnau (Eds.), *Polymer Membranes for Gas and Vapor Separation: Chemistry and Materials Science*. ACS Symposium Series, 1999, pp. 1-27.
- B. D. Freeman, H. Lin, in: H. Czichos, T. Saito, L. Smith (Eds.), *Springer Handbook of Materials Measurement Methods*, Springer, Berlin, German, 2006, pp. 371-87.
- K. Ghosal and B. D. Freeman, Gas separation using polymer membranes: an overview, *Polymers for Advanced Technologies*, 5 (1994) 673-97.
- T. Graham, On the absorption and dialytic separation of gases by colloid septa Part I.- Action of a septum of caoutchouc, *Journal of Membrane Science*, 100 (1995) 27-31.
- M. W. Hellums, W. J. Koros, G. R. Husk, and D. R. Paul, Gas transport in halogen-containing aromatic polycarbonates, *Journal of Applied Polymer Science*, 43 (1991) 1977-86.
- M. W. Hellums, W. J. Koros, G. R. Husk, and D. R. Paul, Fluorinated polycarbonates for gas separation applications, *Journal of Membrane Science*, 46 (1989) 93-112.
- A. J. Hill, S. J. Pas, T. J. Bastow, M. I. Burgar, K. Nagai, L. G. Toy, and B. D. Freeman, Influence of methanol conditioning and physical aging on carbon spin-lattice relaxation times of poly[1-(trimethylsilyl)-1-propyne], *Journal of Membrane Science*, 243 (2004) 37-44.
- K. K. Hsu, S. Nataraj, R. M. Thorogood, and P. S. Puri, Oxygen/nitrogen selectivity improvement for poly[1-(trimethylsilyl)-1-propyne] membranes by UV irradiation and further enhancement by subambient temperature operation, *Journal of Membrane Science*, 79 (1993) 1-10.
- Y. Huang and D. R. Paul, Physical Aging of Thin Glassy Polymer Films Monitored by Optical Properties, *Macromolecules*, 39 (2006) 1554-9.

- Y. Huang, X. Wang, and D. R. Paul, Physical aging of thin glassy polymer films: Free volume interpretation, *Journal of Membrane Science*, 277 (2006) 219-29.
- Y. Ichiraku, S. A. Stern, and T. Nakagawa, An investigation of the high gas permeability of poly[1-(trimethylsilyl)-1-propyne], *Journal of Membrane Science*, 34 (1987) 5-18.
- J. Jia, Gas separation and pervaporation of chemically modified poly[1-(trimethylsilyl)-1-propyne] membranes, Ph.D. Dissertation, Michigan State University, 1999.
- J. Jia and G. L. Baker, Crosslinking of poly[1-(trimethylsilyl)-1-propyne] membranes using bis(aryl azides), *Journal of Polymer Science, Part B: Polymer Physics*, 36 (1998) 959-68.
- S. M. Jordan, G. K. Fleming, and W. J. Koros, Permeability of carbon dioxide at elevated pressures in substituted polycarbonates, *Journal of Polymer Science, Part B: Polymer Physics*, 28 (1990) 2305-27.
- S. M. Jordan, M. A. Henson, and W. J. Koros, The effects of carbon dioxide conditioning on the permeation behavior of hollow fiber asymmetric membranes, *Journal of Membrane Science*, 54 (1990) 103-18.
- S. M. Jordan and W. J. Koros, Characterization of carbon dioxide-induced conditioning of substituted polycarbonates using various "exchange" penetrants, *Journal of Membrane Science*, 51 (1990) 233-47.
- S. M. Jordan, W. J. Koros, and G. K. Fleming, The effects of carbon dioxide exposure on pure and mixed gas permeation behavior: comparison of glassy polycarbonate and silicone rubber, *Journal of Membrane Science*, 30 (1987) 191-212.
- S. D. Kelman, S. Matteucci, C. W. Bielawski, and B. D. Freeman, Crosslinking poly[1-(trimethylsilyl)-1-propyne] and its effect on solvent resistance and transport properties, *Polymer*, 48 (2007) 6881-92.
- S. D. Kelman, S. Matteucci, C. W. Bielawski, and B. D. Freeman, The effect of crosslinking and fumed silica addition on the pure gas sorption and transport properties of poly[1-(trimethylsilyl)-1-propyne], In Preparation, (2007).
- V. L. Khodzaeva, V. G. Zaikin, and V. S. Khotimskii, Thermal oxidation of poly[1-(trimethylsilyl)-1-propyne] studied by IR spectroscopy, *Russian Chemical Bulletin (Translation of Izvestiya Akademii Nauk, Seriya Khimicheskaya)*, 52 (2003) 1333-9.

- J. H. Kim, W. J. Koros, and D. R. Paul, Physical aging of thin 6FDA-based polyimide membranes containing carboxyl acid groups. Part II. Optical properties, *Polymer*, 47 (2006) 3104-11.
- W. J. Koros, D. R. Paul, and G. S. Huvard, Energetics of gas sorption in glassy polymers, *Polymer*, 20 (1979) 956-60.
- W. J. Koros, R. T. Chern, V. Stannett, and H. B. Hopfenberg, A model for permeation of mixed gases and vapors in glassy polymers, *Journal of Polymer Science, Polymer Physics Edition*, 19 (1981) 1513-30.
- R. K. Krishnaswamy and J. Janzen, Exploiting refractometry to estimate the density of polyethylene: The Lorentz-Lorenz approach re-visited, *Polymer Testing*, 24 (2005) 762-5.
- S. S. Kurtz, Jr. and A. L. Ward, Refractivity intercept and the specific refraction equation of Newton. I. Development of the refractivity intercept and comparison with specific-refraction equations, *Journal of the Franklin Institute*, 222 (1936) 563-92.
- S. S. Kurtz, Jr. and A. L. Ward, The refractivity intercept and the specific refraction equation of Newton. II. The electronic interpretation of the refractivity intercept and of the specific refraction equations of Newton, Eykman and Lorentz-Lorenz, *Journal of the Franklin Institute*, 224 (1937) 583-601.
- H. Lin and B. D. Freeman, Gas and vapor solubility in cross-linked poly(ethylene glycol diacrylate), *Macromolecules*, 38 (2005) 8394-407.
- H. A. Lorentz, *The Theory of Electrons and Its Applications*, 2nd ed., Dover, New York, 1953.
- O. Ludtke, R. D. Behling, and K. Ohlrogge, Concentration polarization in gas permeation, *Journal of Membrane Science*, 146 (1998) 145-57.
- P. E. Mallon, in: Y. C. Dean, P. E. Mallon, D. M. Schrader (Eds.), *Positron and Positronium Chemistry*, World Scientific Publishing Co., Singapore, 2003, pp. 253-80.
- T. Masuda, K. Hasegawa, and T. Higashimura, Polymerization of phenylacetylenes. I. Polymerization of phenylacetylene catalyzed by tungsten hexachloride and molybdenum pentachloride, *Macromolecules*, 7 (1974) 728-31.

- T. Masuda, Y. Iguchi, B. Z. Tang, and T. Higashimura, Diffusion and solution of gases in substituted polyacetylene membranes, *Polymer*, 29 (1988) 2041-9.
- T. Masuda, E. Isobe, and T. Higashimura, Polymerization of 1-(trimethylsilyl)-1-propyne by halides of niobium(V) and tantalum(V) and polymer properties, *Macromolecules*, 18 (1985) 841-5.
- T. Masuda, E. Isobe, T. Higashimura, and K. Takada, Poly[1-(trimethylsilyl)-1-propyne]: a new high polymer synthesized with transition-metal catalysts and characterized by extremely high gas permeability, *Journal of the American Chemical Society*, 105 (1983) 7473-4.
- S. Matteucci, Y. Yampolskii, B. D. Freeman, and I. Pinnau, in: Y. Yampolskii, B. D. Freeman, I. Pinnau (Eds.), *Material Science of Membranes for Gas and Vapor Separation*, John Wiley & Sons, New York, 2006, pp. 1-47.
- S. Matteucci, V. A. Kusuma, D. Sanders, S. Swinnea, and B. D. Freeman, Gas transport in TiO₂ nanoparticle-filled poly(1-trimethylsilyl-1-propyne), *Journal of Membrane Science*, 307 (2008) 196-217.
- M. S. McCaig, D. R. Paul, and J. W. Barlow, Effect of film thickness on the changes in gas permeability of a glassy polyarylate due to physical aging part II. Mathematical model, *Polymer*, 41 (1999) 639-48.
- J. S. McHattie, W. J. Koros, and D. R. Paul, Gas transport properties of polysulfones: 3. Comparison of tetramethyl-substituted bisphenols, *Polymer*, 33 (1992) 1701-11.
- J. S. McHattie, W. J. Koros, and D. R. Paul, Gas transport properties of polysulfones. 2. Effect of bisphenol connector groups, *Polymer*, 32 (1991) 2618-25.
- J. S. McHattie, W. J. Koros, and D. R. Paul, Gas transport properties of polysulfones. 1. Role of symmetry of methyl group placement on bisphenol, *Polymer*, 32 (1991) 840-50.
- J. S. McHattie, W. J. Koros, and D. R. Paul, Effect of isopropylidene replacement on gas transport properties of polycarbonates, *Journal of Polymer Science, Part B: Polymer Physics*, 29 (1991) 731-46.
- T. C. Merkel, V. Bondar, K. Nagai, and B. D. Freeman, Sorption and transport of hydrocarbon and perfluorocarbon gases in poly[1-(trimethylsilyl)-1-propyne], *Journal of Polymer Science, Part B: Polymer Physics*, 38 (2000) 273-96.

- T. C. Merkel, V. I. Bondar, K. Nagai, B. D. Freeman, and I. Pinnau, Gas sorption, diffusion, and permeation in poly(dimethylsiloxane), *Journal of Polymer Science, Part B: Polymer Physics*, 38 (2000) 415-34.
- T. C. Merkel, B. D. Freeman, R. J. Spontak, Z. He, I. Pinnau, P. Meakin, and A. J. Hill, Sorption, transport, and structural evidence for enhanced free volume in poly(4-methyl-2-pentyne)/fumed silica nanocomposite membranes, *Chemistry of Materials*, 15 (2003) 109-23.
- T. C. Merkel, R. P. Gupta, B. S. Turk, and B. D. Freeman, Mixed-gas permeation of syngas components in poly(dimethylsiloxane) and poly[1-(trimethylsilyl)-1-propyne] at elevated temperatures, *Journal of Membrane Science*, 191 (2001) 85-94.
- T. C. Merkel, Z. He, I. Pinnau, B. D. Freeman, P. Meakin, and A. J. Hill, Effect of nanoparticles on gas sorption and transport in poly[1-(trimethylsilyl)-1-propyne], *Macromolecules*, 36 (2003) 6844-55.
- T. C. Merkel, L. G. Toy, A. L. Andraday, H. Gracz, and E. O. Stejskal, Investigation of enhanced free volume in nanosilica-filled poly[1-(trimethylsilyl)-1-propyne] by ^{129}Xe NMR spectroscopy, *Macromolecules*, 36 (2003) 353-8.
- A. Morisato, B. D. Freeman, I. Pinnau, and C. G. Casillas, Pure hydrocarbon sorption properties of poly[1-(trimethylsilyl)-1-propyne] (PTMSP), poly(1-phenyl-1-propyne) (PPP), and PTMSP/PPP blends, *Journal of Polymer Science, Part B: Polymer Physics*, 34 (1996) 1925-34.
- K. Nagai, A. Higuchi, and T. Nakagawa, Bromination and gas permeability of poly[1-(trimethylsilyl)-1-propyne] membrane, *Journal of Applied Polymer Science*, 54 (1994) 1207-17.
- K. Nagai, A. Higuchi, and T. Nakagawa, Gas permeation and sorption in brominated poly[1-(trimethylsilyl)-1-propyne] membrane, *Journal of Applied Polymer Science*, 54 (1994) 1353-61.
- K. Nagai, B. D. Freeman, and A. J. Hill, Effect of physical aging of poly[1-(trimethylsilyl)-1-propyne] films synthesized with TaCl_5 and NbCl_5 on gas permeability, fractional free volume, and positron annihilation lifetime spectroscopy parameters, *Journal of Polymer Science, Part B: Polymer Physics*, 38 (2000) 1222-39.

- K. Nagai, A. Higuchi, and T. Nakagawa, Gas permeability and stability of poly(1-trimethylsilyl-1-propyne-co-1-phenyl-1-propyne) membranes, *Journal of Polymer Science, Part B: Polymer Physics*, 33 (1995) 289-98.
- K. Nagai, T. Masuda, T. Nakagawa, B. D. Freeman, and I. Pinnau, Poly[1-(trimethylsilyl)-1-propyne] and related polymers: synthesis, properties and functions, *Progress in Polymer Science*, 26 (2001) 721-98.
- K. Nagai and T. Nakagawa, Oxidation of poly[1-(trimethylsilyl)-1-propyne], *Journal of Applied Polymer Science*, 54 (1994) 1651-8.
- K. Nagai and T. Nakagawa, Effects of aging on the gas permeability and solubility in poly[1-(trimethylsilyl)-1-propyne] membranes synthesized with various catalysts, *Journal of Membrane Science*, 105 (1995) 261-72.
- T. Nakagawa, S. Fujisaki, H. Nakano, and A. Higuchi, Physical modification of poly[1-(trimethylsilyl)-1-propyne] membranes for gas separation, *Journal of Membrane Science*, 94 (1994) 183-93.
- I. Pinnau, C. G. Casillas, A. Morisato, and B. D. Freeman, Hydrocarbon/hydrogen mixed gas permeation in poly[1-(trimethylsilyl)-1-propyne] (PTMSP), poly(1-phenyl-1-propyne) (PPP), and PTMSP/PPP blends, *Journal of Polymer Science, Part B: Polymer Physics*, 34 (1996) 2613-21.
- I. Pinnau, C. G. Casillas, A. Morisato, and B. D. Freeman, Long-term permeation properties of poly[1-(trimethylsilyl)-1-propyne] membranes in hydrocarbon-vapor environment, *Journal of Polymer Science, Part B: Polymer Physics*, 35 (1997) 1483-90.
- I. Pinnau and Z. He, Process of separating a fluid mixture by a polymer membrane containing filler. US Patent, 6,326,684 (2001).
- I. Pinnau and Z. He, Pure- and mixed-gas permeation properties of polydimethylsiloxane for hydrocarbon/methane and hydrocarbon/hydrogen separation, *Journal of Membrane Science*, 244 (2004) 227-33.
- I. Pinnau and L. G. Toy, Transport of organic vapors through poly[1-(trimethylsilyl)-1-propyne], *Journal of Membrane Science*, 116 (1996) 199-209.
- M. Pinteala, V. Harabagiu, B. C. Simionescu, P. Guegan, and H. Cheradame, Ionically conducting networks derived from PEO containing aziridine groups, *Polymer International*, 48 (1999) 1147-54.

- R. S. Prabhakar, R. Raharjo, L. G. Toy, H. Lin, and B. D. Freeman, Self-consistent model of concentration and temperature dependence of permeability in rubbery polymers, *Industrial & Engineering Chemistry Research*, 44 (2005) 1547-56.
- J. Qiu, J. M. Zheng, and K. V. Peinemann, Gas transport properties in a novel poly[1-(trimethylsilyl)-1-propyne] composite membrane with nanosized organic filler trimethylsilylglucose, *Macromolecules*, 39 (2006) 4093-100.
- C. T. Ratcliffe, A. Diaz, C. Nopasit, and G. Munoz, Application of membranes in CO₂ separation from natural gas: pilot plant tests on offshore platforms, *Proceedings - Laurance Reid Gas Conditioning Conference*, (1999) 117-40.
- R. D. Raharjo, Mixed gas sorption and transport study in solubility selective polymers, Ph.D. Dissertation, University of Texas at Austin, 2007.
- R. D. Raharjo, B. D. Freeman, D. R. Paul, and E. S. Sanders, Pure and mixed gas CH₄ and *n*-C₄H₁₀ permeability and diffusivity in poly[1-(trimethylsilyl)-1-propyne], *Polymer*, 48 (2007) 7329-44.
- R. D. Raharjo, B. D. Freeman, and E. S. Sanders, Pure and mixed gas CH₄ and *n*-C₄H₁₀ sorption and dilation in poly(dimethylsiloxane), *Journal of Membrane Science*, 292 (2007) 45-61.
- R. D. Raharjo, B. D. Freeman, and E. S. Sanders, Pure and mixed gas CH₄ and *n*-C₄H₁₀ sorption and dilation in poly[1-(trimethylsilyl)-1-propyne], *Polymer*, 48 (2007) 6097-114.
- W. A. Reinerth, Sr., J. J. Schwab, J. D. Lichtenhan, Q. Liu, D. Hilton, B. D. Freeman, L. Toy, and H. J. Lee, POSSTM/polymer blends for gas separation, *Abstracts of Papers*, 222nd ACS National Meeting, Chicago, IL, United States, August 26-30, 2001, (2001) MTL5-020.
- C. G. Robertson and G. L. Wilkes, Refractive index: a probe for monitoring volume relaxation during physical aging of glassy polymers, *Polymer*, 39 (1998) 2129-33.
- L. M. Robeson, Correlation of separation factor versus permeability for polymeric membranes, *Journal of Membrane Science*, 62 (1991) 165-85.
- C. J. Ruud, J. Jia, and G. L. Baker, Synthesis and characterization of poly[(1-trimethylsilyl-1-propyne)-co-(1-(4-azidobutyl)dimethylsilyl)-1-propyne]] copolymers, *Macromolecules*, 33 (2000) 8184-91.

- E. S. Sanders, W. J. Koros, H. B. Hopfenberg, and V. T. Stannett, Pure and mixed gas sorption of carbon dioxide and ethylene in poly(methyl methacrylate), *Journal of Membrane Science*, 18 (1984) 53-74.
- J. Schultz and K. V. Peinemann, Membranes for separation of higher hydrocarbons from methane, *Journal of Membrane Science*, 110 (1996) 37-45.
- H. Shimomura, K. Nakanishi, H. Odani, and M. Kurata, Effects of physical aging on permeation of gases in a disubstituted polyacetylene, *Reports on Progress in Polymer Physics in Japan*, 30 (1987) 233-6.
- J. M. Smith, H. C. Van Ness, and M. M. Abbot, *Chemical Engineering Thermodynamics* 5th ed., McGraw Hill, New York, 1995.
- R. W. Spillman, Economics of gas separation membranes, *Chemical Engineering Progress*, 85 (1989) 41-62.
- S. Spinner and R. M. Waxler, Relation between refractive index and density of glasses resulting from annealing compared with corresponding relation resulting from compression, *Applied Optics*, 5 (1966) 1887-9.
- R. Srinivasan, S. R. Auvil, and P. M. Burban, Elucidating the mechanism(s) of gas transport in poly[1-(trimethylsilyl)-1-propyne] (PTMSP) membranes, *Journal of Membrane Science*, 86 (1994) 67-86.
- L. C. E. Struik, *Physical Aging in Amorphous Polymers and Other Materials*, Elsevier, Amsterdam, Netherlands, 1978.
- B. Z. Tang, T. Masuda, T. Higashimura, and H. Yamaoka, Radiation effects on silicon-containing polyacetylenes, *Journal of Polymer Science, Part A: Polymer Chemistry*, 27 (1989) 1197-209.
- N. Tanio and T. Nakanishi, Physical aging and refractive index of poly(methyl methacrylate) glass, *Polymer Journal* (Tokyo, Japan), 38 (2006) 814-8.
- V. V. Teplyakov, D. Roizard, E. Favre, and V. S. Khotimsky, Investigations on the peculiar permeation properties of volatile organic compounds and permanent gases through PTMSP, *Journal of Membrane Science*, 220 (2003) 165-75.
- L. G. Toy, Gas and hydrocarbon vapor transport properties of novel disubstituted polyacetylene membranes, Ph.D. Dissertation, North Carolina State University, 2001.

- V. M. Treushnikov, T. V. Telepneva, A. V. Oleinik, E. L. Sorin, V. V. Korshak, E. S. Krongauz, and N. M. Belomoina, Photochemical crosslinking of poly(phenylquinoxalines) with aromatic azides, *Vysokomolekulyarnye Soedineniya, Seriya A*, 28 (1986) 2129-34.
- K. Tsuchihara, T. Masuda, and T. Higashimura, Effects of ultraviolet irradiation on substituted polyacetylenes, *Journal of Polymer Science, Part A: Polymer Chemistry*, 29 (1991) 471-8.
- S. Ulutan and T. Nakagawa, Separability of ethanol and water mixtures through PTMSP-silica membranes in pervaporation, *Journal of Membrane Science*, 143 (1998) 275-84.
- D. W. Van Krevelen, *Properties of Polymers*, 3rd ed., Elsevier, Amsterdam, 2003.
- J. H. Van Santen and W. Opechowski, A generalization of the Lorentz-Lorenz formula, *Physica (The Hague)*, 14 (1948) 545-52.
- J. G. Wijmans and R. W. Baker, The solution-diffusion model: a review, *Journal of Membrane Science*, 107 (1995) 1-21.
- J. D. Wilkinson and H. M. Hudson, High ethane recovery without inlet carbon dioxide removal, *Proceedings of the Gas Conditioning Conference*, 32nd (1982) N1-N21.
- L. C. Witchey-Lakshmanan, H. B. Hopfenberg, and R. T. Chern, Sorption and transport of organic vapors in poly[1-(trimethylsilyl)-1-propyne], *Journal of Membrane Science*, 48 (1990) 321-31.
- Y. P. Yampolskii, A. P. Korikov, V. P. Shantarovich, K. Nagai, B. D. Freeman, T. Masuda, M. Teraguchi, and G. Kwak, Gas permeability and free volume of highly branched substituted acetylene polymers, *Macromolecules*, 34 (2001) 1788-96.
- Y. P. Yampol'skii, S. M. Shishatskii, V. P. Shantarovich, E. M. Antipov, N. N. Kuzmain, S. V. Rykov, V. L. Khodjaeva, and N. A. Plate, Transport characteristics and other physicochemical properties of aged poly[1-(trimethylsilyl)-1-propyne], *Journal of Applied Polymer Science*, 48 (1993) 1935-44.
- M. Yan, S. X. Cai, M. N. Wybourne, and J. F. W. Keana, Evaluation of bis(perfluorophenyl azide)s as cross-linkers for a soluble polyimide, *Journal of Materials Chemistry*, 6 (1996) 1249-52.

- N. Yasuda, S. Yamamoto, H. Adachi, S. Nagae, Y. Wada, and S. Yanagida, A novel photosensitive silicone ladder polymer: synthesis, photochemical, and thermal characteristics, *Bulletin of the Chemical Society of Japan*, 74 (2001) 991-6.
- N. Yasuda, S. Yamamoto, Y. Wada, and S. Yanagida, Photocrosslinking reaction of vinyl-functional polyphenylsilsesquioxane sensitized with aromatic bis(azide) compounds, *Journal of Polymer Science, Part A: Polymer Chemistry*, 39 (2001) 4196-205.

Vita

Scott Douglas Kelman was born on the 30th of December, 1979, and he is the first of two sons to Douglas and Jane Kelman. After attending and graduating from St. Andrew's College in Christchurch, New Zealand, he attended the University of Canterbury in Christchurch and completed a Bachelor of Engineering with 1st Class Honors in Chemical Engineering in November of 2001. In August of 2002 he enrolled at The University of Texas at Austin to pursue a doctoral degree in Chemical Engineering under the guidance of Professor Benny D. Freeman.

Permanent address: 14A Harakeke St.

Riccarton

Christchurch

NEW ZEALAND

This dissertation was typed by Scott Douglas Kelman.